In vivo characterization of present and potentially pre-pandemic viruses —
The SARS-CoV-2 and bat influenza H9N2 examples

Inauguraldissertation

zur

Erlangung des akademischen Grades eines

Doktors der Naturwissenschaften (Dr. rer. nat.)

der

Mathematisch-Naturwissenschaftlichen Fakultät

der

Universität Greifswald

vorgelegt von

Nico Joël Halwe
geb. am 04.10.1995
in Lübbecke

Greifswald, den 24.05.2023

Dekan*in: Prof. Dr. Gerald Kerth

1. Gutachter*in: Prof. Dr. Stefan Finke
2. Gutachter*in: Prof. Dr. Stephan Ludwig
3. Gutachter*in: Prof. Dr. Asisa Volz

Tag der Promotion: Donnerstag, 05.10.2023

Für meine Familie.

--- Table of Content ---

I   Abbreviations

(h/m)ACE2	(Human/mouse) Angiotensin converting enzyme 2
BP	Before present
CDC	Centers for Disease Control and Prevention
CE	Common Era
COVID-19	Coronavirus disease 2019
(H)CoV	(Human)Coronavirus
CRM1	Chromosomal Region Maintenance 1
CTD	C-terminal domain
DBatVir	Database of bat-associated viruses
Dec.	December
DENV	Dengue-virus
dpi	Days post infection
E	Envelope protein (CoVs)
ER	Endoplasmic reticulum
FCS	Furine cleavage site
HA (H1-H18)	Hemagglutinin
EBOV	Ebolavirus
ERGIC	Endoplasmic reticulum-Golgi intermediate compartment
gRNA	Genomic RNA
H1N1pdm09	2009 pandemic swine H1N1
HAV	Hepatitis A virus
HBV	Hepatitis B virus
HIV	Human immunodeficiency virus
HP	Highly pathogenic
HPAIV	Highly pathogenic avian Influenza virus
IAV	Influenza A virus
IVPI/IMPI	Intravenous/intramuscular pathogenicity index
Jan.	January
K18	Keratin-18
kB	Kilobases
KI	Knock-In
LP	Low pathogenic
LRT	Lower respiratory tract
M	Membrane protein (CoVs)
M1/M2	Matrix protein 1/2 (IAVs)
MERS	Middle East Respiratory Syndrome
MHC-II	Major histocompatibility complex II
MARV	Marburg-virus
mRNA	Messenger RNA
MxA	Myxovirus resistance protein 1
N	Nucleocapsid protein (CoVs)

NA (N1-N11)	Neuraminidase
NP	Nucleoprotein
NEP	Nuclear export protein
Nov.	November
NSP1/2	Non-structural protein 1/2
NTD	N-terminal domain
ORF	Open Reading Frame
PA	Polymerase acidic protein
PB1/PB2	Polymerase basic protein 1/2
pp1a/b	Polyprotein 1a/1b
R_0	Basic reproduction number
RABV	Rabies-virus
RBD	Receptor binding domain
RdRp	RNA dependent RNA Polymerase
RKI	Robert-Koch-Institute
RNA	Ribonucleic acid
RO	Replication organelle
RSV	Respiratory syncytial virus
RTC	Replication-transcription complex
RT-qPCR	Real-time quantitative Polymerase chain reaction
S	Spike protein (CoVs)
SARS	Severe acute respiratory syndrome
sgRNA	Subgenomic RNA
(-/+)ssRNA	Negative/positive single stranded RNA
tg	Transgenic
TMD	Transmembrane domain
TMPRSS2	Transmembrane serine protease type II
UK	United Kingdom
UN	United Nations
URT	Upper respiratory tract
VOC	Variant of Concern
vRNA	Viral RNA
vRNP	Viral ribonucleoprotein
WHO	World Health Organization
WOAH	World Organization for Animal Health
WT	Wildtype
wt-S$^{\text{Alpha/Delta/Omicron BA.1}}$	SARS-CoV-2 WT expressing the spike protein of Alpha, Delta or Omicron BA.1
YFV	Yellow-fever virus
ZIKV	Zika-virus

II   Figure Legend

III Table Legend

1   Introduction

1.1   Pandemic outbreaks – From the reservoir hosts to spillover infection to interhuman transmissions

A pandemic is characterized by the rapid and locally unlimited spread of an infectious disease in the human population, often without any pre-existing immunity in respective individuals and without available counteracting treatments. In total, the known pandemics from the past were responsible for hundreds of millions of diseased people and up to millions of human deaths (Piret and Boivin 2020). Recent investigations by researchers led to the conclusion that the world's first pandemic already might have occurred between 6.000 and 5.000 before present (BP), initiated by *Yersinia pestis* (Bouvenot et al. 2021), a bacterium transmitted by fleas (Rascovan et al. 2019). The ability for an animal-to-human interspecies transmission classifies the respective pathogen as being zoonotic (ZOONOSES 1951). All pathogens, naturally circulate in specific so called reservoir hosts (Mandl et al. 2014). Reservoir hosts are characterized by exhibiting disease tolerance to the replication of a specific pathogen, while simultaneously limiting structural and functional host responses independent of the respective pathogen load (Soares et al. 2017).
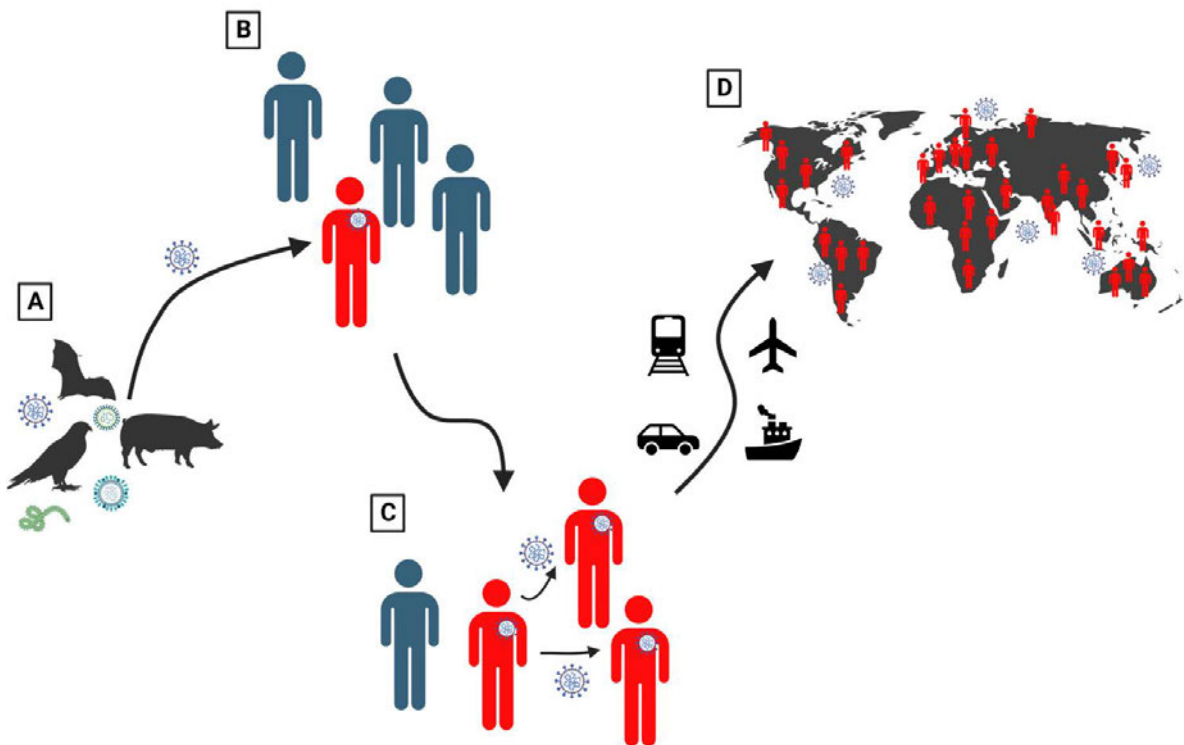

Figure 1: From Spillover to pandemic

Possible chain reaction following a zoonotic pathogen spillover infection to humans, subsequently leading to a pandemic **A** Numerous animal groups can serve as reservoir for different virus families and may finally cause a spillover infection to humans (Mandl et al. 2014; Ellwanger and Chies 2021). **B** In turn, the exposed person might get ill and may spread the zoonotic virus to further human contacts, a prerequisite for the establishment of a pandemic (WHO 2009). **C** The globalized world enables rapid traffic and travel of also potentially infected humans over the globe in a relatively short amount of time (Morens and Fauci 2020; Bickley et al. 2021). **D** The infected person carries the virus all over the globe and exposed contacts get infected via efficient transmission of the pathogen, finally causing a pandemic. Created with Biorender.

When a zoonotic pathogen that is generally circulating in a specific reservoir host population gets transmitted to a new host species, this event is considered to be a spillover infection (Fig. 1A+B) (Ellwanger and Chies 2021). There are multiple potential transmission routes of an infectious agent, either directly or indirectly (Louten 2016). Direct transmission involves physical contact of the new host with e.g. body tissues or fluids of the infected host. Afterwards, the pathogen finally enters the contact host over the mucosal epithelium or open skin lesions, in case of the latter for example by animal bites or scratches (Louten 2016). Examples for pathogens transmitted via the direct route include for example the human immunodeficiency virus (HIV) or hepatitis B virus (HBV) (Shaw and Hunter 2012; Hussein et al. 2022). Direct transmission can also occur via respiratory droplets (> 5 µm) as a consequence of coughing, sneezing or even talking and is differentiated from aerosol transmission as these droplets rapidly fall to the ground (Kutter et al. 2018). The respiratory syncytial virus (RSV) is a prominent example for virus transmission via droplet spread (Kutter et al. 2021b).

Indirect transmission can be achieved via aerosols, vectors or vehicles. Aerosol transmission is achieved mainly by respiratory viruses, for example influenza A viruses (IAVs) or coronaviruses (CoVs) (Lindsley et al. 2016; Prather et al. 2020), which infect their interaction partners mainly over a greater distance via small respiratory droplets (< 5 µm) that can remain infectious in the air for a long time (Louten 2016; Kutter et al. 2021b; Kutter et al. 2021a). Remarkably, it was recently shown that droplets up to a size of 100 µm can sustain in the air for about five seconds at a height of one and a half meters, questioning the current classification of droplet sizes in aerosols (Wang et al. 2021). Indirect transmission via the vector route is established inter alia by animals that can carry the pathogen mechanically from the infected host to the new host (Borremans et al. 2019; Viglietta et al. 2021). For example, human infections with dengue- (DENV), yellow fever- (YFV) or zika-virus (ZIKV) are primarily accomplished by the mosquito *Aedes aegypti* as arthropodal vectors, transferring the pathogen from source to recipient (Souza-Neto et al. 2018). Additionally, such vectors can also serve as so called "mixing vessel", providing a platform for viral recombination events if this host gets

simultaneously infected with two related viruses as it can be seen for pigs and IAVs (Ma et al. 2008; He et al. 2018; Sun et al. 2022). The third route of indirect pathogen transmission encompasses vehicles, such as food or fomites. For example, the hepatitis A virus (HAV), as well as several noroviruses are able to infect a new host via consumption of contaminated food (Randazzo and Sánchez 2020; Elviss et al. 2022). In addition to foodborne transmission, humans or animals can also be infected through contact with inanimate surfaces harboring e.g. noroviruses (Overbey et al. 2021).

Importantly, virus spillover from the source host to the final host can also occur via so called intermediate hosts, as it is likely to have happened with the severe acute respiratory syndrome coronavirus (SARS-CoV) back in 2002/2003 (Cui et al. 2019). The probable origin and coherences of SARS-CoV spillover to humans will be addressed in detail in 1.4.1. In brief, it is hypothesized that SARS-CoV originated through recombination of multiple SARS-CoV-related coronaviruses in horseshoe bats as natural reservoir and subsequently accomplished a spillover to palm civets and raccoon dogs as intermediate host at a Chinese market (Kan et al. 2005; Lau et al. 2005; Li et al. 2005; Song et al. 2005; Cui et al. 2019). In turn, the virus underwent further genetic adaptation in these intermediate hosts, which enabled the jump to humans and caused the SARS-CoV epidemic (Hu et al. 2017; Cui et al. 2019). This scenario highlights the important role of intermediate hosts in the emergence of zoonotic viruses and that some viruses need this intermediate host for further viral adaptation, which can in turn facilitate the spillover to humans.

There are multiple important factors that can positively influence the chance of a successful spillover event and further adaptation to the new host: Firstly, a high percentage of phylogenetic similarities between two viruses can facilitate recombination during a simultaneous host infection, potentially resulting in more virulent and/or transmissive strains, possibly also with an extended host range. These scenarios had already been observed especially with IAVs, but also other viruses, such as middle east respiratory syndrome coronavirus (MERS-CoV) or SARS-CoV-2 (Smith et al. 2009; Xiao et al. 2016; Schroeder et al. 2021; Arora et al. 2022). Secondly, environmental changes can increase the risk for a successful spillover of a zoonotic pathogen. These changes encompass inter alia an intensified agriculture, or environmental factors that directly affect the immune system of hosts inhabiting this specific environmental area (Gibb et al. 2020; Becker et al. 2020; Eby et al. 2022; Hill et al. 2022). In line with that, the interaction frequencies between source and recipient host are increasing (Grange et al. 2021; Eby et al. 2022). Lastly, virus adaptation by the acquisition of nucleotide substitutions in their genome can also promote virulence and transmission efficiency, but most importantly also

contribute to a broader viral host range (Lin et al. 2019; Shuai et al. 2021; Zhou et al. 2021; Scheibner et al. 2023). This may in turn facilitate the spillover of a zoonotic pathogen from an animal reservoir to humans. According to the "WHO pandemic alert system", a high risk for an emerging pandemic exists in case the pathogen finally is also competent to induce human to human transmission events (Fig. 1C) (WHO 2009). The globalization, which includes increasing possibilities for humans to travel around the globe, massively facilitates the swift dissemination of (human-adapted) zoonotic pathogens, eventually leading to a pandemic (Fig. 1D) (Morens and Fauci 2020; Bickley et al. 2021).

1.2   Animal-to-human interface as zoonotic risk factor

On the 15th of November 2022, the United Nations (UN) were celebrating the "Day of 8 Billion", meaning at this date the UN estimates the overall global human population to have reached the milestone of 8 Billion inhabitants (Graham 2022; United Nations 2022). Since the overall human population is still growing, but our planet only has limited space, it becomes obvious that the natural habitat of all animals is narrowed down by humans invading more and more earlier undisturbed environments (Graham et al. 2008; Reperant and M E Osterhaus 2013; Magouras et al. 2020). However, demographics and urbanization are only one small part of many anthropogenic factors massively promoting the animal-to-human interface, which further include domestic food production and trading, as well as migratory movements (Magouras et al. 2020). Now, as the animal-to-human interfaces are continuing to increase, the risk for zoonotic diseases accomplishing spillover infections from an animal reservoir host to humans is becoming greater and greater (Grange et al. 2021). Highly prominent reservoir hosts, which were responsible for several spillover infections of zoonotic viruses leading to severe outbreaks, are especially diverse bat species.

1.2.1 Bats – the perfect home for zoonotic viruses
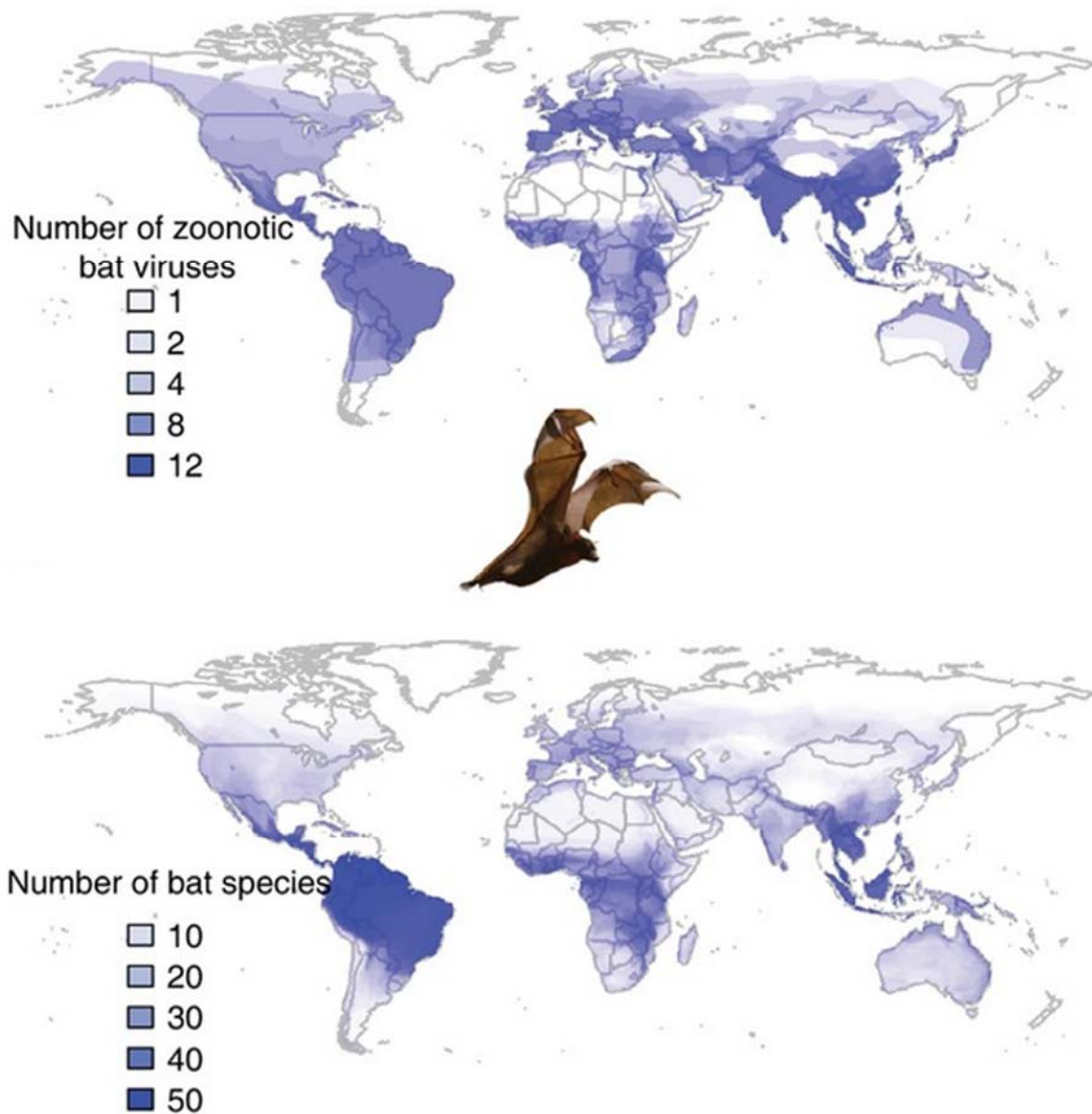
Figure 2: Distribution of bats and their corresponding zoonotic viruses

Adapted from Luis et al. 2015 under the creative commons license CC BY-NC 4.0. Distribution of bat species in comparison to the amount of zoonotic bat-borne viruses detected over the globe.

Bats belong to the class *Mammalia* in the order *Chiroptera*, with different subclades being distributed in specific areas all over the globe (Fig. 2) (Burgin et al. 2018). They provide multiple characteristic traits that qualify them as the perfect reservoir host for viruses. Many of these bat viruses can be classified as zoonotic and human infections with a variety of these bat-borne viruses have been confirmed. Examples for such viruses encompass ebola virus (EBOV) (Leroy et al. 2005), marburg virus (MARV) (Towner et al. 2009), lyssaviruses (Streicker et al. 2010), MERS-CoV (Zaki et al. 2012) and SARS-CoV (Fig. 2) (Lau et al. 2005). Importantly,

the exact progenitor of most viruses causing human outbreaks is not known, so that the knowledge of their origin is limited to close relatives, as demonstrated for SARS-CoV-2 (Zhou et al. 2020; Pekar et al. 2022). In this case, the closest relative was RaTG13, a coronavirus originating from bats, again highlighting the role of bats as a prominent reservoir host for zoonotic viruses (Zhou et al. 2020).

Bats have wings of up to two meters span range, allowing especially migratory bat species to travel many hundreds of miles while potentially carrying pathogens from one place to another (Calisher et al. 2006). A regular exchange of harmless, but also harmful zoonotic viruses between migratory and resident bat species is therefore highly conceivable and allows rapid and transnational distribution of these viruses (Blackwood et al. 2013). Importantly, bats are crepuscular animals that can downregulate their core temperature to up to 10 °C during the day, an ability called torpor (Geiser and Stawski 2011). Additionally, these animals perform hibernation, a more drastic process leading to even higher deceleration of their individual metabolism during the winter period (McGuire et al. 2022). Both abilities, torpor and hibernation, are thought to favor persistence of a huge variety of viruses without causing disease in these animals (George et al. 2011; Subudhi et al. 2017). Disease tolerance against pathogens is highly prominent in bats, which showcase their individual species-dependent disease tolerance mechanism by either limiting pathogen replication or restricting their host immune responses against a specific pathogen to a non-severe pathological threshold (Mandl et al. 2018). The metabolic regulation in bats also contributes to their long-life span of up to 35 years in some species (Wilkinson and Adams 2019; Gorbunova et al. 2020), which in turn has an enormous impact on the basic reproduction number (R_0) of one individual virus-carrying bat (Calisher et al. 2006). Importantly, this does not only include other bat populations, but also other species, such as humans. These events become more and more likely to happen, since the animal-to-human interface, including the bat-to-human interface (Anti et al. 2015; Cappelle et al. 2020), is becoming more tightened and probable, thus facilitating spillover infection of zoonotic viruses from bats to humans. For example, several studies demonstrated recently that Ebola-outbreaks in Africa might be based on a spillover-infection from fruit bats (Leroy et al. 2005; Marí Saéz et al. 2015; Olivero et al. 2020), which is hypothesized to be a reservoir host of this virus (Leroy et al. 2005). It was shown that human behavior massively increases bat-human contacts and therefore the possibility of cross-species spillover events. Examples for this circumstance involve bushmeat consumption and hunting, but also agricultural performance, as fruit bats adapt to and profit by looting from newly available human-cultivated food stocks (Kamins et al. 2011; Centeno-Cuadros et al. 2017).

1.3   Bats as reservoir hosts for influenza A viruses

1.3.1 Discovery of influenza A viruses originating from bat species

IAVs are enveloped, have a negative-sense orientated single-stranded RNA and belong to the *Orthomyxoviridae* family. There are multiple different IAV subtypes, determined by the variable expression of their cell surface proteins hemagglutinin (HA) with 18 subtypes (H1-H18) and neuraminidase (NA) with 11 subtypes (N1-N11) (Taubenberger and Morens 2010; Tong et al. 2012; Tong et al. 2013; Kandeil et al. 2019). Diverse combinations of HA and NA reveal distinct subtypes with specific pathogenicity and viral host range characteristics. For a long time, bats were not taken into consideration as reservoir host for IAVs. Surprisingly, the identification of H17N10 in little yellow-shouldered bats (*Sturnira lilium*) and H18N11 in flat-faced fruit bats *(Artibeus planirostris)* in South America suggested that IAVs might be far more distributed in the order *Chiroptera* than it was assumed before (Tong et al. 2012; Tong et al. 2013). Importantly, the H17N10 and H18N11 IAV subtypes are solely found in bats to date, while subtypes of H1-H16 and N1-N9 are believed to generally circulate in wild waterfowl as natural reservoir host (Olsen et al. 2006). Apart from H17N10 and H18N11, sera from 30 out of 100 sampled frugivorous bats (*Eidolon helvum*) in Ghana showed seropositivity to the avian H9 hemagglutinin subtype (Freidl et al. 2015). These findings presumed the circulation of an H9-influenza A virus in African bats and indeed, another IAV of bat-origin was finally discovered in Old World Egyptian fruit bats (*Rousettus aegyptiacus*) in Egypt in 2019 (Kandeil et al. 2019) and was thereafter classified as bat H9N2. Additionally, more sequences from the bat-borne H9N2 virus originating from Egyptian fruit bats in South Africa were recently published (Rademan et al. 2023), assuming that this bat H9N2 virus is distributed at least over the whole African continent.
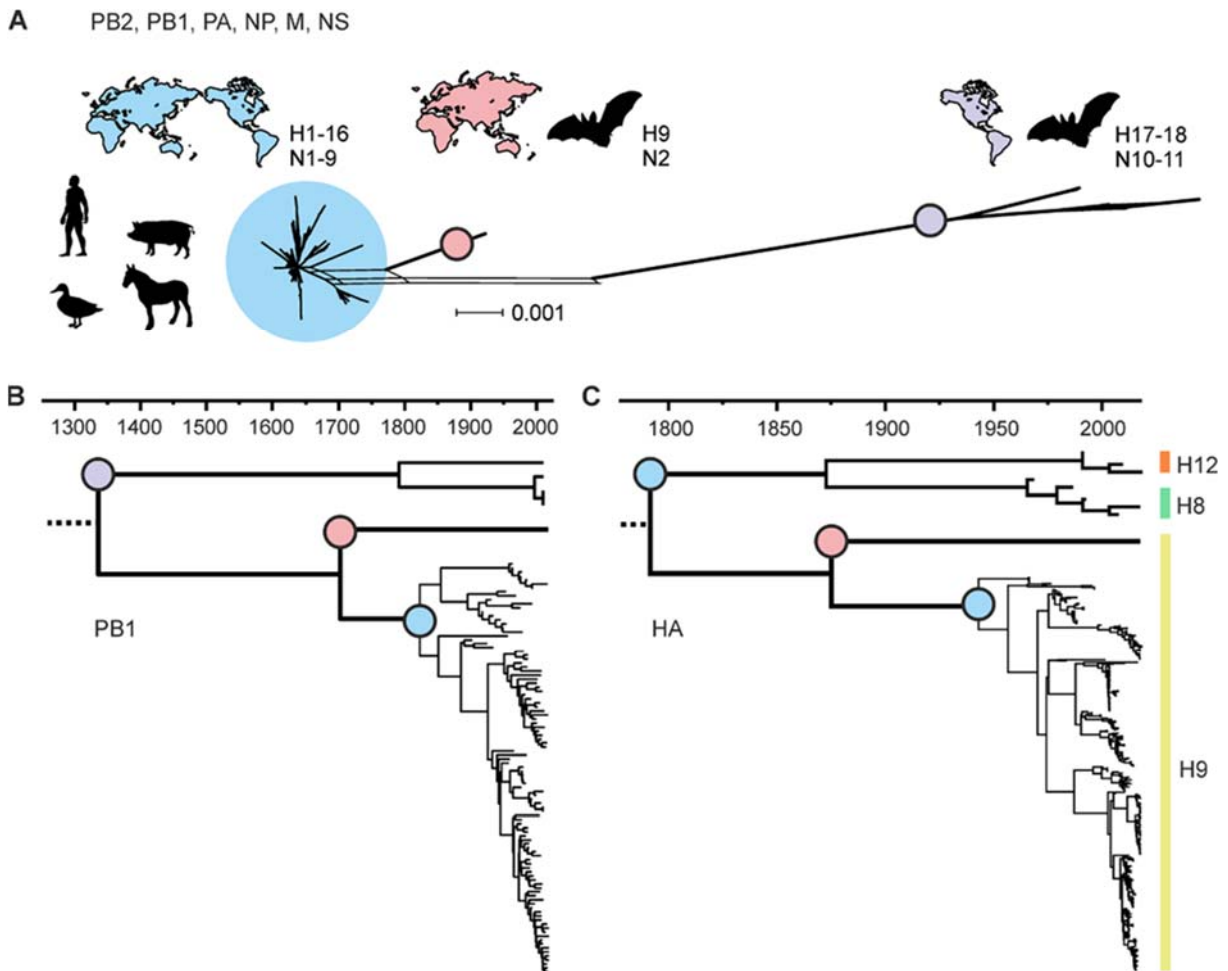
Figure 3: Genetic similarities between bat- and avian influenza A viruses

A Examination of phylogenetic gene segment divergence was accomplished by comparing nucleotide sequences of avian and bat IAVs using a SuperNetwork (Huson and Bryant 2006). Internal avian IAV segments reveal high phylogenetic similarities (blue circle), while Old-World bat H9 and N2 segments, as well as New-World bat-H17/H18 and N10/N11 segments are phylogenetically more diverse to avian IAVs. Importantly, Old World bat segments H9 and N2 demonstrate higher genetical identity to avian IAVs than to New World bat IAV HA and NA segments. **B** Time-calibrated phylogeny of avian and bat-PB1 segments. New World bat PB1 disseminated from avian PB1 around 650 years ago, while Old World bat PB1 disseminated around 300 years ago. **C** Time-calibrated phylogeny of HA, demonstrating phylogenetically younger dissemination of the bat H9 from avian HA segments, indicative of recent recombination events between an Old World bat IAV and avian IAVs. Adapted from Ciminski et al. 2020 under the Creative Common License CC BY 4.0.

Interestingly, phylogenetic comparison of all gene segments from the Old World bat H9N2 IAV demonstrated only little similarities to the New World bat IAVs H17N10 and H18N11, but rather high sequence consensus with avian-origin IAVs of subtype H9N2 (Fig. 3A) (Kandeil et al. 2019; Ciminski et al. 2020). A following deep sequence analysis of the evolutionary background exposed a lineage separation of H17N10 and H18N11 from all other IAVs between the 13th and 14th century (Fig. 3B) (Ciminski et al. 2020). In contrast, lineage separation of internal segments from the Old World bat IAV could be backdated to around the 17th century

(Fig. 3C). However, sequence comparison of the Old World bat IAV HA and NA even shows high similarities to only around 100 years old sequences of avian H9-hemagglutinins and N2-neuraminidases, leading to its classification as subtype bat H9N2 (Fig. 3C) (Ciminski et al. 2020). The composition of the bat H9N2 viral genome may therefore likely be a result of so called recent recombination events between avian IAVs and an ancestral Old World bat flu virus.

1.3.2 General structure and function of influenza A viruses

All influenza A viruses contain a segmented genome of 8 individual parts, coding for specific proteins including polymerase basic protein 1 (PB1), PB2, polymerase (PA), HA, Nucleoprotein (NP), NA, matrix protein (consisting of M1 and M2) and non-structural protein 1 (NS1) (Fig. 4) (Shaw et al. 2008; Chauhan and Gordon 2022). The segmented genome facilitates recombination events between two IAV strains during simultaneous infection of a host in terms of so called reassortment processes, which involves the exchange of gene segments between the different IAV strains and could result in antigenic shifts (Ganti et al. 2021; Marshall et al. 2013). These events finally lead to the emergence of new IAV subtypes that may differ in terms of virulence, antigenicity, transmissive fitness and host range (Mostafa et al. 2020; Sun et al. 2020).
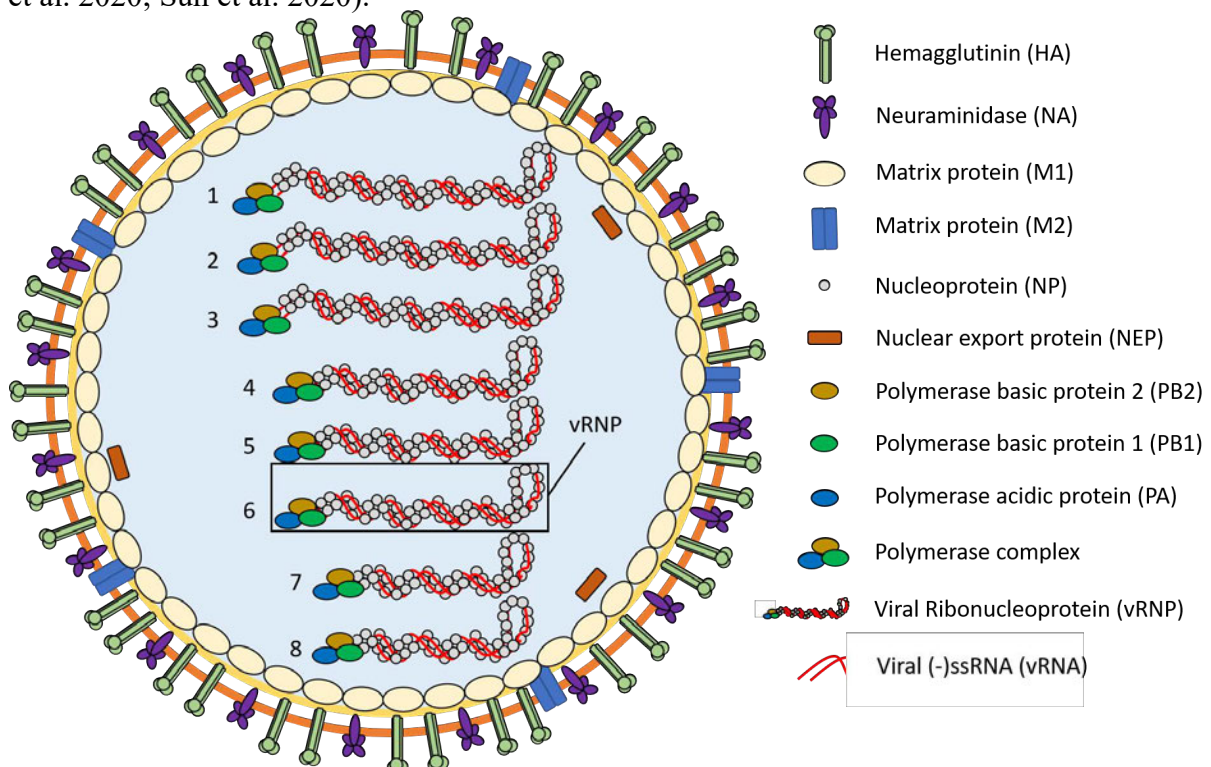
Figure 4: Structure of an influenza A virus virion

The enveloped influenza A virus harbors a single stranded RNA-genome of negative polarity that is distributed in 8 gene segments. These gene segments are coding for the different viral

proteins HA, NA, M (divided in M1 and M2 subunits), NP (incl. NEP), PB1, PB2 and PA and NS. The gene segments are organized in a vRNP-complex, consisting of the viral RNA attached to several NP-proteins, as well as an RdRP-complex including PB1, PB2 and PA. The M1 and M2-subunits are responsible for vRNP-release into the host cell cytoplasm. Additionally, new virion assembly and capsid formation, as well as stabilization of the virus structure is mediated also by the M-protein subunits M1 and M2, respectively. The cell surface proteins HA and NA are important for virus attachment, entry and virion release. NS1, not part of the virion structure, is mainly important to fight against antiviral host immune responses upon IAV infection.

Each viral RNA (vRNA) coding for the respective proteins is assembled to NP-proteins, as well as a heterotrimeric RNA dependent RNA Polymerase (RdRp)-complex consisting of PB1, PB2 and PA, making up one out of eight viral ribonucleoproteins (vRNPs) (Fig. 4) (Eisfeld et al. 2014). HA, NA and M2 are transmembrane proteins embedded in the lipid envelope of the virion (Fig. 4) (Chlanda and Zimmerberg 2016). HA is essential for binding of the viral particle to the appropriate receptors on the host cell surface, thereby initiating virus-cell fusion and entry (Böttcher-Friebertshäuser et al. 2014). Avian IAVs prefer binding to α2,3 sialic acid receptors through HA to mediate these fusion processes (Dou et al. 2018). However, it was also demonstrated that some avian IAVs can also use the α2,6 sialic acid receptor for viral entry, which is normally preferred by mammalian IAVs (Walther et al. 2013; Dou et al. 2018; Xu et al. 2022). The virus can afterwards be taken up by the host cell for example via clathrin-dependent endocytosis (Sieczkarski and Whittaker 2002). The virus subsequently is trafficked to the endosome, which is characterized by a low pH enabling the activation of the proton channel activity of the M2-subunit, as well as the release of the vRNPs from its interaction with M1 (Manzoor et al. 2017; Dou et al. 2018). Acidification of the virion interior by M2 finally leads to the exposure of the HA-fusion peptide, following its insertion into the endosomal membrane, thereby enabling vRNP release into the cytoplasm (Manzoor et al. 2017). Simultaneously, the mission of the NS1 relies in counteracting the antiviral responses of the host by modulating its immune response against IAV infection (Gao et al. 2012; Feng et al. 2017; Sha et al. 2020). Each vRNP contains a nuclear import signal peptide, which enables their transport into the nucleus of the host cell after entry (Samji 2009). Transcription of viral genes is subsequently initiated by the viral RdRp-complex in the nucleus (Stubbs and te Velthuis 2014). The resulting mRNA products still connected to RdRp-complex are finally exported from the nucleus through an interaction between NP, NEP and M1 with the cellular Chromosomal Region Maintenance 1 (CRM1) protein, allowing viral protein translation in the cytoplasm (Elton et al. 2001; Akarsu et al. 2003; Eisfeld et al. 2014). In addition to mRNA transcription, the negative sense vRNA is further transcribed into complementary RNA of positive polarity, allowing the production of new negative sense vRNAs (York et al. 2013).

Freshly translated NP, PA, PB1 and PB2 are first transported back into the nucleus to form vRNPs with newly synthesized vRNA, while translated HA, NA and M are transported to the apical site of the plasma membrane (Dou et al. 2018). Here, assembly and capsid formation are mediated by the viral M1-protein subunits initiating a helical layer arrangement, while simultaneously interacting with the lipid envelope and the mRNA (Noton et al. 2007). Accordingly, the M2-protein functions as a proton-channel, thereby allowing lowering of the interior virion pH, which prevents dissociation of vRNPs from M1 (Pinto and Lamb 2006). Importantly, virus assembly is strongly dependent on particular packaging signals that may differ between specific IAV subtypes and thus determine the reassortment potential (Gerber et al. 2014). Although there are some publications assigning NA a role in the host cell entry processes (Matrosovich et al. 2004; Cohen et al. 2013; Vries et al. 2019), the main function of NA from avian IAVs relies in progeny virion release from the infected host cell. In this process, the NA-protein of avian IAVs mediates catalytical cleavage of host cell sialic acid residues connected to the viral HA-glycoprotein on the progenitor virion surface, thereby allowing budding of new viral particles (Palese et al. 1974; McAuley et al. 2019). All different avian IAV-subtypes further divide up into low pathogenic (LP) and highly pathogenic (HP) IAVs, albeit it is noteworthy that only the subtypes H5 and H7 occur as an HP-phenotype (WOAH 2021; Shi et al. 2023) The LP- or HP-phenotype is generally determined by an intravenous pathogenicity index (IVPI), which involves monitoring of disease and mortality in 4 to 6 week-old chickens after intravenously injecting a specific virus titer. If the IVPI becomes >1.2, the respective IAV subtype has to be classified as HP (WOAH 2021). LP-IAVs do not overcome the threshold of >1.2 in an IVPI, which is mainly based on their differential mechanism of proteolytic cleavage of the HA-protein necessary for viral fusion with the target host cell (Horimoto et al. 1994; Steinhauer 1999; Klenk et al. 2008). LP-IAVs are characterized by a monobasic cleavage site motif resulting in only mild infections. HP-IAV viruses possess a polybasic cleavage site that was proven to be an important factor enhancing virulence and mortality of infected chickens or mammals (Table 1) (Rott 1992; Suguitan et al. 2012; WOAH 2021). This difference is based on the fact that the protease responsible for monobasic HA-cleavage in case of LP-IAVs only exists in the respiratory and enteric tract, while the polybasic cleavage site motif of HP-IAVs can be cleaved by a ubiquitous protease (Klenk and Garten 1994).

1.3.3 Bat- and avian IAVs – Functional comparison

Although bat- and avian IAVs do not differ in their segmented genome arrangement, there are marked functionally differences especially between New World bat-, Old World bat- and avian IAVs (Table 1). Firstly, bat H9N2 and conventional IAVs demonstrate compatible packaging sequences that are necessary to produce viable progeny virions (Gerber et al. 2014; Kandeil et al. 2019). In contrast, studies with H17N10 and H18N11 revealed complete diverse packaging sequences between New World bat IAV- and conventional IAV- gene segments except for M (Yang et al. 2017), which thereby drastically decreases the feasibility of reassortment events between New World bat- and conventional IAVs (Table 1) (Zhou et al. 2014). Secondly, H17N10 and H18N11 rely on the expression of major histocompatibility complex class 2 (MHC-II) to initiate host cell infection, although a direct interaction between H17 or H18 with the MHC-II molecule is yet to be discovered (Table 1) (Karakus et al. 2019). Concurrently, it was demonstrated that the NA-protein of H17N10 and H18N11 does not fulfill a neuraminidase function as the NA of avian IAVs (Table 1) (García-Sastre 2012), but rather that N11 absence promotes viral growth in cell culture (Ciminski et al. 2019). Nevertheless, N11 presence is required for efficient transmission in Neotropical Jamaican fruit bats (*Artibeus jamaicensis*), which was demonstrated by *in vivo* studies in bats and ferrets with a selection and growth promotion of viruses with a full-length NA (Ciminski et al. 2019). Contrastingly, Old World bat H9N2 still uses the conventional α2,3 sialic acid pathway to enter the host cell, just as avian IAVs do (Table 1) (Ciminski et al. 2019). In line with this, embryonated chicken eggs are a suitable source to promote bat H9N2 virus replication (Table 1) (Kandeil et al. 2019). However, it was likewise demonstrated that adult white leghorn chickens were not susceptible to infection with bat H9N2 (Table 1) (Kandeil et al. 2019), suggesting that viral adaptation will be a prerequisite to allow bat H9N2 virus replication in these animals. Accordingly, H17N10 and H18N11 also do not support propagation in embryonated chicken eggs and reassortment with conventional IAVs is impossible without further genetic adaptation (Table 1) (Tong et al. 2012; Tong et al. 2013; Juozapaitis et al. 2014; Zhou et al. 2014). Infection of bats with New World bat IAVs normally results in mild to asymptomatic disease progression and ferrets also remain asymptomatic (Ciminski et al. 2019). Since all three bat influenza A viruses do not support replication in chickens, performing an IVPI in chicken of all three bat influenza A viruses without further genetic adaptations is rendered impossible. However, for all three bat IAVs, sequence analysis revealed a monobasic cleavage site, indicative of low pathogenicity of all these viruses (Table 1) (Tong et al. 2012). Nevertheless, information about viral host range and

zoonotic potential of these bat IAVs, especially bat H9N2, is still limited and should be addressed immediately.

Table 1: Characteristic differences between bat- and avian IAVs

Characteristics	Bat H17N10 / H18N11 (New World bat IAVs)	Bat H9N2 (Old World bat IAV)	Avian IAVs
Cell entry receptor protein	MHC-II	α2,3 Sialic acid	Preferably α2,3, but also α2,6 sialic acid
Neuraminidase	Potential downregulation of MHC-II	Release of progeny particle from producing cell	Release of progeny particle from producing cell
Propagation in adult chicken	No	No	Yes
Propagation in embryonated chicken eggs	No	Yes	Yes
Cleavage site	Monobasic	Monobasic	Monobasic or polybasic
Reassortment	Yes, with New World bat IAVs	Potentially yes, with avian IAVs, for mammalian IAVs unknown	Yes, with IAVs of avian or mammalian origin
Clinical symptoms			
Bats	Mild/asymptomatic	*Part of this thesis*	*Part of this thesis*
Birds	Unsusceptible	Adult chickens unsusceptible *Day-old chicks and turkeys are part of this thesis*	Mild to severe disease depending on subtype
Ferrets	Asymptomatic	*Part of this thesis*	Mild to severe disease depending on subtype
Humans	Unknown	Unknown	Mild to severe disease depending on subtype, sporadic pandemic outbreaks

1.3.4 Reassortment as prerequisite for pandemic outbreaks by IAVs

In humans, two subtypes of IAV are causing re-occurring seasonal Influenza disease outbreaks, namely H1N1 and H3N2, although H3N2 replaced the earlier in humans circulating H2N2 IAV strain (Scholtissek et al. 1978; Lindstrom et al. 2004; Zanobini et al. 2022). However, diverse subtypes of IAVs, including H5N1, H6N1, H7N7, H7N9, or H9N2 have occasionally accomplished spillover infections from reservoir hosts to humans with different patterns of pathogenicity, transmissive fitness and virulence (Scholtissek et al. 1978; Guan et al. 2002; Lindstrom et al. 2004; Wei et al. 2013; Puzelli et al. 2014; Almayahi et al. 2020; Liu et al. 2021b; Zanobini et al. 2022). In general, many of these IAV strains emerged in specific reservoir hosts, mainly swine and diverse bird species (Nelson and Worobey 2018). Pigs, but also turkeys, quails and humans harbor not only α2,3, but also α2,6 sialic acid receptors in their respiratory tract (Kuchipudi et al. 2021), thereby serving as potential "mixing vessel" for reassortment events between human and avian IAVs (Hennig et al. 2022). The reassortment processes between these IAVs of different species origin may facilitate adaptation to a distinct and new host population, in turn leading to cross-species spillover infections. Several pandemic outbreaks in the 20th or 21st century have been associated with spillover events of IAVs and concomitant reassortment (Dawood et al. 2012). A popular example is represented by the so-called "Spanish flu", which emerged during World War I in 1918 based on a spillover infection of an IAV of subtype H1N1 with avian origin (Taubenberger 2006), consequently resulting in approximately 50 million fatal cases (Taubenberger and Morens 2006). Interestingly, the amino acid sequences of the 1918 pandemic H1N1 IAV internal proteins (PB1, PB2, PA, NS1, NP and M) demonstrate high similarities to modern avian IAVs (Reid et al. 2004; Worobey et al. 2014). These observations support the assumption that the origin of this virus relies in wild waterfowl (Reid et al. 2004; Nelson and Worobey 2018; Taubenberger and Morens 2020). Although the swine is questioned to be a potential intermediate host for the transmission of the 1918 pandemic H1N1 virus from birds finally to humans, this virus was only detected in swine for the first time in 1919 and became enzootic afterwards (Walia et al. 2019; Taubenberger and Morens 2020). Therefore, it is rather unlikely that the pandemic H1N1 had circulated for a longer period of time in for example the pig as intermediate host before finally accomplishing the spillover to humans (Reid et al. 2004; Nelson and Worobey 2018). Another example for a noteworthy pandemic outbreak encompasses the Asian flu from 1957, with the H2N2 IAV strain of avian origin as causative agent (Jones et al. 2014). This virus likely originated in wild ducks and finally underwent reassortment processes with a human IAV, consequently able to induce a successful spillover event to humans (Kawaoka et al. 1989; Joseph et al. 2014). The

pandemic outbreak of the Asian flu globally resulted in around 1 million deaths (Viboud et al. 2016). In the following, the 1968-1970 "Hong Kong flu" pandemic emerged as a reassortant with a newly acquired avian H3 and the N2 of the H2N2 Asian flu from 1957 (Kawaoka et al. 1989; Chauhan and Gordon 2022). This virus had great transmissive potential comparable to the 1918 H1N1 pandemic IAV strain, but the disease severity was considerably less (Jester et al. 2020; Piret and Boivin 2020; Jinjarak et al. 2021). After the pandemic, the H3N2 virus has acquired many antigenic changes in the HA, which likely provided immune evasive fitness and thereby facilitated its development in a concerning seasonal IAV strain (Jester et al. 2020).

The most recent pandemic outbreak of an influenza virus strain is backdated to the 2009 pandemic swine H1N1 IAV (H1N1pdm09) (Smith et al. 2009). It was proven that the virus, which was eventually able to succeed with a spillover infection to humans, derived from reassortment processes of multiple IAV lineages of avian, swine and human origin with the swine as a common reservoir host, as "mixing vessel" (Smith et al. 2009). Estimations of human deaths associated with H1N1pdm09 by the CDC add up to nearly 300.000 during the pandemic wave in 2009, but the virus still circulates as a seasonal strain and contributed to an estimate of 25.000 deaths in the United States alone during the Influenza season 2019-2020 (Dawood et al. 2012; CDC 2022). Importantly, recurrent spillback from humans to pigs on the basis of H1N1 has led to the appearance of multiple reassortants with unknown consequences for their viral host range and transmissibility or virulence (Henritzi et al. 2020).

These examples prove that IAVs that are able to cross the species barrier to humans circulate in multiple different reservoir host populations and pose a constant threat to the human population due to their major reassortment potential.

As mentioned earlier, reassortment processes of New World bat IAVs with conventional IAVs could not be proven without further genetic modifications to date (Juozapaitis et al. 2014). Nevertheless, the bat H9N2 gene segment packaging sequences are compliant with that of conventional IAVs and could therefore enable reassortment with conventional IAVs, although evidence for this is still lacking (Table 1) (Gerber et al. 2014; Kandeil et al. 2019). At this point, it is worth highlighting again that the bat H9N2 virus originates from a mammalian species, which enables and drastically facilitates the adaptation to diverse mammalian species and therefore also humans. Therefore, a deep characterization of emerging and newly discovered IAVs with zoonotic potential, especially bat H9N2, is needed to enhance the pandemic preparedness.

1.4   Bats as reservoir for coronaviruses

Apart from influenza A and other zoonotic viruses originating from bats, a wide variety of CoVs can be found in bat species. According to the database of bat-associated viruses (DBatVir), nearly 5000 coronaviruses have been discovered in bats to date (Chen et al. 2014; Ruiz-Aravena et al. 2022). Among these, human pathogenic coronaviruses solely belong to the taxonomic genera alpha- and betacoronaviruses (Su et al. 2016; Schoeman et al. 2022). So far, human coronavirus (HCoV)-OC43, NL63, HKU1 and 229E have been linked to the induction of mostly mild common colds in humans (Su et al. 2016; Ye et al. 2020). However, three viral species have been linked to cause severe respiratory infections in humans, including SARS-CoV and MERS-CoV, along with the recently discovered SARS-CoV-2 and are therefore considered as high-impact coronaviruses (Peiris et al. 2003; Zaki et al. 2012; Zhu et al. 2020). As already described earlier, bats frequently come in contact with humans through anthropogenic factors favoring the animal-to-human interface, thereby facilitating spillover events between bats, humans and also intermediate hosts (Centeno-Cuadros et al. 2017; Kamins et al. 2011).

1.4.1 Pandemic outbreaks associated with coronaviruses

Numerous coronaviruses are concerning zoonotic viruses and have been associated with epidemic or pandemic outbreaks in the past. MERS-CoV caused a disease outbreak first reported in Saudi Arabia in 2012 (Zaki et al. 2012). Symptoms of MERS-CoV infections range from human common colds to severe pneumonia and multiple organ failure that may result in fatal cases (Zaki et al. 2012). To date, over 2500 cases including over 900 deaths have been reported and still, infections are registered regularly (WHO 2022). MERS is believed to originate from bats, albeit transmission to humans is mediated by dromedary camels where the virus is circulating (Memish et al. 2013; Munster et al. 2016; Chu et al. 2014; Shalhoub and Omrani 2016).

Another concerning epidemic outbreak attributed to coronaviruses includes the SARS-CoV-related epidemic in 2002/2003 with over 8000 confirmed human infections including nearly 800 deaths (WHO 2015). As mentioned in the beginning, the origin of the SARS-CoV epidemic is hypothesized to have involved an intermediate host as a bridge for the spillover from bats to humans (Cui et al. 2019). In detail, SARS-CoV presence could be confirmed in 91 palm civets and 15 racoon dogs traded at an animal market in China, although the virus could not be detected in over a 1000 palm civets sampled in further 12 provinces around this market (Tu et al. 2004; Kan et al. 2005). This suggested that the spillover to palm civets and raccoon dogs

likely occurred through another animal exactly at this market. Furthermore, closely related SARS-CoV-like coronaviruses had been detected at the same time in horseshoe bats, and further studies discovered multiple SARS-CoV-related viruses that markedly differ in their Spike (S), open-reading-frame 3 (ORF3) and ORF8 sequence information (Lau et al. 2005; Li et al. 2005; Hu et al. 2017). These discoveries suggested that recombination of multiple SARS-CoV-related viruses might have occurred in horseshoe bats to finally result in the progenitor of SARS-CoV (Hu et al. 2017). Interestingly, the genomic sequences of SARS-CoV from humans and civets are nearly identical except for the S and ORF8, which indicates that there has been ongoing adaptation of SARS-CoV during the 2002-2003 epidemic (Song et al. 2005; Cui et al. 2019). Therefore, it is conceivable that SARS-CoV arose through recombination of multiple SARS-CoV-like viruses in horseshoe bats, which in turn transmitted the virus to palm civets or raccoon dogs that finally might have accomplished SARS-CoV spillover infection to humans by serving as intermediate host.

Lastly, the SARS-CoV-2 pandemic was initiated by a spillover infection of the zoonotic SARS-CoV-2 from a currently unknown source (Zhu et al. 2020). However, recent evidence suggests the Huanan Seafood Wholesale market as a striking epicenter for the first SARS-CoV-2 outbreak (Worobey et al. 2022). This is because the virus was first isolated and sequenced from a sample of a patient from Wuhan (China) who was hospitalized with severe pneumonia in December 2019 (ISIDProMed 2019). Later on, it was proven that most of the early infected patients have visited the "Huanan Seafood Wholesale Market" in Wuhan (Worobey et al. 2022). From this epicenter, the virus rapidly spread over the whole globe and revealed severe disease progression especially in elderly persons and people with co-morbidities (Bonanad et al. 2020; Gao et al. 2020). Additionally, among all coronavirus disease 2019 (COVID-19) survivors, some faced more or less severe Long-COVID symptoms ranging from small fatigue to neuropathological signs (Groff et al. 2021). Moreover, genetic similarities between SARS-CoV-2 and a related coronavirus originating from a *Rhinopholus* bat species highly suggest a bat origin also of SARS-CoV-2 (Zhou et al. 2020). Additionally, pangolin-originated coronaviruses also show high genetic sequence similarities to SARS-CoV-2, which complicates the answer of the true animal reservoir of SARS-CoV-2 (Xiao et al. 2020). Nevertheless, multiple factors underpin the hypothesis of an intermediate host playing an important role in transmission of SARS-CoV-2 from reservoir bats to the human host. Since the beginning of the first outbreak, the coronavirus disease 2019 (COVID-19) induced by SARS-CoV-2 accounts for over 700 million confirmed human infections including nearly 7 million SARS-CoV-2-associated deaths (WHO as of 24th March 2023).

Listing all these diverse disease-related pandemic and epidemic outbreaks along with the high numbers of severe illnesses and fatal cases highlight the importance of a detailed surveillance and of a deep characterization of emerging zoonotic pathogens in addition to SARS-CoV-2 in terms of virulence, pathogenicity, transmission efficiency, immune escape and viral host range.

1.4.2 SARS-CoV-2 life cycle and proteins functions

SARS-CoV-2 is a spherical, enveloped betacoronavirus belonging to the *Coronaviridae* family, order *Nidovirales*, and has a single-stranded RNA genome of positive polarity (Rota et al. 2003; Zaki et al. 2012; Zhu et al. 2020). The spike gene of the virus shares around 76% genetic sequence identity with SARS-CoV, a related betacoronavirus that already accomplished spillover infections to humans and was responsible for the 2002-2003 SARS-CoV epidemic (Cherry 2004; Wu et al. 2020). The SARS-CoV-2 genome comprises nearly 30 kB distributed in 10 open reading frames (ORFs) (Wang et al. 2020b). Just as SARS-CoV, the genome of SARS-CoV-2 is encoding four structural proteins, Spike (S), Envelope (E), Membrane (M) and Nucleocapsid (N), as well as eight further accessor-proteins (Fig. 5) (Wang et al. 2020b). The virion envelope is strewn with S-proteins, necessary for host cell attachment and entry (Fig. 5) (Huang et al. 2020).
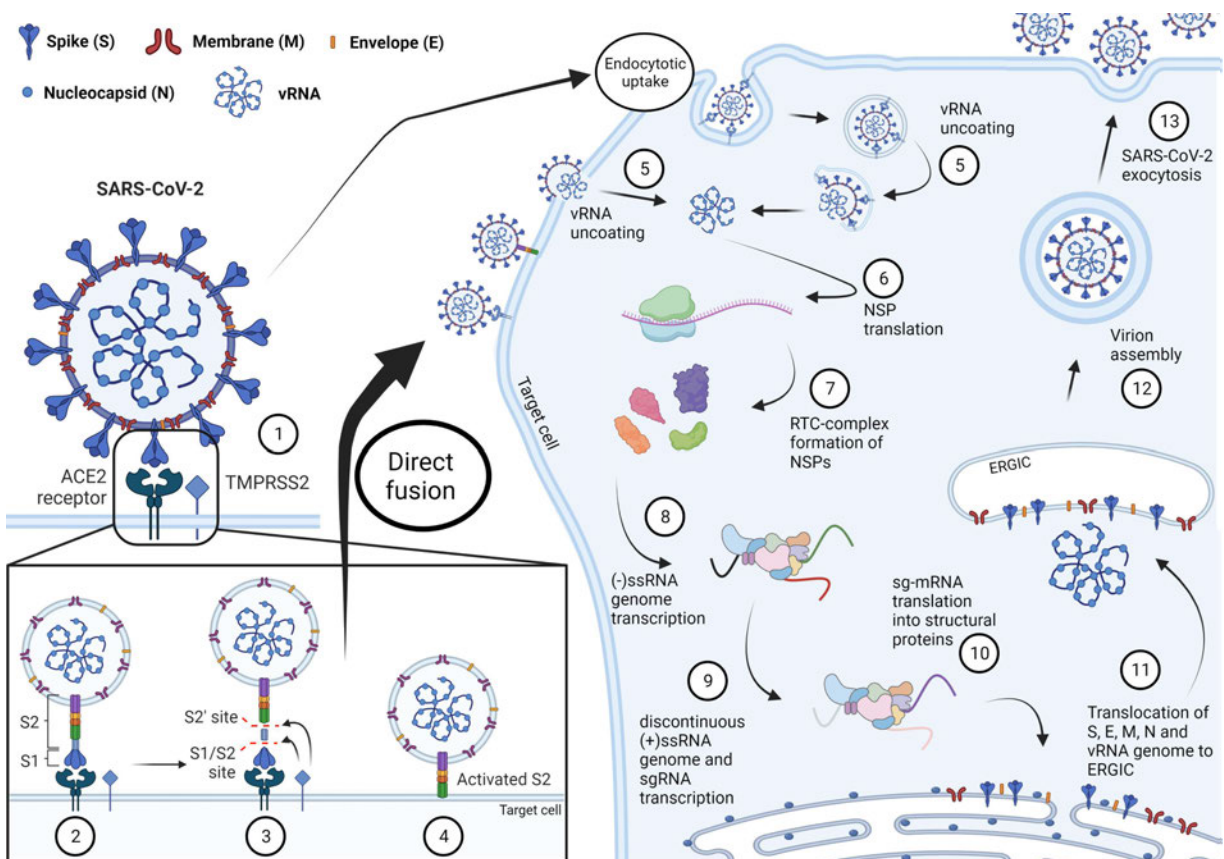
Figure 5: Viral entry of SARS-CoV-2

SARS-CoV-2 encodes the structural proteins S, M, E and N and encapsidates its viral RNA (vRNA) (Wang et al. 2020a; Wang et al. 2020b). 1/2) Entry via direct fusion is mediated by binding of S to the host-cell resident receptor ACE2 (Huang et al. 2020). 3) Proteolytic cleavage by TMPRSS2 leads to a conformational change of S (Hoffmann et al. 2020) and finally leads to 4) the insertion of the fusion peptide of S into the target membrane (Jackson et al. 2022), in turn developing a fusion pore to 5) finally release of the vRNA into the cytoplasm (Jackson et al. 2022). Viral entry can also be established through an endocytotic uptake involving clathrin. In turn, endosomes incorporating virions get acidified, leading to S-protein activation through cathepsins that eventually cause vRNA release into the cytoplasm (Jackson et al. 2022). 6) Non-structural protein (NSP) translation is initiated by host ribosomes, 7) resulting in 16 NSPs forming the replication-transcription-complex (RTC) (Malone et al. 2022) essential to 8) perform transcription of the SARS-CoV-2 negative sense (-)ssRNA genome (Schubert et al. 2020). 9) The resulting (-)ssRNA genome can finally serve as template for discontinuous transcription to generate the whole (+)ssRNA genome of SARS-CoV-2 or the structural proteins (Sola et al. 2015; Parker et al. 2021) that 10) in turn get translated in the cytoplasm and finally get transported to the ER for further post-translational modifications (Cortese et al. 2020). 11) Translocation of the structural proteins and vRNA-genome to the endoplasmic reticulum-Golgi intermediate compartement (ERGIC) initiates 12) virion assembly (Liao et al. 2006) and the viral particle lastly is released from the host cell by 13) exocytosis or lysosomal traffic (Ghosh et al. 2020; Di Chen et al. 2021). Created with Biorender.

The trimeric S-protein consists of an intracellular C-terminal domain (CTD), a transmembrane domain (TMD) and an extracellular N-terminal domain (NTD) (Fig. 5) (Wang et al. 2020a). During host cell entry via the dominant direct fusion pathway, the receptor binding domain (RBD) in the S1 subunit of the SARS-CoV-2 S protein binds to the angiotensin converting enzyme 2 (ACE2)-receptor on the host cell (Fig. 5.2) (Yan et al. 2020). In contrast to SARS-CoV, SARS-CoV-2 is comprised of a polybasic furin cleavage site (FCS)-motif within the S-protein, which allows priming of S for viral fusion by the cellular transmembrane serine protease type II (TMPRSS2) (Fig. 5.3) (Bertram et al. 2013; Hoffmann et al. 2020). Interestingly, *in vitro* passaging of SARS-CoV-2 on VeroE6 cells leads to loss of the FCS, and following *in vivo* studies demonstrated that this loss results in attenuated pathogenicity and transmission efficacy of this virus (Davidson et al. 2020; Johnson et al. 2021; Peacock et al. 2021). These observations highly suggest an important role for FCS-presence in the SARS-CoV-2 S-protein necessary for spread and disease severity of this virus. TMPRSS2 proteolytically cleaves the S1-subunit from the S2-subunit (Fig. 5.3), thereby allowing exposure and insertion of the S2-subunit-associated fusion peptide into the cellular membrane (Fig. 5.4), which allows uncoating of the vRNA through a developing fusion pore between the viral and host cell membrane into the cytoplasm (Fig. 5.5) (Jackson et al. 2022). Another possible mechanism of SARS-CoV-2 cell entry relies in classical clathrin-mediated endocytosis (Fig. 5) (Jackson et al. 2022). In this case, the acidification of the virus incorporating endosomes induces S-protein activation through cathepsins, finally enabling the release of the vRNA into

the cytoplasm (Fig. 5) (Bayati et al. 2021; Jackson et al. 2022; Mao et al. 2022). Subsequent to vRNA uncoating, replication of ORF1a and ORF1b is initiated by utilizing host ribosomes, resulting in the production of replicase polyprotein pp1a and pp1ab (Fig. 5.6) (Malone et al. 2022). The resulting 16 NSPs are crucial to downregulate host mRNA transcription processes, whereas the remaining NSPs assemble in so called replication-transcription complexes (RTCs) that mediate the production of new vRNA (Fig. 5.7) (Schubert et al. 2020). This complex incorporates an RdRp, as well as other NSPs necessary to construct so called replication organelles (ROs) by exploiting cellular ER-membrane components (Snijder et al. 2020). ROs are therefore hypothesized to provide a defined location for structured replication processes of CoVs in general (Snijder et al. 2020). Transcription of SARS-CoV-2 gRNA leads to an antisense RNA of negative polarity, which can either serve as template for new SARS-CoV-2 full-length (+)gRNA replication or as a template for discontinuous transcription (Fig. 5.8) (Sola et al. 2015). This discontinuous transcription, a hallmark of coronaviruses, allows the production of new, positive-sense subgenomic mRNAs (sg-mRNAs) that code for the structural proteins S, M, E and N of SARS-CoV-2 (Fig. 5.9) (Parker et al. 2021). After cytosolic translation of the structural proteins, the proteins are allocated to the ER by specific signal sequences for ER-orientated traffic (Fig. 5.10) (Yadav et al. 2021). Further post-translational modifications enable viral protein maturation, which can finally assemble into new virions at the endoplasmic reticulum-Golgi intermediate compartment (ERGIC) (Fig. 5.11) (Cortese et al. 2020). In this assembly process (Fig. 5.12), N mainly condenses the viral genome, while E may act as a viroporin (Liao et al. 2006). Furthermore, the M-protein serves as interaction partner for N, E and S, thereby facilitating incorporation of all proteins in a new viral particle (Neuman et al. 2010). Besides translation of structural proteins, there are numerous other ORFs coding for accessory proteins that are not essential for virus production, but are hypothesized to have an important assistant role in host immune evasion processes (Redondo et al. 2021). Virus budding of SARS-CoV-2 is not fully elucidated yet, although there is evidence for either an exocytotic or lysosomal trafficking pathway (Fig. 5.13) (Ghosh et al. 2020; Di Chen et al. 2021).
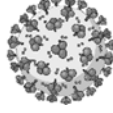
1.4.3 Evolution of the SARS-CoV-2 pandemic

The host cell-resident entry mediator ACE2, which is highly conserved among mammalian species (Damas et al. 2020), enables SARS-CoV-2 infection in multiple mammalian host species and may also have contributed to the spillover of SARS-CoV-2 to humans (MacLean et al. 2021; Michelitsch et al. 2021). The ability of a highly efficient interhuman transmission

finally enabled the pandemic situation by countless virus transfers from person to person mainly via an aerosol-based transmission route (Phan et al. 2020; Wang et al. 2021). Efficient transmission is a prerequisite for virus adaptation (Simmonds et al. 2019), as the virus develops new quasi-species in its infected contact host resulting also in amino acid sequence mutations, which might lead to a charge or conformational change of the respective residues (Yang et al. 2021a). In turn, this can provoke either a replication, transmission or immune escape advantage of the new quasi-species over the previous virus strain (Frost et a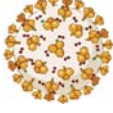l. 2018). Consequently, this evolved virus variant gets predominantly transmitted to further contacts. Among billions of SARS-CoV-2 interhuman transmission events, the ancestral SARS-CoV-2 virus isolated in Wuhan (Wu-1) has rapidly evolved by acquiring fitness-providing amino acid substitutions, insertions or deletions over time. The first identified high-impact mutation within the SARS-CoV-2 pandemic period relies in a single amino acid substitution from aspartic acid to glycine at position 614 in the S-protein (mutation D614G) (Korber et al. 2020). In the following, multiple research groups gave experimental evidence of a replicative and transmissive fitness advantage of this new variant over the ancestral SARS-CoV-2 D614 strain *in vitro*, *ex vivo* and *in vivo* (Hou et al. 2020; Korber et al. 2020; Zhou et al. 2021). Identification of virus variants in infected patients by high-throughput sequencing methods allowed the determination of specific variant frequencies in the human population, which evidenced that the D614G variant rapidly prevailed over its ancestor over the globe and is now globally approved as WT SARS-CoV-2 (Korber et al. 2020). Afterwards, diverse SARS-CoV-2 variants have emerged with multiple mutations especially in the S-protein (Aleem et al. 2022), among which several have initially been classified as "Variant of Concern (VOC)" by the WHO (WHO as of 1st december 2022), such as Alpha (also known as B.1.1.7), Beta (also known as B.1.351), Gamma (also known as P.1), Delta (also known as B.1.617) and Omicron (also known as B.1.1.529) (See Table 2 for references). As of March 2023, the WHO classified the Alpha, Beta, Gamma, Delta and the parental Omicron lineage B.1.1.529 as previously circulating VOCs (WHO 2023). These VOCs have characteristic amino acid mutation profiles that lead to variant competitions during simultaneous host infection (Somerville et al. 2021; Aleem et al. 2022). More precisely, fitness advantages in terms of immune escape, replication and/or transmission finally decide which VOC gets preferentially transmitted to contacts (Zhou et al. 2021; Liu et al. 2022b). As a result, the global population has been facing diverse and consecutive variant waves over time until today (See Table 2). In line with that, several breakthrough infections have already been confirmed with a variety of VOCs that have emerged throughout the pandemic, in principal proving that individuals can be infected multiple times with this virus and its respective variants

(Kroidl et al. 2021; Rovida et al. 2021; Duerr et al. 2022; Tan et al. 2023). Alpha VOC, containing 17 non-synonymous mutations, has been the first major VOC that rapidly predominated over WT SARS-CoV-2 during a time of no available COVID-19 vaccines or counteracting treatments and an immunologically naïve population (Table 2) (Washington et al. 2021). Beta and Gamma were among the first variants identified harboring diverse immune escape-promoting mutations and were detected in multiple countries over the globe (Table 2) (Fujino et al. 2021; Tegally et al. 2021; Andeweg et al. 2022). As more and more people became convalescent and the first commercially available vaccines against SARS-CoV-2 developed by various pharmaceutical companies were licensed (GOV.UK 2020), the Delta variant with increased transmissibility and an additional immune escape potential has become predominant in early 2021 (Table 2) (Cherian et al. 2021). Finally, in late 2021, the VOC Omicron BA.1 has been detected in multiple countries over the globe displaying in total 50 amino acid mutations in its whole genome, with 39 in its S-protein alone (Jung et al. 2022). Originating from this VOC, several different sub-lineages with unique mutations developed, of which the sub-lineages Omicron BA.2, BA.4/5 and BQ.1.1 have predominated in short sequential time frames lately in 2022 (Scarpa et al. 2022; Wang et al. 2022b). Although there are still many open questions on which mutations exactly were crucial for VOC Omicron dominance, there is large experimental evidence that neutralizing antibodies from vaccinated or convalescent individuals only insufficiently eliminate the virus, thereby enabling global breakthrough infections (Hachmann et al. 2022; Wang et al. 2022c). Nevertheless, several *in vivo* experiments also demonstrated that VOC Omicron and its subvariants are less pathogenic than its progenitor variants (Uraki et al. 2022; Yuan et al. 2022). An overview of most important characteristic fitness traits of a variety of SARS-CoV-2 VOCs with appropriate references can be seen in Table 2. Detailed experimental *in vivo* characterization of the distinct variants has therefore always been and still is an important tool to estimate the fitness potential and predict the circulation of future SARS-CoV-2 VOCs in the human population.

Table 2: Major characteristics of SARS-CoV-2 VOCs

| Previous SARS-CoV-2 Variants of Concern (VOCs)							
VOC	**Alpha B.1.1.7**	**Beta B.1.351**	**Gamma P.1**	**Delta B.1.617**	**Omicron BA.1**	**Omicron BA.2**	**Omicron BA.4/5**

Prevalence over time in Germany	

Figure 6: Prevalence of SARS-CoV-2 VOCs in Germany from Jan. 2021 - Nov. 2022
Data source for this graph was the Whole Genome Sequencing Data from the RKI (RKI 2021). Blue: Alpha VOC; green: Beta VOC; grey: Gamma VOC; purple: Delta VOC; saffron: Omicron BA.1 VOC; dark brown: Omicron BA.2 VOC; light brown: Omicron BA.4/5 VOCs. Colors of VOC Alpha, Beta, Delta and Omicron BA.1 are in accordance with the respective VOC-colors used in the publications associated with this dissertation.

First discovered	UK	South Africa	Brazil	India	South Africa	South Africa	South Africa
Date of VOC declaration	Dec. 2020	Dec. 2020	Jan. 2021	May. 2021	Nov. 2021	Nov. 2021	Jan. 2022
Reference	(ECDC as of 2023)						
S-protein mutations	9	9	10	9-11, depends on strain	39	31	35
	(Faria et al. 2021); (Tegally et al. 2021); (Yang et al. 2021b); (Suratekar et al. 2022); (McCallum et al. 2021); (Kumar et al. 2022); (Tegally et al. 2022)						

Key fitness advantages to WT SARS-CoV-2

ACE2-binding	+++	+	++	+	+	++	++
	(Liu et al. 2022a); (Hoffmann et al. 2022); (Cao et al. 2022); (Li et al. 2022b)						
Transmission	+	+	+	++	+++	+++	+++
	(Wang et al. 2022a); (Suzuki et al. 2022); (Tegally et al. 2022)						
Immune escape	o/+	+	++	+	+++	+++	+++
	(Uriu et al. 2021); (Uraki et al. 2023); (Kurhade et al. 2022)						
BNT162b vaccine effectiveness	88%	72%	63%	77,8%	55,9%	Likely lower than BA.1	Likely lower than BA.2
	(Butt et al. 2021); (Esper et al. 2022; Feikin et al. 2023);						

Disease severity	+	+	+	++	--	-	-
	(Singer et al. 2021); (Gram et al. 2022); (Kirsebom et al. 2022); (Møller Kirsebom et al. 2022)						

1.5 Popular animal models for IAV and SARS-CoV-2 research

Although no single animal model is qualified to exactly mimic disease progression and severity, replication or transmission efficiency, as well as pathogenicity of a specific human pathogen yet, the evaluation of pathogen behavior in multiple animal models has been the most powerful tool to estimate the danger arising from a newly discovered pathogen for a long time. Furthermore, *in vivo* characterization of zoonotic pathogens in general leads to a better understanding of emerging viruses, e.g. concerning their zoonotic potential or also the risk of new animal reservoirs. There are multiple different standard animal models that are suitable for specific viruses, depending on the desired conclusions to draw, which include for example general virus characterization or vaccine development (Fig. 7) (Muñoz-Fontela et al. 2020; Hoffmann et al. 2021; Nguyen et al. 2021; Ran et al. 2022). In the following, the most important standard animal models for IAV and SARS-CoV-2 research will be introduced in more detail.
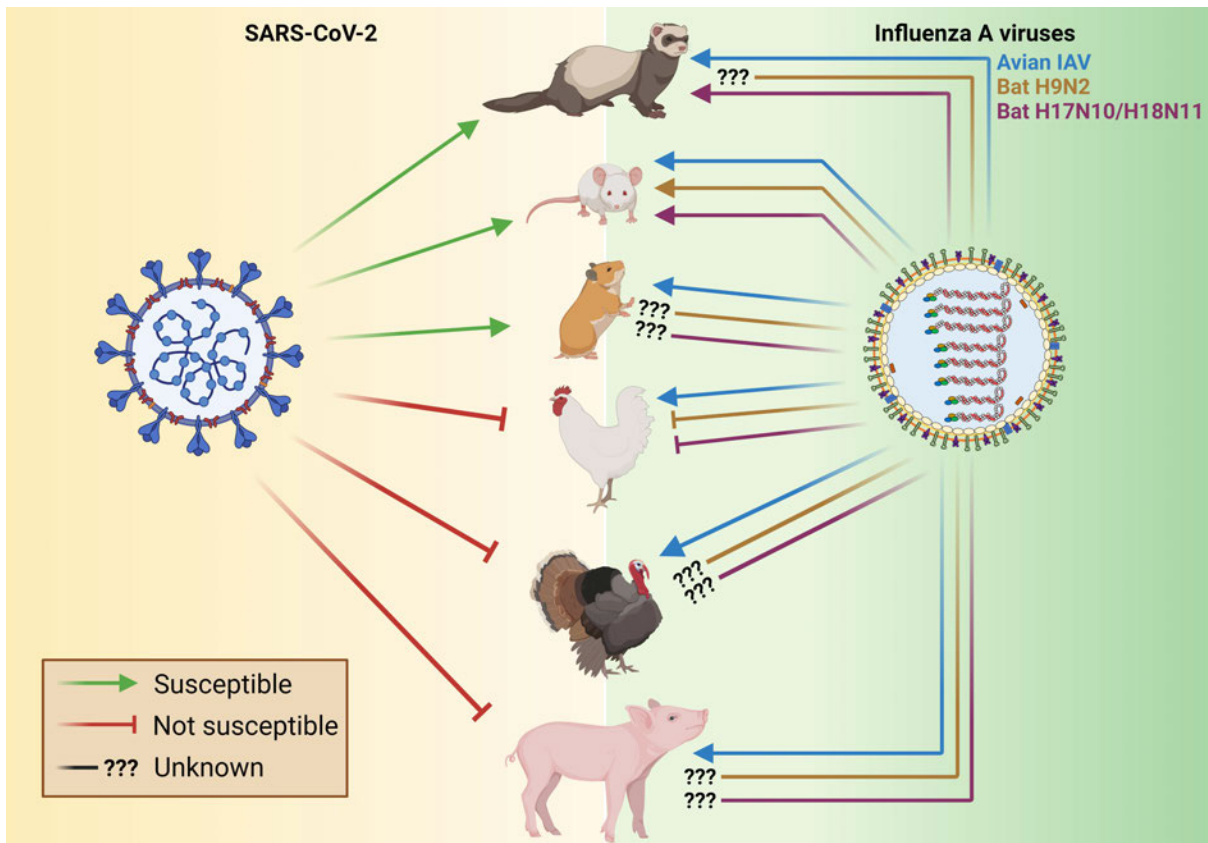
Figure 7: Susceptibility of different experimental animal models for SARS-CoV-2 and avian or bat IAVs

Several animal models reveal specific susceptibilities for either SARS-CoV-2 or the different avian or bat IAVs. SARS-CoV-2 is known to successfully infect ferrets, specific transgenic hACE2-containing mice and Syrian hamsters as standard animal models (Muñoz-Fontela et al. 2020; Michelitsch et al. 2021), but cannot infect diverse bird species or pigs (Schlottau et al. 2020; Berhane et al. 2021). Avian IAVs are able to infect ferrets, genetically unmodified mice, Syrian hamsters, chicken and turkeys, as well as pigs (Iwatsuki-Horimoto et al. 2018; Slomka et al. 2018; Nguyen et al. 2021; Fan et al. 2022). In contrast, the Old World bat H9N2 is not able to infect adult chickens, but C57/Bl6 and BALB/c mice were shown to be susceptible to this virus (Kandeil et al. 2019). If the bat H9N2 also infects Syrian hamsters or pigs is currently unknown, and the evaluation of turkey and ferret susceptibility to this virus is part of this thesis. For the New World bat IAVs H17N10 and H18N11, it is known that they are able to infect ferrets and genetically unmodified C57/Bl6 mice, but chickens are not susceptible to these viruses (Tong et al. 2013; Tong et al. 2012; Juozapaitis et al. 2014; Ciminski et al. 2019). If turkeys, pigs or Syrian hamsters are susceptible to these New World bat IAVs has not been evaluated yet. The figure was created with BioRender.

1.5.2 Ferrets

The lung physiology of the ferret reveals multiple similarities with humans, including the distribution of sialic acid receptors (Belser et al. 2011; Flerlage et al. 2021). Additionally, the pattern of viral attachments (PVAs) for zoonotic IAVs in humans are highly similar to those from especially ferrets and pigs (van Riel et al. 2007; Flerlage et al. 2021). Moreover, immune responses, disease progression, pathogenesis and clinical signs as a consequence of an IAV-

infection are similar in humans and cannot be as prominently observed in the mouse or guinea pig model (Maher and DeStefano 2004; Belser et al. 2018; Belser et al. 2020; Nguyen et al. 2021). Most importantly, the ferret still resembles one of the currently best known animal model for IAV transmission, especially concerning aerosol- and droplet spread-based virus transmission (Richard et al. 2020; Le Sage et al. 2021; Nguyen et al. 2021; Zhang et al. 2022). Ferrets are also a valuable model to study vaccine safety, immunogenicity and effectiveness especially in the case of vaccine development against IAV infection (Schön et al. 2020; Liu et al. 2021a; Stadlbauer et al. 2021; Vidaña et al. 2021). All these advantages and utilities of this famous animal model have even led authorities to include this animal in the "Influenza Risk Assessment Tool (IRAT)" and the "Tool for Influenza Pandemic Risk Assessment (TIPRA)" as a precautionary measure in respect of pandemic preparedness (Cox et al. 2014; WHO 2016; Belser et al. 2018). Importantly, the ferret is also susceptible to New World bat IAVs (Ciminski et al. 2019). Taken together, the ferret is one of the most important and valuable animal models in IAV research, independent from the desired conclusions to draw.

After SARS-CoV-2 emergence, the ferret also rapidly evinced also as a suitable model for this virus mimicking generally mild SARS-CoV-2 infections in humans. More specifically, the virus can be efficiently transmitted among ferrets, but clinical signs are rather absent and replication is restricted to the upper respiratory tract (URT) (Schlottau et al. 2020; Berhane et al. 2021; Zhou et al. 2021). In some preclinical studies, ferrets are also considered a valuable model for SARS-CoV-2 vaccine development (An et al. 2021; Li et al. 2021; Boley et al. 2023). Conclusively, the ferret represents a highly valuable model for IAV and SARS-CoV-2 research in all different questions of translational research, which range from general virus characterization to specific vaccine development. On the other side, the available immunological tools are limited for the ferret, and handling of the animals requires respective training of the animal caretakers and researchers. This is especially important when working under high biosecurity levels (Pickering et al. 2019; Wong et al. 2019; Nguyen et al. 2021).

1.5.1 Laboratory mice

For basic research and also pre-clinical studies, C57/Bl6 and BALB/c are commonly used as laboratory mice models (Zhu et al. 2013; Bleul et al. 2020; Magaña-Guerrero et al. 2020; Li et al. 2022a). A well examined immune system, as well as fully available genome sequences and great potential of genetic modification in these animals (e.g. gene knock-out) are the main criteria of mouse model popularity in research (Rosenthal and Brown 2007). In many cases of experimental IAV-infection of mouse models, the animals develop severe clinical signs that

may even lead to fatalities (Margine and Krammer 2014; Gunther et al. 2021; Okda et al. 2021). It was also shown that C57/Bl6 mice are susceptible to H18N11, and C57/Bl6 as well as BALB/c mice are susceptible to bat H9N2 (Ciminski et al. 2019; Kandeil et al. 2019) Transgenic C57/Bl6 mice expressing the human myxovirus resistance protein 1 (MxA) were demonstrated to exhibit remarkably lower clinical signs and disease progression of a variety of diseases, including IAV infections (Hefti et al. 1999; Haller and Kochs 2020). Interestingly, researchers suggest that MxA is a major restriction factor for IAVs and that these viruses have to escape from MxA to establish a seasonal IAV strain circulating in the global population (Dittmann et al. 2008; Götz et al. 2016; Deeg et al. 2017). Therefore, identifying an MxA escape by experimentally using transgenic MxA mice is rendered an important step to unravel potential pre-pandemic IAV strains.

For SARS-CoV-2 research, especially genetically modified, transgenic K18-hACE2-mice, which express - in addition to their murine ACE2 (mACE2) receptor - the human ACE2-receptor under the keratin 18 promotor, and transgenic hACE2-knock-in (hACE2-KI) mice (expressing hACE2 instead of the mouse homolog mACE2) are used, since both models are highly susceptible to SARS-CoV-2 infection (Dong et al. 2022; Winkler et al. 2022). Importantly, the very early SARS-CoV-2 variants are not able to efficiently use the murine ACE2 (mACE2) protein as cellular receptor and therefore research makes use of genetically modified mice or mouse-adapted SARS-CoV-2 virus strains (Zhou et al. 2020; Ren et al. 2021; Sun et al. 2021). However, SARS-CoV-2 infection in K18-hACE2 mice can exhibit severe clinical signs by artificial neuroinvasion, since the hACE2 receptor here is ubiquitously expressed including the brain (Chan et al. 2022; Fumagalli et al. 2022). This is not the case for the hACE2-KI mice, as the mACE2 receptor in these animals is exchanged by the hACE2-receptor (Winkler et al. 2022).

Taken together, the mouse model still is a highly valuable animal model for IAV and also SARS-CoV-2 research, which is mainly based on and facilitated by the availability of several genetically modified mice strains.

1.5.4 Syrian hamster

The Golden Syrian hamster is generally susceptible to IAV-infection, but still is not the most favorite animal model for this virus type (Fan et al. 2022). However, the Syrian hamster may become a more relevant model for IAV infections in the future, since researchers showed that an H3N2 virus was able to successfully infect Syrian hamsters, but not mice (Iwatsuki-Horimoto et al. 2018). For bat IAVs, it is currently unknown if these animals are susceptible to

these viruses. All in all, the Syrian hamster could represent a good model for specific IAV strains in the future and it shows the dynamics of the development of *in vivo* research following the adaptive potential of novel virus strains.

In contrast, SARS-CoV-2 infection of Syrian hamsters, especially with WT SARS-CoV-2 and the early variants Alpha, Beta and Delta, results in severe disease with striking pneumonia that may even lead to fatal cases (Muñoz-Fontela et al. 2020; Tostanoski et al. 2020; Yuan et al. 2022). SARS-CoV-2 infection of Syrian hamsters moreover efficiently enables viral replication and transmission of all known SARS-CoV-2 variants and is therefore one of the most suitable used animals in SARS-CoV-2 research (O'Donnell et al. 2021; Yuan et al. 2022). This model is also becoming more and more relevant in respect of vaccine development, as there are already many research groups performing preclinical trials with all different kinds of vaccine prototypes in Syrian hamsters (Trimpert et al. 2021; Maruggi et al. 2022; Roth et al. 2023).

1.5.3 Poultry

Experimental inoculation of turkeys and chicks with SARS-CoV-2 was abortive, which assumes that these animals are not susceptible to SARS-CoV-2 infection (Schlottau et al. 2020; Berhane et al. 2021).

Multiple IAVs have an avian origin with seasonally occurring, sometimes massive wide ranging avian influenza virus (AIV) infections in wild birds and poultry farms (Artois et al. 2018; Adlhoch et al. 2022). Therefore, chicks, turkeys, ducks, but also embryonated chicken eggs (ECEs) are indispensable for IAV research in terms of characterization of emerging IAV-strains (Saito et al. 2009; Slomka et al. 2018). In contrast to the Old World bat H9N2 IAV, the New World bat IAVs do not even replicate in embryonated chicken eggs (Tong et al. 2012; Tong et al. 2013; Kandeil et al. 2019).

1.5.3.1   **Embryonated chicken eggs**

Since a long time, embryonated chicken eggs serve as highly suitable platform for avian IAV or bat H9N2 replication and is therefore a useful method for virus propagation in the lab (Burnet and Bull 1943). This method is considered to be the gold-standard method in influenza A virus detection and isolate generation, although being time-intensive with an inconvenient protocol (WOAH 2022). Moreover, *in ovo* inoculation and passaging experiments with several IAV strains have facilitated and augmented the understanding of how and why HPAIVs develop from LPAIV precursory strains (Laleye and Abolnik 2020; Seekings et al. 2020).

1.5.3.2   Chicken, turkeys and ducks

In recent years, European countries were affected by the strongest epizootic HPAIV outbreaks in known history not only in wild or captive birds, but also poultry farms (King et al. 2022; Pohlmann et al. 2022). In case of poultry farms, especially farms keeping layer chicken and turkeys have been identified as an HPAIV outbreak location (King et al. 2022). Chicken and turkeys that become infected with an HPAIV strain, such as H5N1, will lead to fatal cases in the short time frame of a few days, while infection with LPAIVs results in usually marginal clinical signs (Morales et al. 2009; Aldous et al. 2010). Concerning bat IAVs, it is known that the bat H9N2 is not able to infect adult white leghorn chicks, although efficiently replicating in embryonated chicken eggs (Kandeil et al. 2019). For turkeys and ducks, susceptibility to bat H9N2 or New World bat IAVs has not been investigated yet. Since all HPAIVs develop from LPAIV precursors (Laleye and Abolnik 2020; Seekings et al. 2020), it is important to track AIV occurrence via a detailed PCR-based and also serological surveillance. Apart from the surveillance, chicks, turkeys and ducks are also valuable animal models for experimental infections *in vivo*, for example to determine the IVPI or the intramuscular pathogenicity index (IMPI) of specific IAVs (Grund et al. 2018). Importantly, for a wide variety of IAV strains, ducks do not exhibit clinical signs as a consequence of IAV infection despite the detection of substantial viral load in swabs and organ samples during the acute phase of infection (Kim et al. 2009; Grund et al. 2018; Campbell et al. 2021). Due to the absence of symptoms, it is believed that ducks are one of the main reservoir hosts for IAVs massively facilitating the spread of HPAIV among birds, which highlights their importance as research model to study the transmissive capacity of newly discovered IAV strains (Kim et al. 2009; Grund et al. 2018). In contrast, chicks and turkeys develop severe clinical signs upon HPAIV infection including nasal discharge, lethargy and death (Smith et al. 2015; Hemmink et al. 2018; Nguyen et al. 2021; Blaurock et al. 2022). One discussed explanation for the clinical differences between chicks, turkeys and ducks involves their differential immune response upon IAV infection, since chicks and turkeys elicit a much stronger immune response upon IAV infection than ducks do (Powell et al. 2009; Smith et al. 2015; Pantin-Jackwood et al. 2017; Blaurock et al. 2022). Chicks, turkeys and ducks thus represent important animal models for IAV research, with the advantage of minimal cost at a simultaneous high availability (Nguyen et al. 2021). On the other hand, only mammalian animal models, such as the ferret or the pig, are suitable for the characterization of human IAVs, which is mainly based on the different receptor specificity of avian (α2,3 sialic acid) or mammalian IAVs (α2,6 sialic acid) (Campbell and Magor 2020; Kuchipudi et al. 2021). Accordingly, either the α2,3- or the α2,6 sialic acid receptor is more

abundantly expressed in the respective avian or mammalian species (Hemmink et al. 2018; Campbell and Magor 2020; Kuchipudi et al. 2021; Nguyen et al. 2021). In turn, infections of poultry with human IAV strains is extremely rare and without obvious clinical signs in the animals, resulting in a low relevance of poultry for the characterization of human IAVs (Kalthoff et al. 2010; Berhane et al. 2016; Hemmink et al. 2018).

1.5.4 Swine

Over a long period of time, the pig is considered as one of the most important "mixing and reassortment vessels" for avian and mammalian IAVs, which is based on the presence of both α2,3- and α2,6 sialic acid receptors in the respiratory tract of these animals allowing efficient (simultaneous) replication of both avian and mammalian IAVs (Nelson and Worobey 2018; Nguyen et al. 2021; Hennig et al. 2022). While the α2,3- sialic acid receptor is more abundantly expressed in the LRT of the pig, the α2,6 sialic acid receptor is predominantly apparent in their URT (Nelson and Worobey 2018). As already elucidated in chapter 1.3.4, the swine is often connected with several pandemic IAV outbreaks from the past, assigning this animal a role as intermediate host and "mixing vessel" to facilitate the spillover of the respective pandemic IAV strain to humans (Smith et al. 2009; Dawood et al. 2012; Walia et al. 2019; Taubenberger and Morens 2020). Importantly, interspecies transmission of IAVs between pigs and humans can occur via both ways, from pigs to humans and from humans to pigs (Nelson and Vincent 2015; Hennig et al. 2022). In general, the pig develops obvious clinical signs upon IAV infection that include for example fever and dyspnea, while the lower and upper extremities of either an asymptomatic or a fatal IAV infection in these animals are rarely observed (Duerrwald et al. 2013; Hemmink et al. 2016; Ryt-Hansen et al. 2019). To date, it is unknown if pigs are susceptible to any bat-related IAVs. Transmission between these animals can occur via respiratory droplets, aerosols and direct contact (Lange et al. 2009; Rajao and Vincent 2015; Lopez Moreno et al. 2021). The swine shares multiple anatomic, physiological and genomic traits with humans, which include for example the general body size, their lung physiology and similarities in their cardiovascular system (Rajao and Vincent 2015; Zettler et al. 2020). Through these similarities, the pig qualifies as an excellent translational research model for IAV infection in humans. Nevertheless, the challenging housing conditions and animal handling along with non-negligible expenses complicates their utility under infection conditions.

The use of a variety of standard animal models paves the way for a deep characterization of zoonotic viruses in all kinds of research questions. Since all animal models have their specific

advantages and disadvantages, it is required to analyze specific and especially newly emerging viruses in more than one animal model. Depending on the virus, there may be complementary results in terms of transmission efficiency, replication capacity or the general viral host range of this specific virus, which can only be fully elucidated by establishing a multi-species characterization approach (Nguyen et al. 2021; Zhou et al. 2021; Muñoz-Fontela et al. 2020). For the purpose of wildlife reservoir or potential intermediate host identification for specific viruses, it may also become necessary to use or sample more exotic animal models, as it had been for example the case for SARS-CoV-2 and raccoon dogs, bank voles, white-tailed deer or minks (Freuling et al. 2020; Ulrich et al. 2021; Pickering et al. 2022; Vandegrift et al. 2022; Virtanen et al. 2022). Numerous animal trials in multiple species have led to an overwhelming knowledge about useful and susceptible animals to IAV or SARS-CoV-2 (Fig. 7) (Muñoz-Fontela et al. 2020; Schlottau et al. 2020; Michelitsch et al. 2021; Nguyen et al. 2021).

2   Study objectives

Preparedness for potentially pre-pandemic pathogens, as well as preventive actions for onward transmission of already pandemic pathogens are indispensable to better understand and minimize the overall infection risk of the global population (Lal et al. 2020). Characterization of pathogens fulfilling these requirements in specific animal models have therefore always been a tool of utmost importance to rapidly estimate e.g. the zoonotic risk for humans (Kash et al. 2004; Kash et al. 2006; Claire et al. 2017; Schlottau et al. 2020).

In this doctoral thesis, the objectives were to tackle both concerns with the examples of the potentially pre-pandemic bat IAV H9N2, as well as the already pandemic SARS-CoV-2 virus. This study thus provides important insights into mechanisms of action in case of two major objectives:

I)   **Pandemic preparedness** – bat H9N2, a potentially zoonotic pathogen whose pre-pandemic potential is currently unknown and has to be evaluated, and

II)   **Pandemic control and precaution** – SARS-CoV-2, an already pandemic pathogen with continuously adapting virus strains of uncertain capabilities concerning virulence, immune escape and transmission efficacy.

I)   *In vivo* characterization of emerging bat IAV H9N2 to estimate its zoonotic/pandemic potential

Firstly, *in vivo* characterization of bat H9N2 in its natural host *Rousettus aegyptiacus* was performed and compared to an infection of the same bat species with an avian H9N2 **(Publication I)**. This study was performed to directly investigate bat H9N2 pathogenicity, transmission, disease progression, clinical signs and viral spread in organs of infected bats of this newly described virus in its natural host. Secondly, ferrets, transgenic MxA mice, as well as turkey and chicken hatchlings were experimentally infected with the bat H9N2 virus for analyzing both the zoonotic potential but also the risk of adapting to poultry reservoirs **(Publication II)**.

II)   *In vivo* competitive infections with SARS-CoV-2 VOCs to unravel their specific fitness advantages

The SARS-CoV-2 pandemic was and still is driven by frequent emergence of VOCs and related variants, and the role of specific fitness advantages over their respective precursors are a matter of debate (RKI 2021). The aim of the second objective was thus to characterize the fitness

advantages of emerging VOCs during the progression of the pandemic. Firstly, potential fitness advantages of emerging SARS-CoV-2 VOCs Alpha and Beta and their genetic fitness determinants compared to WT SARS-CoV-2 were examined in competitive infection and transmission approaches in the ferret, golden Syrian hamster, as well as K18-hACE2 and hACE2-KI mice models **(Publication III)**. Secondly, the same competitive infection and transmission studies were also performed with the lately emerged SARS-CoV-2 Delta and Omicron VOC **(Publication IV)**, now taking the pandemic situation at that timepoint into consideration by using vaccinated animals in addition. Additionally, single infection studies with both Delta and Omicron in ferrets were performed to directly compare the disease parameters including shedding, transmission, pathology and viral load distribution in organs of infected animals, also with competitively inoculated animals **(Publication IV)**. Finally, the generation of recombinant SARS-CoV-2 WT viruses expressing the spike protein of the respective VOCs Delta or Omicron should determine the influence of spike-associated mutations in terms of fitness (dis-)advantages **(Publication IV)**.

3   Publications

I

<u>Publication I</u>

Egyptian Fruit Bats (*Rousettus aegyptiacus*) Were Resistant to Experimental Inoculation with Avian-Origin Influenza A Virus of Subtype H9N2, But Are Susceptible to Experimental Infection with Bat-Borne H9N2 Virus

<u>Nico Joël Halwe*</u>, Marco Gorka, Bernd Hoffmann, Melanie Rissmann, Angele Breithaupt, Martin Schwemmle, Martin Beer, Ahmed Kandeil, Mohamed A. Ali, Ghazi Kayali, Donata Hoffmann, Anne Balkema-Buschmann

Viruses, 2021

viruses

MDPI

Article

Egyptian Fruit Bats (*Rousettus aegyptiacus*) Were Resistant to Experimental Inoculation with Avian-Origin Influenza A Virus of Subtype H9N2, But Are Susceptible to Experimental Infection with Bat-Borne H9N2 Virus

Nico Joel Halwe [1], Marco Gorka [1], Bernd Hoffmann [1], Melanie Rissmann [2], Angele Breithaupt [3], Martin Schwemmle [4,5], Martin Beer [1], Ahmed Kandeil [6], Mohamed A. Ali [6], Ghazi Kayali [7,8], Donata Hoffmann [1,*] and Anne Balkema-Buschmann [2]

[1] Institute of Diagnostic Virology, Friedrich-Loeffler-Institut, 17493 Greifswald, Insel Riems, Germany; nico.halwe@fli.de (N.J.H.); marco.gorka@fli.de (M.G.); Bernd.Hoffmann@fli.de (B.H.); Martin.Beer@fli.de (M.B.)

[2] Institute of Novel and Emerging Infectious Diseases, Friedrich-Loeffler-Institut, Insel Riems, 17493 Greifswald, Insel Riems, Germany; Melanie.Rissmann@fli.de (M.R.); anne.buschmann@fli.de (A.B.-B.)

[3] Department of Experimental Animal Facilities and Biorisk Management, Friedrich-Loeffler-Institut, 17493 Greifswald, Insel Riems, Germany; angele.breithaupt@fli.de

[4] Institute of Virology, Medical Center-University of Freiburg, 79104 Freiburg, Germany; martin.schwemmle@uniklinik-freiburg.de

[5] Faculty of Medicine, University of Freiburg, 79104 Freiburg, Germany

[6] Center of Scientific Excellence for Influenza Viruses, National Research Centre, Dokki, Giza 12311, Egypt; Ahmed.Kandeil@human-link.org (A.K.); Mohamed.Ali@human-link.org (M.A.A.)

[7] Department of Epidemiology, Human Genetics and Environmental Sciences, University of Texas Health Sciences Center, Houston, TX 77030, USA; ghazi@human-link.org

[8] Human Link, Dubai, United Arab Emirates

* Correspondence: donata.hoffmann@fli.de

check for **updates**

Abstract: Influenza A viruses (IAV) of subtype H9N2, endemic in world-wide poultry holdings, are reported to cause spill-over infections to pigs and humans and have also contributed substantially to recent reassortment-derived pre-pandemic zoonotic viruses of concern, such as the Asian H7N9 viruses. Recently, a H9N2 bat influenza A virus was found in Egyptian fruit bats (*Rousettus aegyptiacus*), raising the question of whether this bat species is a suitable host for IAV. Here, we studied the susceptibility, pathogenesis and transmission of avian and bat-related H9N2 viruses in this new host. In a first experiment, we oronasally inoculated six Egyptian fruit bats with an avian-related H9N2 virus (A/layer chicken/Bangladesh/VP02-plaque/2016 (H9N2)). In a second experiment, six Egyptian fruit bats were inoculated with the newly discovered bat-related H9N2 virus (A/bat/Egypt/381OP/2017 (H9N2)). While *R. aegyptiacus* turned out to be refractory to an infection with H9N2 avian-type, inoculation with the bat H9N2 subtype established a productive infection in all inoculated animals with a detectable seroconversion at day 21 post-infection. In conclusion, Egyptian fruit bats are most likely not susceptible to the avian H9N2 subtype, but can be infected with fruit bat-derived H9N2. H9-specific sero-reactivities in fruit bats in the field are therefore more likely the result of contact with a bat-adapted H9N2 strain.

Keywords: influenza virus; H9N2; *Rousettus aegyptiacus*; avian-related H9N2; bat-related H9N2

1. Introduction

Low-pathogenic avian influenza viruses (LPAIV) of subtype H9N2 are globally widespread in poultry and endemic in China and Eurasian countries [1,2]. While causing severe losses in poultry production, spill-over infections of H9N2 and its reassortants pose a constant threat to the human population [3–5]. In 1999, the first isolation of H9N2 from

two diseased children in Hong Kong was published [6]. In addition, H9N2 viruses are able to replicate in further mammalian species, such as pigs or mice [7]. Multiple cases of H9N2 outbreaks in avian species in Africa have been reported inter alia from Egypt [8,9], where the virus is endemic [2].

The first evidence of influenza A and influenza A-like viruses originating from different bat species was found in 2012 and 2013: two novel influenza A-like viruses, provisionally designated as H17N10 and H18N11, were identified via next-generation sequencing in the feces of a little yellow-shouldered fruit bat (*Sturnira lilium*) and a South American flat-faced fruit-eating bat (*Artibeus planirostris*), respectively [10,11]. These findings raised the question of bats in general being a reservoir host for multiple influenza A viruses. Most importantly, however, these findings opened questions about an evolutionary relationship between avian and bat-borne influenza A viruses. Furthermore, H9-specific sero-reactivity was demonstrated in 30% of straw-colored fruit bats (*Eidolon helvum*) in Ghana [12]. Furthermore, only recently, a new distinct influenza A virus was found and isolated from Egyptian fruit bats (*Rousettus aegyptiacus*) in Egypt. Interestingly, the hemagglutinin (HA) and neuraminidase (NA) encoding segments of this particular virus were closely related to avian H9N2-viruses [13,14].

Considering the findings of influenza A and influenza A-like viruses and specific antibodies in multiple bat species, bats in general might be involved in influenza A virus transmission cycles and might represent a potential vessel for reassortment processes [14,15]. However, to what extent Egyptian fruit bats support infection with IAV, including the newly described bat H9N2 subtype, remains to be shown.

In order to specifically investigate susceptibility, pathogenesis and virus shedding, we oronasally infected two groups of Egyptian fruit bats (*Rousettus aegyptiacus*) with either a poultry-origin H9N2 strain of clade G1 (A/layer chicken/Bangladesh/VP02-plaque/2016) or the fruit bat-derived strain A/bat/Egypt/381OP/2017 (H9N2). The latter group was cohoused with naïve contact bats (24 h post-infection) to further elucidate H9N2 bat flu virus transmission.

2. Materials and Methods

2.1. Viruses

LPAIV H9N2 of clade G1, namely A/layer chicken/Bangladesh/VP02-plaque/2016 (accession numbers EPI1807182-1807189), was obtained from the Friedrich-Loeffler-Institut (FLI) virus repository [9]. The virus stock was propagated in Madin-Darby Canine Kidney (MDCK) type II cells (Collection of Cell Lines in Veterinary Medicine CCLV RIE1061) for two days at 37 °C under 5% CO2 atmosphere using a mixture of equal volumes of Eagle Minimum Essential Medium (MEM) (Hank's balanced salts solution) and Eagle MEM (Earle's balanced salts solution), 2 mM L-Gln, nonessential amino acids, adjusted to 850 mg/L NaHCO3, 120 mg/L sodium pyruvate, pH 7.2 in the presence of tosylsulfonyl phenylalanyl chloromethyl ketone (TPCK)-treated trypsin (Sigma, Munich, Germany). The LPAIV H9N2 A/bat/Egypt/381OP/2017 virus isolate (accession numbers MH376902.1-MH376909.1) was propagated via infection of embryonated chicken eggs for 72 h. Hereafter, the allantoic fluid was harvested and stored at −80 °C. This virus stock was once more propagated in cell culture on CCLV RIE1495 MDCK cells for two days at 37 °C, 5% CO2 using the MEM mixture mentioned above. Viral supernatants of both avian and bat H9N2 were harvested, cleared of debris and stored at −80 °C. Viral titers were determined by virus titration and calculated by the Reed–Muench method [16].

2.2. Experimental Inoculation and Sampling of Bats

Overall, all 20 Egyptian fruit bats (*Rousettus aegyptiacus*) from both experiments were reared at FLI and tested negative for influenza A reactive antibodies via immunofluorescence analysis (IFA) using the inoculation viruses. Six bats in each experiment were anesthetized by inhalation of 5% isoflurane in O2 and oronasally inoculated with 100 μL H9N2 (A/layer chicken/Bangladesh/VP02-plaque/2016) distributed equally into each

nostril and mouth at a concentration of $10^{4.7}$ TCID$_{50}$ per animal (Figure 1) or with 100 µL $10^{4.7}$ TCID$_{50}$ per animal of A/bat/Egypt/381OP/2017 (H9N2) (Figure 2), respectively. The remaining two animals in the first experiment served as negative controls and were mock-infected with the same volume of PBS (Figure 1). The six naïve animals in the second experiment (Figure 2) were co-housed with the inoculated animals 24 h post-infection. Clinical signs (nasal discharge, reduced activity, neurological symptoms and dyspnea) were monitored daily. In the second experiment, all infected and two contact animals carried a temperature transponder (Anipill, Bodycap, Hérouville Saint-Clair, France) that had been surgically implanted under general anesthetics into the abdominal cavity two weeks prior to infection. The transponder automatically transmitted the body core temperature to the monitor device every 15 min. In addition, rectal temperature, body weight and oral and rectal swabs were collected at two-day intervals using plain swab sterile paper applicator cotton tipped 164C, Copan, Brescia, Italy. The swabs were transferred to 2 mL of cell culture medium containing 1% Baytril (Bayer, Leverkusen, Germany), 0.5% Lincomycin (WDT, Garbsen, Germany) and 0.2% Amphotericin/Gentamycin (Fisher Scientific Waltham, MA, USA), followed by 30 min. incubation at room temperature under roughly shaking at 300 rpm (KS 260 control, IKA, Staufen, Germany). In the first experiment, all bats were sacrificed 21 dpi, whereas in the second experiment, two inoculated and two naïve animals were sacrificed at day seven, while the residual eight animals were kept until day 21. At necropsy, samples were obtained from the following organs: conchae, trachea, lung (left caudal lung lobe and right cranial lung lobe), heart, kidney, liver, spleen, duodenum, jejunum, colon, rectum, skeletal muscle and thigh muscles. One part of each tissue was fixed in 10% neutral-buffered formalin and another part was stored at −80 °C until further processing. Blood samples for serology were collected from final bleed during the euthanasia procedure.
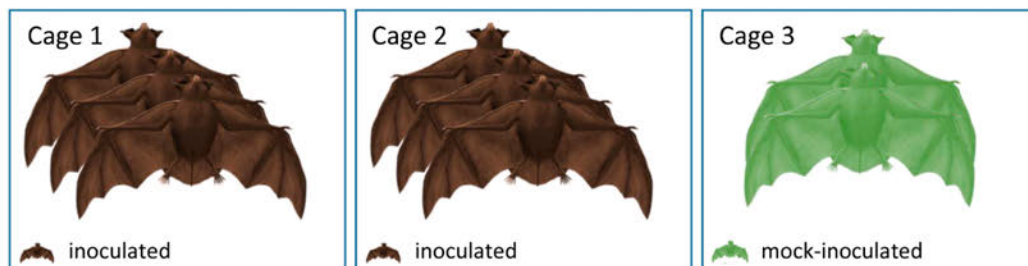
Figure 1. Experimental design of the experiment with "A/layer chicken/Bangladesh/VP02-plaque/2016 (H9N2)". Three inoculated bats each were housed in two separate cages. The two mock-inoculated individuals were housed separately in cage 3.
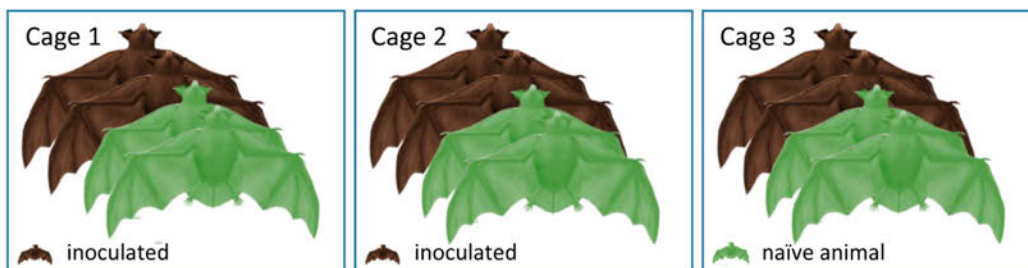
Figure 2. Experimental design of the experiment with A/bat/Egypt/381OP/2017 (H9N2). On 1 dpi, two inoculated and two naïve bats were mixed and housed in each of the three cages. This animal distribution was eventually maintained until the end of the experiment.

2.3. Organ Homogenization

Organ pieces (approximately 2 × 2 × 2 mm) were transferred into 2 mL collection tubes prepared with a stainless-steel bead (diameter 5 mm) and 1 mL of DMEM supplemented with antibiotics (1% penicillin-streptomycin, Biochrome, Berlin, Germany). Homogenization was performed using a TissueLyser II instrument (Qiagen, Hilden, Germany) for 2 min at 300 Hz. Supernatants for RNA extractions were acquired following centrifugation at 13,000 rpm for 2 min.

2.4. RNA Isolation

RNA extraction of all oral and rectal swabs, as well as organ samples after euthanasia from both experiments was performed via the NucleoMag Vet kit (Macherey-Nagel, Düren, Germany) according to manufacturer's instructions on a Biosprint 96 platform (Qiagen, Hilden, Germany).

2.5. Real-Time RT-PCR (RT-qPCR)

RT-qPCRs of organs, oral and rectal swabs in the first experiment (avian origin H9N2) were performed as described before [17].

In order to detect A/bat/Egypt/381OP/2017 (H9N2) viral RNA in the second experiment, a specific primer and probe system was designed (Table 1). For process control, a genomic nucleic acid was co-amplified in the PCR runs using the HEX channel [18]. The final composition of the RT-qPCR reactions was 1.75 μL of RNase-free water, 6.25 μL of 2x qScript XLT One-Step RT-qPCR ToughMix (Quanta, Beverly, MA, USA), 1 μL of primer-probe-mix-FAM, 1 μL of beta-actin DNA-mix2-HEX and 2.5 μL of template RNA. All RT-qPCRs were run on the CFX 96 real-time PCR cycler (Bio-Rad, Hercules, CA, USA). The temperature profile used was 10 min at 50 °C (reverse transcription), 1 min at 95 °C (inactivation of the reverse transcriptase/activation Taq polymerase) followed by 45 cycles of 10 s at 95 °C (denaturation), 30 s at 57 °C (annealing) and 30 s at 68 °C (elongation). Fluorescence values (FAM, HEX) were collected during the annealing step. Absolute quantification was done using a standard of known concentrations, corresponding to the RNA of the original virus used for inoculation. Quantification was established by the QX200 Droplet Digital PCR System in combination with the 1-Step RT-ddPCR Advanced Kit for Probes (BioRad, Hercules, CA, USA).

Table 1. Probes and primers for detection of A/bat/Egypt/381OP/2017 (H9N2) viral RNA (specifically designed for this study) and A/layer chicken/Bangladesh/VP02-plaque/2016 (H9N2) viral RNA.

Primer/Probe	Sequence	Concentration	Accession Number
Detection of A/bat/Egypt/381OP/2017 (H9N2) viral RNA			
H9N2-PB1-101Fv2	tga tcc acc cta cag cca tg	20 μM	MH376908 (Pos. 78-97)
H9N2-PB1-180Rv2	ctt ttt ctg aat att gat gag tcc ta	20 μM	MH376908 (Pos. 132-157)
H9N2-PB1-125FAMv2	FAM-tgg cac agg ata tac aat gga cac cgt-BHQ1	5 μM	MH376908 (Pos. 102-128)
Detection of A/layer chicken/Bangladesh/VP02-plaque/2016 (H9N2) viral RNA			
IAV-PB1_120F	cat ttg aat gga ygt caa ycc ga	20 μM	
IAV-PB1_271R	ctg ttd acy gtg tcc atd gtg ta	20 μM	[17]
IAV-PB1_247as_FAM	FAM-ccw gty ccy gty cca tgg ctg ta-BHQ1	5 μM	

2.6. Histopathology

Based on RT-qPCR data, selected organs from bats sacrificed at 7 dpi were trimmed for paraffin-embedding: nasal atrium (non-respiratory region), nasal conchae (respiratory and olfactory region), duodenum, jejunum, colon and rectum of inoculated #5 and #6, as well

as transmission #11 and #12. Tissue sections were stained with hematoxylin and eosin (HE). Immunohistochemistry for viral antigen detection using a primary antibody against the M protein of IAV (ATCC clone HB-64) was performed on consecutive slides as described earlier [19]. The severity of lesions was recorded on an ordinal scoring scale with scores 0 = no lesion, 1 = minimal or <5% per affected cells/tissue slide; 2 = mild or 6–40% affected; 3 = moderate or 41–80% affected; and 4 = severe or > 80% affected. The distribution of antigen was semi-quantitatively scored on an ordinal 0–4 scale: 0 = negative; 1 = focal or oligofocal, 2 = multifocal, 3 = coalescing and 4 = diffuse immunoreactive cells. Evaluation and interpretation were performed by a board-certified pathologist (DiplECVP).

2.7. Propagation of A/Bat/Egypt/381OP/2017 (H9N2) Virus Isolates from Bat Samples

Animal samples were initially diluted in medium (see section "Experimental inoculation and sampling of bats"), whereupon 200 µL was transferred into the allantoic cavity of embryonated chicken eggs (three eggs per sample) followed by incubation for five days at 37 °C. Afterwards, the eggs were placed at −80 °C for 30 min to ensure the death of the chicken embryo, whereupon the egg was opened to allow harvesting of the allantoic fluid. The fluid was centrifuged at 3500 rpm for 10 min, followed by a TRIzol LS reagent (life technologies, Carlsbad, CA, USA)-based RNA extraction (according to manufacturer's instructions). Existence of A/bat/Egypt/381OP/2017 (H9N2) viral RNA and thereby evidence for successful propagation of A/bat/Egypt/381OP/2017 (H9N2) was finally verified via RT-qPCR as described before.

2.8. Serology

All serum samples were heat-inactivated at 56 °C for 30 min and animal sera from both experiments were analyzed by a commercial enzyme-linked immunosorbent assay (ELISA) for the presence of antibodies against the IAV nucleoprotein (NP) according to manufacturer's instructions (ID-Vet, Montepellier, France). In addition, a virus neutralization assay was performed in the first experiment. In brief, 50 µL of medium containing H9N2 (A/layer chicken/Bangladesh/VP02-plaque /2016) at a concentration of $10^{3.3}$ $TCID_{50}/_{mL}$ was mixed with the same volume of diluted sera. Each serum was prepared in triplicate in a 96-well plate. After incubation for 2 h at 37 °C, the samples were transferred into a second 96-well plate prepared 24 h earlier containing 100 µL medium on 24 h grown MDCK II cells. Viral replication was assessed after an incubation period of 5 days (37 °C, 5% CO2) via visualization of the cytopathic effect. Validation was achieved by titration of the virus dilutions. In the second experiment, seroconversion was investigated via IFA as well. For that reason, MDCK cells were seeded in a 96-well plate and were grown for 24 h. Afterwards, cells were infected with A/bat/Egypt/381OP/2017 (H9N2) for 24 h followed by cell fixation with 4% paraformaldehyde (PFA), as well as permeabilization with 0.5% Triton-X-100 in PBS. Cells were then stained for 1 h with a dilution series from 1:10–1:256 of the appropriate animal serum, followed by three PBS-washing steps and the incubation with a secondary goat-α-bat IgG (H + L) antibody (Novus biologicals, Wiesbaden Nordenstadt, Germany) for 1 h. Subsequently, cells were washed three times with PBS again, followed by the addition of an Alexa Fluor 488-coupled chicken-α-goat IgG (H + L) third antibody for 1 h to allow visualization under the fluorescence microscope after a final three-times PBS-wash procedure.

3. Results

3.1. Egyptian Fruit Bats Are Resistant to Infection with an Avian H9N2 Strain

Following oronasal inoculation of Egyptian fruit bats (*Rousettus aegyptiacus*) with $10^{4.7}$ TCID50 per animal of A/layer chicken/Bangladesh/VP02-plaque /2016 (H9N2), neither clinical signs nor any significant changes in body weight or body temperature could be observed during the experiment. In addition, no viral RNA was detected in organs, oral or rectal swabs. Samples below 10 viral genome copy numbers per mL (equivalent to Ct 39.2) were considered negative. At necropsy, no macroscopic lesions were evident. Analysis

of sera until 21 dpi by IAV-antibody-ELISA and serum neutralization assay revealed no evidence of seroconversion. Taken together, these observations strongly suggest that this H9N2 subtype of avian origin fails to replicate in Egyptian fruit bats.

3.2. Egyptian Fruit Bats Are Susceptible to Natural Infection with Bat-Origin H9N2 A/Bat/Egypt/381OP/2017

After infection with the H9N2 subtype of bat origin, none of the inoculated or contact animals showed any obvious clinical signs of an infection, such as anorexia, depression or signs of a respiratory infection. The temperature monitoring data did not reveal any obvious deviation from the physiological oscillation that ranges mainly between 34 and 41 °C (Figure 3), depending on the time of day and the animals' activity. While only one of six contact animals (contact animal #4) displayed altogether two temperature maxima reaching 41 °C within 21 dpi, all six inoculated animals showed at least one maximum exceeding 40 °C, with two animals showing 11 temperature peaks > 40 °C (inoculated animal #2) or six peaks > 40 °C (inoculated animal #4) within the same time period. Inoculated animal #2 reached 41 °C twice during the experiment (Figure 3). Notably, contact animal #4 and inoculated animal #2 were kept in the same cage.

Inoculation of Egyptian fruit bats with 100 µL (dose $10^{4.7}$ TCID$_{50}$) per animal of A/bat/Egypt/381OP/2017 (H9N2) established a productive infection in these animals. At 1 dpi, one out of six oral swabs, as well as two rectal swabs from the inoculated animals, were positive for the H9N2 bat flu viral genome using RT-qPCR (Figures 4 and 5). At 3 dpi, oral swabs of five out of six inoculated animals, and one rectal swab (inoculated animal #10), were positive for viral genome, ranging from 30 up to 4.6×10^3 viral genome copy numbers per mL (Figures 4 and 5). Three oral swabs and one rectal swab of the inoculated animals after 5 dpi and two oral swabs from inoculated animals after 7 dpi, as well as one oral swab of an inoculated animal after 9 dpi were still positive for A/bat/Egypt/381OP/2017 (H9N2) genome. From 11 dpi until the end of the experiment at 21 dpi, all oral and rectal swabs were negative for H9N2 bat flu RNA (Figures 4 and 5).

Nasal conchae samples of two inoculated animals sacrificed at 7 dpi tested positive in both inoculated animals (Figure 6). Moreover, viral RNA was also detected from the trachea samples of both inoculated animals. As summarized in Figure 6, nasal conchae from two of four inoculated animals sacrificed at day 21 of the animal experiment were still positive for viral RNA of H9N2 bat flu.

Fecal samples of animal cage one were positive for A/bat/Egypt/381OP/2017 (H9N2) viral RNA at 4 and 7 dpi and samples from cage two were positive at 3, 4, 6 and 8 dpi, with maximum viral loads of 4×10^3 genome copies per mL detected in the sample collected at 8 dpi. Only one fecal sample collected from cage three was positive at 3 dpi, while the residual samples were negative for A/bat/Egypt/381OP/2017 (H9N2) viral RNA.

Histopathology identified an oligo-focal, minimal to mild rhinitis in all animals evaluated at 7 dpi (inoculated animal #5 and #6) and 6 days post-contact (contact animal #5 and #6). Additionally, inoculated animal #6 showed a moderate transmigration of granulocytes and lymphocytes as well as intraluminal cellular debris within the nasolacrimal duct (Figure 7A). Contact animal #6 exhibited loss of cilia and moderate degeneration of the mucosal epithelium of the nasal-associated lymphoid tissue (Figure 7C). No lesions were observed in the intestinal tract. Viral antigen could not be detected in the nasal cavity or in the intestinal tract using immunohistochemistry. In summary, Egyptian fruit bats can be productively infected with A/bat/Egypt/381OP/2017 (H9N2) resulting in fecal secretion with maximum viral loads at 8 dpi, whereas transmission to contact animals was rather inefficient and did not result in a sustained infection.
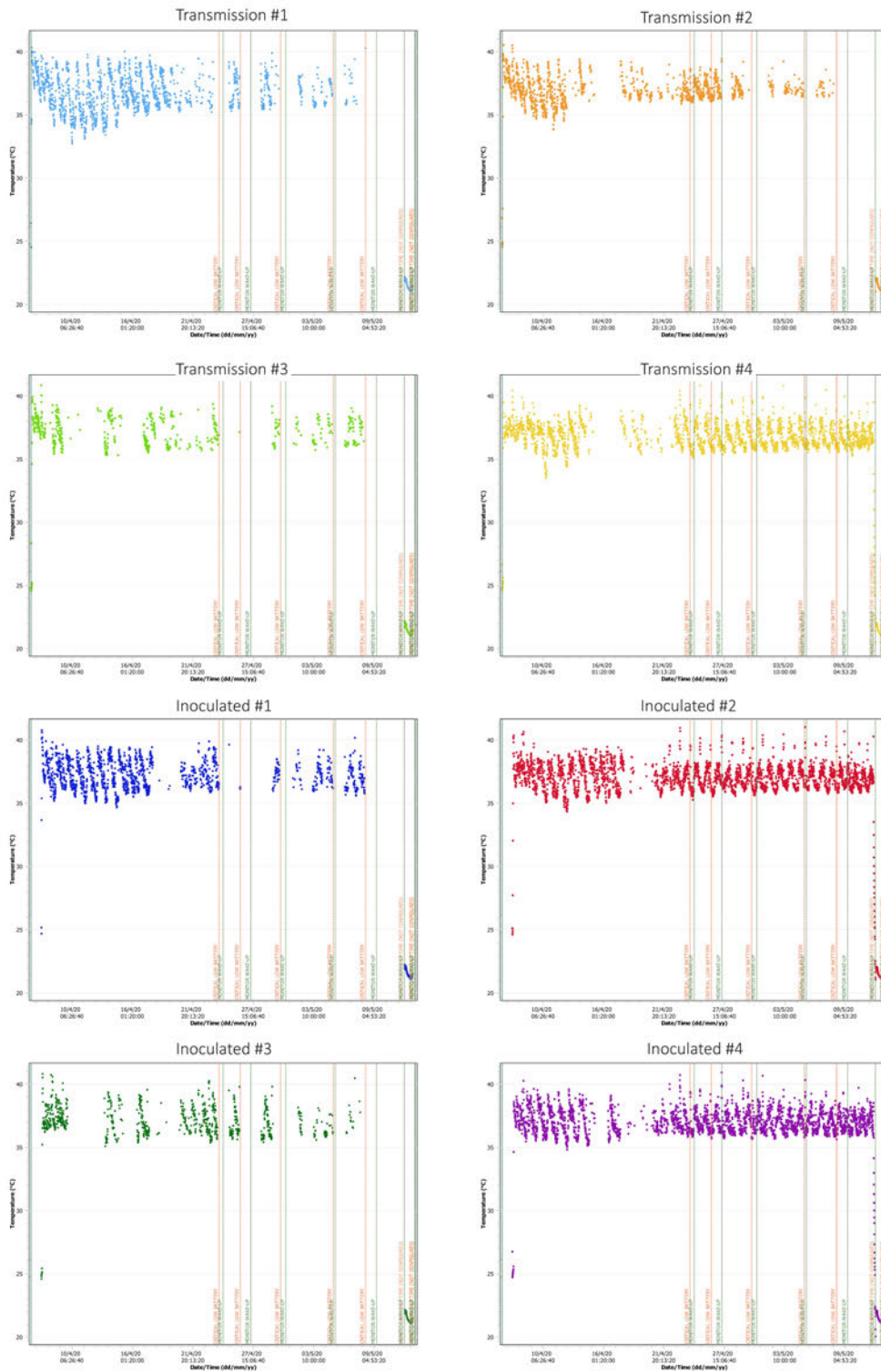
Figure 3. Temperature data of four infected and four contact animals. Body core temperatures were recorded every 15 min, some of the signals were lost due to the experimental setup (metal cages interfere with signal transduction to the monitor). Blue vertical line indicates challenge; red horizontal line shows 41 °C.
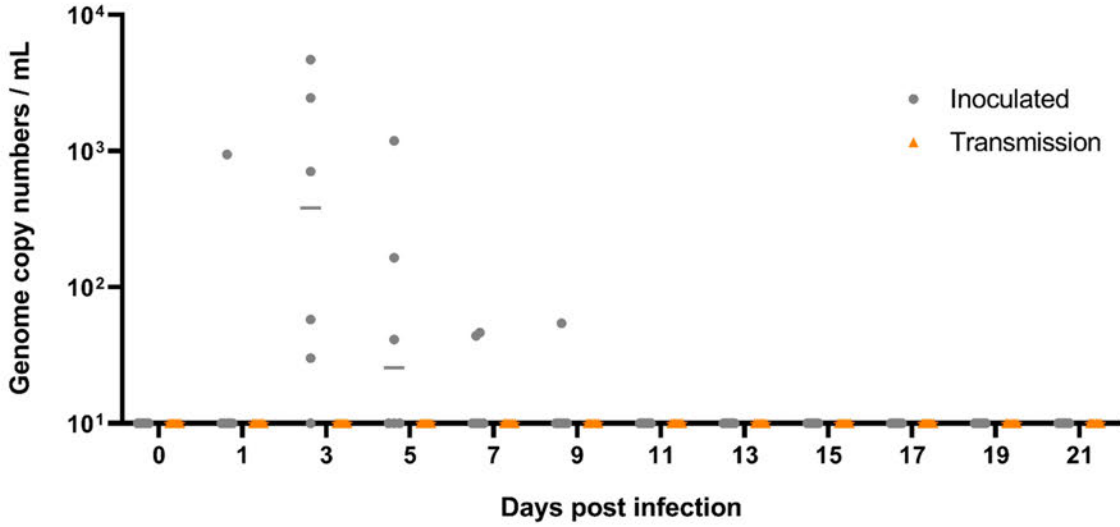
Figure 4. Viral shedding from oral swabs of the *Rousettus* bats following A/bat/Egypt/381OP/2017 (H9N2) infection. Viral shedding was monitored by RT-qPCR from swabs taken from the oral cavity. Swabs of six inoculated animals (grey dots) and six contact animals (orange triangles) were taken individually every other day. Samples below 10 viral genome copy numbers per mL (equivalent to Ct 39.2) were considered negative. DPI = Days post infection.

Figure 5. Viral shedding from rectal swab samples of the *Rousettus* bats following infection with A/bat/Egypt/381OP/2017 (H9N2). Viral shedding was monitored by RT-qPCR from rectal swabs. Swabs of six inoculated animals (grey dots) and six contact animals (orange triangles) were taken individually every other day. Samples below 10 viral genome copy numbers per mL (equivalent to Ct 39.2) were considered negative. DPI = Days post infection.
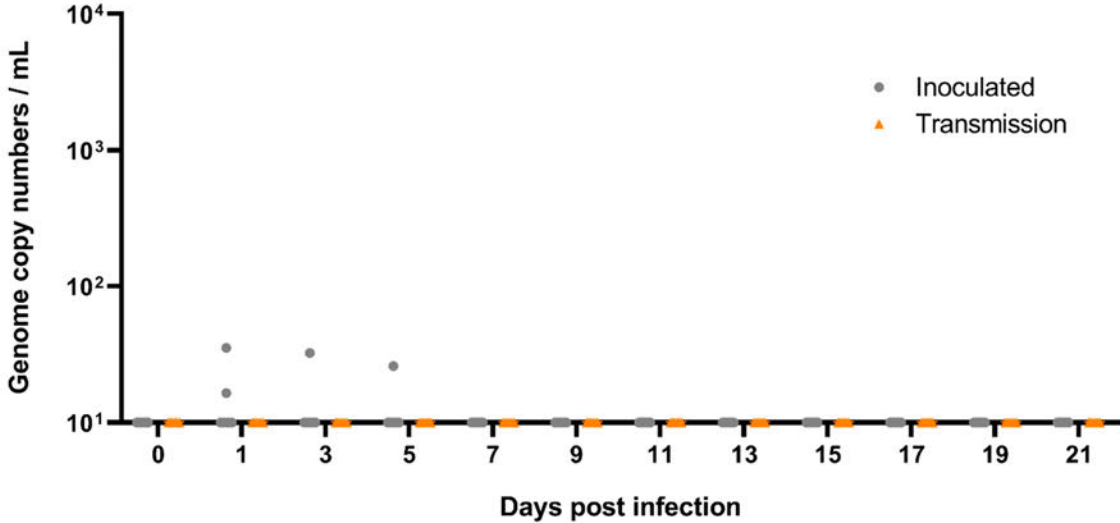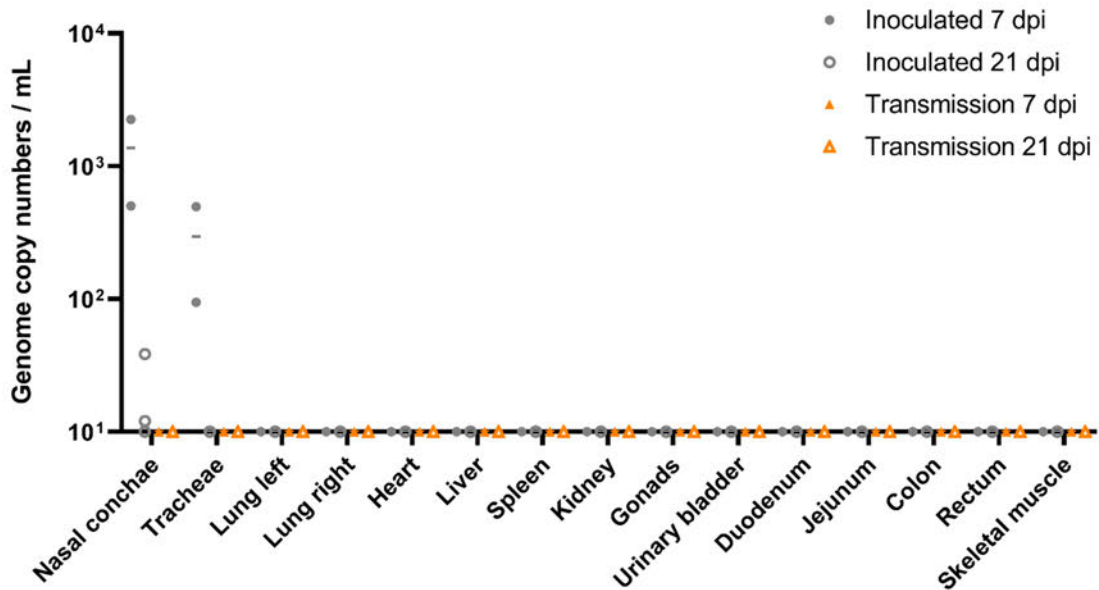
Figure 6. Viral loads in organs of A/bat/Egypt/381OP/2017 (H9N2)-inoculated Egyptian fruit bats. Individual results of detected viral RNA are depicted. Organs from two inoculated (filled grey dots) and two contact animals (filled orange triangles) were taken at 7 dpi, while organs from the residual four inoculated (open grey dots) and contact animals (open orange triangles) were taken after euthanasia at 21 dpi. Samples below 10 viral genome copy numbers per mL (equivalent to Ct 39.2) were considered negative.
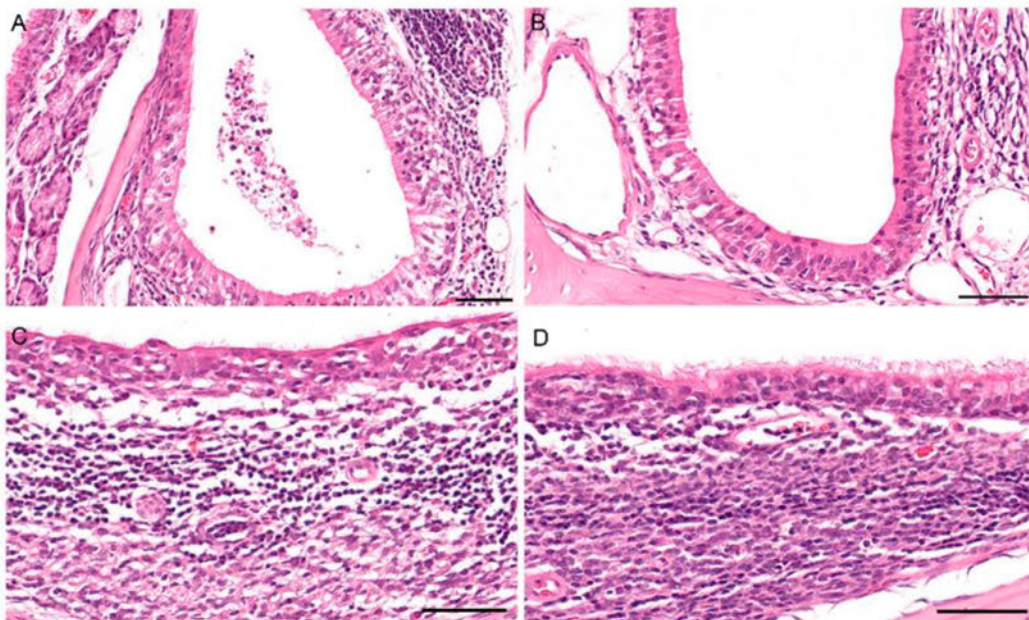
Figure 7. Histopathology in the nasal mucosa of fruit bats after infection with bat-origin H9N2 (A/bat/Egypt/381OP/2017), 7 dpi. (**A**) Inoculated animal #5: moderate transmigration of granulocytes and lymphocytes as well as intraluminal cellular debris within the nasolacrimal duct. (**B**) Unaffected nasolacrimal duct for comparison. (**C**) Contact animal #6: loss of cilia and moderate degeneration of the mucosal epithelium of the nasal-associated lymphoid tissue (NALT). (**D**) Unaffected NALT for comparison. All bars = 50 μm.

3.3. A/Bat/Egypt/381OP/2017 (H9N2) Was Effectively Isolated and Propagated from the Experimental Egyptian Fruit Bat Samples

Since it has been shown previously that A/bat/Egypt/381OP/2017 (H9N2) efficiently replicates in embryonated chicken eggs [13], we attempted to propagate the virus from two RT-qPCR-positive Egyptian fruit bat oral swabs (inoculated animal #3 and inoculated animal #6), as well as from one RT-qPCR-positive nasal turbinate sample (inoculated animal #6) using three replicates, respectively.

As shown in Table 2, all three eggs inoculated with the oral swab sample of inoculated animal #3 (initial Ct-value 30.11) were confirmed to contain A/bat/Egypt/381OP/2017 (H9N2) viral RNA with Ct-values ranging from 31 to 34, suggesting that viral replication may have occurred to a certain extent. However, two out of three eggs inoculated either with the oral swab (initial CT value 28.90) or the nasal conchae organ sample of inoculated animal #6 (initial Ct-value 31.74) showed striking evidence for successful viral replication, with Ct-values of 14 and 13, respectively, whereas the third egg replicate of both samples revealed Ct-values of 28 and 34, respectively. In order to demonstrate that even the least positive Ct-value detected from the respective samples out of the three egg replicates was indicative for A/bat/Egypt/381OP/2017 replication, we infected MDCK-cells with 100 µL of the aforementioned egg samples and incubated the cells at 37 °C for three days. As expected, a cytopathic effect (CPE) was observed in all of the three infected samples, thereby further confirming the successful re-isolation after inoculation of the embryonated eggs. Together, these observations indicate that Egyptian fruit bats experimentally infected with A/bat/Egypt/381OP/2017 (H9N2) shed infectious virus.

Table 2. Summary of the isolation and propagation experiments of fruit bat samples inoculated with A/bat/Egypt/381OP/2017 (H9N2) in embryonated chicken eggs.

	Inoculated Animal #3 Oral Swab, 3 DPI	Inoculated Animal #6 Oral Swab, 3 DPI	Inoculated Animal #6 Nasal Conchae, 7 DPI
Initial Ct-value	30.11	28.90	31.74
Egg 1	31.68	28.64	34.61
Egg 2	31.82	14.58	13.55
Egg 3	34.11	14.05	13.47

3.4. Egyptian Fruit Bats Seroconvert upon Inoculation with A/Bat/Egypt/381OP/2017 (H9N2)

As shown by an indirect immunofluorescence assay, all directly inoculated animals sacrificed at day 21 had seroconverted against A/bat/Egypt/381OP/2017 (H9N2), whereas all contact animals remained seronegative (Table 3, Supplementary Figure S1). Interestingly, only one out of two inoculated animals sacrificed at 7 dpi was seropositive against A/bat/Egypt/381OP/2017 (H9N2) (inoculated animal #5), while the two contact bats introduced at 1 dpi were seronegative (contact animals #5 and #6). These observations were substantiated by ELISA, where we were able to detect IAV-NP reactive antibodies in two out of four inoculated animals (inoculated animals #1 and #3 at 21 dpi) (Table 3, Supplementary Table S1). A third animal (inoculated animal #2) had a reaction conspicuously higher than the sera taken from naïve animals and was therefore categorized as "questionable". A similar observation was also applicable to one IFA-seropositive animal (inoculated animal #4) euthanized at 21 dpi and to one out of two IFA-seropositive animals (inoculated animal #5) euthanized at 7 dpi. Here, both animals did not overcome the threshold to be placed from "negative" to "questionable" in the ELISA, although signals showed a higher reactivity than the non-inoculated contact animals (Supplementary Materials Table S1). However, particularly concerning inoculated animal #4, this might also be explained by the observations in RT-qPCR, where we could only detect 58 viral genome copy numbers per mL, which does not necessarily lead to a strong seroconversion. Overall, these observations further document the successful infection of Egyptian fruit bats with A/bat/Egypt/381OP/2017 (H9N2).

Table 3. Summary of antibody detection from samples of six fruit bats inoculated with A/bat/Egypt/381OP/2017 (H9N2) and six contact Egyptian fruit bats.

Egyptian Fruit Bats ID	Immunofluorescence Assay */ELISA °		
	0 dpi	7 dpi	21 dpi
Contact animal #1	neg/neg	nd	neg/neg
Contact animal #2	neg/neg	nd	neg/neg
Contact animal #3	neg/neg	nd	neg/neg
Contact animal #4	neg/neg	nd	neg/neg
Contact animal #5	neg/neg	neg/neg	nd
Contact animal #6	neg/neg	neg/neg	nd
Inoculated animal #1	neg/neg	nd	pos/pos
Inoculated animal #2	neg/neg	nd	pos/quest
Inoculated animal #3	neg/neg	nd	pos/pos
Inoculated animal #4	neg/neg	nd	pos/neg
Inoculated animal #5	neg/neg	pos/neg	nd
Inoculated animal #6	neg/neg	neg/neg	nd

* Values considered positive at a dilution > 1:64; nd not done; ° values considered positive according to manufacturer's instructions.

4. Discussion

Our study shows for the first time that oronasal inoculation using LPAIV of subtype H9N2 (A/layer chicken/Bangladesh/VP02-plaque/2016) does not result in any virus replication or specific seroconversion in an experimental setup with Egyptian fruit bats. This suggests that these fruit bats are not susceptible to an avian-origin H9N2 influenza A virus infection. This was of special interest since there was, contrastingly, a clear indication of H9-specific antibodies in African fruit bats [12]. Therefore, the observed insensitivity against avian influenza of subtype H9N2 was unexpected but could have several reasons. On the one hand, the virus strain we used could be incompatible to Egyptian fruit bats. The Eurasian avian H9N2 lineage is divided into three different sub lineages, consisting of the Korean, also called Y439, lineage, the diverse Y280 lineage and the G1 lineage with the reference strain A/Quail/Hong Kong/G1/1997 [20,21]. The strain A/layer chicken/Bangladesh/VP02-plaque/2016 accounts to the latter lineage, which is extremely diverse and contains multiple sub lineages as well [22]. Thus, we cannot fully exclude that Egyptian fruit bats could be susceptible to a different avian H9N2 virus of the G1 lineage. However, it appears to be more likely that Egyptian fruit bats are simply not susceptible to avian H9N2 viruses coming directly from poultry without any adaptation processes. In contrast, in vitro replication studies using lung epithelial cells derived from three different bat species demonstrated a general permissiveness of these cells for other avian influenza viruses, e.g., subtype H6N1 and H2N3 [23]. On the other hand, the host species chosen to be inoculated might have been erroneous. Although specific antibodies against influenza A viruses of subtype H9N2 were demonstrated particularly in straw-colored fruit bats (*Eidolon helvum*) [12], this observation does not likewise guarantee replication of avian H9N2 in Egyptian fruit bats (*Rousettus aegyptiacus*). In addition, the infection dose of $10^{4.7}$ TCID$_{50}$ per animal used in this experimental inoculation could be another factor, potentially in combination with the application route. However, oral swabs taken from naturally infected Egyptian fruit bats were more likely to be tested positive for viral RNA than rectal swabs, highlighting that oral epithelial cells of Egyptian fruit bats are able to replicate IAV [13].

Bat Influenza Viruses May Be Highly Adapted to Particular Bat Species

Despite the fact that bat borne H9N2 showed strong genetic similarities to avian H9N2 viruses, the phylogeny revealed that in contrast to the HA and NA, all inner segments were very divergent from the recent AIV [13,14]. Therefore, this kind of bat flu virus might also exist in straw-colored fruit bats in Ghana and is the reason for the reported H9-seroreactivity [12].

Overall, although inoculation of Egyptian fruit bats with A/layer chicken/Bangladesh/VP02-plaque/2016 (H9N2) did not result in a productive infection of these animals, inoculation and thereby infection of the same species with A/bat/Egypt/381OP/2017 (H9N2) was successful. First indications for a successful infection were detected by a permanent temperature monitoring of four infected and four contact animals, which only showed subtle differences between both groups, that would have been unnoticed by monitoring of the rectal temperature alone. Therefore, monitoring of the body core temperature independent of any manipulation of the animal is important for challenge experiments where only mild or even no clinical signs are to be expected in the infected animals. Although we were not able to detect viral RNA related to A/bat/Egypt/381OP/2017 (H9N2) in oral/rectal swabs and organ samples from the direct contact animals, we demonstrated mucosal epithelium degeneration via histopathologic analysis in contact animal #6 (Figure 7), indicating that the virus was able to be transmitted from bat to bat. Furthermore, we could show that the isolation and propagation of A/bat/Egypt/381OP/2017 (H9N2) from three different Egyptian fruit bat samples of our experiment was successful in embryonated chicken eggs.

In addition to virus isolation and propagation, we observed that all animals directly inoculated with A/bat/Egypt/381OP/2017 (H9N2) and euthanized at 21 dpi displayed seroconversion. Although we could not demonstrate threshold-exceeding seropositivity of all animals in the ELISA that were seropositive in the IFT, we nevertheless saw obvious differences in the data values of these animals compared to the naïve animals (Supplementary Materials Table S1). Taken together, these serological observations further support the evidence of a successful replication of A/bat/Egypt/381OP/2017 (H9N2) in Egyptian fruit bats after direct inoculation, and the RT-qPCR results moreover provide some evidence that the virus is able to be transmitted from bat to bat.

Recently published observations concerning the replication of another bat influenza A virus, H18N11, in various animal models proved that H18N11 is being transmitted among and is able to replicate in bats, whereas replication in mice and ferrets was only weakly detectable [24]. Thus, bat influenza A virus susceptibility, transmission and replication could be species-specific and bats in general might not be susceptible to influenza viruses originating from a non-bat host.

This hypothesis could thereby explain why the same species of flying foxes are susceptible to infection with A/bat/Egypt/381OP/2017 (H9N2), but not to A/layer chicken/Bangladesh/VP02-plaque/2016 (H9N2). However, due to the rapid adaptation processes of influenza viruses in general, the zoonotic potential of these viruses should not be underestimated and cannot be excluded without further experiments. Therefore, future studies will focus in more detail on the different influenza virus infections of fruit bats and the necessary adaptation processes. Our study provided first insights into the host range of different H9N2 viruses and the adaptation of bat-origin H9N2 to Egyptian fruit bats. Future studies will focus on the minimum infectious dose or the reactivity of the host following bat-origin H9N2 infection.

Author Contributions: Conceptualization, D.H., A.B.-B. and M.B.; methodology, N.J.H., M.G., B.H., M.R. and A.B.; formal analysis, N.J.H., A.B. and B.H.; investigation, M.G., N.J.H. and M.R.; data curation, D.H. and A.B.-B.; writing—original draft preparation, N.J.H. and M.G.; writing—review and editing, A.K.; M.A.A., D.H., M.S., M.B. and G.K.; supervision, B.H.; project administration, D.H.; funding acquisition, M.B. and A.B.-B. All authors have read and agreed to the published version of the manuscript.

References

1. Li, C.; Wang, S.; Bing, G.; Carter, R.A.; Wang, Z.; Wang, J.; Wang, C.; Wang, L.; Wu, G.; Webster, R.G.; et al. Genetic evolution of influenza H9N2 viruses isolated from various hosts in China from 1994 to 2013. *Emerg. Microbes Infect.* **2017**, *6*, e106. [CrossRef] [PubMed]

2. Peacock, T.P.; James, J.; Sealy, J.E.; Iqbal, M. A Global Perspective on H9N2 Avian Influenza Virus. *Viruses* **2019**, *11*, 620. [CrossRef] [PubMed]

3. Lam, T.T.-Y.; Wang, J.; Shen, Y.; Zhou, B.; Duan, L.; Cheung, C.-L.; Ma, C.; Lycett, S.J.; Leung, C.Y.-H.; Chen, X.; et al. The genesis and source of the H7N9 influenza viruses causing human infections in China. *Nat. Cell Biol.* **2013**, *502*, 241–244. [CrossRef]

4. Liu, D.; Shi, W.; Shi, Y.; Wang, D.; Xiao, H.; Li, W.; Bi, Y.; Wu, Y.; Li, X.; Yan, J.; et al. Origin and diversity of novel avian influenza A H7N9 viruses causing human infection: Phylogenetic, structural, and coalescent analyses. *Lancet* **2013**, *381*, 1926–1932. [CrossRef]

5. Pan, Y.; Cui, S.; Sun, Y.; Zhang, X.; Ma, C.; Shi, W.; Peng, X.; Lu, G.; Zhang, D.; Liu, Y.; et al. Human infection with H9N2 avian influenza in northern China. *Clin. Microbiol. Infect.* **2018**, *24*, 321–323. [CrossRef] [PubMed]

6. Peiris, M.; Yuen, K.; Leung, C.; Chan, K.; Ip, P.; Lai, R.; Orr, W.; Shortridge, K. Human infection with influenza H9N2. *Lancet* **1999**, *354*, 916–917. [CrossRef]

7. Sun, H.; Wang, K.; Yao, W.; Liu, Q.; Yang, J.; Teng, Q.; Li, X.; Li, Z.; Chen, H. H9N2 Viruses Isolated From Mammals Replicated in Mice at Higher Levels Than Avian-Origin Viruses. *Front. Microbiol.* **2019**, *10*, 416. [CrossRef] [PubMed]

8. Naguib, M.M.; Arafa, A.-S.; Parvin, R.; Beer, M.; Vahlenkamp, T.; Harder, T.C. Insights into genetic diversity and biological propensities of potentially zoonotic avian influenza H9N2 viruses circulating in Egypt. *Virology* **2017**, *511*, 165–174. [CrossRef] [PubMed]

9. Parvin, R.; Begum, J.A.; Chowdhury, E.H.; Islam, M.R.; Beer, M.; Harder, T. Co-subsistence of avian influenza virus subtypes of low and high pathogenicity in Bangladesh: Challenges for diagnosis, risk assessment and control. *Sci. Rep.* **2019**, *9*, 8306. [CrossRef]

10. Tong, S.; Zhu, X.; Li, Y.; Shi, M.; Zhang, J.; Bourgeois, M.; Yang, H.; Chen, X.; Recuenco, S.; Gomez, J.; et al. New World Bats Harbor Diverse Influenza A Viruses. *PLoS Pathog.* **2013**, *9*, e1003657. [CrossRef]

11. Tong, S.; Li, Y.; Rivailler, P.; Conrardy, C.; Castillo, D.A.A.; Chen, L.-M.; Recuenco, S.; Ellison, J.A.; Davis, C.T.; York, I.A.; et al. A distinct lineage of influenza A virus from bats. *Proc. Natl. Acad. Sci. USA* **2012**, *109*, 4269–4274. [CrossRef] [PubMed]

12. Freidl, G.S.; Binger, T.; Müller, M.A.; De Bruin, E.; Van Beek, J.; Corman, V.M.; Rasche, A.; Drexler, J.F.; Sylverken, A.; Oppong, S.K.; et al. Serological Evidence of Influenza A Viruses in Frugivorous Bats from Africa. *PLoS ONE* **2015**, *10*, e0127035. [CrossRef] [PubMed]

13. Kandeil, A.; Gomaa, M.R.; Shehata, M.M.; El Taweel, A.N.; Mahmoud, S.H.; Bagato, O.; Moatasim, Y.; Kutkat, O.; Kayed, A.S.; Dawson, P.; et al. Isolation and Characterization of a Distinct Influenza A Virus from Egyptian Bats. *J. Virol.* **2018**, *93*, e01059-18. [CrossRef]

14. Ciminski, K.; Pfaff, F.; Beer, M.; Schwemmle, M. Bats reveal the true power of influenza A virus adaptability. *PLoS Pathog.* **2020**, *16*, e1008384. [CrossRef] [PubMed]

15. Brunotte, L.; Beer, M.; Horie, M.; Schwemmle, M. Chiropteran influenza viruses: Flu from bats or a relic from the past? *Curr. Opin. Virol.* **2016**, *16*, 114–119. [CrossRef]

16. Reed, L.; Muench, H. A Simple Method of Estimating Fifty Per Cent Endpoints. *Am. J. Epidemiol.* **1938**, *27*, 493–497. [CrossRef]

17. Grund, C.; Hoffmann, D.; Ulrich, R.; Naguib, M.; Schinköthe, J.; Hoffmann, B.; Harder, T.; Saenger, S.; Zscheppang, K.; Tönnies, M.; et al. A novel European H5N8 influenza A virus has increased virulence in ducks but low zoonotic potential. *Emerg. Microbes Infect.* **2018**, *7*, 132. [CrossRef]

18. Toussaint, J.-F.; Sailleau, C.; Mast, J.; Houdart, P.; Czaplicki, G.; Demeestere, L.; Vandenbussche, F.; Van Dessel, W.; Goris, N.; Bréard, E.; et al. Bluetongue in Belgium, 2006. *Emerg. Infect. Dis.* **2007**, *13*, 614–616. [CrossRef]

19. Graaf, A.; Ulrich, R.; Maksimov, P.; Scheibner, D.; Koethe, S.; Abdelwhab, E.M.; Mettenleiter, T.C.; Beer, M.; Harder, T. A viral race for primacy: Co-infection of a natural pair of low and highly pathogenic H7N7 avian influenza viruses in chickens and embryonated chicken eggs. *Emerg. Microbes Infect.* **2018**, *7*, 204. [CrossRef]

20. Dong, G.; Luo, J.; Zhang, H.; Wang, C.; Duan, M.; Deliberto, T.J.; Nolte, D.L.; Ji, G.; He, H. Phylogenetic diversity and genotypical complexity of H9N2 influenza A viruses revealed by genomic sequence analysis. *PLoS ONE* **2011**, *6*, e17212. [CrossRef]

21. Guo, Y.J.; Krauss, S.; Senne, D.A.; Mo, I.P.; Lo, K.S.; Xiong, X.P.; Norwood, M.; Shortridge, K.F.; Webster, R.G.; Guan, Y. Characterization of the Pathogenicity of Members of the Newly Established H9N2 Influenza Virus Lineages in Asia. *Virology* **2000**, *267*, 279–288. [CrossRef] [PubMed]

22. Pusch, E.A.; Suarez, D.L. The Multifaceted Zoonotic Risk of H9N2 Avian Influenza. *Vet. Sci.* **2018**, *5*, 82. [CrossRef] [PubMed]

23. Slater, T.; Eckerle, I.; Chang, K.-C. Bat lung epithelial cells show greater host species-specific innate resistance than MDCK cells to human and avian influenza viruses. *Virol. J.* **2018**, *15*, 68. [CrossRef] [PubMed]

24. Ciminski, K.; Ran, W.; Gorka, M.; Lee, J.; Malmlov, A.; Schinköthe, J.; Eckley, M.; Murrieta, R.A.; Aboellail, T.A.; Campbell, C.L.; et al. Bat influenza viruses transmit among bats but are poorly adapted to non-bat species. *Nat. Microbiol.* **2019**, *4*, 2298–2309. [CrossRef] [PubMed]

Supplementary Data
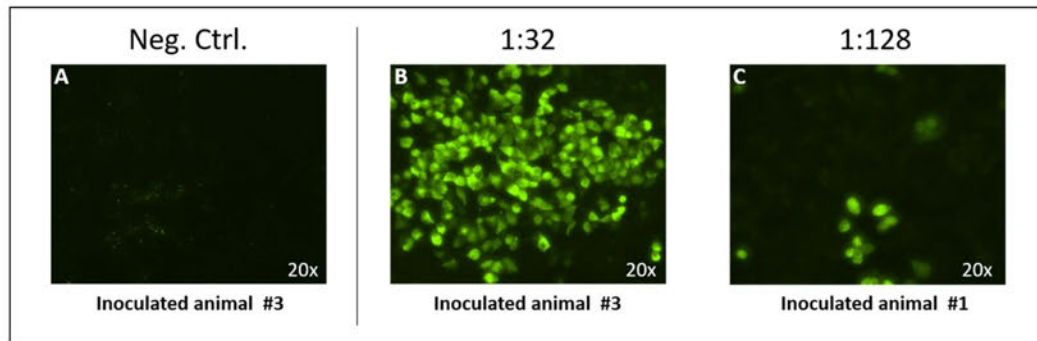
Supplementary Figure S1: Immunofluorescence assay of animal sera showing
sero-reactivity after infection of Egyptian fruit bats with A/bat/Egypt/381OP/2017 (H9N2). Cells were
seeded in a 96-well plate and grown for 24 hours. Afterwards, cells were infected with
A/bat/Egypt/381OP/2017 (H9N2) for 24 hours, followed by fixation with 4% paraformaldehyde (PFA)
and permeabilization with 0.5% Triton-X-100 in PBS. Finally, cells were incubated for 1 h with the
respective animal sera in a dilution series of 1:10 – 1:256, as well as with a negative serum sample of
each respective animal taken before start of the experiment. Pictures were taken at a 20x
magnification **A** Fixed and permeabilized infected cells were incubated for 1 h with negative serum of
the respective animal taken before start of the experiment. **B** Fixed and permeabilized infected cells
were incubated for 1 h with a 1:32 dilution of serum taken from the respective inoculated animal #3
at 21 dpi **C** Fixed and permeabilized infected cells were incubated for 1 h with a 1:128 dilution of
serum taken from the respective inoculated animal #1 at 21 dpi.

Supplementary Table S1: S/P-values of the NP-ELISA with sera collected from animals that were
infected with A/bat/Egypt/381OP/2017 (H9N2)

	S/P-value d0	S/P-value d7	S/P-value d21
Contact animal #1	106,4039871		105,6568482
Contact animal #2	106,8042283		99,92884341
Contact animal #3	103,9224447		101,1295883
Contact animal #4	104,9719806		99,17281922
Contact animal #5	110,0951702	101,2630056	
Contact animal #6	109,9261799	98,55021231	
Inoculated animal #1	105,8169531		21,02641578
Inoculated animal #2	105,3633365		45,21924945
Inoculated animal #3	107,7292534		13,25269088
Inoculated animal #4	107,4268458		53,20644148
Inoculated animal #5	107,1422194	70,62172262	
Inoculated animal #6	108,6631637	82,27341541	

≤45% positive; 45% - 50% questionable; ≥50 % negative

II

<u>Publication II</u>

The bat-borne influenza A virus H9N2 exhibits a set of unexpected pre-pandemic features

<u>Nico Joël Halwe</u>, Lea Hamberger, Julia Sehl-Ewert, Christin Mache, Jacob Schön, Lorenz Ulrich, Sten Calvelage, Mario Tönnies, Jonas Fuchs, Pooja Bandawane, Madhumathi Loganathan, Anass Abbad, Juan Manuel Carreño, Maria C Bermúdez-González, Viviana Simon, Ahmed Kandeil, Rabeh El-Shesheny, Mohamed A. Ali, Ghazi Kayali, Matthias Budt, Stefan Hippenstiel, Andreas C. Hocke, Florian Krammer, Thorsten Wolff, Martin Schwemmle, Kevin Ciminski*, Donata Hoffmann*, Martin Beer*

Submitted to **Nature Medicine, 2023**

(Contacted potential reviewers on the 19ᵗʰ of May, 2023)

manuscripttracking**system**   nature**medicine**

| tracking system home | submission guidelines | reviewer instructions | help | logout | journal home |

Detailed Status Information

Manuscript #	NMED-BC126191
Current Revision #	0
Submission Date	15th May 23
Current Stage	Manuscript under consideration
Title	The bat-borne influenza A virus H9N2 exhibits a set of unexpected pre-pandemic features
Manuscript Type	Brief Communication
Manuscript Comment	We suggest the following reviewers: Rafael Medina (rafael.medina@emory.edu) Daniel R Perez (dperez1@uga.edu) Wanda Markotter (wanda.markotter@up.ac.za) Malik Peiris (malik@hku.hk) Jürgen Richt (jricht@vet.k-state.edu)
Corresponding Author	Professor Martin Beer (Martin.Beer@fli.de) (Friedrich-Loeffler-Institute)
Contributing Authors	Mr Nico Halwe , Lea Hamberger , Julia Sehl-Ewert , Christin Mache , Jacob Schön , Dr Lorenz Ulrich , Sten Calvelage , Dr Jonas Fuchs , Ms Pooja Bandawane , Ms Madhumathi Loganathan , Anass Abbad , Juan Manuel Carreño , Dr Viviana Simon , Dr Ghazi Kayali , Mario Tönnies , Ahmed Kandeil , Rabeh El-Shesheny , Professor Mohamed Ali , Dr Thorsten Wolff , Matthias Budt , Mr Stefan Hippenstiel , Professor Andreas Hocke , Professor Florian Krammer , Professor Martin Schwemmle , Dr Kevin Ciminski , Dr Donata Hoffmann , Maria Bermudez-Gonzalez
Authorship	Yes
Abstract	An Old-World bat H9N2 influenza A virus (IAV) identified in Egypt exhibits high replication and transmission potential in ferrets, efficient infection of human lung explant cultures and marked escape from the antiviral activity of MxA. Together with low antigenic similarity to N2 of seasonal human strains, bat H9N2 meets key criteria for pre-pandemic IAVs.
Subject Terms	Biological sciences/Microbiology/Virology/Influenza virus Health sciences/Diseases/Infectious diseases/Influenza virus Biological sciences/Microbiology/Virology/Viral epidemiology
Show Author Information	Allow Reviewers to see Author information.
Research Square author dashboard	I understand that my manuscript and associated personal data will be shared with Research Square for the delivery of the author dashboard.
In Review	Yes, my co-authors and I would like to opt in to *In Review*
Competing interests policy	**Yes** there is potential Competing Interest. The Icahn School of Medicine at Mount Sinai has filed patent applications relating to influenza virus vaccines, SARS-CoV-2 serological assays and SARS-CoV-2 vaccines which list Florian Krammer as co-inventor. Viviana Simon is also listed as co-inventor on patent applications for SARS-CoV-2 serological assays. Mount Sinai has spun out companies, Kantaro and Castlevax, to market the SARS-CoV-2 related technologies. Florian Krammer has consulted for Merck and Pfizer (before 2020), and is currently consulting for Pfizer, Seqirus, 3rd Rock Ventures, GSK and Avimex. The Krammer laboratory is also collaborating with Pfizer on animal models of SARS-CoV-2 and with Dynavax on universal influenza virus vaccines. All other authors declare no competing interests.
Applicable Funding Source	No Applicable Funding
Previous Interactions	Submitted due to previous interactions with an editor on the journal Editor: Alison Farrell

Stage	Start Date
Manuscript under consideration	20th May 23
Contacting Potential Reviewers	19th May 23
Manuscript under consideration	15th May 23
Editor assigned	15th May 23
Manuscript received	15th May 23
Manuscript submitted	9th May 23

eJournalPress

1 # The bat-borne influenza A virus H9N2 exhibits a set of

2 # unexpected pre-pandemic features

3 Nico Joel Halwe[1], Lea Hamberger[2,3], Julia Sehl-Ewert[4], Christin Mache[5], Jacob

4 Schön[1], Lorenz Ulrich[1], Sten Calvelage[1], Mario Tönnies[6], Jonas Fuchs[2,3], Pooja

5 Bandawane[7,8], Madhumathi Loganathan[7,8], Anass Abbad[7,8], Juan Manuel Carreño[7,8],

6 Maria C Bermúdez-González[7,8], Viviana Simon[7,8,9,10,11], Ahmed Kandeil[12], Rabeh El-

7 Shesheny[12], Mohamed A. Ali[12], Ghazi Kayali[13], Matthias Budt[5], Stefan Hippenstiel[14],

8 Andreas C. Hocke[14], Florian Krammer[7,8,9], Thorsten Wolff[5], Martin Schwemmle[2,3],

9 Kevin Ciminski[2,3*], Donata Hoffmann[1*], Martin Beer[1*]

10

11 [1] Institute of Diagnostic Virology, Friedrich-Loeffler-Institut, 17493 Greifswald, Insel Riems, Germany

12 [2] Institute of Virology, Medical Center-University of Freiburg, 79104 Freiburg, Germany

13 [3] Faculty of Medicine, University of Freiburg, 79104 Freiburg, Germany

14 [4] Department of Experimental Animal Facilities and Biorisk Management, Friedrich-Loeffler-Institut,
15 17493 Greifswald, Insel Riems, Germany

16 [5] Unit 17, Influenza and Other Respiratory Viruses, Robert Koch-Institut, Seestraße 10, 13353 Berlin,
17 Germany

18 [6] HELIOS Clinic Emil von Behring, Department of Pneumology and Department of Thoracic Surgery,
19 Chest Hospital Heckeshorn, Berlin, Germany.

20 [7] Department of Microbiology, Icahn School of Medicine at Mount Sinai, New York, NY 10029, USA

21 [8] Center for Vaccine Research and Pandemic Preparedness (C-VaRPP), Icahn School of Medicine at
22 Mount

23 [9] Department of Pathology, Molecular and Cell Based Medicine, Icahn School of Medicine at Mount
24 Sinai, New York, NY, USA

25 [10] Division of Infectious Diseases, Department of Medicine, Icahn School of Medicine at Icahn School
26 of Medicine at Mount Sinai, New York, NY, USA

27 [11] The Global Health and Emerging Pathogens Institute, Icahn School of Medicine at Mount Sinai, New
28 York, NY, USA

29   [12] Center of Scientific Excellence for Influenza Viruses, National Research Centre, Giza, 12622, Egypt

30   [13] Human Link, Dubai, United Arab Emirates

31   [14] Charité - Universitätsmedizin Berlin, Corporate Member of Freie Universität Berlin and Humboldt-
32   Universität zu Berlin, Department of Infectious Diseases, Respiratory Medicine and Critical Care,
33   Berlin, Germany.

34   *Corresponding authors

2

- 54 -

35 **Abstract**

36 An Old World bat H9N2 influenza A virus (IAV) identified in Egypt exhibits high replication and

37 transmission potential in ferrets, efficient infection of human lung explant cultures and marked

38 escape from the antiviral activity of MxA. Together with low antigenic similarity to N2 of

39 seasonal human strains, bat H9N2 meets key criteria for pre-pandemic IAVs.

40

3

41 **Main**

42 Influenza A viruses (IAVs) are highly infectious viral pathogens that can cross interspecies

43 barriers and infect a wide range of avian and mammalian species[1]. Although bats have long

44 been known to be reservoirs for a variety of viruses[2], they were only recently found to also

45 harbor IAVs[3,4]. While H17N10 and H18N11 strains were first identified in Central and South

46 American bat species[3,4], H9N2 viruses have recently been isolated from Egyptian fruit bats

47 (*Rousettus aegyptiacus*) in the Nile Delta region[5]. Phylogenetic analyses suggest that this Old

48 World bat H9N2 virus is distinct from New World bat IAVs and emerged as a reassortant from

49 an ancestral bat backbone and avian IAV H9 and N2 segments[6]. Avian H9N2 viruses were

50 first isolated from turkeys in North American poultry farms in 1966[7] and subsequently became

51 endemic in poultry farms in many countries in the Middle East and Asia[8,9]. Since then, avian

52 H9N2 viruses have become widespread and have undergone extensive reassortment with

53 other circulating avian IAVs, resulting in at least 74 different lineages[10]. Over the past two

54 decades, avian H9N2 infections have been recorded in swine populations and mink farms[11,12].

55 Furthermore, since 1998, the WHO has reported 82 human spill-over infections with avian IAVs

56 in China or Cambodia, resulting in mild to severe disease[13]. Interestingly, sero-epidemiological

57 data from Ghanaian straw-colored fruit bats showed a high prevalence of H9-specific

58 antibodies (30%)[14], and bat H9N2 was also recently detected in South African bats[15],

59 suggesting widespread circulation of bat H9N2 in African bat populations. Similar to avian

60 H9N2, bat H9N2 initiates infection by utilizing avian IAV-like α2,3 sialic acid receptors, and

61 replicates in mice, but not in adult chickens[5]. Here, we investigated whether bat H9N2 is of

62 zoonotic concern.

63

64 As H9N2 viruses were originally isolated from turkeys[7], we first determined the replication

65 properties of bat H9N2 in one-day-old turkeys. Following oro-nasal inoculation, bat H9N2

66 replicated efficiently to 10^5 to 10^7 copies mL^{-1} at 1 day post infection (dpi; Extended Data Fig.

67 1a). Thereafter, viral loads rapidly decreased but again reached titers of 5×10^5 copies mL^{-1}

68 between 5 to 8 dpi. Infectious virus was isolated from oral swabs collected at 5 dpi (Extended

69 Data Fig. 1a). At 11 dpi, all but one oral swab was negative for viral RNA (Extended Data Fig.

70 1a) and no viral RNA was detected in cloacal swabs at any time point measured. All turkey

71 hatchlings seroconverted with antibodies targeting the viral nucleoprotein (NP) at 21 dpi

72 (Extended Data Fig. 1b,c), demonstrating that bat H9N2 maintained its ability to replicate in

73 turkeys. In contrast, and in agreement with previous reports[5], bat H9N2 failed to replicate

74 efficiently in one-day-old chicken and did not elicit an antibody response (Extended Data Fig.

75 1d,e).

76

4

77 In order to assess the zoonotic potential and transmissibility of bat H9N2 in the model most
78 relevant to humans, we infected 15 donor ferrets and co-housed three naïve contact animals
79 from 1 to 12 dpi (Fig. 1a). Quantification of viral RNA obtained from nasal lavages revealed
80 substantial viral replication (10^6 to 10^8 copies mL^{-1}) within the first two days after infection and
81 continuous shedding of viral genomes up to 10 dpi (Fig. 1a). Strikingly, all contact animals
82 immediately acquired a viral infection from donor ferrets after co-housing with peak titers (10^7
83 copies mL^{-1}) at 4 days post exposure (dpe) (Fig. 1a). To determine whether bat H9N2
84 replication is limited to the upper respiratory tract, we next measured viral titers in the organs
85 of six donor ferrets euthanized at 6 dpi (Fig. 1b). While all ferrets had substantial viral genome
86 copies in the nasal conchae and five of six animals had moderate levels in the trachea, 1 of 6
87 ferrets had moderate viral genome levels in the cranial lung lobe, 2 in the medial and caudal
88 lung lobes, and 1 ferret even had low viral copies in the colon (Fig. 1b). We did not observe
89 severe body weight loss in most donor and any contact ferrets, although two donor animals
90 exhibited ~15% weight loss at 6 and 12 dpi (Fig. 1c), which was most likely unrelated to
91 infection. Elevated body temperatures ranging from 39 to 41°C were observed at 2 dpi in 14
92 of 15 donor ferrets (Fig. 1d) and all contact animals had elevated body temperatures from 1
93 dpe onwards (Fig. 1d). Seroconversion with NP-specific antibodies was detected as early as
94 6 dpi in donor ferrets, and all donor and contact ferrets examined at 21 dpi exhibited a robust
95 NP-specific antibody response (Fig. 1e). Furthermore, at 21 dpi we determined antibodies with
96 a strong neutralizing capacity against bat H9N2 and some degree of cross-neutralization
97 against the avian H9N2 A/layer chicken/Bangladesh/VP02-plaque/2016 isolate (Fig. 1f).
98 Histopathological examination revealed severe purulent to necrotizing rhinitis with viral antigen
99 in the respiratory and olfactory epithelia of all ferrets at 6 dpi (Fig 1g). We observed mild
100 infection-induced changes characterized by focal to oligofocal epithelial necrosis and mild
101 infiltration of the lamina propria in the trachea of four animals. No influenza-associated
102 pathology was detected in the lungs.
103
104 Because severe courses of influenza in humans almost always affect the lower respiratory
105 tract[16], we next infected human *ex vivo* lung cultures with bat H9N2, a prototypic human
106 seasonal H3N2 isolate (A/Panama/2007/1999) or chicken H9N2 and determined viral growth
107 properties. Intriguingly, bat H9N2 replicated to comparable or even higher viral titers than
108 human H3N2, reaching peak titers of 3×10^4 plaque-forming units (PFU) mL^{-1} at 48 hours post
109 infection (hpi; Fig. 2a). In contrast, chicken H9N2 showed minimal viral replication in human
110 lung tissue. Immunostaining of lung explants at 24 hpi revealed that all viruses infected alveolar
111 type II cells (Fig. 2b), which is the primary cellular tropism of IAV in the lung[17].
112

5

113   Next, we studied whether bat H9N2 is able to escape human MxA, a crucial innate antiviral
114   factor which restricts IAVs by inhibiting their polymerase activity[18]. Human-adapted IAVs, such
115   as the pandemic H1N1 virus A/Hamburg/4/2009 (pdmH1N1), acquire characteristic clusters of
116   adaptive mutations in NP that enable escape from MxA[18,19], whereas such clusters are virtually
117   absent in IAVs of avian origin including the highly-pathogenic H5N1 strain A/Thailand/1(KAN-
118   1)/2004 (KAN-1). Bat H9N2 NP also lacks the residues described as conferring MxA resistance
119   (Extended Data Fig. 2a). Thus, as expected, bat H9N2 exhibited a high degree of MxA-
120   sensitivity as demonstrated by infecting MDCK cells stably overexpressing either wild-type
121   MxA (MDCK-MxA) or the antivirally inactive MxA_{T103A} variant (MDCK-MxA_{T103A})[20]. While
122   pdmH1N1, KAN-1 and bat H9N2 replicated efficiently in MDCK-MxA_{T103A} cells to titers between
123   1.3×10^7 and 7×10^8 PFU mL^{-1} at 48 hpi (Fig. 2c), KAN-1 was nearly completely inhibited in
124   MDCK-MxA cells whereas peak titers of pdmH1N1 decreased only 5-fold. Replication of bat
125   H9N2 was potently restricted in the presence of MxA as illustrated by residual viral titers $\leq 10^2$
126   PFU mL^{-1} between 24-48 hpi (Fig. 2c).
127
128   To assess the importance of MxA in controlling bat H9N2 *in vivo*, we intranasally infected wild
129   type C57BL/6 (B6), which lack a functional Mx protein, and human MxA-transgenic (hMxA$^{tg/tg}$)
130   mice with bat H9N2. Surprisingly, lung viral titers were similar in both B6 and MxA-transgenic
131   mice[21] at 3 dpi (5×10^5 PFU mL^{-1}; Fig. 2d), as confirmed by comparable NP levels in lung
132   homogenates detected by Western blotting (Fig. 2f). Interestingly, MxA expression was not
133   observed in the lungs of infected hMxA$^{tg/tg}$ mice, but could be potently induced by IFN-α
134   pretreatment 18 h prior to challenge infection with bat H9N2. Under these conditions, we
135   observed induction of MxA (Fig. 2f) and 10-fold lower lung viral lung titers in hMxA$^{tg/tg}$ compared
136   to B6 mice (Fig. 2c), suggesting that MxA, when induced, reduces bat H9N2 replication.
137
138   Finally, because there is little serological evidence for H9-specific antibodies in the human
139   population[22,23], we wondered whether the antibody responses to circulating seasonal H1N1
140   and H3N2 strains as well as vaccination would be cross-reactive for bat N2. Serum collected
141   from 15 healthy adults before and after seasonal influenza vaccination in 2022/23 revealed no
142   reactivity to bat N2 (Extended Data Fig. 2b,e), but robust reactivity to N2 from the seasonal
143   A/Kansas/14/2017 (H3N2) isolate (Extended Data Fig. 2d).
144
145   Our study shows that the Old World bat H9N2 virus meets key characteristics of a pre-
146   pandemic IAV, including replication in and efficient transmission between ferrets, the ability to
147   replicate efficiently in human lung explants and evasion from MxA-mediated restriction.
148   Intriguingly, bat H9N2 exhibits an immediate (at 1 dpe) and highly efficient transmission
149   potential (100%) not previously observed in any avian-derived H9N2 isolate[24], which may also

6

- 58 -

150 allow for spread among and further adaptation to humans. Our data also suggests that bat
151 H9N2 can suppress the expression of MxA, thereby overcoming this important restriction factor
152 for zoonotic spill-over[25]. This is in strong contrast to zoonotic H5N1 and H7N9 viruses of avian
153 origin that are potently inhibited in hMxA$^{tg/tg}$ mice[21]. Given the ability of bat H9N2 to infect turkey
154 hatchlings, introduction of bat H9N2 into poultry farms and reassortment with avian IAV cannot
155 be ruled out, necessitating increased attention and close monitoring of possible human spill-
156 over infections in Africa.
157
158 A further prerequisite of pre-pandemic viruses is their antigenic novelty to the human immune
159 system. Since the human population is presently exposed only to the currently-circulating
160 H1N1 and H3N2 subtypes, a lack of humoral immunity to bat H9N2 is very likely. Indeed, our
161 serological data demonstrates that seasonal influenza vaccines containing H1N1 and H3N2
162 do not elicit cross-reactive antibodies to the bat N2 protein, substantiating the general pre-
163 pandemic features of bat H9N2.

7

164   **Material and Methods**

165   **Virus**

166   The bat-derived H9N2 A/bat/Egypt/381OP/2017 isolate was propagated in embryonated SPF-
167   chicken eggs for 5 days at 37 °C. Subsequently, the allantoic fluid was harvested and used as
168   virus stock. The chicken H9N2 isolate A/layer chicken/Bangladesh/VP02-plaque/2016 was
169   obtained from the Friedrich-Loeffler-Institut (FLI) virus repository[26]. Virus stocks of the human
170   seasonal A/Panama/2007/1999 (H3N2) isolate were generated by propagation on MDCKII
171   cells. Recombinant A/Hamburg/4/2009 (pdmH1N1) and A/Thailand/1(KAN-1)/2004 (H5N1)
172   were generated utilizing the eight-plasmid pHW2000-based rescue system[27]. All recombinant
173   viruses were plaque purified and then used for stock generation. Stock titers were determined
174   by a plaque assay on MDCKII cells.

175   **Cells**

176   Madin-Darby Canine Kidney (MDCK) type II cells (Collection of Cell Lines in Veterinary
177   Medicine CCLV RIE1061) were used. Cells were incubated at 37 °C under 5% CO_2
178   atmosphere using a mixture of equal volumes of Eagle Minimum Essential Medium (MEM)
179   (Hank's balanced salts solution) and Eagle MEM (Earle's balanced salts solution), 2 mM L-
180   Gln, nonessential amino acids, adjusted to 850 mg L^{-1} NaHCO3, 120 mg L^{-1} sodium pyruvate,
181   pH 7.2 with 10% FCS (Bio & Sell GmbH) or without FCS in the presence of tosylsulfonyl
182   phenylalanyl chloromethyl ketone (TPCK)-treated trypsin (Sigma) after virus addition. MDCK-
183   MxA and MDCK-MxA$_{T103A}$ were cultured in Dulbecco's modified Eagle's medium (DMEM,
184   Gibco, Thermo Fisher Scientific) containing 10% fetal calf serum (FCS), 100 U penicillin and
185   100 µg streptomycin mL^{-1} at 37 °C and 5% CO_2.

186   **Virus infections**

187   MDCK-MxA and MDCK-MxA$_{T103A}$ cells were seeded and grown in 6-well plates. Prior to
188   infection cells were washed with phosphate buffered saline (PBS) containing 0.2% bovine
189   serum albumin (BSA) and then infected with the indicated virus at an MOI of 0.001 in infection
190   medium (DMEM, containing 0.2% BSA and 100 U penicillin and 100 µg streptomycin $µL^{-1}$). For
191   bat H9N2 and pdmH1N1 1 µg mL^{-1} TPCK-treated trypsin was added into the infection medium.
192   Viral titers were determined by plaque assay.

193   **Infection of human lung explants**

194   Fresh lung explants were obtained from patients suffering from lung carcinoma and undergoing
195   lung resection at local thoracic surgeries. Written informed consent was obtained from all

8

196 patients and the study was approved by the ethics committee at the Charité clinic (project
197 EA2/079/13). Tumor-free peripheral lung tissue was cut into small pieces and incubated
198 overnight at 37°C with 5% CO_2 in Roswell Park Memorial Institute (RPMI) 1640 medium. The
199 next day, lung tissue was infected with 1×10^6 PFU of either human seasonal H3N2, chicken
200 H9N2 or bat H9N2 for 1.5 h under shaking conditions and excess virus was removed by three
201 washing steps with PBS. Infected lung tissues were incubated at 37°C and 5% CO_2 for up to
202 72 h in RPMI 1640 medium supplemented with 2 mM L-glutamine and 0.3% BA. Viral titers
203 were determined by plaque assay.

204 **Western blot**

205 Mouse lung samples were incubated at 95°C in Laemmli buffer and subsequently separated
206 by sodium dodecyl sulfate polyacrylamide gel electrophoresis (SDS–PAGE). Separated
207 protein samples were blotted onto a nitrocellulose membrane. Proteins were detected using
208 specific antibodies against the highly conserved G domain in MxA (M143)23, NP (Gene Tex,
209 GTX125989, 1:1,000), or actin (Sigma-Aldrich, A3853; 1:1,000), respectively. Primary
210 antibodies were detected using peroxidase-conjugated secondary antibodies (Jackson
211 ImmunoResearch, 1:5,000).

212 **Animal experiment ethics declarations**

213 All ferret and hatchling experiments were evaluated by the responsible ethics committee of the
214 State Office of Agriculture, Food Safety, and Fishery in Mecklenburg–Western Pomerania
215 (LALLF M-V) and gained governmental approval under the registration numbers LVL MV
216 TSD/7221.3-1-029/22 and 7221.3-1-003/22. All mouse experiments were performed in
217 accordance with the guidelines of the German animal protection law and were approved by
218 the state of Baden-Württemberg (Regierungspräsidium Freiburg; reference number: 35-
219 9185.81/G-19/05).

220 **Animals**

221 One-day-old chickens, one-day-old turkeys, ferrets as well as C57BL/6 (B6) mice and human
222 MxA transgenic (hMxA$^{tg/tg}$) mice were used for this study. Chicks were bread at the FLI from
223 SPF-chicken eggs (VALOBioMedia, Germany) and one-day-old turkeys were ordered and
224 shipped on hatching day from a local breeding facility (Bösel) to the FLI. The ferrets were
225 obtained from the in-house breeding program at the FLI. B6 mice were obtained from Janvier
226 and hMxA$^{tg/tg}$ mice were bred in-house at the Institute of Virology, Freiburg.

227 **One-day-old chicken and turkey studies**

9

228 At the day of hatching, one-day-old turkeys were inoculated with 10^5 TCID$_{50}$ per animal and
229 one-day-old chicks were inoculated with $10^{3.9}$ TCID$_{50}$ per animal, calculated by back-titration
230 of the original inoculum. All hatchlings were sampled daily via cloacal and oro-pharyngeal
231 swabs until 21 dpi or until the animal samples tested negative in a bat H9N2-specific RT-qPCR.
232 Oro-pharyngeal and cloacal swabs were taken using plain swab sterile paper applicator cotton
233 tips 164C (Copan, Brescia, Italy). The swabs were immediately transferred into 1 mL of cell
234 culture medium containing 1% Baytril (Bayer, Leverkusen, Germany), 0.5% lincomycin (WDT,
235 Garbsen, Germany) and 0.2% amphotericin/gentamycin (Fisher Scientific Waltham, MA,
236 USA). After euthanasia, nasal conchae and colon organ samples were taken for investigation
237 of viral genome loads via RT-qPCR analysis in the respective organs. Clinical status of the
238 animals was checked daily.

239 **Ferret study**

240 Ferrets (*Mustela putorius furo*) were housed in multiple connected cage units. Before
241 inoculation, blood samples and nasal washings were collected to confirm naivety to IAV of all
242 animals via serological analysis (ELISA) and RT-qPCR. Body weight, body temperature as
243 well as physical condition of all animals was monitored regularly throughout the animal trial.
244 Nasal washing samples were taken under a short-term isoflurane inhalation anesthesia by
245 applying 750 µl of PBS into each nostril and collecting the efflux. Rectal swabs were taken
246 using plain swab sterile paper applicator cotton tips 164C (Copan). The swabs were
247 immediately transferred into 1 mL of cell culture medium containing 1% Baytril (Bayer,
248 Leverkusen, Germany), 0.5% lincomycin (WDT, Garbsen, Germany) and 0.2%
249 amphotericin/gentamycin (Fisher Scientific Waltham, MA, USA). After one week of
250 acclimatization to their new environment (0 dpi), 15 ferrets were intranasally inoculated with
251 $10^{4.8}$ TCID$_{50}$ per animal in a 200 µL volume (calculated by back-titration of the original material).
252 The inoculum was evenly distributed into each nostril (approximately 100 µl per nostril). At 1
253 dpi, three direct contact animals were co-housed with the donor ferrets. All animals were
254 sampled via nasal washings and rectal swabs daily until 10 dpi and afterwards every second
255 day until 21 dpi or until the samples tested negative via bat H9N2 specific RT-qPCR analysis.
256 Clinical signs of disease (nasal discharge, reduced activity, fever, neurological symptoms and
257 dyspnea), body temperature and body weight were monitored daily. At 6 dpi, in the acute phase
258 of the infection, six donor ferrets were euthanized and subject to necropsy for
259 pathomorphological investigation and analysis of viral genome loads in the upper and lower
260 respiratory organs, as well as in the intestinal tract. The residual animals were kept until the
261 end of the study at 21 dpi to allow for seroconversion. Nasal conchae organ samples from
262 animals euthanized at 21 dpi were analyzed with a bat H9N2-specific RT-qPCR.

10

263 **Mouse study**

264 For infection experiments, mice were anaesthetized with a mixture of ketamine (100 mg per g
265 body weight) and xylazine (5 mg per g body weight) administered intraperitoneally and were
266 subsequently inoculated intranasally with 40 µL of the indicated virus dose diluted in Opti-MEM
267 containing 0.3% BSA. For interferon pretreatment 2 µg per 100 µL IFN-α was administered
268 subcutaneously 18 hours prior to challenge with the indicated virus. Throughout the
269 experiment, mice were monitored daily for changes in body weight and other signs of disease.
270 At 3 dpi mice were sacrificed and the lung was dissected. Organs were homogenized in 1 mL
271 PBS by three subsequent rounds of mechanical treatment for 25 s each at 6.5 ms^{-1}. Tissue
272 debris was removed by centrifuging homogenates for 5 min at 5,000 rpm at 4°C and samples
273 were stored at -80°C until further processing. Viral organ titers were determined by plaque
274 assay.

275 **Propagation of bat H9N2 virus isolates from turkey samples**

276 For isolation of bat H9N2 from turkey hatchlings, swab material was used for inoculation of
277 embryonated chicken eggs. Briefly, 200 µl of selected animal samples were transferred into
278 the allantoic cavity of embryonated SPF-chicken eggs (three eggs per sample), followed by
279 incubation for 5 days at 37°C. Viral genome material was extracted from the allantoic fluid and
280 detected by RT-qPCR analysis.

281 **Pathomorphology and immunohistochemistry**

282 For the ferret histopathology, nasal conchae, trachea, right cranial, medial and caudal lung
283 lobes as well as the colon were sampled. Tissues were fixed in 10% neutral buffered formalin,
284 embedded in paraffin wax and cut at 3 µm sections. To assess tissue architecture and cell
285 morphology sections were stained with hematoxylin and eosin following standard procedures.
286 For viral antigen detection immunohistochemistry was performed using an in house derived
287 rabbit polyclonal primary antibody directed against the influenza nucleoprotein (NP, 1:750)[28].
288 Lesions and cellular vial antigen localization were determined and evaluated by a board-
289 certified pathologist (DiplACVP).
290 To analyze the cellular tropism of IAV infection in human lung tissue samples, tissues
291 were fixed with 4 % paraformaldehyde for 48 h, embedded in paraffin and processed for
292 immunohistochemistry. Lung tissue was then blocked with 5% adequate serum and incubated
293 with primary antibodies direct to CD68 (abcam, Cambridge, UK, 1:50), HT2-280 (terrace
294 biotech, 1:200) and EMP2 (atlas antibodies, 1:50). Viral antigens were stained with polyclonal
295 antibodies to IAV (Serotec, Puchheim, Germany, 1:50) conjugated to a fluorophore (DyLight
296 488, Thermo Fisher). Primary antibodies were detected using a corresponding secondary

11

297 labeling kits (OPAL Polaris, Akoyabio) and nuclear counterstaining was performed using DAPI
298 (Sigma, Hamburg, Germany). Finally tissue sections were mounted in Mowiol, and analyzed
299 using a LSM 780 spectral confocal microscope (objectives 63x Plan-Apochromat/oil, NA 1.4,
300 Zeiss, Germany).

301 **Experimental sample work-up and analysis**

302 Animal organ samples of about 0.1 cm^3 size were first homogenized in a 2 mL Eppendorf-tube
303 containing 1 mL of Hank's balanced salts MEM and Earle's balanced salts MEM (2 mM L-
304 glutamine, 850 mg L^{-1} NaHCO3, 120 mg L^{-1} sodium pyruvate, and 1% penicillin–streptomycin)
305 at 300 Hz using a Tissuelyser II (Qiagen, Hilden, Germany). From each homogenized organ,
306 swab or nasal wash sample, 100 µl was extracted via the NucleoMag Vet kit (Macherey&Nagel,
307 Düren, Germany) according to the manufacturer's instructions on a Biosprint 96 platform
308 (Qiagen). Viral RNA was detected by RT-qPCR using bat H9N2-specific primers and probes[29].
309 Absolute quantification was done using a standard of known concentrations, corresponding to
310 the RNA of the original virus used for inoculation. Quantification was established by the QX200
311 Droplet Digital PCR System in combination with the 1-Step RT-ddPCR Advanced Kit for
312 Probes (BioRad, Hercules, CA, US).

313 **Human sera collected before and after seasonal influenza vaccination**

314 The observational study protocol IRB-16-00772 was reviewed and approved by the Mount
315 Sinai Hospital Institutional Review Board. All study participants provided written informed
316 consent before biospecimens, and data were collected. Permissions to store and share
317 biospecimen were also obtained from all participants. All specimens were coded before
318 processing and analysis. Whole blood was collected through venipuncture into serum
319 separator tubes and sera were stored at −80 °C until analysis.

320 **Serology**

321 Serological analysis of blood samples from all animals at respective blood collection time
322 points was performed by using a commercial IAV-specific enzyme-linked immunosorbent
323 assay (ELISA) detecting NP-specific antibodies (ID-Vet, Montpellier, France) according to the
324 manufacturer's instructions. The antibody titers were expressed as "% inhibition", which was
325 calculated as ((OD_{450} negative control − OD_{450} sample) / OD_{450} negative control) × 100.
326 Neutralizing antibody titers were determined in a virus neutralization test (VNT). Briefly,
327 MDCK cells seeded and grown in 96-well plates 24 hours before infection. Serum samples
328 were serially diluted in DMEM containing 1 µg mL^{-1} TPCK-treated trypsin and then and mixed
329 with 100 $TCID_{50}$ mL^{-1} of either bat or chicken H9N2. After incubation for two hours at 37°C and
330 5% CO_2, the serum-virus mixture was transferred onto MDCK and incubated for 72 hours.

12

331   Neutralization was evaluated by light microscopy for the absence of specific cytopathic effect
332   (CPE), and the corresponding VNT titer was determined from the last serum dilution in which
333   no CPE was observed.
334   ELISAs with human sera against a recombinant version of the N2 NA of H9N2 virus
335   A/bat/Egypt/381OP/2017 were performed as described in detail before[30]. Recombinant NA
336   from human seasonal H3N2 strain A/Kansas/14/2017 was used as to show positive reactivity,
337   recombinant NA from the Wuhan spiny eel influenza virus[31] (to which humans are naïve) was
338   used as contrast to show negative reactivity. Recombinant proteins were expressed as
339   described previously[32]. Sera collected from 15 study participants before and after receiving the
340   2022/23 seasonal influenza vaccination were used to determine reactivity to N2 from H9N2,
341   N2 from seasonal H3N2 or to the Wuhan spiny eel influenza virus NA. Monoclonal antibody
342   1G01[33] was used as positive control in all cases.

13

Acknowledgements

360

14

361 **Author contributions**

362 N.J.H., D.H. and M.Be. conceived the study. N.J.H., J.S., L.U. and D.H. designed and
363 performed turkey, chicken and ferret experiments. J.S.E. and L.U. performed ferret pathology.
364 C.M., M.T., M.Bu., S.H., A.C.H. and T.W. designed and performed human lung explant
365 infection experiments. L.H., J.F. and K.C. designed and performed mouse infections. P.B.,
366 M.L., A.A., J.M.C., V.S. and F.K. collected serum samples, and designed and performed
367 serological analysis. A.K., R.E.S., M.A.A. and G.K. provided reagents. S.C. performed
368 computational analysis. N.J.H., M.S., K.C. and M.Be. wrote the original draft. N.J.H., J.S.E.,
369 L.U., F.K., M.S., K.C., D.H. and M.Be. reviewed and edited the paper. T.W., S.H., A.C.H., M.S.,
370 K.C. and M.Be. acquired funds.

371

15

- 67 -

372 **Competing interests**

382

- 17 -

383 **Data and materials availability**

384 All data are available in the main text or supplementary materials.

385

17

References

1   Long, J. S., Mistry, B., Haslam, S. M. & Barclay, W. S. Host and viral determinants of influenza A virus species specificity. *Nat Rev Microbiol* **17**, 67-81, doi:10.1038/s41579-018-0115-z (2019).

2   Letko, M., Seifert, S. N., Olival, K. J., Plowright, R. K. & Munster, V. J. Bat-borne virus diversity, spillover and emergence. *Nat Rev Microbiol* **18**, 461-471, doi:10.1038/s41579-020-0394-z (2020).

3   Tong, S. *et al.* A distinct lineage of influenza A virus from bats. *Proc Natl Acad Sci U S A* **109**, 4269-4274, doi:10.1073/pnas.1116200109 (2012).

4   Tong, S. *et al.* New world bats harbor diverse influenza A viruses. *PLoS Pathog* **9**, e1003657, doi:10.1371/journal.ppat.1003657 (2013).

5   Kandeil, A. *et al.* Isolation and Characterization of a Distinct Influenza A Virus from Egyptian Bats. *J Virol* **93**, doi:10.1128/JVI.01059-18 (2019).

6   Ciminski, K., Pfaff, F., Beer, M. & Schwemmle, M. Bats reveal the true power of influenza A virus adaptability. *PLoS Pathog* **16**, e1008384, doi:10.1371/journal.ppat.1008384 (2020).

7   Homme, P. J. & Easterday, B. C. Avian influenza virus infections. I. Characteristics of influenza A-turkey-Wisconsin-1966 virus. *Avian Dis* **14**, 66-74 (1970).

8   Afifi, M. A., El-Kady, M. F., Zoelfakar, S. A. & Abdel-Moneim, A. S. Serological surveillance reveals widespread influenza A H7 and H9 subtypes among chicken flocks in Egypt. *Trop Anim Health Prod* **45**, 687-690, doi:10.1007/s11250-012-0243-9 (2013).

9   Li, C. *et al.* Genetic evolution of influenza H9N2 viruses isolated from various hosts in China from 1994 to 2013. *Emerg Microbes Infect* **6**, e106, doi:10.1038/emi.2017.94 (2017).

10   Dong, G. *et al.* Phylogenetic diversity and genotypical complexity of H9N2 influenza A viruses revealed by genomic sequence analysis. *PLoS One* **6**, e17212, doi:10.1371/journal.pone.0017212 (2011).

11   Cong, Y. L. *et al.* Swine infection with H9N2 influenza viruses in China in 2004. *Virus Genes* **36**, 461-469, doi:10.1007/s11262-008-0227-z (2008).

12   Zhang, C. *et al.* Avian influenza virus H9N2 infections in farmed minks. *Virol J* **12**, 180, doi:10.1186/s12985-015-0411-4 (2015).

13   WHO. *Avian Influenza Weekly Update Number 877*, <https://www.who.int/docs/default-source/wpro---documents/emergency/surveillance/avian-influenza/ai_20230106.pdf?sfvrsn=5f006f99_108> (2023).

18

424   14   Freidl, G. S. *et al.* Serological evidence of influenza A viruses in frugivorous
425   bats from Africa. *PLoS One* **10**, e0127035, doi:10.1371/journal.pone.0127035
426   (2015).

427   15   Rademan, R., Geldenhuys, M. & W., M. Detection and Characterization of an
428   H9N2 Influenza A Virus in the Egyptian Rousette Bat in Limpopo, South Africa.
429   *Viruses* **15**, doi:10.3390/v15020498 (2023).

430   16   Taubenberger, J. K. & Morens, D. M. The pathology of influenza virus
431   infections.   *Annu   Rev   Pathol   3,   499-522,*
432   doi:10.1146/annurev.pathmechdis.3.121806.154316 (2008).

433   17   Weinheimer, V. K. *et al.* Influenza A viruses target type II pneumocytes in the
434   human lung. *J Infect Dis* **206**, 1685-1694, doi:10.1093/infdis/jis455 (2012).

435   18   Zimmermann, P., Manz, B., Haller, O., Schwemmle, M. & Kochs, G. The viral
436   nucleoprotein determines Mx sensitivity of influenza A viruses. *J Virol* **85**,
437   8133-8140, doi:10.1128/JVI.00712-11 (2011).

438   19   Manz, B. *et al.* Pandemic influenza A viruses escape from restriction by human
439   MxA through adaptive mutations in the nucleoprotein. *PLoS Pathog* **9**,
440   e1003279, doi:10.1371/journal.ppat.1003279 (2013).

441   20   Ashenberg, O., Padmakumar, J., Doud, M. B. & Bloom, J. D. Deep mutational
442   scanning identifies sites in influenza nucleoprotein that affect viral inhibition
443   by MxA. *PLoS Pathog* **13**, e1006288, doi:10.1371/journal.ppat.1006288 (2017).

444   21   Deeg, C. M. *et al.* In vivo evasion of MxA by avian influenza viruses requires
445   human signature in the viral nucleoprotein. *J Exp Med* **214**, 1239-1248,
446   doi:10.1084/jem.20161033 (2017).

447   22   Nachbagauer, R. *et al.* Defining the antibody cross-reactome directed against
448   the influenza virus surface glycoproteins. *Nat Immunol* **18**, 464-473,
449   doi:10.1038/ni.3684 (2017).

450   23   Meade, P. *et al.* Influenza Virus Infection Induces a Narrow Antibody Response
451   in Children but a Broad Recall Response in Adults. *mBio* **11**,
452   doi:10.1128/mBio.03243-19 (2020).

453   24   Wan, H. *et al.* Replication and transmission of H9N2 influenza viruses in
454   ferrets: evaluation of pandemic potential. *PLoS One* **3**, e2923,
455   doi:10.1371/journal.pone.0002923 (2008).

456   25   Ciminski, K., Chase, G. P., Beer, M. & Schwemmle, M. Influenza A Viruses:
457   Understanding Human Host Determinants. *Trends Mol Med* **27**, 104-112,
458   doi:10.1016/j.molmed.2020.09.014 (2021).

459   26   Parvin, R. *et al.* Co-subsistence of avian influenza virus subtypes of low and
460   high pathogenicity in Bangladesh: Challenges for diagnosis, risk assessment
461   and control. *Sci Rep* **9**, 8306, doi:10.1038/s41598-019-44220-4 (2019).

19

462 27 Hoffmann, E., Krauss, S., Perez, D., Webby, R. & Webster, R. G. Eight-plasmid
463   system for rapid generation of influenza virus vaccines. *Vaccine* **20**, 3165-
464   3170, doi:10.1016/s0264-410x(02)00268-2 (2002).

465 28 Abdelwhab el, S. M. *et al.* Prevalence of the C-terminal truncations of NS1 in
466   avian influenza A viruses and effect on virulence and replication of a highly
467   pathogenic   H7N1   virus   in   chickens.   *Virulence*   **7**,   546-557,
468   doi:10.1080/21505594.2016.1159367 (2016).

469 29 Halwe, N. J. *et al.* Egyptian Fruit Bats (Rousettus aegyptiacus) Were Resistant
470   to Experimental Inoculation with Avian-Origin Influenza A Virus of Subtype
471   H9N2, But Are Susceptible to Experimental Infection with Bat-Borne H9N2
472   Virus. *Viruses* **13**, doi:10.3390/v13040672 (2021).

473 30 Carreno, J. M. *et al.* Activity of convalescent and vaccine serum against SARS-
474   CoV-2 Omicron. *Nature* **602**, 682-688, doi:10.1038/s41586-022-04399-5
475   (2022).

476 31 Arunkumar, G. A. *et al.* Functionality of the putative surface glycoproteins of
477   the   Wuhan   spiny   eel   influenza   virus.   *Nat   Commun*   **12**,   6161,
478   doi:10.1038/s41467-021-26409-2 (2021).

479 32 Margine, I., Palese, P. & Krammer, F. Expression of functional recombinant
480   hemagglutinin and neuraminidase proteins from the novel H7N9 influenza
481   virus using the baculovirus expression system. *J Vis Exp*, e51112,
482   doi:10.3791/51112 (2013).

483 33 Stadlbauer, D. *et al.* Broadly protective human antibodies that target the
484   active site of influenza virus neuraminidase. *Science* **366**, 499-504,
485   doi:10.1126/science.aay0678 (2019).

486

20

487 **Figure Legends**

488 **Fig. 1: Ferrets are highly susceptible to bat H9N2. a** Ferrets (n= 15) were inoculated with
489 $10^{4.8}$ TCID$_{50}$ of bat H9N2 IAV per animal. At 1 dpi, direct contact animals (n= 3) were co-
490 housed. Viral shedding was measured by nasal lavage. Dashed line indicates detection limit.
491 **b** Organs collected from euthanized ferrets (n= 6) at 6 dpi with bat H9N2 were tested by RT-
492 qPCR to determine viral genome copies. Dashed line indicates detection limit. Data are mean
493 ± SD. **c** Changes in body weight relative to 0 dpi of bat H9N2-infected (n= 15) and contact (n=
494 3) ferrets were monitored throughout the course of the experiment. **d** Body temperatures of
495 donor and naïve contact ferrets were monitored from 0 to 14 dpi. Dashed line at 40°C indicates
496 fever. **e** Ferret serum antibody titers in an IAV NP-specific ELISA at the indicated time points.
497 Dashed lines indicates threshold between 45% and 50% inhibition. Mean antibody titers are
498 indicated. **f** Ferret neutralizing antibody titers against bat H9N2 and chicken H9N2. **g**
499 Histopathologic findings with detection of viral antigen in the nasal mucosa of bat H9N2-
500 infected ferrets (n= 6) at 6 dpi. Acute severe rhinitis with diffuse necrosis of the olfactory
501 epithelium (arrow) and infiltrating neutrophils (asterisk) (1). Intralesional viral antigen (NP) is
502 abundant in degenerated and desquamated epithelial cells (arrowhead) (2). The inset (3) is a
503 higher magnification of the center of the image (2). Scale bar, 100 µm (main panels), 25 µm
504 (inset).

505

506 **Fig. 2: Bat H9N2 replicates in human lung explants and suppresses induction of MxA in**
507 **MxA-transgenic mice. a** Human lung tissue explants (n= 4) were infected with human H3N2,
508 chicken H9N2 or bat H9N2 with 1×10^6 PFU, and viral titers were determined at the indicated
509 time points. Error bars indicate standard deviation and statistical analysis was performed using
510 non-paired, non-parametric Kruskal-Wallis test (*p<0.05). Data are mean ± SE of n= 4
511 independent experiments. **b** At 24 hpi, human lung explants were stained for alveolar type I
512 (AT1) (cyan) and type II (AT2) cells (yellow), CD68 indicating alveolar macrophages (green)
513 and IAV antigens (red). Note, in chicken H9N2 and bat H9N2 infected cells, AT2 labeling was
514 omitted for better visualization. White arrows indicate infected cells. Scale bar, 10 µm. **c** MDCK
515 cells overexpressing MxA or inactive MxA$_{T103A}$ were infected with human-adapted pdmH1N1,
516 avian KAN-1 or bat H9N2 at an MOI of 0.001, and viral titers were determined at the indicated
517 time points. Data are mean ± SD of n= 3 independent experiments; statistical analysis was
518 performed using two-tailed t-tests; **P=0.01; ****P=0.0001. Dashed line indicates detection
519 limit. **d** hMxA$^{tg/tg}$ (n= 8) or wild-type B6 mice (n= 8) were infected with 1×10^4 PFU. Lung viral
520 titers were determined 3 dpi. **e** hMxA$^{tg/tg}$ (n= 6) or wild-type B6 mice (n= 7) were pretreated
521 with IFN-α 18 h prior to infection with 1×10^4 PFU. Lung viral titers were determined 3 dpi. Data

21

522 are mean ± SD; statistical analysis was performed using two-tailed *t*-tests; ****P=0.0001. **f**
523 MxA, NP and actin protein levels in homogenized lungs from IFN-α pretreated or infected mice
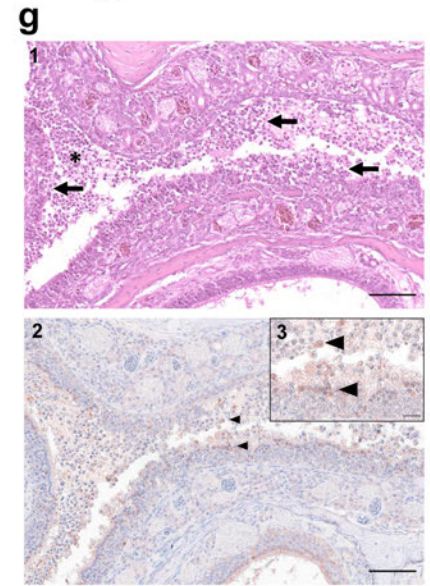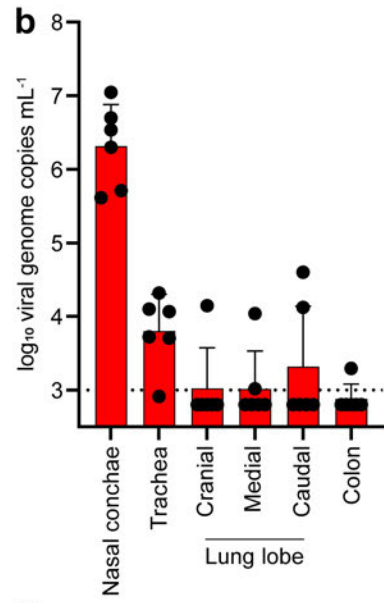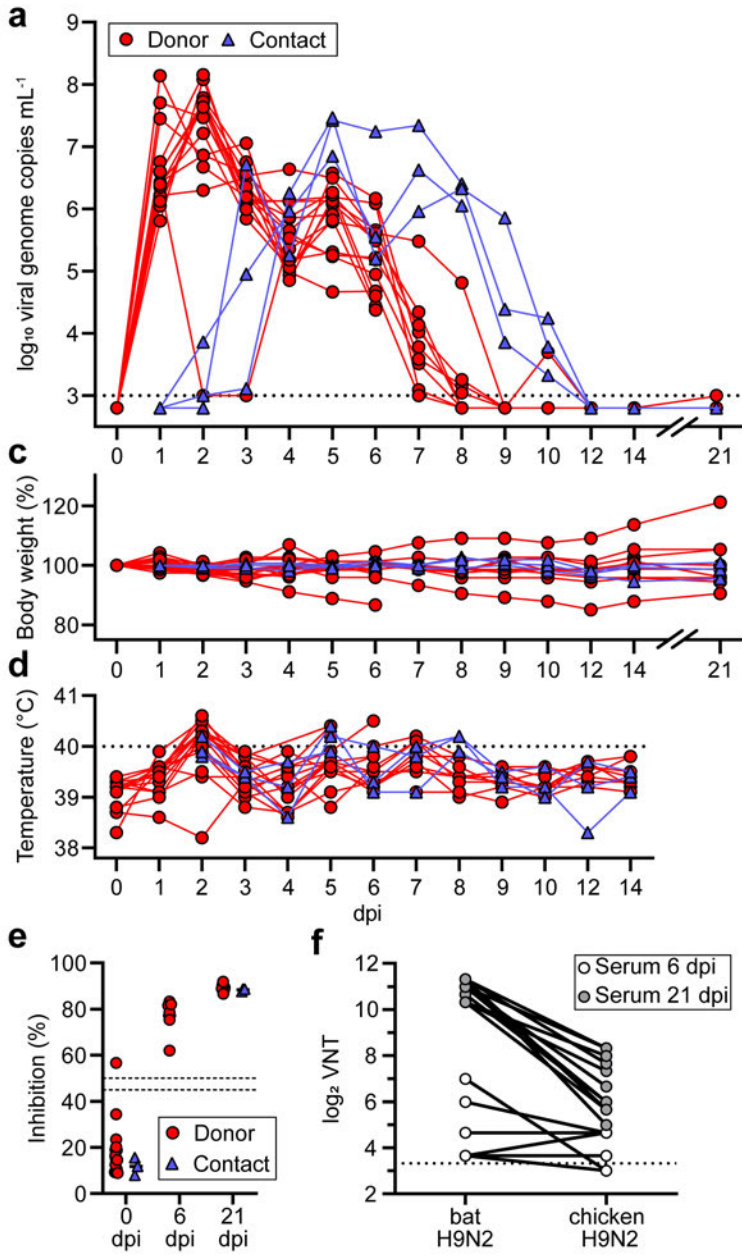524 from (**d,e**) were detected by Western blot.

525

526 **Extended Data Fig. 1: Bat H9N2 replicates efficiently in turkey but not chicken**
527 **hatchlings. a** Turkey hatchlings (*n*= 13) were oro-nasally inoculated with bat H9N2 and viral
528 shedding was monitored by RT-qPCR analysis of oro-pharyngeal swab samples. Asterisk
529 indicates successful virus isolation from swab material. Dashed line indicates detection limit.
530 **b** Serum antibody titers of turkey hatchlings before and after bat H9N2 infection were
531 determined by an IAV NP-specific ELISA. Dashed lines indicates threshold between 45% and
532 50% inhibition. Mean antibody titers are indicated. **c** Neutralizing antibody titers against bat
533 H9N2. **d** A group of chicken hatchlings (*n*= 13) was oro-nasally inoculated with bat H9N2 and
534 viral shedding was monitored by RT-qPCR analysis of oro-pharyngeal swab samples. Dashed
535 line indicates detection limit. **e** Serum antibody titers of chicken hatchlings at 21 dpi with bat
536 H9N2 were determined by an IAV NP-specific ELISA. Dashed lines indicate threshold area
537 between 45% and 50% inhibition. Mean antibody titers are indicated.

538

539 **Extended Data Fig. 2: No cross-reactive antibodies to bat N2 among individuals**
540 **vaccinated against seasonal influenza. a** Known MxA escape mutations in NP from the
541 1918 and the 2009 pdmH1N1 strains are highlighted in red and the resistance patch of the
542 Eurasian avian-like swine isolate Belzig is shown in blue. Note that the avian-adapted IAV
543 KAN-1 and bat H9N2 do not harbor any of the known MxA-resistance amino acid residues.
544 The NP model was created with PyMol based on the available crystal structure (PDB code:
545 2Q06). **b** Reactivity of sera from 15 healthy adults taken before the 2022/23 seasonal influenza
546 vaccination to recombinant N2 from bat H9N2. **c,d** Reactivity of the same sera against the
547 recombinant N2 of a recent seasonal H3N2 strain (**c**) and the recombinant NA of the Wuhan
548 spiny eel influenza virus (**d**). **e** Pre- and post- seasonal vaccination reactivity of sera from 15
549 healthy adults who received the 2022/23 seasonal influenza virus vaccine against recombinant
550 N2 from the bat H9N2 virus. Reactivity was quantified as area under the curve (AUC). A paired
551 *t*-test was used to determine statistical differences. For **b, c** and **d,** mAb 1G01 was used as
552 positive control, an irrelevant human mAbs was used as negative control.

553

22

nature portfolio

Corresponding author(s):   Kevin Ciminski
Donata Hofmmann
Martin Beer

Last updated by author(s):   May 11, 2023
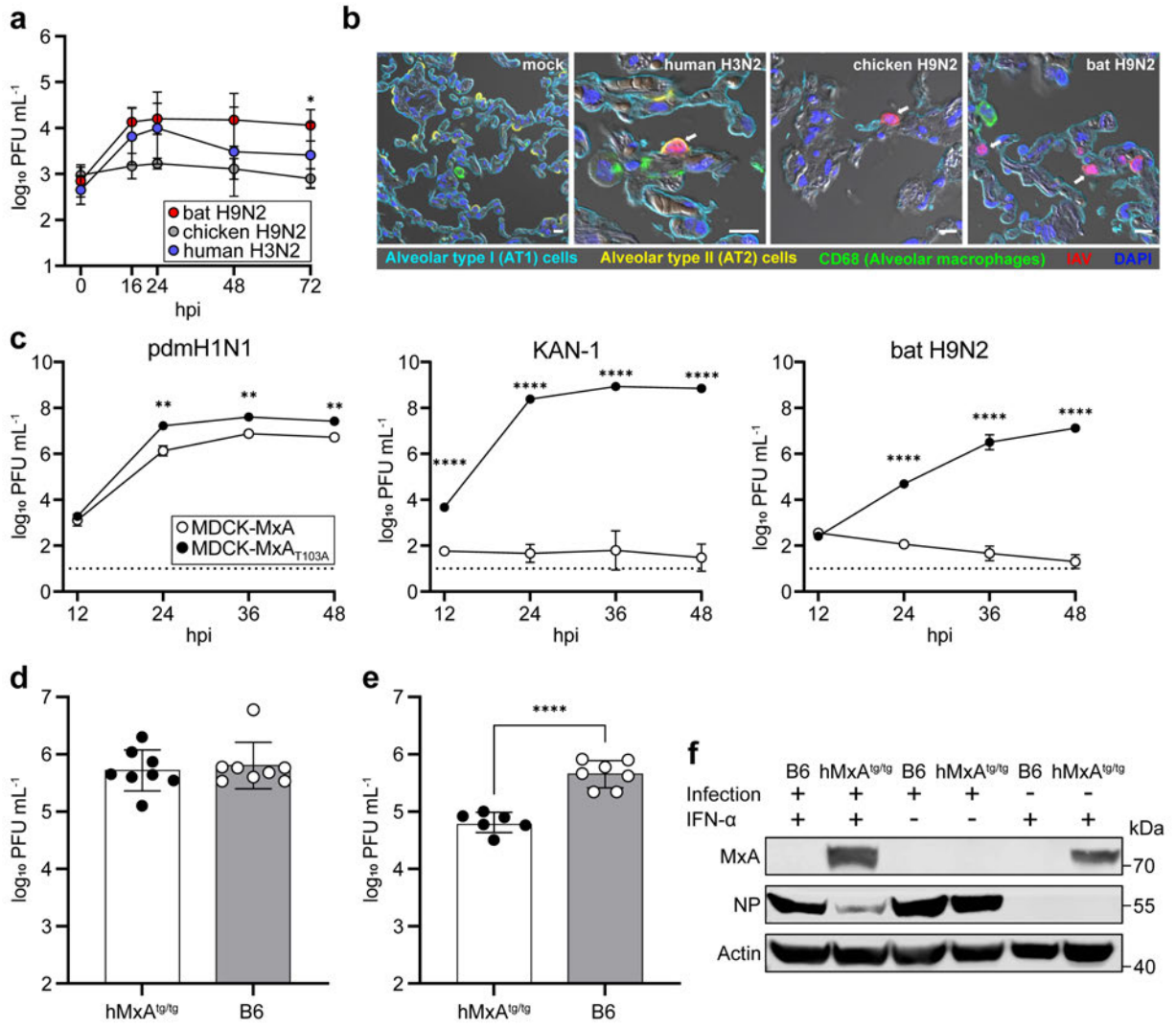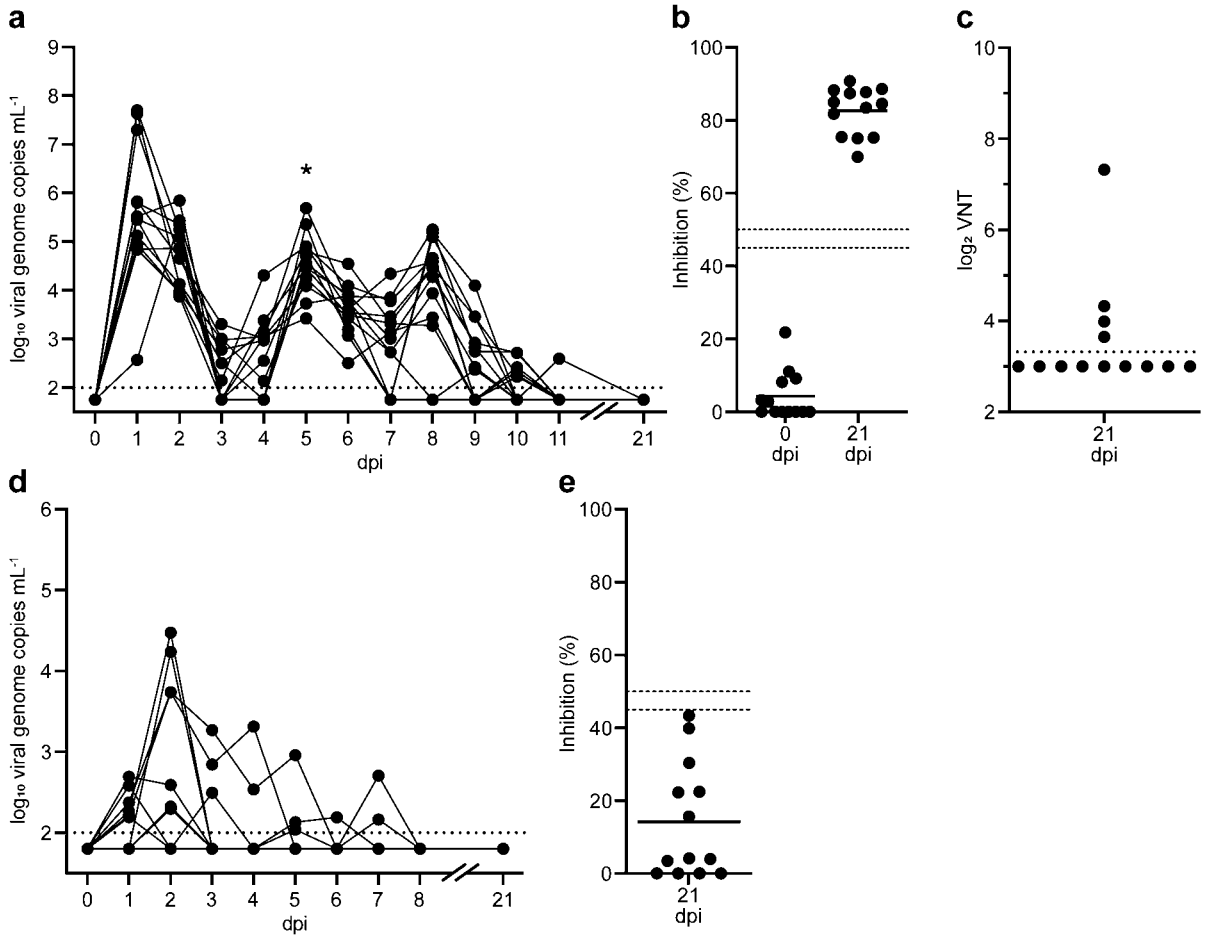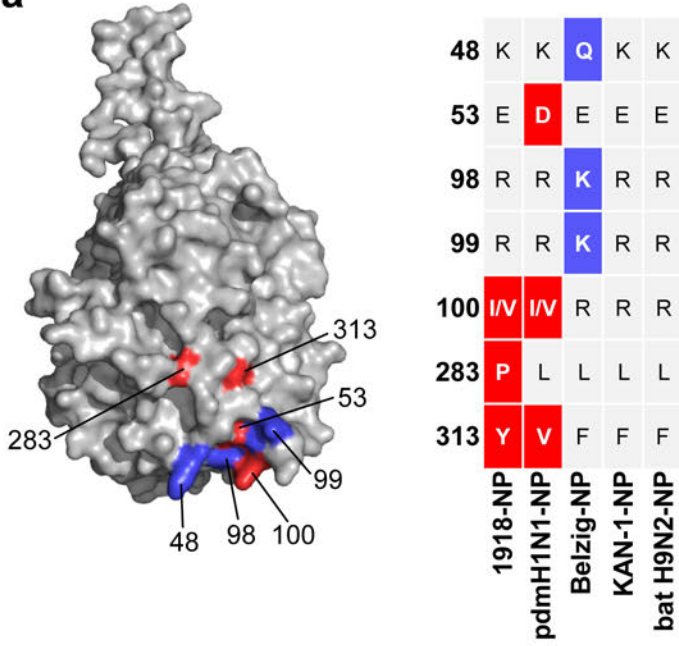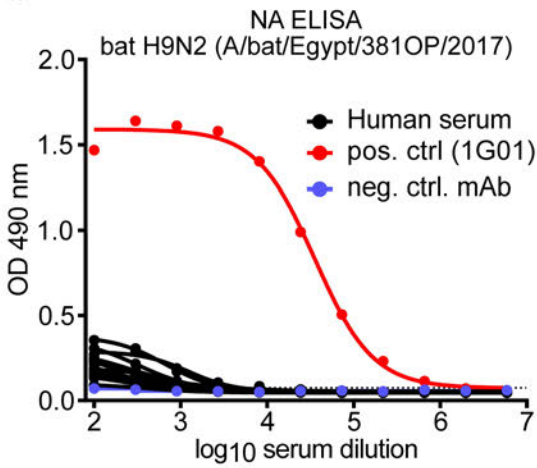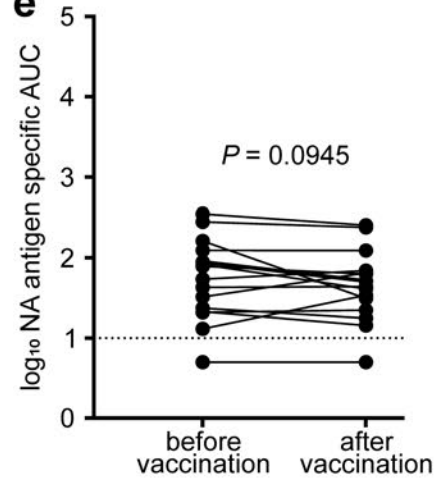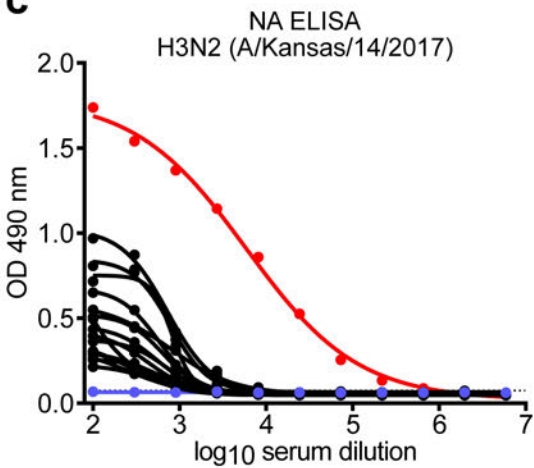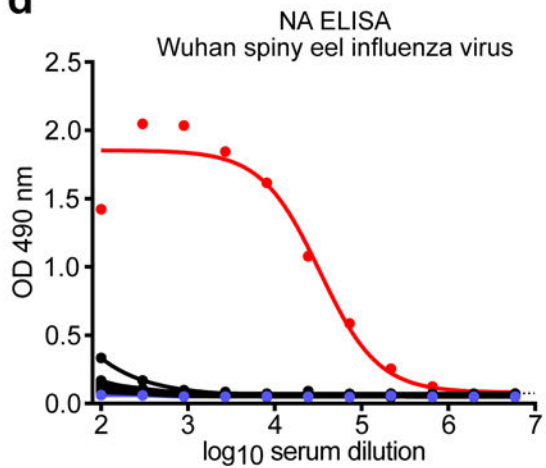
Editorial Policy Checklist

This form is used to ensure compliance with Nature Portfolio editorial policies related to research ethics and reproducibility. For further information, please see our **editorial policies** site. All relevant questions on the form must be answered.

Competing interests

Policy information about **competing interests**

In the interest of transparency and to help readers form their own judgements of potential bias, Nature Portfolio journals require authors to declare any competing financial and/or non-financial interest in relation to the work described in the submitted manuscript.

Competing interests declaration

☐ We declare that none of the authors have competing financial or non-financial interests as defined by Nature Portfolio.

☒ We declare that one or more of the authors have a competing interest as defined by Nature Portfolio.

The Icahn School of Medicine at Mount Sinai has filed patent applications relating to influenza virus vaccines, SARS-CoV-2 serological assays and SARS-CoV-2 vaccines which list Florian Krammer as co inventor. Viviana Simon is also listed as co-inventor on patent applications for SARS-CoV-2 serological assays. Mount Sinai has spun out companies, Kantaro and Castlevax, to market the SARS-CoV-2 related technologies. Florian Krammer has consulted for Merck and Pfizer (before 2020), and is currently consulting for Pfizer, Seqirus, 3rd Rock Ventures, GSK and Avimex. The Krammer laboratory is also collaborating with Pfizer on animal models of SARS CoV 2 and with Dynavax on universal influenza virus vaccines. All other authors declare no competing interests.

Authorship

Policy information about **authorship**

Prior to submission all listed authors must agree to all manuscript contents, the author list and its order and the author contribution statements. Any changes to the author list after submission must be approved by all authors.

☒ We have read the Nature Portfolio Authorship Policy and confirm that this manuscript complies.

Policy information about Authorship: inclusion & ethics in global research

All authors are encouraged to provide an "Inclusion & Ethics" statement where relevant.

☐ We have provided an "Inclusion & Ethics" statement.

Data availability

Policy information about **availability of data**

Data availability statement

All manuscripts must include a **data availability statement**. This statement should provide the following information, where applicable:
- Accession codes, unique identifiers, or web links for publicly available datasets
- A description of any restrictions on data availability
- For clinical datasets or third party data, please ensure that the statement adheres to our **policy**

☒ We have provided a full data availability statement in the manuscript.

Mandated accession codes (where applicable)

Confirm that all relevant data are deposited into a public repository and that accession codes are provided.

☒ All relevant accession codes are provided   ☐ Accession codes will be available before publication   ☐ No data with mandated deposition

Code availability

Policy information about availability of computer code

Code availability statement

For all studies using custom code or mathematical algorithm that is deemed central to the conclusions, the manuscript must include a statement under the heading "Code availability" describing how readers can access the code, including any access restrictions. Code availability statements should be provided as a separate section after the data availability statement but before the References.

☐ We have provided a full code availability statement in the manuscript

Data presentation

For all data presented in a plot, chart or other visual representation confirm that:

n/a	Confirmed	
☐	☒	Individual data points are shown when possible, and always for $n \leq 10$
☐	☒	The format shows data distribution clearly (e.g. dot plots, box-and-whisker plots)
☒	☐	Box-plot elements are defined (e.g. center line, median; box limits, upper and lower quartiles; whiskers, 1.5x interquartile range; points, outliers)
☐	☒	Clearly defined error bars are present and what they represent (SD, SE, CI) is noted

Image integrity

Policy information about image integrity

☒ We have read Nature Portfolio's image integrity policy and all images comply.

Unprocessed data must be provided upon request. Please double-check figure assembly to ensure that all panels are accurate (e.g. all labels are correct, no inadvertent duplications have occurred during preparation, etc.).

Where blots and gels are presented, please take particular care to ensure that lanes have not been spliced together, that loading controls are run on the same blot, and that unprocessed scans match the corresponding figures.

Additional policy considerations

Some types of research require additional policy disclosures. Please indicate whether each of these apply to your study. If you are not certain, please read the appropriate section before selecting a response.

Does not apply	Involved in the study
☒ ☐	Macromolecular structural data
☒ ☐	Unique biological materials
☐ ☒	Research animals and/or animal-derived materials that require ethical approval
☒ ☐	Human embryos, gametes and/or stem cells
☐ ☒	Human research participants
☒ ☐	Clinical data
☒ ☐	Archaeological, geological, and palaeontological materials

Research animals

Policy information about studies involving animals; ARRIVE guidelines recommended for reporting animal research

Ethical compliance

☒ We have complied with all relevant ethical regulations and include a statement affirming this in the manuscript.

Ethics committee

☒ We have disclosed the name(s) of the board and institution that approved the study protocol in the manuscript.

2

Human research participants

Policy information about studies involving human research participants

Ethical compliance

☒ We have complied with all relevant ethical regulations and include a statement affirming this in the manuscript.

Ethics committee

Confirm that the manuscript states the name(s) of the board and/or institution that:

☒ Approved the study protocol   -OR-   ☐ Provided guidelines for study procedures (if protocol approval is not required)

Informed consent

☒ We have obtained informed consent from all participants and this is noted in the manuscript.

Identifiable images

For publication of identifiable images of research participants, confirm that consent to publish was obtained and is noted in the Methods.

Authors must ensure that consent meets the conditions set out in the Nature Portfolio participant release form.

☐ Yes   ☒ No identifiable images of human research participants

---

I certify that all the above information is complete and correct.

Typed signature   Martin Beer   Date   12.05.2023

nature portfolio

Corresponding author(s): Kevin Ciminski
Donata Hoffmann
Martin Beer

Last updated by author(s): May 11, 2023

Reporting Summary

Nature Portfolio wishes to improve the reproducibility of the work that we publish. This form provides structure for consistency and transparency in reporting. For further information on Nature Portfolio policies, see our Editorial Policies and the Editorial Policy Checklist.

Statistics

For all statistical analyses, confirm that the following items are present in the figure legend, table legend, main text, or Methods section.

n/a	Confirmed	
☐	☒	The exact sample size (n) for each experimental group/condition, given as a discrete number and unit of measurement
☒	☐	A statement on whether measurements were taken from distinct samples or whether the same sample was measured repeatedly
☐	☒	The statistical test(s) used AND whether they are one- or two-sided *Only common tests should be described solely by name; describe more complex techniques in the Methods section.*
☒	☐	A description of all covariates tested
☒	☐	A description of any assumptions or corrections, such as tests of normality and adjustment for multiple comparisons
☐	☒	A full description of the statistical parameters including central tendency (e.g. means) or other basic estimates (e.g. regression coefficient) AND variation (e.g. standard deviation) or associated estimates of uncertainty (e.g. confidence intervals)
☒	☐	For null hypothesis testing, the test statistic (e.g. F, t, r) with confidence intervals, effect sizes, degrees of freedom and P value noted *Give P values as exact values whenever suitable.*
☒	☐	For Bayesian analysis, information on the choice of priors and Markov chain Monte Carlo settings
☒	☐	For hierarchical and complex designs, identification of the appropriate level for tests and full reporting of outcomes
☒	☐	Estimates of effect sizes (e.g. Cohen's d, Pearson's r), indicating how they were calculated

Our web collection on statistics for biologists contains articles on many of the points above.

Software and code

Policy information about availability of computer code

Data collection	ELISA: Tecan i-control 2014 1.11
Data analysis	relative quantification: Bio-Rad CFX Maestro 1.1 Version 4.1.2433.1219
	sequence analysis: Geneious Prime ® 2019.2.3
	figures: GraphPad Prism 8.4.2 (679) for Windows, Microsoft PowerPoint 2016 (16.0.4266.1001)
	NGS: Genome Sequencer Software Suite (version 2.6; Roche, https://roche.com), variant analysis tool integrated in Geneious Prime (2019.2.3)
	ELISA: Microsoft Excel 2016 (16.0.5188.1000)

For manuscripts utilizing custom algorithms or software that are central to the research but not yet described in published literature, software must be made available to editors and reviewers. We strongly encourage code deposition in a community repository (e.g. GitHub). See the Nature Portfolio guidelines for submitting code & software for further information.

1

Data

Policy information about <u>availability of data</u>

All manuscripts must include a <u>data availability statement</u>. This statement should provide the following information, where applicable:

- Accession codes, unique identifiers, or web links for publicly available datasets
- A description of any restrictions on data availability
- For clinical datasets or third party data, please ensure that the statement adheres to our <u>policy</u>

> All data are available in the main text or the supplementary materials.

Human research participants

Policy information about <u>studies involving human research participants and Sex and Gender in Research.</u>

Reporting on sex and gender	Human sera from both male and female adult study participants were tested for reactivity to N2 of bat H9N2, N2 of seasonal H3N2 or to the Wuhan spiny eel influenza virus NA
Population characteristics	Paired sera from 15 healthy adults collected before and after seasonal influenza vaccination (2022/23 season) were used. Total number of sera: 30
Recruitment	IRB-16-00772 is an observational longitudinal study which collects biospecimen before and after seasonal influenza vaccination. All participants provided written consent form prior to sample and data collection. All participants provided permission for sample banking and sharing.
Ethics oversight	The observational longitudinal study protocol IRB-16-00772 was reviewed and approved by the Mount Sinai Hospital Institutional Review Board Fresh lung explants were obtained from patients suffering from lung carcinoma and undergoing lung resection at local thoracic surgeries. Written informed consent was obtained from all patients and the study was approved by the ethics committee at the Charité clinic (projects EA2/050/08 and EA2/023/07).

Note that full information on the approval of the study protocol must also be provided in the manuscript.

Field-specific reporting

Please select the one below that is the best fit for your research. If you are not sure, read the appropriate sections before making your selection.

☒ Life sciences   ☐ Behavioural & social sciences   ☐ Ecological, evolutionary & environmental sciences

For a reference copy of the document with all sections, see nature.com/documents/nr-reporting-summary-flat.pdf

Life sciences study design

All studies must disclose on these points even when the disclosure is negative.

Sample size	Used amounts of samples were based on in-house protocols and are stated in the respective Material and Methods sections
Data exclusions	No data were excluded from analysis.
Replication	Experiments were performed according to best practices and as described in the methods.
Randomization	PCR-analysis and ELISA do not require randomization Animals were randomly assigned to the respective study groups, no further criteria for assignment were defined
Blinding	Blinding was not done.

Reporting for specific materials, systems and methods

We require information from authors about some types of materials, experimental systems and methods used in many studies. Here, indicate whether each material, system or method listed is relevant to your study. If you are not sure if a list item applies to your research, read the appropriate section before selecting a response.

Materials & experimental systems

n/a	Involved in the study
☐	☒ Antibodies
☐	☒ Eukaryotic cell lines
☒	☐ Palaeontology and archaeology
☐	☒ Animals and other organisms
☒	☐ Clinical data
☒	☐ Dual use research of concern

Methods

n/a	Involved in the study
☒	☐ ChIP-seq
☒	☐ Flow cytometry
☒	☐ MRI-based neuroimaging

Antibodies

Antibodies used	-rabbit polyclonal anti-IAV-NP (1:750) was described previously (https://doi.org/10.1080/21505594.2016.1159367) -mouse monoclonal anti-MxA (1:1,000) was described previously (https://doi.org/10.1016/S0014-5793(99)01598-7) -rabbit monoclonal anti-IAV-NP (Gene Tex, GTX125989, 1:1,000) -mouse monoclonal anti-actin (Sigma-Aldrich, catalog# A3853, 1:1000) -Peroxidase-conjugated anti-mouse IgG (Jackson ImmunoResearch, catalog# 315-035-045, 1:5000) -Peroxidase-conjugated anti-rabbit IgG (Jackson ImmunoResearch, catalog# 111-035-045, 1:5000) -goat anti-Influenza A (Bio Rad, catalog# OBT1551, 1:50) -DyLight™ Microscale Antibody Labeling Kit 488 or 594 (Thermo Fisher Scientific, catalog# 53025 or 53045) -mouse monoclonal anti-HT2-280 (terrace biotech, catalog# TB-27AHT2-280, 1:200) -mouse monoclonal anti-CD68 (abcam, catalog# ab955, 1:50) -rabbit polyclonal anti-EMP2 (atlas antibodies, catalog# HPA014711, 1:50) -Opal 6-Plex Manual Detection Kit (akoyabio, catalog# NEL861001KT)
Validation	-rabbit polyclonal anti-IAV-NP was validated on bat H9N2-infected and mock-infected cell lysates -mouse monoclonal anti-MxA was validated on MxA-expressing cells and MxA-negative cells. -rabbit polyclonal anti-IAV-NP purchased from GeneTex was validated on bat H9N2-infected and mock-infected cell lysates; see also validation statement on the manufacturer's website (www.genetex.com) -mouse monoclonal anti-actin was validated on whole-cell lysates; see also validation statement on the manufacturer's website (www.sigmaaldrich.com) -Peroxidase-conjugated anti-mouse and anti-rabbit IgG was validated by omission of the primary antibody

Eukaryotic cell lines

Policy information about cell lines and Sex and Gender in Research

Cell line source(s)	-MDCK type II cells: Collection of Cell Lines in Veterinary Medicine CCLV RIE 1061 -MDCK-MxA and MDCK-MxAT103A were obtained by Jesse D. Bloom (Fred Hutchinson Cancer Research Center, United States) and described previously (https://doi.org/10.1371/journal.ppat.1006288)
Authentication	in-house authentication for cell lines was not performed
Mycoplasma contamination	in-house Mycoplasma exclusion is performed regularly
Commonly misidentified lines (See ICLAC register)	Name any commonly misidentified cell lines used in the study and provide a rationale for their use.

Animals and other research organisms

Policy information about studies involving animals; ARRIVE guidelines recommended for reporting animal research, and Sex and Gender in Research

Laboratory animals	-1 to 3 year old adult ferrets (Mustela putorius furo; 10 males and 8 females) -One-day-old chicken and one-day-old turkeys, male and female -6-10 weeks old C57BL/6 mice (8 males and 7 females) and hMxAtg/tg mice (7 males and 7 females)
Wild animals	No wild animals were used
Reporting on sex	Sex was not considered in the study design, as no differences in the results was assumed in this study.
Field-collected samples	Field samples were not collected
Ethics oversight	All ferret and hatchling experiments were evaluated by the responsible ethics committee of the State Office of Agriculture, Food Safety, and Fishery in Mecklenburg–Western Pomerania (LALLF M-V) and gained governmental approval under the registration numbers LVL MV TSD/7221.3-1-029/22 and 7221.3-1-003/22. All mouse experiments were performed in accordance with the guidelines of the German animal protection law and were approved by the state of Baden-Württemberg (Regierungspräsidium

Freiburg; reference number: 35-9185.81/G-19/05).

Note that full information on the approval of the study protocol must also be provided in the manuscript.

III

Publication III

Enhanced fitness of SARS-CoV-2 variant of concern Alpha but not Beta

Lorenz Ulrich*, **Nico Joël Halwe***, Adriano Taddeo*, Nadine Ebert*, Jacob Schön, Christelle Devisme, Bettina Salome Trüeb, Bernd Hoffmann, Manon Wider, Xiaoyu Fan, Meriem Bekliz, Manel Essaidi-Laziosi, Marie Luisa Schmidt, Daniela Niemeyer, Victor Max Corman, Anna Kraft, Aurélie Godel, Laura Laloli, Jenna N. Kelly, Brenda M. Calderon, Angele Breithaupt, Claudia Wylezich, Inês Berenguer Veiga, Mitra Gultom, Sarah Osman, Bin Zhou, Kenneth Adea, Benjamin Meyer, Christiane S. Eberhardt, Lisa Thomann, Monika Gsell, Fabien Labroussaa, Jörg Jores, Artur Summerfield, Christian Drosten, Isabella Anne Eckerle, David E. Wentworth, Ronald Dijkman, Donata Hoffmann, Volker Thiel, Martin Beer & Charaf Benarafa

Article

Enhanced fitness of SARS-CoV-2 variant of concern Alpha but not Beta

Lorenz Ulrich[1,17], Nico Joel Halwe[1,17], Adriano Taddeo[2,3,17], Nadine Ebert[2,3,17], Jacob Schön[1], Christelle Devisme[2,3], Bettina Salome Trüeb[2,3,4], Bernd Hoffmann[1], Manon Wider[5], Xiaoyu Fan[6], Meriem Bekliz[7], Manel Essaidi-Laziosi[7], Marie Luisa Schmidt[8], Daniela Niemeyer[8,9], Victor Max Corman[8,9], Anna Kraft[1], Aurélie Godel[2,3], Laura Laloli[5,10], Jenna N. Kelly[2,3], Brenda M. Calderon[6], Angele Breithaupt[11], Claudia Wylezich[1], Inês Berenguer Veiga[2,3], Mitra Gultom[5,10], Sarah Osman[6], Bin Zhou[6], Kenneth Adea[7], Benjamin Meyer[12], Christiane S. Eberhardt[12,13,14], Lisa Thomann[2,3], Monika Gsell[5], Fabien Labroussaa[4], Jörg Jores[4], Artur Summerfield[2,3], Christian Drosten[8,9], Isabella Anne Eckerle[7,15,16], David E. Wentworth[6], Ronald Dijkman[5,18], Donata Hoffmann[1,18], Volker Thiel[2,3,18]✉, Martin Beer[1,18]✉ & Charaf Benarafa[2,3,18]✉

Emerging variants of concern (VOCs) are driving the COVID-19 pandemic[1,2]. Experimental assessments of replication and transmission of major VOCs and progenitors are needed to understand the mechanisms of replication and transmission of VOCs[3]. Here we show that the spike protein (S) from Alpha (also known as B.1.1.7) and Beta (B.1.351) VOCs had a greater affinity towards the human angiotensin-converting enzyme 2 (ACE2) receptor than that of the progenitor variant S(D614G) in vitro. Progenitor variant virus expressing S(D614G) (wt-S[614G]) and the Alpha variant showed similar replication kinetics in human nasal airway epithelial cultures, whereas the Beta variant was outcompeted by both. In vivo, competition experiments showed a clear fitness advantage of Alpha over wt-S[614G] in ferrets and two mouse models—the substitutions in S were major drivers of the fitness advantage. In hamsters, which support high viral replication levels, Alpha and wt-S[614G] showed similar fitness. By contrast, Beta was outcompeted by Alpha and wt-S[614G] in hamsters and in mice expressing human ACE2. Our study highlights the importance of using multiple models to characterize fitness of VOCs and demonstrates that Alpha is adapted for replication in the upper respiratory tract and shows enhanced transmission in vivo in restrictive models, whereas Beta does not overcome Alpha or wt-S[614G] in naive animals.

Uncontrolled transmission of SARS-CoV-2 in the human population has contributed to the persistence of the COVID-19 pandemic. The emergence of new variants in largely immunologically naive populations suggests that adaptive mutations in the viral genome continue to improve the fitness of this zoonotic virus. In March 2020, a single amino acid change in the S protein at position 614 (S(D614G)) was identified in a small fraction of sequenced samples—this became the predominant variant worldwide within a few weeks[4]. The fitness advantage conferred by this single amino acid change was supported by major increases in infectivity, viral load and transmissibility in vitro and in animal models[3,5,6].

In the second half of 2020, SARS-CoV-2 VOCs with a combination of several mutations emerged, including Alpha, first described in southeast England[7], and Beta, first identified in South Africa[8]. In February–March 2021, Alpha rapidly became the prevailing variant in many regions of the world and a higher reproduction number was inferred from early epidemiological data[9–11]. Beyond S(D614G), Alpha has 18 further mutations in its genome compared with the progenitor, with two deletions and six substitutions within the *S* gene[12]. Some of the S mutations, such as N501Y and the H69/V70 deletion, have been hypothesized to enhance replication and transmission, but there is a lack of clear experimental evidence for this[13,14]. Beta has nine mutations in S, including N501Y,

[1]Institute of Diagnostic Virology, Friedrich-Loeffler-Institut, Greifswald-Insel Riems, Germany. [2]Institute of Virology and Immunology, Mittelhäusern, Switzerland. [3]Department of Infectious Diseases and Pathobiology, Vetsuisse Faculty, University of Bern, Bern, Switzerland. [4]Institute of Veterinary Bacteriology, Vetsuisse Faculty, University of Bern, Bern, Switzerland. [5]Institute for Infectious Diseases, University of Bern, Bern, Switzerland. [6]CDC COVID-19 Emergency Response, Centers for Disease Control and Prevention, Atlanta, GA, USA. [7]Department of Microbiology and Molecular Medicine, Faculty of Medicine, University of Geneva, Geneva, Switzerland. [8]Charité–Universitätsmedizin Berlin, Institute of Virology, Berlin, Germany. [9]German Centre for Infection Research (DZIF), Berlin, Germany. [10]Graduate School for Biomedical Science, University of Bern, Bern, Switzerland. [11]Department of Experimental Animal Facilities and Biorisk Management, Friedrich-Loeffler-Institut, Greifswald-Insel Riems, Germany. [12]Centre for Vaccinology, Department of Pathology and Immunology, University of Geneva, Geneva, Switzerland. [13]Division of General Paediatrics, Department of Woman, Child and Adolescent Medicine, Faculty of Medicine, University of Geneva, Geneva, Switzerland. [14]Center for Vaccinology, Geneva University Hospitals, Geneva, Switzerland. [15]Division of Infectious Disease, Geneva University Hospitals, Geneva, Switzerland. [16]Division of Laboratory Medicine, Laboratory of Virology, Geneva University Hospitals, Geneva, Switzerland. [17]These authors contributed equally: Lorenz Ulrich, Nico Joel Halwe, Adriano Taddeo, Nadine Ebert. [18]These authors jointly supervised this work: Ronald Dijkman, Donata Hoffmann, Volker Thiel, Martin Beer, Charaf Benarafa. ✉e-mail: volker.thiel@vetsuisse.unibe.ch; martin.beer@fli.de; charaf.benarafa@vetsuisse.unibe.ch

Article
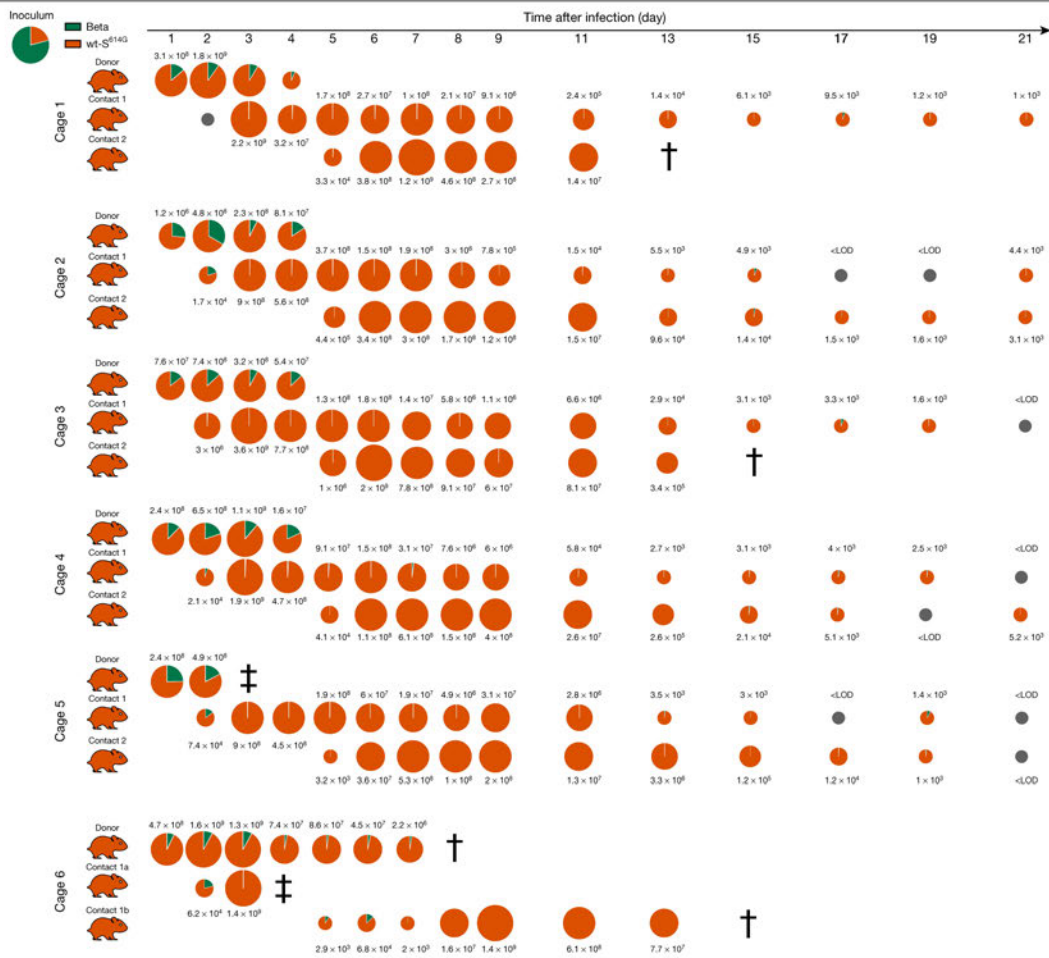
Fig. 1 | Competitive replication and transmission of Beta and wt-S[614G] in Syrian hamsters. Six donor hamsters were each inoculated with a median tissue culture infectious dose (TCID$_{50}$) of 10[4.25], determined by back titration and comprising a mixture of wt-S[614G] (orange) and Beta (green) at a 1:3.8 ratio, determined by quantitative PCR with reverse transcription (RT–qPCR). Donor, contact 1 and contact 2 hamsters were co-housed sequentially as shown in Extended Data Fig. 2a. Nasal washes were performed daily from 1–9 dpi and then every 2 days until 21 dpi. Pie charts show the ratio of variants detected in nasal washes at the indicated dpi. Pie chart sizes are proportional to the total number of viral genome copies per ml, as shown above or below each chart. Grey pies indicate values below the limit of detection (LOD; <10[3] viral genome copies per ml). Hamster silhouettes are coloured according to the dominant variant (>66%) detected in the last positive sample from each animal. Daggers indicate that the animal reached the humane endpoint; double daggers indicate a hamster that died during inhalation anaesthesia at 3 and 4 dpi. This required changes in the group composition in cage 6—the donor hamster was kept until 7 dpi and was co-housed in two different pairs: donor–contact 1a and donor–contact 1b.

and two in the S receptor-binding domain (RBD), K417N and E484K. E484K is thought to be responsible for the ability of Beta to escape neutralization by plasma from convalescent individuals[15–17]. Whether S mutations are solely responsible for the putative fitness advantage and if so, which ones, remains unknown.

Here we investigate the fitness of Alpha and Beta VOCs relative to wt-S[614G], the predominant parental strain containing the S(D614G) substitution—in relevant primary airway culture systems in vitro, and in ferrets, Syrian hamsters and two mouse models expressing human ACE2—to assess specific advantages in replication and transmission and to evaluate the effects of Alpha S mutations alone in vivo. Neither Alpha nor Beta showed enhanced replication in human airway epithelial cell (AEC) cultures compared with wt-S[614G]. Competitive transmission experiments in Syrian hamsters showed similar replication and transmission of wt-S[614G] and Alpha, which both outcompeted Beta. However, competitive experiments in ferrets and transgenic mice expressing human ACE2 controlled by the *KRT18* promoter (hACE2-K18Tg), which overexpress human ACE2 in epithelial cells, showed increased fitness of Alpha compared with wt-S[614G]. Finally, Alpha and a recombinant clone of progenitor virus expressing the Alpha S protein (wt-S[Alpha]) both outcompeted the parental wt-S[614G] strain, resulting in higher virus load in the upper respiratory tract (URT) of mice expressing human ACE2 instead of mouse ACE2 under the endogenous mouse *Ace2* promoter (hACE2-KI mice). Similar to results from AEC cultures, Beta showed lower fitness than wt-S[614G] in hACE2-KI mice. Infections with Alpha and wt-S[614G] virus resulted in similar pathologies in all the in vivo models.
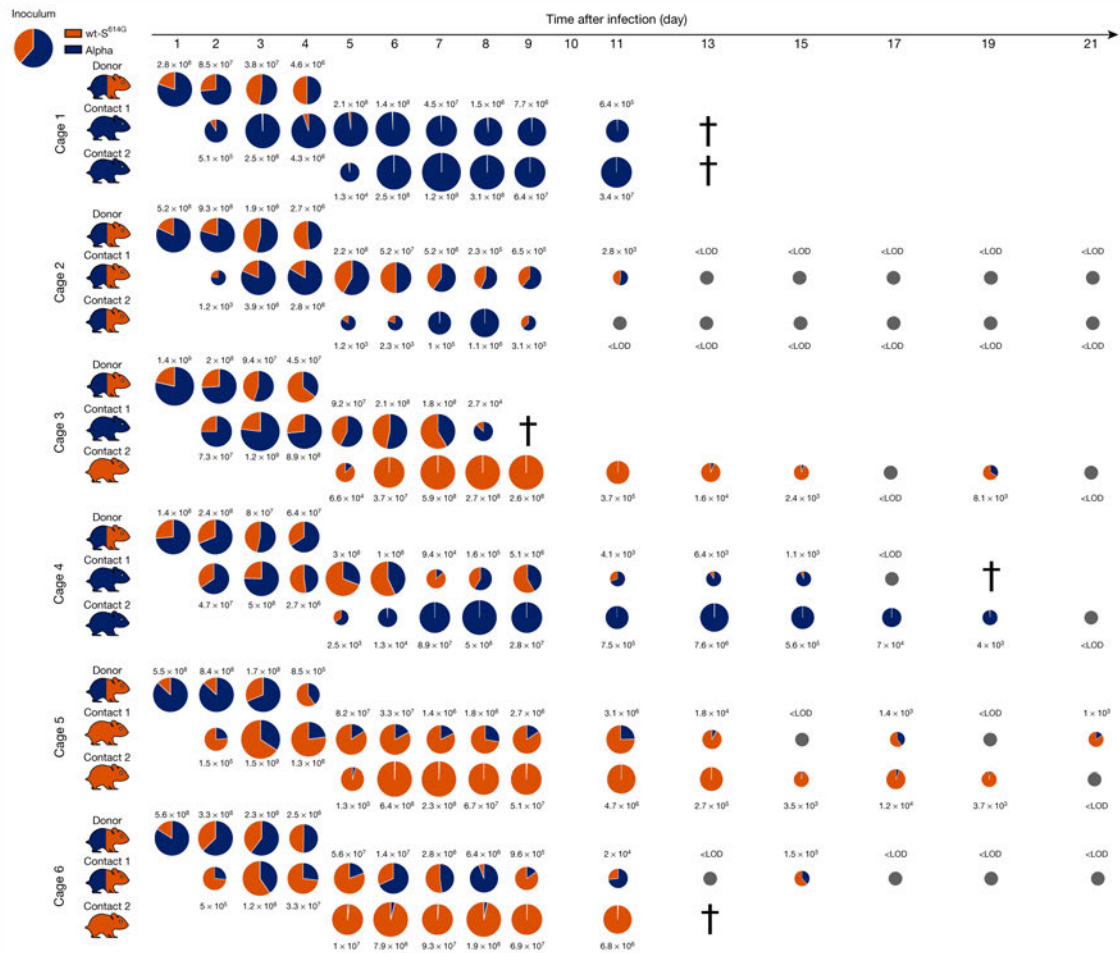
Fig. 2 | Competitive replication and transmission of Alpha and wt-S^614G in Syrian hamsters. Six donor hamsters were each inoculated with a TCID$_{50}$ of 10^{4.3}, determined by back titration and comprising a mixture of wt-S^614G and Alpha at a 1:1.6 ratio, determined by RT–qPCR. Donor, contact 1 and contact 2 hamsters were co-housed sequentially as shown in Extended Data Fig. 2a. Nasal washes were performed daily from 1–9 dpi and then every 2 days until 21 dpi. Pie charts show the ratio of variants detected in nasal washes at the indicated dpi.

Pie chart sizes are proportional to the total number of viral genome copies per ml, as shown above or below each chart. Grey pies indicate values below the LOD. Hamster silhouettes are coloured to indicate the dominant variant (>66%) detected in the last positive sample from each hamster; a silhouette with two colours indicates that there is no dominant variant. Daggers indicate that the hamster reached the humane endpoint.

Binding and replication of VOCs in vitro

The evolution of SARS-CoV-2 variants is associated with accumulation of mutations in the S protein. We determined dissociation constant (K_D) values for recombinant trimeric S with immobilized dimeric human ACE2 using bio-layer interferometry. S protein from Alpha (S^Alpha) or Beta (S^Beta) exhibited a fourfold higher affinity for human ACE2 than that of S(D614G) protein (Extended Data Fig. 1a). Replication kinetics of Alpha, Beta and a wild-type clinical isolate with the S(D614G) mutation were similar in relation to viral copies and titres in AEC cultures incubated at 33 and 37 °C (Extended Data Fig. 1b). However, in direct competition experiments in AEC cultures, Alpha had no advantage over wt-S^614G, whereas Beta was outcompeted by both Alpha and wt-S^614G (Extended Data Fig. 1c), indicating that competition experiments can expose differences in replication that are not detected in individual growth kinetic assays.

Alpha and wt-S^614G outcompete Beta in hamsters

We inoculated groups of six Syrian hamsters intranasally with a mixture of two SARS-CoV-2 strains comprising equivalent numbers of genome copies in three one-to-one competition experiments: Alpha versus Beta, Beta versus wt-S^614G, and Alpha versus wt-S^614G. All experimentally infected 'donor' hamsters were kept strictly in isolation cages to prevent intergroup spill-over infections. Each donor hamster was co-housed with a naive 'contact 1' hamster 1 day post infection (dpi), creating six donor–contact 1 pairs to evaluate shedding and transmission. At 4 dpi, donor hamsters were euthanized and six subsequent transmission pairs were set up by co-housing each contact 1 hamster with a naive contact 2 hamster (Extended Data Fig. 2a).

In two competition experiments, wt-S^614G and Alpha outcompeted Beta, as indicated by nasal washes of the donor hamsters from 1 dpi until

Article
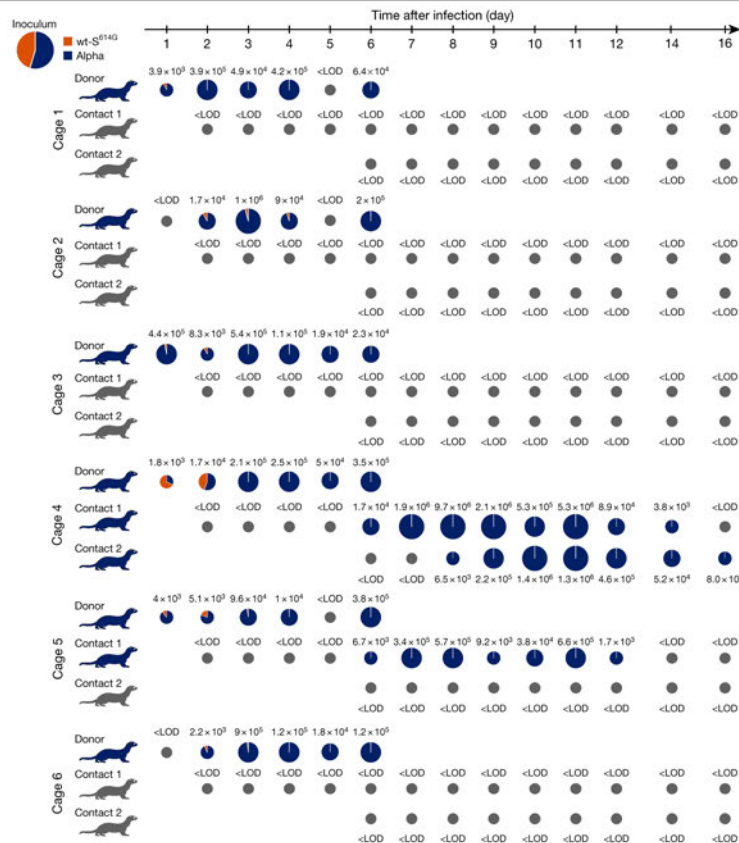
Fig. 3 | Replication and transmission of SARS-CoV-2 Alpha and wt-S^614G in ferrets. Six donor ferrets were each inoculated with a TCID$_{50}$ of $10^{5.9}$, determined by back titration and comprising a mixture of wt-S^614G and Alpha at a 1:1.2 ratio, determined by RT–qPCR. Donor, contact 1 and contact 2 ferrets were co-housed sequentially as shown in Extended Data Fig. 2b. Pie charts show the ratio of variants detected in nasal washes at the indicated dpi. Pie chart sizes are proportional to the total number of viral genome copies per ml, as shown above or below each chart. Grey pies indicate values below the LOD. Viral genome copies were below the LOD at 18 and 20 dpi (not shown). Ferret silhouettes are coloured to indicate the dominant SARS-CoV-2 variant (>66%) detected in the last positive sample from each ferret.

euthanasia at 4 dpi. The viral load reached 10^9 genome copies (gc) per ml for wt-S^614G and Alpha, whereas Beta viral loads were tenfold lower at corresponding time points. Consequently, transmission of Beta was limited or undetectable in contact 1 and contact 2 hamsters compared with the competing variants wt-S^614G (Fig. 1) and Alpha (Extended Data Fig. 3). Transmission to contact hamsters was associated with clinical signs and weight loss (Extended Data Fig. 4a, b). In donor and contact hamsters, viral genome loads in the URT (comprising nasal conchae and trachea) revealed increased replication of Alpha and wt-S^614G compared with Beta (Extended Data Fig. 5a, b), which may explain the lower transmission rate of Beta in a competition context. Of note, Beta replicated to high titres in the lower respiratory tract (LRT; comprising cranial, medial and caudal lung lobes) of donor hamsters, similar levels as observed for the competing Alpha and wt-S^614G virus (Extended Data Fig. 5a, b).

Competition between Alpha and wt-S^614G showed no clear difference in virus titres in nasal washes of donor hamsters, and both variants were detected at all time points in each donor with numbers of individual variants ranging from 10^5 to 10^9 gc ml^{-1} (Fig. 2). Of note, Alpha was dominant over wt-S^614G in the donor hamsters at 1 dpi, but these strains were balanced by the endpoint at 4 dpi. In organ samples from the donor hamsters, the highest viral loads were found in the LRT, where Alpha was predominant

(more than 66% of genome copies) overall with more than tenfold more viral genome copies than wt-S^614G in 14 out of 18 lung samples from the 6 donor hamsters (Extended Data Fig. 5c). Sequential transmission to contact animals was associated with body weight loss (Extended Data Fig. 4c) and was highly efficient for Alpha and wt-S^614G variants, which were both detected in nasal washes of almost all contact 1 hamsters (Fig. 2). Whereas all donor and contact 1 hamsters transmitted both viruses to their respective contacts, contact 2 hamsters mainly shed one variant at high levels in nasal washes, demonstrating similar transmission ability for wt-S^614G and Alpha. At the individual endpoints for contact 1 hamsters, Alpha appeared to dominate in the LRT when both variants were found at similar levels in the nasal washes and URT. In contact 2 hamsters, the variant that was dominant in the URT was also dominant in the LRT (Extended Data Fig. 5c). High levels of SARS-CoV-2 replication in hamsters induced a rapid humoral immune response, as shown by serum reactivity in RBD-based ELISA in all but one of the contact hamsters (Extended Data Fig. 6a–c). We observed a twofold increase in in vitro binding affinity of recombinant trimeric S^Alpha to hamster ACE2 compared with S(D614G) (Extended Data Fig. 1d). These findings suggest that although S^Alpha has an increased binding affinity for ACE2, this factor was not predictive of the outcome of experimental infections in hamsters.

Alpha dominates wt-S⁶¹⁴ᴳ in ferrets

In a similar approach, we inoculated six donor ferrets with a mixture of wt-S^{614G} and Alpha at equivalent numbers of genome copies and monitored sequential transmission in naive contact 1 and contact 2 ferrets (Extended Data Fig. 2b). Alpha rapidly became the dominant variant in nasal washes from 2 dpi with up to 10^5 gc ml^{-1} (Fig. 3). Correspondingly, the nasal concha of donor ferrets revealed high levels of replication in the nasal epithelium and up to 100-fold higher load of Alpha (up to $10^{8.2}$ gc ml^{-1}) than wt-S^{614G} (up to $10^{6.5}$ gc ml^{-1}) (Extended Data Fig. 7a). Although histopathological analysis clearly indicated viral replication in the nasal epithelium of the donor ferrets (Extended Data Fig. 7b–e), we did not observe severe clinical signs of infection (Extended Data Fig. 4d, e). Transmission to contact 1 ferrets was detected in only two pairs of ferrets, and only one contact 1 ferret transmitted the virus to the contact 2 ferret. However, in each of these three transmission events, the Alpha variant was highly dominant and replicated to similarly high titres as in donor ferrets (Fig. 3). The 3 contact ferrets with virus shedding seroconverted by 15–20 days post contact (dpc), confirming active infection (Extended Data Fig. 6d).

Alpha dominates wt-S⁶¹⁴ᴳ in K18Tg mice

To assess further adaptation of Alpha to human ACE2, four hACE2-K18Tg mice, which overexpress hACE2 in respiratory epithelium[18], were inoculated with a mixture of SARS-CoV-2 wt-S^{614G} and Alpha with equivalent numbers of genomic copies (Fig. 4a). Each inoculated mouse was co-housed with a contact hACE2-K18Tg mouse at 1 dpi. Alpha was dominant in the oropharyngeal samples of all four inoculated mice from 1 to 4 dpi with up to 10^6 gc ml^{-1}. The increased replicative fitness of Alpha over wt-S^{614G} was further reflected throughout the respiratory tract, with higher numbers of genome copies in nose, lungs, olfactory bulb and most brain samples at 4 dpi (Fig. 4a), and inoculated mice showed loss of body weight at 4 dpi (Extended Data Fig. 8a). A relatively high infectious dose was used to promote transmission in these experiments, and was associated with high viral load (up to 10^8 viral genome copies per sample) in the lung and brain, leading to encephalitis—as previously reported in hACE2-K18Tg mice[19,20]. Viral loads were lower in nasal and oropharyngeal swabs from these mice, and only limited transmission was observed from these samples (two out of four contacts). None of the contact mice lost weight, but only Alpha was detectable in the lungs of contact mice at 7 dpc (Extended Data Fig. 8b).

We performed a similar competition experiment between wt-S^{614G} and an isogenic recombinant virus expressing S^{Alpha} (wt-S^{Alpha}). We inoculated hACE2-K18Tg mice with an equal mixture of wt-S^{Alpha} and wt-S^{614G} and housed them with a contact hACE2-K18Tg mouse at 1 dpi. The replicative advantage of wt-S^{Alpha} was less clear in this experiment, and both wt-S^{Alpha} and wt-S^{614G} were present with similarly high numbers of viral genome copies in lung and brain samples (Fig. 4b). Transmission to contact mice was inefficient, and wt-S^{Alpha} was the only virus detected in lungs of contact mice at 7 dpc (Extended Data Fig. 8b). These results indicate that the S^{Alpha} spike mutations contribute to the replication advantage of Alpha over wt-S^{614G} in the URT of mice that express high levels of human ACE2.

Competition in hACE2-KI mice

To further address this question, we next used hACE2-KI homozygous mice[3]. In contrast to hACE2-K18Tg mice, hACE2-KI mice show physiological expression of human ACE2, with no ectopic expression of human ACE2 in the brain, and no expression of mouse ACE2, which has been shown to be permissive to the spike mutation N501Y contained in S^{Alpha}. We inoculated 4 groups of hACE2-KI mice intranasally with 10^4 plaque-forming units (PFU) per mouse of either wt-S^{614G}, Alpha, wt-S^{Alpha} or Beta (n = 8 mice per group) as individual virus infections.
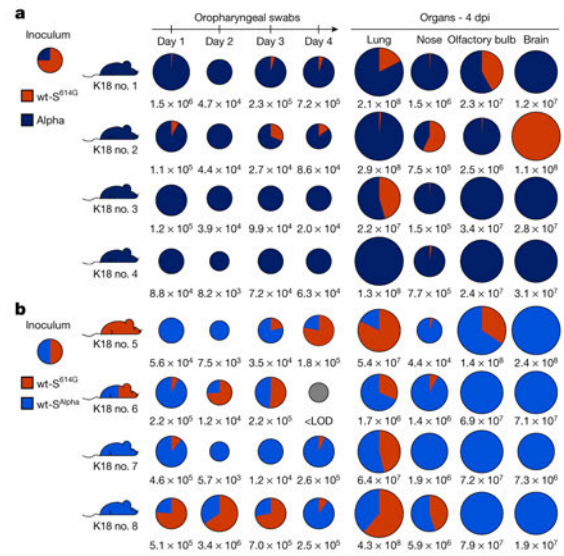
Fig. 4 | Replication of Alpha, wt-S^{Alpha}, and wt-S^{614G} in hACE2-K18Tg mice. a, b, Two groups of four donor hACE2-K18Tg mice were inoculated with 1×10^4 PFU, determined by back titration and comprising a mixture of wt-S^{614G} (orange) and Alpha (dark blue) at a 3:1 ratio (**a**), or a mixture of wt-S^{614G} and wt-S^{Alpha} (light blue) at a 1:1 ratio (**b**). Pie charts show the ratio of variants detected in each sample at the indicated dpi. Pie chart sizes are proportional to the total number of viral genome copies per ml (swabs) or per sample (tissues), as shown below each chart. Grey pies indicate values below the LOD. Mouse silhouettes are coloured to indicate the dominant SARS-CoV-2 variant (>66%) in the last positive swab sample from the corresponding mouse; a silhouette with two colours indicates that there is no dominant variant. K18 nos. 1 to 8 denote individual hACE-K18Tg donor mice.

We observed significantly higher viral genome copy numbers in mice infected with Alpha, wt-S^{Alpha} or Beta compared with wt-S^{614G} in oropharyngeal swabs at 1 dpi (Extended Data Fig. 9a). Moreover, there were significantly higher numbers of viral genome copies of Alpha and wt-S^{Alpha} in the nose at 2 dpi and in the olfactory bulb at 4 dpi compared with wt-S^{614G} and Beta (Extended Data Fig. 9b). Of note, viral titres in the nasal airways and lungs showed SARS-CoV-2 persistence at 4 dpi in 3 out of 4 mice infected with either Alpha or with wt-S^{Alpha}, but not in mice inoculated with wt-S^{614G}, whereas Beta persisted in the lungs of 2 out of 4 mice (Extended Data Fig. 9c). The apparent discrepancy between genome copy number and PFU reflects the non-homogeneous distribution of the virus in the different samples processed for each assay. We observed no difference in weight loss (Extended Data Fig. 9d) or lung histopathology score (Supplementary Table 1) between groups.

Finally, we performed competition experiments to compare the replication of the VOCs in groups of hACE2-KI mice. We observed a complete predominance of Alpha and wt-S^{Alpha} over wt-S^{614G} (Fig. 5a–c). By contrast, Beta showed reduced fitness compared with wt-S^{614G} (Fig. 5d). Together, the two mouse models support enhanced fitness of SARS-CoV-2 Alpha VOC over its progenitor wt-S^{614G} with increased replication and persistence in the URT and more systemic spread, mediated in part by changes in the Alpha S sequence.

Discussion

Epidemiological data indicate that new SARS-CoV-2 variant lineages with specific amino acid changes have a fitness advantage over

Article
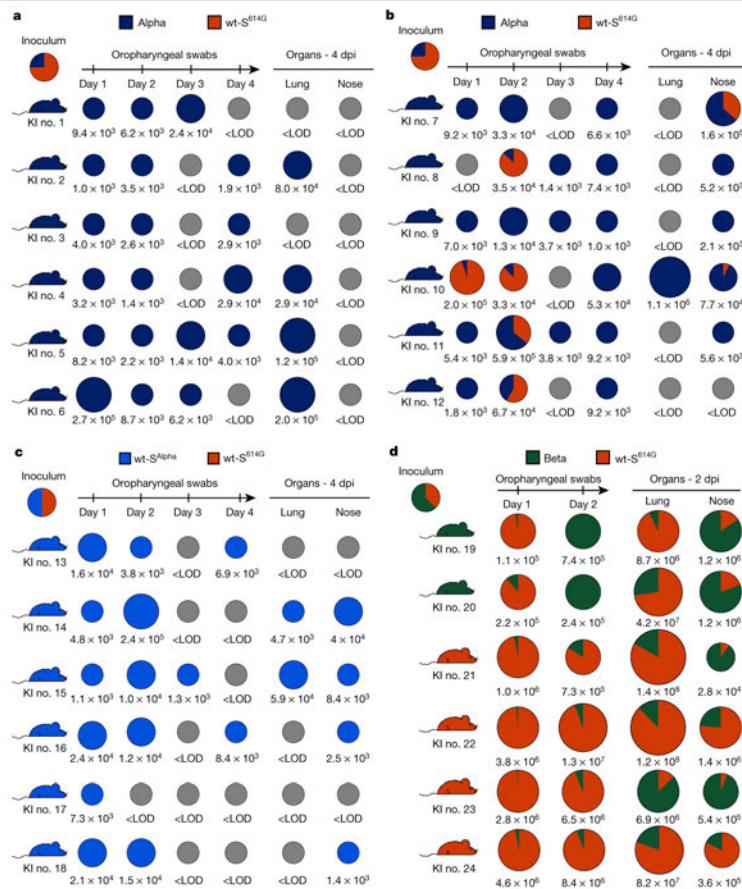
Fig. 5 | Replication of Alpha, wt-S^{Alpha}, and Beta in competition with wt-S^{614G} in hACE2-KI mice. a–d, Groups of hACE2-KI male (**a**, **c**, **d**) and female (**b**) mice were inoculated with 1×10^4 PFU, determined by back titration and comprising a mixture of wt-S^{614G} and Alpha at a 3:1 ratio (**a**, **b**), a mixture of wt-S^{614G} and wt-S^{Alpha} at a 1:1 ratio (**c**), and a mixture of wt-S^{614G} and Beta at a 1:1.6 ratio (**d**). Pie charts show the ratio of variants detected in each sample at the indicated dpi.

Pie chart sizes are proportional to the total number of viral genome copies per ml (swabs) or per sample (tissues), as shown below each chart. Grey pies indicate values below the LOD. Mouse silhouettes are coloured to indicate the dominant SARS-CoV-2 variant (>66%) in the last positive swab sample from the corresponding mouse. KI nos. 1 to 24 denote individual hACE2-KI mice.

contemporary strains. VOCs such as Alpha and Beta are particularly concerning for their hypothesized ability to supersede progenitor strains and establish immune escape properties, respectively. Here we provide experimental evidence that SARS-CoV-2 Alpha has a clear replication advantage over wt-S614G in ferrets and in two humanized mouse models. Moreover, Alpha was exclusively transmitted to contact animals in competition experiments, in which ferrets and hACE2-K18Tg mice were inoculated with mixtures of Alpha and wt-S^{614G}. Because SARS-CoV-2 replicates to lower levels in ferrets and hACE2-KI mice, the inability to detect wt-S^{614G} in some samples from inoculated animals also reflects the limit of detection of the assays using PCR with reverse transcription (RT–PCR) (approximately 10^3 gc ml^{-1}).

We have shown that the molecular mechanism underlying the fitness advantage of Alpha in vivo is largely dependent on a few changes in S, including three amino acid deletions (H69, V70 and Y144) and six substitutions (N501Y, A570D, P681H, T716I, S982A and D1118H). In hACE2-KI mice, higher genome copies and/or titres of Alpha and wt-S^{Alpha} compared with wt-S^{614G} were found in the URT (oropharynx and nose) and olfactory bulb. Increased replication and transmission of wt-S^{Alpha} over

wt-S^{614G} were also evident in hACE2-K18Tg mice. Transmission events are rare in mice; however, we observed transmission of Alpha and wt-S^{Alpha} in 50% of the contact hACE2-K18Tg mice and no detection of wt-S^{614G} in any contact mouse. In vitro, Alpha S mutations increased its affinity for hamster and human ACE2 by twofold and fourfold, respectively, indicating an overall improvement in binding abilities rather than a specialization towards human ACE2.

Beta showed a higher binding affinity for human ACE2 than its progenitor wt-S^{614G} and an equal level of replication to Alpha and wt-S^{614G} in single infections of AEC cultures and in hACE2-KI mice. However, Beta replication was outcompeted in direct competition with wt-S^{614G} in vitro and in hACE2-KI mice. In hamsters, wt-S^{614G} and Alpha also outcompeted Beta in relation to replication and transmission to contact animals, in which Beta was outnumbered by one or two orders of magnitude. This reduced fitness was also evident in previous experiments in K18-hACE2 mice[21]. The relative reduced intrinsic fitness of Beta in immunologically naive hosts supports the hypothesis that the epidemiological advantage of Beta may be principally owing to immune escape, as indicated by reduced efficiency in serum neutralization tests[16]. In convalescent

or vaccinated populations, the immune escape advantage of Beta may prove to be sufficient to compensate its reduced intrinsic fitness and explains, for example, the low prevalence of this variant in regions with a mainly naive population.

Alpha and wt-S^{614G} exhibited similar replication and transmission in hamsters, a model with very high susceptibility and replication efficacy, in which the impact of a marginally fitter SARS-CoV-2 variant may not become apparent. Indeed, efficient simultaneous transmission of both variants to contact hamsters was observed in association with high viral loads in infected animals. In models supporting high replication, such as human AEC cultures and hamsters, only major improvements in replication and transmission can be detected when the variants compared already have a high fitness. By contrast, in ferrets and mouse models—in which SARS-CoV-2 replication is overall less efficient—VOCs with modestly enhanced replication and transmission can be identified. The similar replication and transmission efficacies in hamsters are in line with recent publications using VOCs in the hamster model[22].

The basal rate of replication is an important factor in the assertion of a variant over a contemporary variant in a naive population. Some individuals with higher bioaerosol exhalation levels can initiate disproportionate numbers of transmission events, possibly because of higher viral load in the URT, and are therefore called 'superspreaders'[23]. The hamster model might thus resemble the human superspreader scenario, since there is no clear indication of a specific predominance in transmission between two SARS-CoV-2 variants with high fitness levels, such as wt-S^{614G} and Alpha. However, we did not perform strict aerosol transmission studies, so this remains only a proposition. The ferret and hACE2-KI models are more restricted in that infection is predominantly in the URT. Therefore, these models more closely mimic the situation in humans, in which infections are predominantly mild. Although the rate of transmission was not high overall (3 out of 8 pairs in ferrets, and 4 out of 8 pairs in hACE2-K18Tg mice), the almost exclusive transmission of Alpha relative to wt-S^{614G} mirrored increased transmission of Alpha in the human population; Alpha has been responsible for more than 90% of infections in most countries in Europe[24].

Overall, our study demonstrates that multiple complementary models are necessary to comprehensively evaluate different aspects of human SARS-CoV-2 infection and the impact of emerging VOCs on the course of the ongoing pandemic. The hamster and ferret provide complementary models for transmission efficiency. The mouse models used here may become critical for VOCs demonstrating higher specificity for binding to human ACE2 relative to those from other species. Together, our results show the clear fitness advantage of Alpha and a concomitant disadvantage of Beta, in line with the observed epidemiological predominance of Alpha in the context of a relatively naive population. Notably and reassuringly, despite the apparent fitness differences of these VOCs, there is no indication of different pathologies.

Online content

Any methods, additional references, Nature Research reporting summaries, source data, extended data, supplementary information, acknowledgements, peer review information; details of author contributions and competing interests; and statements of data and code availability are available at https://doi.org/10.1038/s41586-021-04342-0.

1. Harvey, W. T. et al. SARS-CoV-2 variants, spike mutations and immune escape. *Nat. Rev. Microbiol.* **19**, 409–424 (2021).
2. Tao, K. et al. The biological and clinical significance of emerging SARS-CoV-2 variants. *Nat. Rev. Genet.* **22**, 757–773 (2021).
3. Zhou, B. et al. SARS-CoV-2 spike D614G change enhances replication and transmission. *Nature* **592**, 122–127 (2021).
4. Korber, B. et al. Tracking changes in SARS-CoV-2 spike: evidence that D614G increases infectivity of the COVID-19 virus. *Cell* **182**, 812–827.e819 (2020).
5. Plante, J. A. et al. Spike mutation D614G alters SARS-CoV-2 fitness. *Nature* **592**, 116–121 (2021).
6. Hou, Y. J. et al. SARS-CoV-2 D614G variant exhibits efficient replication ex vivo and transmission in vivo. *Science* **370**, 1464–1468 (2020).
7. Volz, E. et al. Assessing transmissibility of SARS-CoV-2 lineage B.1.1.7 in England. *Nature* **593**, 266–269 (2021).
8. Tegally, H. et al. Detection of a SARS-CoV-2 variant of concern in South Africa. *Nature* **592**, 438–443 (2021).
9. Davies, N. G. et al. Estimated transmissibility and impact of SARS-CoV-2 lineage B.1.1.7 in England. *Science* **372**, eabg3055 (2021).
10. Washington, N. L. et al. Emergence and rapid transmission of SARS-CoV-2 B.1.1.7 in the United States. *Cell* **184**, 2587–2594.e7 (2021).
11. Weber, S., Ramirez, C. M., Weiser, B., Burger, H. & Doerfler, W. SARS-CoV-2 worldwide replication drives rapid rise and selection of mutations across the viral genome: a time-course study—potential challenge for vaccines and therapies. *EMBO Mol. Med.* **13**, e14062 (2021).
12. Galloway, S. E. et al. Emergence of SARS-CoV-2 B.1.1.7 lineage—United States, December 29, 2020–January 12, 2021. *Morb. Mortal. Wkly Rep.* **70**, 95–99 (2021).
13. Liu, Y. et al. The N501Y spike substitution enhances SARS-CoV-2 infection and transmission. *Nature* https://doi.org/10.1038/s41586-021-04245-0 (2021).
14. Kemp, S. et al. Recurrent emergence and transmission of SARS-CoV-2 spike deletion H69/V70 and its role in the Alpha variant B.1.1.7. *Cell Rep.* **35**, 109292 (2021).
15. Cele, S. et al. Escape of SARS-CoV-2 501Y.V2 from neutralization by convalescent plasma. *Nature* **593**, 142–146 (2021).
16. Hoffmann, M. et al. SARS-CoV-2 variants B.1.351 and P.1 escape from neutralizing antibodies. *Cell* **184**, 2384–2393.e2312 (2021).
17. Wibmer, C. K. et al. SARS-CoV-2 501Y.V2 escapes neutralization by South African COVID-19 donor plasma. *Nat. Med.* **27**, 622–625 (2021).
18. McCray, P. B., Jr et al. Lethal infection of K18-hACE2 mice infected with severe acute respiratory syndrome coronavirus. *J. Virol.* **81**, 813–821 (2007).
19. Yinda, C. K. et al. K18-hACE2 mice develop respiratory disease resembling severe COVID-19. *PLoS Pathog.* **17**, e1009195 (2021).
20. Zheng, J. et al. COVID-19 treatments and pathogenesis including anosmia in K18-hACE2 mice. *Nature* **589**, 603–607 (2021).
21. Hoffmann, D. et al. CVnCoV and CV2CoV protect human ACE2 transgenic mice from ancestral B BavPat1 and emerging B.1.351 SARS-CoV-2. *Nat. Commun.* **12**, 4048 (2021).
22. Abdelnabi, R. et al. Comparing infectivity and virulence of emerging SARS-CoV-2 variants in Syrian hamsters. *EBioMedicine* **68**, 103403 (2021).
23. Edwards, D. A. et al. Exhaled aerosol increases with COVID-19 infection, age, and obesity. *Proc. Natl Acad. Sci. USA* **118**, e2021830118 (2021).
24. Variants of concern. *European Centre for Disease Prevention and Control* https://www.ecdc.europa.eu/en/covid-19/variants-concern (accessed 3 June 2021).

Article

Methods

Cell lines

Vero E6 cells (ATCC CRL-1586) (provided by D. Muth, M. Müller and C. Drosten) or Vero-TMPRSS2[25] (provided by S. Pöhlmann) were propagated in Dulbecco's Modified Eagle Medium-GlutaMAX supplemented with 1 mM sodium pyruvate, 10% (v/v) heat-inactivated fetal bovine serum (FBS), 100 μg ml^{-1} streptomycin, 100 IU ml^{-1} penicillin, 1% (w/v) nonessential amino acids and 15 mM HEPES (Gibco). Cells were maintained at 37 °C in a humidified incubator with 5% CO$_2$.

Viruses

Viruses are listed in Extended Data Table 1 together with the corresponding in vitro and in vivo experiments in which they were used. Specific amino acid changes are shown schematically in Extended Data Fig. 10. Contemporary clinical isolates from the B.1.160 (S^{D614G}) (EPI_ISL_414019), Alpha (EPI_ISL_2131446, EPI_ISL_751799 (L4549)) and Beta (EPI_ISL_803957 (L4550)) were isolated and minimally passaged on Vero E6 cells. Beta (EPI_ISL_981782) was initially isolated on A549 cells expressing human ACE2 before passaging on Vero E6 cells. SARS-CoV-2 Alpha (L4549) and Beta (L4550)[21] were received from the Robert-Koch-Institut Berlin, Germany. Isogenic variants with the Alpha spike (wt-S^{Alpha}) or individual Alpha spike mutations were introduced into a wild-type SARS-COV-2 'Wuhan' backbone strain comprising the D614G amino acid change (wt-S^{614G}), as described[3,26]. Isogenic viruses were grown on Vero-TMPRSS2 cells after one passage on human bronchial airway epithelial cells. All viruses were verified by performing whole-genome next generation sequencing (NGS). For SARS-CoV-2 Alpha (L4549, SARS-CoV-2 B.1.1.7 NW-RKI-I-0026/2020 passage 3), one silent mutation in the ORF1a (sequence position 11741) was determined (C to T with 27% T, 57% strand bias). For SARS-CoV-2 Beta (L4550, available under ENA study accession number MZ433432), one nucleotide exchange was detected (A12022C) resulting in the amino acid exchange D3923A in ORF1a and one SNP at sequence position 11730 (C to T with 41%, stand bias 52%).

For all in vivo virus competition experiments, we generated inoculum mixtures aiming for a 1:1 ratio of each variant based on virus stock titres. The reported mixture inoculum titres are based on back-titration of the inoculum mixtures and the indicated ratio of each variant was determined by standard RT–qPCR. SARS-CoV-2 wt-S^{614G} (PRJEB45736; wt-S614G ID#49 vial 2) and SARS-CoV-2 Beta (L4550) were used to inoculate hamsters in the wt-S^{614G} versus Beta study; SARS-CoV-2 Alpha (L4549), and SARS-CoV-2 Beta (L4550) were used for inoculation in the Alpha versus Beta hamster study. SARS-CoV-2 wt-S^{614G}, wt-S^{Alpha}, Alpha (L4549) and Beta (L4550) were used to inoculate hACE2 humanized mice in all single virus or mixed virus competition experiments.

Next-generation sequencing

NGS was used to verify the sequence of isolates and isogenic clones prior to experimentation. RNA was extracted using the RNAdvance Tissue kit (Beckman Coulter) and the KingFisher Flex System (Thermo Fisher Scientific). Subsequently, RNA was transcribed into cDNA and sequencing libraries were generated as described[27] and were sequenced using the Ion Torrent S5XL Instrument (ThermoFisher). Samples with C_t values >20 for SARS-CoV-2 were additionally treated with RNA baits (myBaits, Arbor Biosciences) for SARS-CoV-2 enrichment before sequencing[28]. Sequence datasets were analysed by reference mapping with the Genome Sequencer Software Suite (version 2.6, Roche), default software settings for quality filtering and mapping using EPI_ISL_414019 (Alpha), EPI_ISL_2131446 (Alpha) and EPI_ISL_981782 (Beta) as references. To identify potential single nucleotide polymorphisms in the read data, the variant analysis tool integrated in Geneious Prime (2019.2.3) was applied (default settings).

AEC cultures

Human nasal AEC cultures were purchased from Epithelix (EP02MP Nasal MucilAir, pool of 14 donors). Maintenance of primary nasal AEC cultures were performed according to manufacturer's guidelines. Individual SARS-CoV-2 infections with contemporary virus isolates were conducted at either 33 °C or 37 °C as described elsewhere[29] using a multiplicity of infection (MOI) of 0.02, whereas all competition experiments and replication kinetics were performed with an MOI of 0.005 as described[30]. Quantification of viral load of individual SARS-CoV-2 infections with contemporary virus isolates was performed using the NucliSens easyMAG (BioMérieux) and RT–qPCR targeting the E gene of SARS-CoV-2 as described[31,32]. In competition experiments, nucleic acids were extracted using the Quick-RNA Viral 96 kit (Zymo research) and RT–qPCR primers and probe sequences are shown in Extended Data Table 2. The viral replication of individual isogenic variants was monitored by plaque assay.

Plaque titration assay

Viruses released into the apical compartments were titrated by plaque assay on Vero E6 cells as described[30,33]. In brief, 2×10^5 cells per ml were seeded in 24-well plates 1 day prior to titration and inoculated with tenfold serial dilutions of virus solutions. Inocula were removed 1 h post-infection and replaced with overlay medium consisting of DMEM supplemented with 1.2% Avicel (RC-581, FMC biopolymer), 15 mM HEPES, 5 or 10% heat-inactivated FBS, 100 μg ml^{-1} streptomycin and 100 IU ml^{-1} penicillin. Cells were incubated at 37 °C, 5% CO$_2$ for 48 h, fixed with 4% (v/v) neutral buffered formalin, and stained with crystal violet.

Protein expression, purification and bio-layer interferometry assay

SARS-CoV-2 S protein expression plasmids were constructed to encode the ectodomain of S protein S(D614G) or S^{Alpha} (residues 1–1208, with a mutated furin cleavage site and K986P/V987P substitutions) followed by a T4 fold on the trimerization domain and a polyhistidine purification tag. ACE2 protein (human, hamster or ferret) expression plasmids were constructed to encode the ectodomain of ACE2 followed by a human IgG1 Fc purification tag. The recombinant proteins were expressed using the Expi293 Expression system (ThermoFisher Scientific) and purified with HisTrap FF columns (for polyhistidine-tagged spike proteins) or with HiTrap Protein A column (for Fc-tagged ACE2 proteins) in FPLC (Cytiva) system. Recombinant proteins were further purified with Superose 6 Increase 10/300 GL column (Cytiva) as needed.

Binding affinity between the trimeric spike and dimeric ACE2 was evaluated using an Octet RED96e instrument at 30 °C with a shaking speed of 1,000 rpm (ForteBio). Anti-human IgG Fc biosensors (ForteBio) were used. Following 20 min of pre-hydration of anti-human IgG Fc biosensors and 1 min of sensor check, 7.5 nM of human ACE2–Fc, 7.5 nM of hamster ACE2–Fc in 10× kinetic buffer (ForteBio) were loaded onto the surface of anti-human IgG Fc biosensors for 5 min. After 1.5 min of baseline equilibration, 5 min of association was conducted at 10–100 nM S(D614G), S^{Alpha} or S^{Beta}, followed by 5 min of dissociation in the same buffer, which was used for baseline equilibration. The data were collected using ForteBio Data Acquisition Software 12.0.1 and corrected by subtracting signal from the reference sample and a 1:1 binding model with global fit was used for determination of affinity constants.

Animal experiment ethics declarations

All ferret and hamster experiments were evaluated by the responsible ethics committee of the State Office of Agriculture, Food Safety, and Fishery in Mecklenburg–Western Pomerania (LALLF M-V) and gained governmental approval under registration number LVL MV TSD/7221.3-1-004/21. Mouse studies were approved by the Commission for Animal Experimentation of the Cantonal Veterinary Office of Bern and

conducted in compliance with the Swiss Animal Welfare legislation and under license BE-43/20.

Hamster studies

Six Syrian hamsters (*Mesocricetus auratus*) (Janvier Labs) were inoculated intranasally under a brief inhalation anaesthesia with a 70 µl mixture of two SARS-CoV-2 VOCs (wt-S[614G] and Alpha mixture, wt-S[614G] and Beta mixture, or Alpha and Beta mixture). Each inoculum was back-titrated and ratios of each variant were determined by RT–qPCR. The wt-S[614G] and Alpha mixture held a 1:1.6 ratio with TCID$_{50}$ of $10^{4.3}$ per hamster, the wt-S[614G] versus Beta mixture held a 1:3.8 ratio with TCID$_{50}$ of $10^{4.25}$ per hamster, and the Alpha versus Beta mixture held a 1.8:1 ratio with TCID$_{50}$ of $10^{5.06}$ per hamster.

Inoculated donor hamsters were isolated in individually ventilated cages for 24 h. Thereafter, contact hamster 1 was co-housed with each donor, creating six donor–contact 1 pairs (Extended Data Fig. 2a). The housing of each hamster pair was strictly separated in individual cage systems to prevent spillover between different pairs. At 4 dpi, the individual donor hamsters (inoculated animal) were euthanized. To simulate a second transmission cycle, the original contact hamsters (referred to as contact 1) were commingled with a further six naive hamsters (referred to as contact 2), which equates to another six contact 1 and contact 2 pairs (Extended Data Fig. 2a). These pairs were co-housed until the end of the study at 21 dpi. Because the first contact hamster (cage 6) in the competition trial wt-S[614G] versus Alpha, died at 2 dpc, the second contact hamster for this cage was also co-housed with the donor hamster; thus the first and second contact hamsters in this cage were labelled contact 1a and contact 1b, respectively. To enable sufficient contact between the donor hamster and contact 1b hamster, which was commingled routinely on 4 dpi, the donor hamster was euthanized at 7 dpi (instead of at 4 dpi), when it reached the humane end-point criterion for bodyweight (below 80% of 0 dpi body weight).

Viral shedding was monitored by nasal washes in addition to a daily physical examination and body weighing routine. Nasal wash samples were obtained under a short-term isoflurane anaesthesia from individual hamsters by administering 200 µl PBS to each nostril and collecting the reflux. Animals were sampled daily from 1 dpi to 9 dpi, and then every other day until 21 dpi. Under euthanasia, serum samples and an organ panel comprising representative URT and LRT tissues were collected from each hamster. All animals were observed daily for signs of clinical disease and weight loss. Hamsters reaching the humane endpoint, that is, falling below 80% of the initial body weight relative to 0 dpi, were humanely euthanized.

Ferret studies

Similar to the hamster study, 12 ferrets (six donor ferrets and six transmission 1 ferrets) from the FLI in-house breeding were housed pairwise in strictly separated cages to prevent spillover contamination. Of these, six ferrets were inoculated with an equal 250 µl mixture of SARS-CoV-2 wt-S[614G] and Alpha. The inoculum was back-titrated and the ratio of each variant was determined by RT–qPCR. The wt-S[614G] versus Alpha mixture held a 1:1.2 ratio with $10^{5.875}$ TCID$_{50}$ distributed equally into each nostril of donor ferrets. Ferrets were separated for the first 24 h following inoculation. Subsequently, the ferret pairs were co-housed again, allowing direct contact of donor to contact 1 ferrets. All ferrets were sampled via nasal washes with 750 µl PBS per nostril under a short-term inhalation anaesthesia. Donor ferrets were sampled until euthanasia at 6 dpi, which was followed by the introduction of one additional naive contact 2 ferret per cage (*n* = 6), resulting in a 1:1 pairwise setup with contact 1 and contact 2 ferrets (Extended Data Fig. 2b). All ferrets, which were in the study group on the respective days, were sampled on the indicated days. Bodyweight, temperature and physical condition of all ferrets were monitored daily throughout the experiment. URT and LRT organ samples, as well as blood samples of all ferrets were taken at respective euthanasia time points.

Full autopsy was performed on all animals under BSL3 conditions. The lung, trachea and nasal conchae were collected and fixed in 10% neutral-buffered formalin for 21 days. The nasal atrium, decalcified nasal turbinates (cross-sections every 3–5 mm), trachea and all lung lobes were trimmed for paraffin embedding. Based on PCR results, tissue sections (3 µm) of all donors (day 6) and one recipient (no. 8, day 20) were cut and stained with haematoxylin and eosin for light microscopical examination. Immunohistochemistry was performed using an anti-SARS nucleocapsid antibody (Novus Biologicals NB100-56576, dilution 1:200) according to standardized avidin–biotin–peroxidase complex-method producing a red labelling and haematoxylin counterstain. For each immunohistochemistry staining, positive control slides and a negative control for the primary antibodies were included. Histopathology was performed on at least five consecutive tissue samples per animal, yielding comparable results in all cases. Lung tissue pathology was evaluated according to a detailed score sheet developed by Angele Breithaupt (DipECVP) (Supplementary Table 2). Evaluation and interpretation was performed by board-certified veterinary pathologists (DiplECVP) (AB, IBV).

Mouse studies

hACE2-KI mice (B6.Cg-*Ace2*[tm1(ACE2)Dwnt]) and hACE2-K18Tg mice (Tg(K18-hACE2)2Prlmn) were described previously[3,18]. All mice were produced at the specific-pathogen-free facility of the Institute of Virology and Immunology (Mittelhäusern), where they were maintained in individually ventilated cages (blue line, Tecniplast), with 12-h:12-h light:dark cycle, 22 ± 1 °C ambient temperature and 50 ± 5% humidity, autoclaved food and acidified water. At least 7 days before infection, mice were placed in individually HEPA-filtered cages (IsoCage N, Tecniplast). Mice (10 to 12 weeks old) were anaesthetized with isoflurane and infected intranasally with 20 µl per nostril with the virus inoculum described in the results section. One day after inoculation, infected hACE2-K18Tg mice were placed in the cage of another hACE2-K18Tg contact mouse. Mice were monitored daily for bodyweight loss and clinical signs. Oropharyngeal swabs were collected under brief isoflurane anaesthesia using ultrafine sterile flock swabs (Hydraflock, Puritan, 25-3318-H). The tips of the swabs were placed in 0.5 ml of RA1 lysis buffer (Macherey-Nagel, 740961) supplemented with 1% β-mercaptoethanol and vortexed. At 2 or 4 dpi, mice were euthanized, and organs were aseptically dissected. Systematic tissue sampling was performed as detailed previously[3].

Animal specimens work up, viral RNA detection and quantification

Organ samples from ferrets and hamsters were homogenized in a 1 ml mixture composed of equal volumes of Hank's balanced salts MEM and Earle's balanced salts MEM containing 2 mM L-glutamine, 850 mg l^{-1} NaHCO3, 120 mg l^{-1} sodium pyruvate and 1% penicillin–streptomycin at 300 Hz for 2 min using a Tissuelyser II (Qiagen) and centrifuged to clarify the supernatant. Organ samples from mice were either homogenized in 0.5 ml of RA1 lysis buffer supplemented with 1% β-mercaptoethanol using a Bullet Blender Tissue Homogenizer (Next-Advance) or in Tube M (Miltenyi Biotech, 130-096-335) containing 1 ml of DMEM using a gentleMACS Tissue Dissociator (Miltenyi Biotech). Nucleic acid was extracted from 100 µl of the nasal washes or 200 µl mouse oropharyngeal swabs after a short centrifugation step or 100 µl of organ sample supernatant using the NucleoMag Vet kit (Macherey Nagel). Nasal washes, oropharyngeal swabs, and organ samples were tested by RT–qPCR analysis for the ratio of the two different viruses used for inoculation, by applying two different assays, each of them specific for one variant: either the wt-S[614G], Alpha or Beta variant (Extended Data Tables 2, 3). Viral RNA copies in swabs and organs in studies using a single variant inoculum in mice were determined using the E protein RT–qPCR exactly as described[3].

Four specific RT–qPCR assays for SARS-CoV-2 wt-S[614G], Alpha and Beta were designed based on the specific genome deletions within ORF1

Article

and the *S* gene (Extended Data Table 2). Here, virus-specific primers were used to achieve a high analytical sensitivity (less than 10 genome copies per μl template) of the PCR assays, and in samples with a high genome load of the non-matching virus.

The RT–qPCR reaction was prepared using the qScript XLT One-Step RT–qPCR ToughMix (QuantaBio) (hamsters and ferrets) or the AgPath-ID One-Step RT–PCR (ThermoFisher Scientific) (hACE2-K18Tg and hACE2-KI mice) in a volume of 12.5 μl including 1 μl of the respective FAM mix and 2.5 μl of extracted RNA. The reaction was performed for 10 min at 50 °C for reverse transcription, 1 min at 95 °C for activation, and 42 cycles of 10 s at 95 °C for denaturation, 10 s at 60 °C for annealing and 20 s at 68 °C for elongation. Fluorescence was measured during the annealing phase. RT–qPCRs were performed on a BioRad real-time CFX96 detection system (Bio-Rad) (hamsters and ferrets) or an Applied Biosystems 7500 Real-Time PCR System (ThermoFisher Scientific) (mice). Validation work was performed by comparison with established protocols (https://www.who.int/docs/default-source/coronaviruse/eal-time-rt-pcr-assays-for-the-detection-of-sars-cov-2-institut-pasteur-paris.pdf?sfvrsn=3662fcb6_2 and ref. [31]).

Serological tests of hamsters and ferrets

Serum samples from the wt-S^{614G} versus Alpha, wt-S^{614G} versus Beta, and Alpha versus Beta co-inoculated hamsters and ferrets were tested by ELISA for sero-reactivity against the RBD domain[34] using a Tecan i-control 2014 1.11 plate reader and data was analysed using Microsoft Excel 16.0. All samples were generated at the time point of euthanasia of the individual animal.

Statistical analysis

Statistical analysis was performed using GraphPad Prism 8 or R[35] (version 4.1), using the packages tidyverse[36] (v1.3.1), ggpubr (v0.4.0) and rstatix (v.0.7.0). Unless noted otherwise, the results are expressed as mean ± s.d. Two-way analysis of variance (ANOVA) with Tukey honest significance differences post hoc test was used to compare competition results at different time points after infection in vitro. One-way ANOVA with Tukey's multiple comparisons test was used to compare viral genome copies or titres at different time points post infection in individual virus mouse infection studies. Significance was defined as $P < 0.05$.

Reporting summary

Further information on research design is available in the Nature Research Reporting Summary linked to this paper.

Data availability

Sequence data are available on the NCBI Sequence Read Archive (SRA) under the accession numbers PRJEB45736 and PRJNA784099, or in Gen-Bank under the accession numbers MT108784, MZ433432, OL675863, OL689430 and OL689583 as shown in Extended Data Table 1. Source data are provided with this paper.

25. Hoffmann, M. et al. SARS-CoV-2 cell entry depends on ACE2 and TMPRSS2 and is blocked by a clinically proven protease inhibitor. *Cell* **181**, 271–280.e278 (2020).
26. Thi Nhu Thao, T. et al. Rapid reconstruction of SARS-CoV-2 using a synthetic genomics platform. *Nature* **582**, 561–565 (2020).
27. Wylezich, C., Papa, A., Beer, M. & Hoper, D. A versatile sample processing workflow for metagenomic pathogen detection. *Sci. Rep.* **8**, 13108 (2018).
28. Wylezich, C. et al. Next-generation diagnostics: virus capture facilitates a sensitive viral diagnosis for epizootic and zoonotic pathogens including SARS-CoV-2. *Microbiome* **9**, 51 (2021).
29. Essaidi-Laziosi, M. et al. Propagation of respiratory viruses in human airway epithelia reveals persistent virus-specific signatures. *J. Allergy Clin. Immunol.* **141**, 2074–2084 (2018).
30. V'Kovski, P. et al. Disparate temperature-dependent virus-host dynamics for SARS-CoV-2 and SARS-CoV in the human respiratory epithelium. *PLoS Biol.* **19**, e3001158 (2021).
31. Corman, V. M. et al. Detection of 2019 novel coronavirus (2019-nCoV) by real-time RT-PCR. *Euro Surveill.* **25**, 2000045 (2020).
32. Baggio, S. et al. SARS-CoV-2 viral load in the upper respiratory tract of children and adults with early acute COVID-19. *Clin. Infect. Dis.* **73**, 148–150 (2021).
33. Jonsdottir, H. R. & Dijkman, R. Characterization of human coronaviruses on well-differentiated human airway epithelial cell cultures. *Methods Mol. Biol.* **1282**, 73–87 (2015).
34. Wernike, K. et al. Multi-species ELISA for the detection of antibodies against SARS-CoV-2 in animals. *Transbound. Emerg. Dis.* **68**, 1779–1785 (2020).
35. R: A language and environment for statistical computing (R Core Team, 2021).
36. Wickham, H. et al. Welcome to the Tidyverse. *J. Open Source Softw.* **4**, 1686 (2019).

Extended Data Fig. 1 | ACE2 receptor binding and replication kinetics of SARS-CoV-2 VOC in vitro. (a) Affinity between spike (S^{614G}, S^{Alpha}, and S^{Beta}) protein trimers and hACE2 dimers determined by Bio-layer interferometry. (b) Viral replication kinetics of SARS-CoV-2 Alpha, Beta, and wt-S^{614G} (MOI 0.02) at 33 °C and 37 °C in primary human nasal airway epithelial cell (AEC) cultures. (c) Viral replication kinetics of pairwise competition assays in primary nasal AEC cultures at 33 °C (MOI 0.005). (b, c) Data are presented as individual points with mean (line) and standard deviation; (b) n = 2 (Alpha and Beta), n = 4

(wt-S^{614G}), (c) n = 3 independent biological replicates. (c) P-values were determined by two-way ANOVA and Tukey Honest Significant Differences (HSD) post-hoc test. (d) Affinity between spike (S^{614G}, S^{Alpha}) protein trimers with hamster ACE2 determined by Bio-layer interferometry. (a, d) ACE2 with IgG1 Fc tag were loaded on anti-human IgG Fc biosensors and binding kinetics were conducted using indicated concentrations of spike trimers. Data is representative of 3 independent experiments.

Article
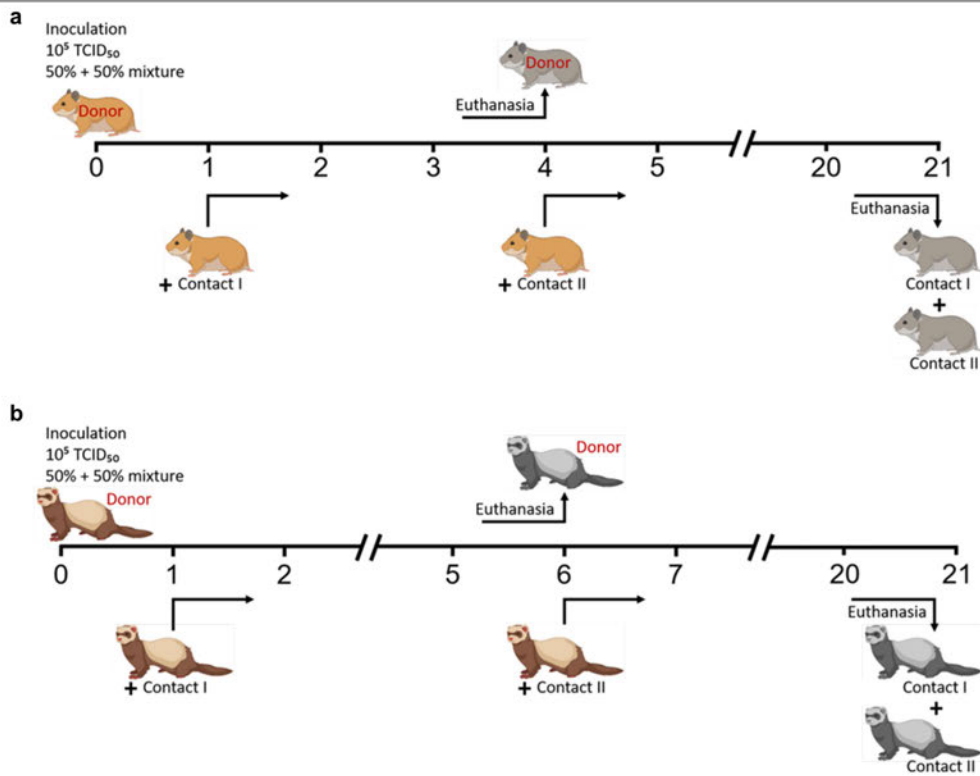
Extended Data Fig. 2 | Experimental workflow of competitive transmission experiments in Syrian hamsters and ferrets. (**a**) Timeline of the hamster experiments. Six intranasally inoculated donor hamsters each were co-housed with one naïve contact hamster (1 dpi), building six respective donor-contact I pairs. At 4 dpi, the donor hamsters were euthanized and the initial contact hamsters I were co-housed with one additional hamster (Contact II). (**b**) Timeline of the ferret experiment. The scheme was generated with BioRender (https://biorender.com/).
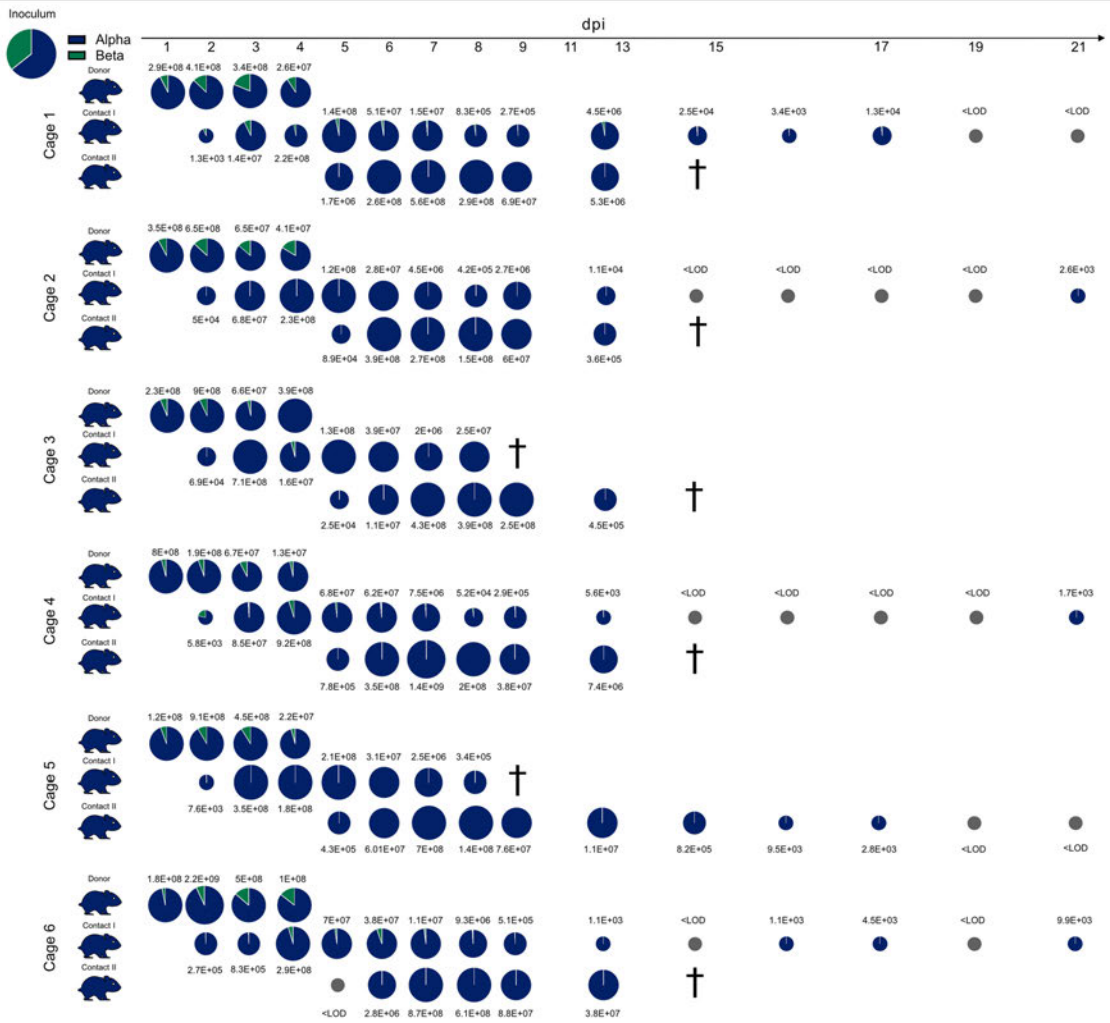
Extended Data Fig. 3 | Competitive transmission between Alpha and Beta in Syrian hamsters. Six donor hamsters were each inoculated with $10^{5.06}$ TCID$_{50}$ determined by back titration and composed of a mixture of Alpha (dark blue) and Beta (green) at 1.8:1 ratio determined by RT-qPCR. Donor hamsters, contact I and II hamsters were co-housed sequentially as shown in Extended Data Fig. 2a. Nasal washings were performed daily from 1–9 dpi and afterwards every two days until 21 dpi. Pie chart colors illustrate the ratio of variants detected in nasal washings at the indicated dpi. Pie chart sizes are proportional to the total viral genome copies reported above or below respective pies. Grey pies indicate values below the LOD (<103 viral genome copies per sample). Hamster silhouettes are colored according to the dominant variant (>66%) detected in the latest sample of each animal. † indicate that the corresponding animal reached the humane endpoint.

Article
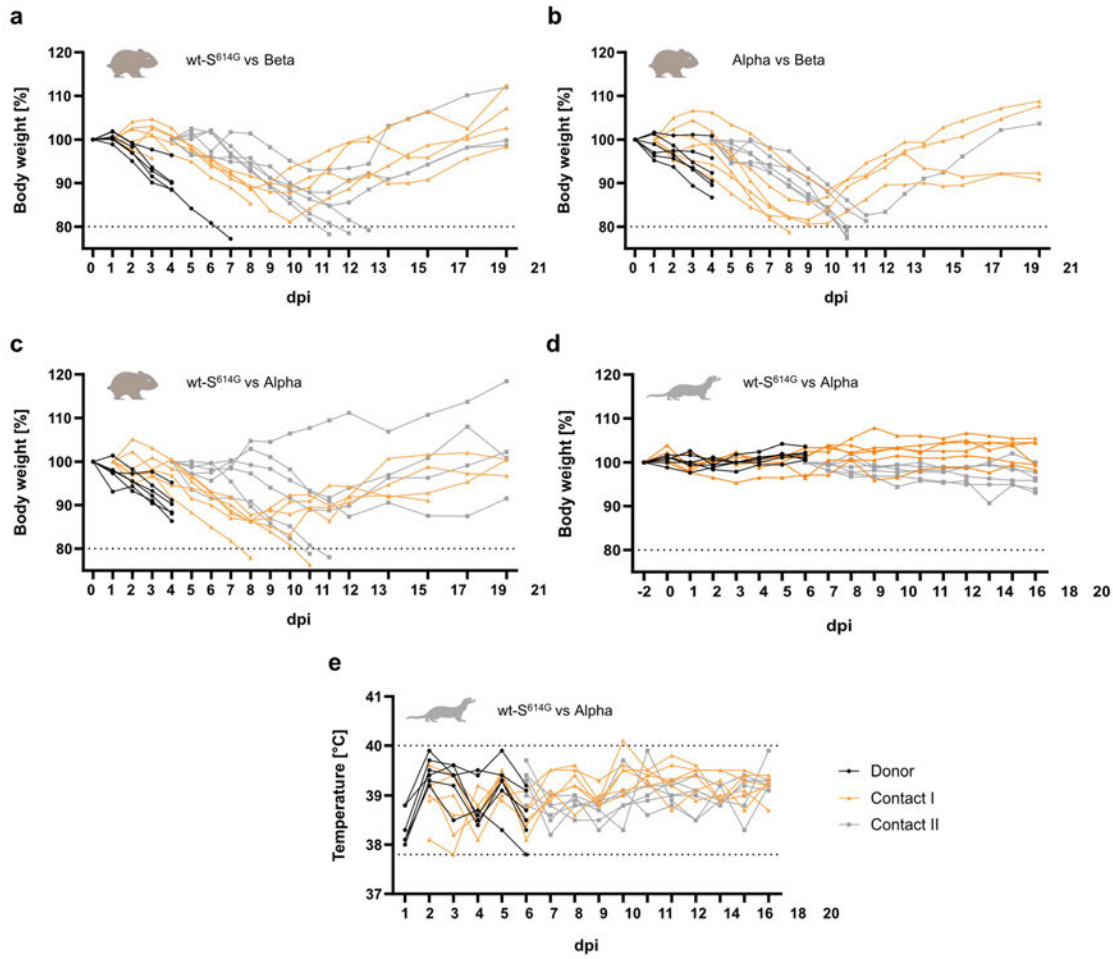
Extended Data Fig. 4 | Clinical features of hamsters and ferrets. (**a**–**c**) Syrian hamsters were inoculated with comparable genome equivalent mixture of either wt-S[614G] and Beta (**a**), Alpha and Beta (**b**), or wt-S[614G] and Alpha (**c**). In hamsters, body weight was monitored daily until 13 dpi, afterwards every two days until 21 dpi and plotted relative to body weight of day 0. The dotted line indicates the humane endpoint criterion of 20% body weight loss from initial body weight at which hamsters were promptly euthanized for animal welfare reasons. (**d**, **e**) Ferrets were inoculated intranasally with an equal mixture of wt-S[614G] and Alpha. Body weight (**d**) and temperature (**e**) were monitored daily in ferrets until 12 dpi, and afterwards every 2 days. Grey dotted lines in e indicate the physiologic range for body temperature in ferrets.
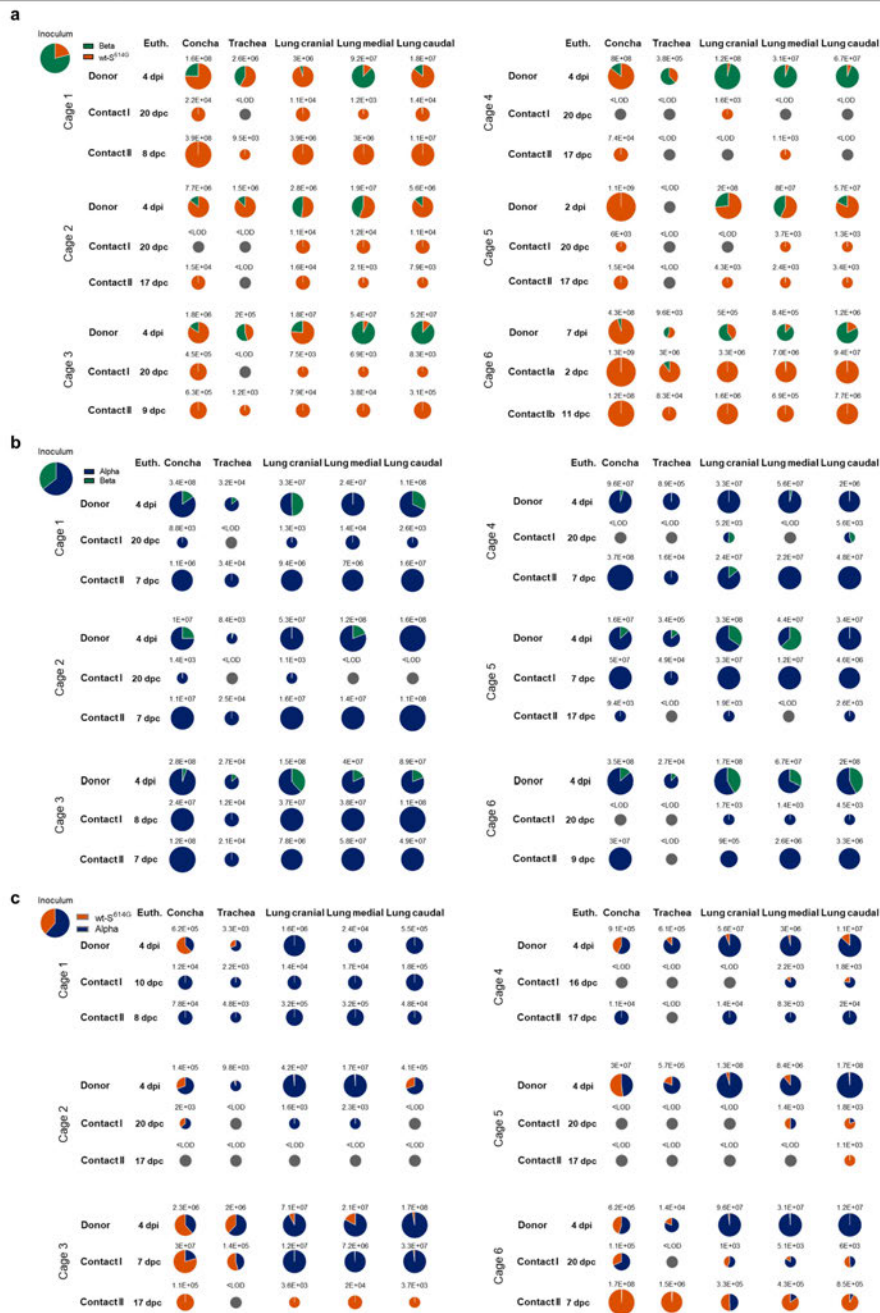
Extended Data Fig. 5 | Viral genome load in upper (URT) and lower (LRT) respiratory tract tissues of Syrian hamsters in the competitive transmission experiment between SARS-CoV-2 VOCs. (a–c) Syrian hamsters were inoculated with comparable genome equivalent mixture of either wt-S[614G] and Beta (**a**), Alpha and Beta (**b**), or wt-S[614G] and Alpha (**c**). Absolute quantification was performed by RT–qPCR analysis of tissue homogenates of donor, contact I and contact II hamsters in relation to a set of defined standards. Tissue samples were collected at euthanasia (Euth.). Pie chart colors illustrate the ratio of variants detected in each sample at the indicated dpi or days post contact (dpc). Pie chart sizes are proportional to the total viral genome copies reported below. Grey pies indicate values below the LOD (<10[3] viral genome copies per sample).

Article

a wt-S^{614G} vs Beta

b Alpha vs Beta

c wt-S^{614G} vs Alpha

d wt-S^{614G} vs Alpha

● Donor
▲ Contact I
■ Contact II
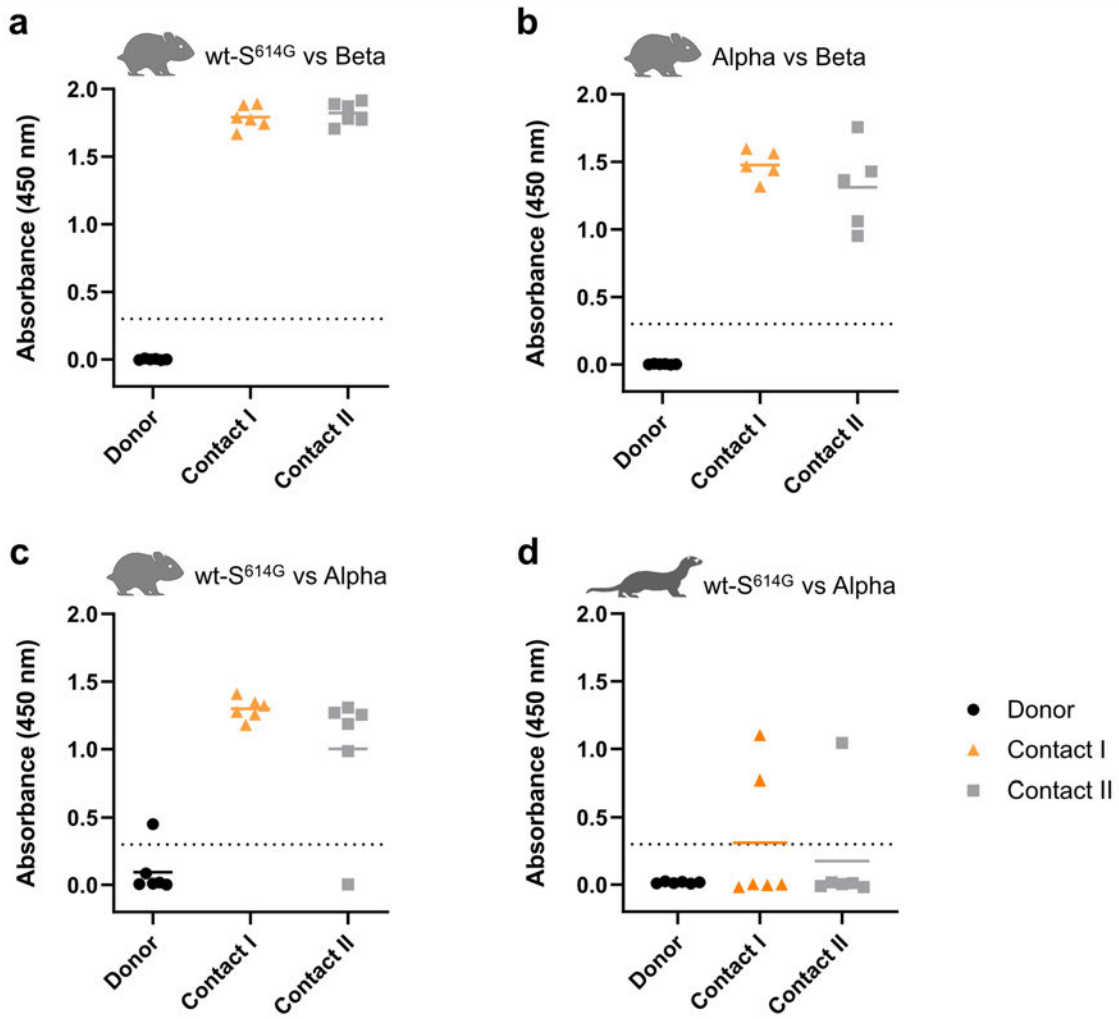
Extended Data Fig. 6 | Indirect ELISA against the RBD of SARS-CoV-2. Sera of donor hamsters (**a**, **b**, **c**) and ferrets (**d**) inoculated with the indicated SARS-CoV-2 VOC mixtures and sera of contact I and II animals were collected at their respective experimental endpoints. All sera were tested for specific reactivity against the SARS-CoV-2 RBD-SD1 domain (wt-S amino acids 319-519).
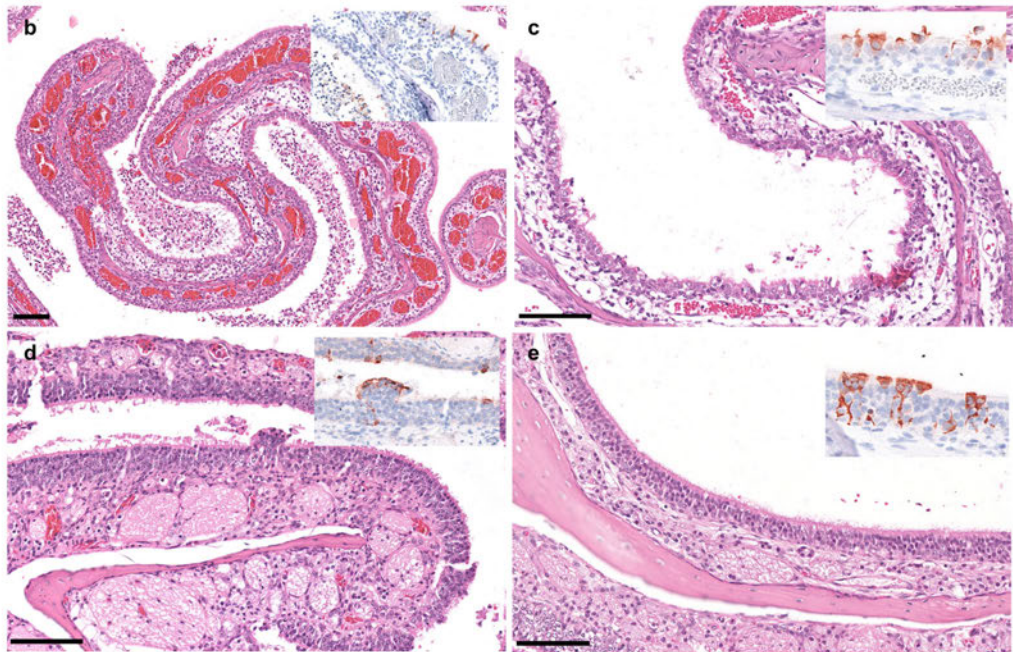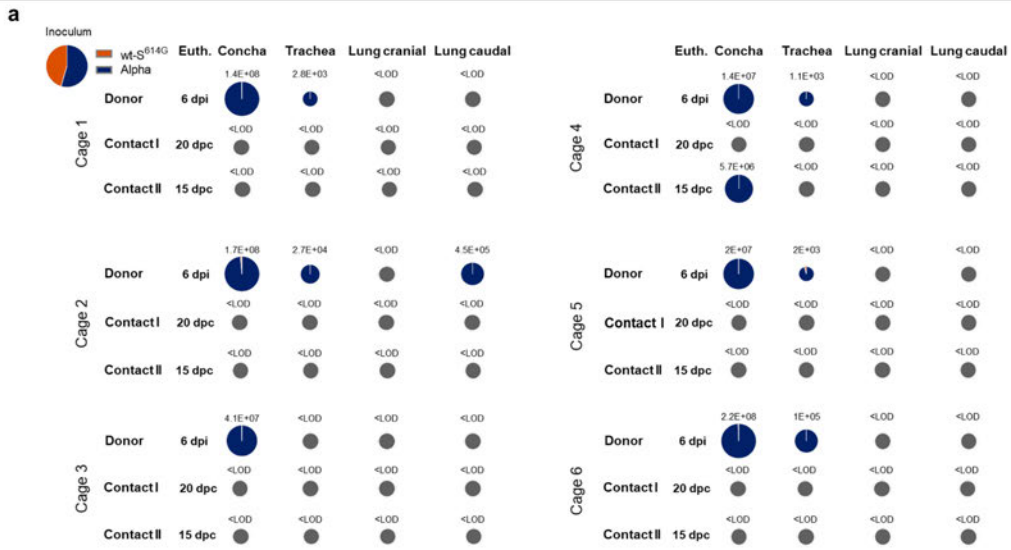
Extended Data Fig. 7 | Viral genome load in upper (URT) and lower (LRT) respiratory tract tissue of ferrets in the competitive transmission experiment between SARS-CoV-2 Alpha and wt-S⁶¹⁴ᴳ. (**a**) Absolute quantification was performed by RT–qPCR analysis of tissue homogenates of donor, contact I and contact II ferrets in relation to a set of defined standards. Tissue samples were collected at euthanasia (Euth.). Pie chart colors illustrate the ratio of variants detected in each sample at the indicated dpi or dpc. Pie chart sizes are proportional to the total viral genome copies reported below. Grey pies indicate values below the LOD (<10³ viral genome copies per sample).

(**b**–**e**) Representative micrographs of hematoxylin and eosin staining of 3 µm sections of nasal conchae of donor ferrets (n = 6) 6 dpi with wt-S⁶¹⁴ᴳ and Alpha. Micrographs are representative of 5 consecutive tissue samples of each animal. Insets show immunohistochemistry staining of SARS-CoV-2 with anti-SARS nucleocapsid antibody with hematoxylin counterstain. The respiratory (**b**, **c**) and olfactory (**d**, **e**) nasal mucosa exhibited rhinitis with varying severity. Lesion-associated antigen was found in ciliated cells of the respiratory epithelium (**b**, **c**) and in sustentacular cells of the olfactory epithelium (**d**, **e**) in all donor animals (n = 6) at 6 dpi. Scale bars are 100 µm.

Article

a

b
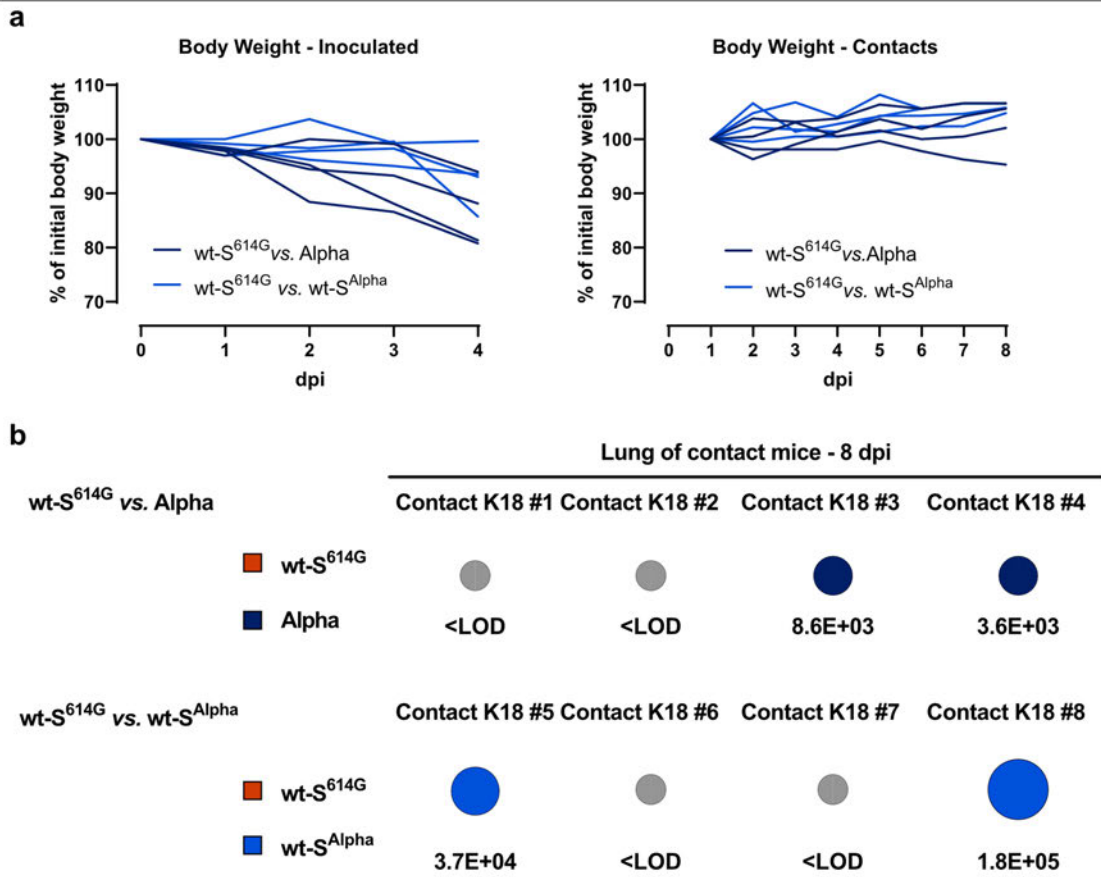
Extended Data Fig. 8 | Bodyweight and transmission in hACE2-K18Tg mice.
hACE2-K18Tg mice inoculated with a mixture of wt-S^{614G} and Alpha, or wt-S^{614G} and wt-S^{Alpha}. (**a**) Relative body weight of individual donor mice (n = 4 mice/group; left panel), and contact mice (n = 4 mice/group; right panel). (**b**) Pie chart colors illustrate the ratio of wt-S^{614G} (orange) with Alpha (dark blue), or with wt-S^{Alpha} (light blue) in corresponding experiments in lung homogenates of contact mice at 7 dpc (i.e., 8 dpi of donor mice). Pie chart sizes are proportional to the total viral genome copies reported below. Grey pies indicate values below the LOD (<10^3 viral genome copies per sample).
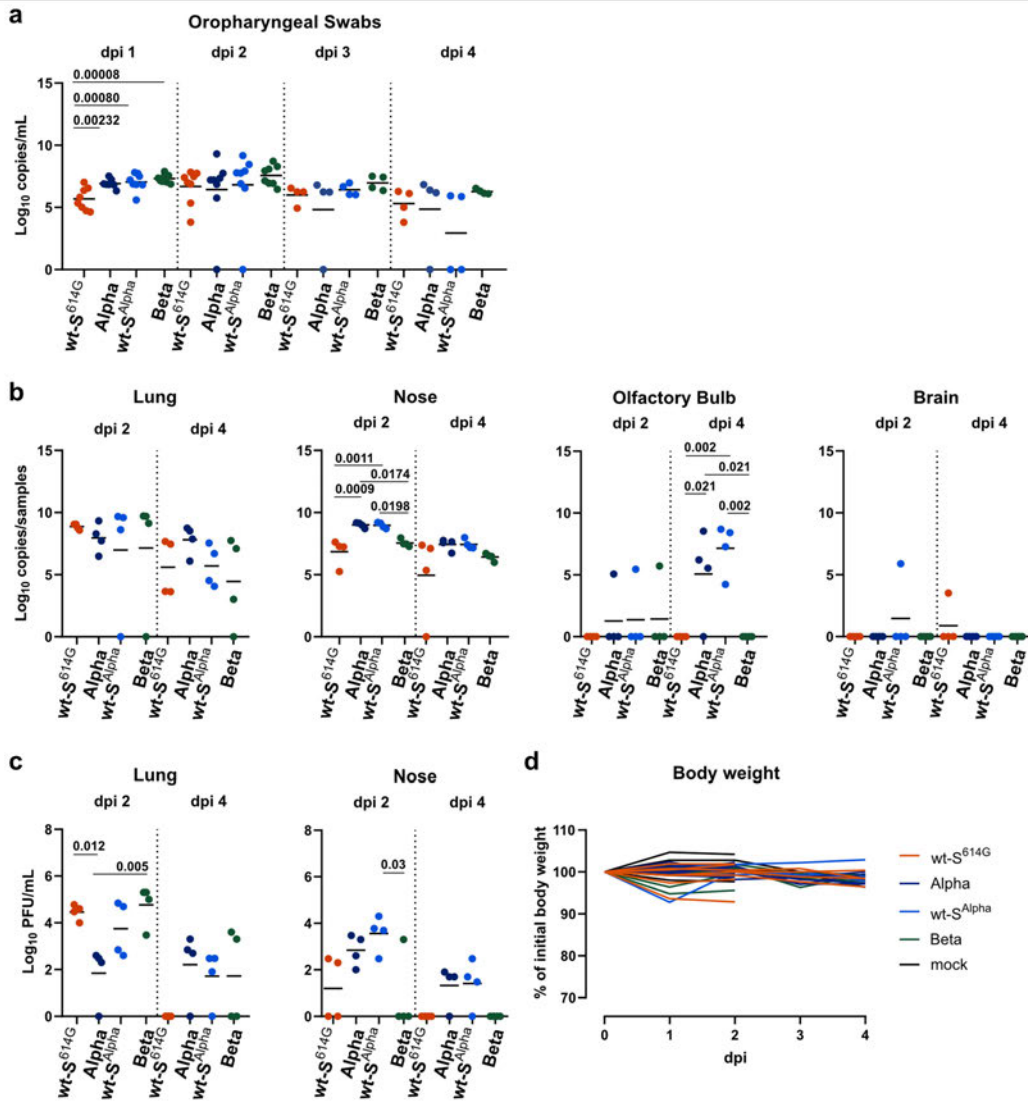
Extended Data Fig. 9 | Replication of VOC in hACE2-KI mice. (a–d) Groups hACE2-KI male mice were inoculated intranasally with 10^4 PFUs of SARS-CoV-2 wt-S^{614G}, Alpha, wt-S^{Alpha} and Beta (n = 8 mice/group). Genome copy numbers in daily oropharyngeal swabs **(a)** and in tissues **(b)**, and virus titers **(c)** in tissues were determined at indicated dpi. Data were log10 transformed and presented as individual values and mean. * p<0.05, **p<0.01 by one-way ANOVA with Tukey's multiple comparisons test comparing the four groups. **(d)** Relative body weight of individual hACE2-KI mice overtime relative to weight at infection (n = 8 mice/group until 2 dpi, and n = 4 mice/group from 3 dpi).

Article
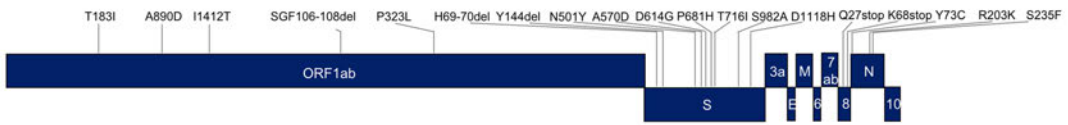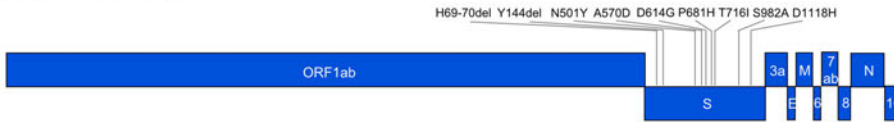
Extended Data Fig. 10 | Genome sequences of used SARS-CoV-2 variants. Colors of the variants represent respective viruses in the different experiments. Grey lines indicate positions of known mutations of each virus strain.

Extended Data Table 1 | Sequence mutations in S in SARS-CoV-2 recombinant strains

SARS-CoV-2 viruses	Mutations in S	Use	Accession ID (BioProject / GenBank / GISAID)
Isolates:			
wt-S^{614G} (B.1.610)	D614G	Kinetics in vitro	OL675863, EPI_ISL_414019
Alpha	H69/V70del, Y144del, N501Y, A570D, D614G, P681H, T716I, S982A, D1118H	Kinetics in vitro	OL689430, EPI_ISL_2131446
Beta	L18F, D80A, D215G, L242/A243/L244del, K417N, E484K, N501Y, D614G, A701V,	Kinetics in vitro	OL689583, EPI_ISL_981782
Alpha (L4549)	H69/V70del, Y144del, N501Y, A570D, D614G, P681H, T716I, S982A, D1118H	Competition wt-S^{614G} vs Alpha; in vitro, hamster, ferret, and mice Individual virus infection, mice	PRJEB45736, SARS-CoV-2 B.1.1.7 NW-RKI-I-0026/2020 passage 3 L4549, EPI_ISL_803957
Beta (L4550) (Ref. 21)	L18F, D80A, D215G, L242/L243/A244del K417N, E484K, N501Y, D614G, A701V	Competition wt-S^{614G} vs Beta; hamster, mice Competition Alpha vs Beta; hamster	MZ433432, L4550, EPI_ISL_751799
Recombinant clones:			
wt-S^{614G} (Ref. 3)	D614G	Competition wt-S^{614G} vs Beta; in vitro, hamster, mice Competition wt-S^{614G} vs Alpha; in vitro, mice Competition wt-S^{614G} vs wt-S^{Alpha}; mice Single virus infection, mice	MT108784
wt-S^{614G} (*) (L4595)	D614G, R685S	Competition wt-S^{614G} vs Alpha; hamster and ferret	PRJEB45736, wt-S614G ID#49 vial 2, L4595
wt-S^{Alpha}	H69/V70del, Y144del, N501Y, A570D, D614G, P681H, T716I, S982A, D1118H	Competition wt-S^{614G} vs wt-S^{Alpha}; mice Single virus infection, mice	PRJNA784099

(*) SARS-CoV-2 wt-S^{614G} used for the competitive experiments between wt-S^{614G} vs. Alpha in hamsters and ferrets had an exchange in 54% of the analyzed contigs from C to A in position 23615, located in the S gene.

Article

Extended Data Table 2 | Sequences of primer and probes for RT-qPCR assays

Oligo name	Sequence (5´- 3´)	Conc.	Position
SARS-CoV-2 wt-S^{614G} -ORF1 assay			
wt-S^{614G} -ORF1-1.2F	TGG TTG ATA CTA GTT TGT CTG GT	10 μM	11271-11293 *
wt-S^{614G} -ORF1-1.3R	GCA CCA TCA TCA TAC ACA GTT C	10 μM	11379-11358 *
wt-S^{614G} -ORF1-1FAM	FAM-TGC ATC AGC TGT AGT GTT ACT AAT CC-BHQ1	5 μM	11320-11345 *
SARS-CoV-2 wt-S^{614G} -S assay			
wt-S^{614G} -S-1.2F	TAC TTG GTT CCA TGC TAT ACA TGT	10 μM	21748-21771 *
wt-S^{614G} -S-1.5R	CCA ACT TTT GTT GTT TTT GTG GTA ATA	10 μM	22018-21992 *
wt-S^{614G} -S-1FAM	FAM-ACC CTG TCC TAC CAT TTA ATG ATG-BHQ1	5 μM	21804-21827 *
SARS-CoV-2 Alpha -ORF1 assay			
B117-ORF1-2.1F	GAT ATG GTT GAT ACT AGT TTG AAG	10 μM	11265-11288 **
wt-S^{614G} -ORF1-1.3R	See above		
wt-S^{614G} -ORF1-1FAM	See above		
SARS-CoV-2 Alpha -S assay			
B117-S-1.2F	TTA CTT GGT TCC ATG CTA TMT C	10 μM	21736-21757 **
B117-S-1.3R	AAC TTT TGT TGT TTT TGT GGT AAA C	10 μM	21996-21972 **
wt-S^{614G} -S-1FAM	See above		

* Position based on NC_045512; ** Position based on MW963651. Conc, concentration.

Extended Data Table 3 | Attribution of RT-qPCR assays used for the individual competitive transmission experiments

Assay	For detection of
wt-S^{614G} vs Alpha (hamsters, ferrets)	
SARS-CoV-2 wt-S^{614G} -ORF1 assay	SARS-CoV-2 wt-S^{614G}
SARS-CoV-2 Alpha -ORF1 assay	SARS-CoV-2 Alpha
wt-S^{614G} vs Alpha (human AEC cultures, mice)	
SARS-CoV-2 wt-S^{614G} -S assay	SARS-CoV-2 wt-S^{614G}
SARS-CoV-2 Alpha -S assay	SARS-CoV-2 Alpha
SARS-CoV-2 Alpha -S assay	SARS-CoV-2 wt-S^{Alpha}
wt-S^{614G} vs Beta (human AEC cultures, hamsters and mice)	
SARS-CoV-2 wt-S^{614G} -ORF1 assay	SARS-CoV-2 wt-S^{614G}
SARS-CoV-2 Alpha -ORF1 assay	SARS-CoV-2 Beta
Alpha vs Beta (human AEC cultures, hamsters)	
SARS-CoV-2 Alpha -S assay	SARS-CoV-2 Alpha
SARS-CoV-2 wt-S^{614G} -S assay	SARS-CoV-2 Beta

nature portfolio

Corresponding author(s): Charaf Benarafa, Martin Beer, Volker Thiel

Last updated by author(s): Nov 26, 2021

Reporting Summary

Nature Portfolio wishes to improve the reproducibility of the work that we publish. This form provides structure for consistency and transparency in reporting. For further information on Nature Portfolio policies, see our Editorial Policies and the Editorial Policy Checklist.

Statistics

For all statistical analyses, confirm that the following items are present in the figure legend, table legend, main text, or Methods section.

n/a	Confirmed	
☐	☒	The exact sample size (*n*) for each experimental group/condition, given as a discrete number and unit of measurement
☐	☒	A statement on whether measurements were taken from distinct samples or whether the same sample was measured repeatedly
☐	☒	The statistical test(s) used AND whether they are one- or two-sided. *Only common tests should be described solely by name; describe more complex techniques in the Methods section.*
☐	☒	A description of all covariates tested
☐	☒	A description of any assumptions or corrections, such as tests of normality and adjustment for multiple comparisons
☐	☒	A full description of the statistical parameters including central tendency (e.g. means) or other basic estimates (e.g. regression coefficient) AND variation (e.g. standard deviation) or associated estimates of uncertainty (e.g. confidence intervals)
☐	☒	For null hypothesis testing, the test statistic (e.g. F, t, r) with confidence intervals, effect sizes, degrees of freedom and P value noted. *Give P values as exact values whenever suitable.*
☒	☐	For Bayesian analysis, information on the choice of priors and Markov chain Monte Carlo settings
☒	☐	For hierarchical and complex designs, identification of the appropriate level for tests and full reporting of outcomes
☒	☐	Estimates of effect sizes (e.g. Cohen's *d*, Pearson's *r*), indicating how they were calculated

Our web collection on statistics for biologists contains articles on many of the points above.

Software and code

Policy information about availability of computer code

Data collection	ELISA: Tecan i-control 2014 1.11 qRT-PCR: QuantStudio™ Real-Time PCR Software (v1.7.1), or 7500 Fast System SDS Software Version 1.4 Viral titers: manual counting, registered in Microsoft Excel 2016 (16.0.5239.1001) BLI: Octet RED96e instrument with ForteBio Data Acquisition Software (Version: 12.0.1.8)
Data analysis	relative variant quantification: Bio-Rad CFX Maestro 1.1 Version 4.1.2433.1219 sequence analysis: Geneious Prime * 2019.2.3 figures: GraphPad Prism 8.4.2 (679) for Windows, Microsoft PowerPoint 2016 (16.0.4266.1001), Adobe Photoshop CS5 64 bit NGS: Genome Sequencer Software Suite (version 2.6; Roche, https://roche.com), variant analysis tool integrated in Geneious Prime (2019.2.3) digital PCR: QuantaSoft Analysis Pro software (version 1.0.596) ELISA: Microsoft Excel 2016 (16.0.5188.1000) Statistical analysis: GraphPad Prism version 8 or R (version 4.1), using the packages tidyverse (v1.3.1), ggpubr (v0.4.0), rstatix (v.0.7.0). BLI: ForteBio Data Analysis Software (Version 12.0.1.2)

For manuscripts utilizing custom algorithms or software that are central to the research but not yet described in published literature, software must be made available to editors and reviewers. We strongly encourage code deposition in a community repository (e.g. GitHub). See the Nature Portfolio guidelines for submitting code & software for further information.

Data

Policy information about availability of data

All manuscripts must include a data availability statement. This statement should provide the following information, where applicable:
- Accession codes, unique identifiers, or web links for publicly available datasets
- A description of any restrictions on data availability
- For clinical datasets or third party data, please ensure that the statement adheres to our policy

Sequence data are available on the NCBI Sequence Read Archive (SRA) under the accession numbers PRJEB45736, and PRJNA784099, or in GenBank under the accession numbers MT108784, MZ433432, OL675863, OL689430, and OL689583 as shown in Extended Data Table 1. Source data are provided with this paper.

Field-specific reporting

Please select the one below that is the best fit for your research. If you are not sure, read the appropriate sections before making your selection.

☒ Life sciences ☐ Behavioural & social sciences ☐ Ecological, evolutionary & environmental sciences

For a reference copy of the document with all sections, see nature.com/documents/nr-reporting-summary-flat.pdf

Life sciences study design

All studies must disclose on these points even when the disclosure is negative.

Sample size	No sample size calculations were performed. Number of animals used in experiments were based on our previous comparative studies of fitness of SARS-CoV-2 variants.
Data exclusions	No data were excluded from analysis.
Replication	Binding Assays (BLI): data are representative of 3 independent experiments. Airway epithelial cell (AEC) cultures in vitro: All attempts at replication were successful; experiments were performed independently on different biological donors according to best practices and as described in the Methods. In vivo: Competition experiments between two VOCs were performed on groups of 6 infected animals and replicated in 4 animal models. Competition between wt-S614G and Alpha was replicated in males and females. All attempts at replication were successful. Single VOC infections were performed in groups of 8 mice for each variant.
Randomization	No randomization was required for all in vitro and in vivo competition experiments because the viral and host response parameters were measured within each cell culture insert or each animal. For single infection with VOCs, hACE2-KI were randomly assigned to the respective study groups.
Blinding	Investigators were blinded during analysis of viral plaque and qRT-PCR assays of in vitro and in vivo experiments. Blinding was also not relevant for in vivo competition experiments as both arms of the comparison were in single animals.

Reporting for specific materials, systems and methods

We require information from authors about some types of materials, experimental systems and methods used in many studies. Here, indicate whether each material, system or method listed is relevant to your study. If you are not sure if a list item applies to your research, read the appropriate section before selecting a response.

Materials & experimental systems

n/a	Involved in the study
☐	☒ Antibodies
☐	☒ Eukaryotic cell lines
☒	☐ Palaeontology and archaeology
☐	☒ Animals and other organisms
☒	☐ Human research participants
☒	☐ Clinical data
☒	☐ Dual use research of concern

Methods

n/a	Involved in the study
☒	☐ ChIP-seq
☒	☐ Flow cytometry
☒	☐ MRI-based neuroimaging

Antibodies

Antibodies used	anti-SARS nucleocapsid antibody (Novus Biologicals #NB100-56576)

2

Validation	relevant validation information can be accessed at https://www.novusbio.com/products/sars-nucleocapsid-protein-antibody_nb100-56576#reviews-publications

Eukaryotic cell lines

Policy information about cell lines

Cell line source(s)	Vero E6 cells (FLI): Collection of Cell Lines in Veterinary Medicine CCLV RIE 0929 Vero E6 cells (IVI, IFIK): cells were kindly provided by Doreen Muth, Marcel Müller, and Christian Drosten, Charité, Berlin, Germany (ATCC CRL-1586) Vero-TMPRSS2 cells were kindly provided by Stefan Pöhlmann, German Primate Center - Leibniz Institute for Primate Research, Göttingen, Germany) Primary human nasal cells were commercially procured from Epithelix, in Geneva, Switzerland. Expi293F cells: ThermoFisher Scientific, USA. A549-hACE2 cells were derived from ATCC CCL-185 and kindly provided by M. Schmolke, B. Mazel-Sanchez, and F. Abdul, Faculty of Medicine, Geneva
Authentication	in-house authentication for cell lines was not performed
Mycoplasma contamination	Cell lines were tested negative for mycoplasma contamination.
Commonly misidentified lines (See ICLAC register)	None

Animals and other organisms

Policy information about studies involving animals; ARRIVE guidelines recommended for reporting animal research

Laboratory animals	Mustela putorius furo, ferrets, neutered male and female, 8 - 23 months Mesocricetus auratus, Syrian hamster, male, 7-12 weeks Mus musculus, mice B6.Cg-Tg(K18-ACE2)2Prlmn/J, male and female, 10-12 weeks Mus musculus, mice B6.Cg-Ace2<tm1(ACE2)Dwnt>, male and female, 10-12 weeks
Wild animals	No wild animals were used
Field-collected samples	Field samples were not collected
Ethics oversight	Ferrets/hamsters: State Office of Agriculture ethics committee, Food Safety, and Fishery in Mecklenburg–Western Pomerania, Germany, registration number LVL MV TSD/7221.3-1-004/21 Mice: Commission for Animal Experimentation, Cantonal Veterinary Office of Bern, Switzerland, license BE-43/20

Note that full information on the approval of the study protocol must also be provided in the manuscript.

nature portfolio | reporting summary

March 2021

3

IV

Publication IV

The spike gene is a major determinant for the SARS-CoV-2 Omicron-BA.1 phenotype

G. Tuba Barut*, **Nico Joël Halwe***, Adriano Taddeo*, Jenna N. Kelly*, Jacob Schön, Nadine Ebert, Lorenz Ulrich, Christelle Devisme, Silvio Steiner, Bettina Salome Trüeb, Bernd Hoffmann, Inês Berenguer Veiga, Nathan Georges François Leborgne, Etori Aguiar Moreira, Angele Breithaupt, Claudia Wylezich, Dirk Höper, Kerstin Wernike, Aurélie Godel, Lisa Thomann, Vera Flück, Hanspeter Stalder, Melanie Brügger, Blandina I. Oliveira Esteves, Beatrice Zumkehr, Guillaume Beilleau, Annika Kratzel, Kimberly Schmied, Sarah Ochsenbein, Reto M. Lang, Manon Wider, Carlos Machahua, Patrick Dorn, Thomas M. Marti, Manuela Funke-Chambour, Andri Rauch, Marek Widera, Sandra Ciesek, Ronald Dijkman, Donata Hoffmann, Marco P. Alves, Charaf Benarafa, Martin Beer & Volker Thiel

The spike gene is a major determinant for the SARS-CoV-2 Omicron-BA.1 phenotype

A list of authors and their affiliations appears at the end of the paper

Variant of concern (VOC) Omicron-BA.1 has achieved global predominance in early 2022. Therefore, surveillance and comprehensive characterization of Omicron-BA.1 in advanced primary cell culture systems and animal models are urgently needed. Here, we characterize Omicron-BA.1 and recombinant Omicron-BA.1 spike gene mutants in comparison with VOC Delta in well-differentiated primary human nasal and bronchial epithelial cells in vitro, followed by in vivo fitness characterization in hamsters, ferrets and hACE2-expressing mice, and immunized hACE2-mice. We demonstrate a spike-mediated enhancement of early replication of Omicron-BA.1 in nasal epithelial cultures, but limited replication in bronchial epithelial cultures. In hamsters, Delta shows dominance over Omicron-BA.1, and in ferrets Omicron-BA.1 infection is abortive. In hACE2-knock-in mice, Delta and a Delta spike clone also show dominance over Omicron-BA.1 and an Omicron-BA.1 spike clone, respectively. Interestingly, in naïve K18-hACE2 mice, we observe Delta spike-mediated increased replication and pathogenicity and Omicron-BA.1 spike-mediated reduced replication and pathogenicity, suggesting that the spike gene is a major determinant of replication and pathogenicity. Finally, the Omicron-BA.1 spike clone is less well-controlled by mRNA-vaccination in K18-hACE2-mice and becomes more competitive compared to the progenitor and Delta spike clones, suggesting that spike gene-mediated immune evasion is another important factor that led to Omicron-BA.1 dominance.

On a global scale, SARS-CoV-2 evolution can be tracked by identifying independently emerging variants of concern (VOCs), with VOC Alpha, Delta, and Omicron dominating successively. Delta carries two deterministic mutations potentially leading to increased fitness: L452R, conferring immune escape[1], and P681R, conferring enhanced transmission[2]. Omicron-BA.1 holds in total up to 50 mutations, with 34 located in the spike (S) gene, 15 of which are within the receptor-binding domain (RBD)[3]. A defining Omicron-BA.1 mutation is ins214EPE, a three-amino acid insertion, whose role for viral fitness is still unknown. However, this VOC is characterized by its remarkable ability to evade neutralizing antibodies up to 40 times more efficiently than the ancestral SARS-CoV-2 and pre-Omicron variants[4,5]. In January 2022, the Omicron-BA.1 lineage became predominant in most countries worldwide[6] and has since then largely been replaced by the related Omicron-BA.2 and other Omicron sublineages. It remains elusive if the rapid spread of Omicron-BA.1 and the replacement of Delta is due to increased fitness and transmission, or if it is mainly based on its immune escape ability allowing efficient infection and transmission chains among double-vaccinated and even boosted individuals. The genetic determinants for the Omicron-BA.1 phenotype also remain largely undefined. With high prevalence of concurrent VOCs and reports of recombination events in communities[7], it is crucial to characterize differences in viral fitness and immune escape of emerging and prevailing VOCs in advanced cell culture and animal models[8].

While mouse models expressing human angiotensin-converting enzyme 2 (hACE2) and Syrian hamsters are highly susceptible for SARS-CoV-2 and show signs of severe disease, ferrets display subclinical infection despite efficient viral replication of SARS-CoV-2 in the

✉ e-mail: marco.alves@vetsuisse.unibe.ch; charaf.benarafa@vetsuisse.unibe.ch; martin.beer@fli.de; volker.thiel@vetsuisse.unibe.ch

Article   https://doi.org/10.1038/s41467-022-33632-y

upper respiratory tract (URT)[9,10]. An experimental setup applying competitive infection and transmission experiments in different species has become a gold-standard method to investigate VOC fitness[9–12]. With this experimental approach, the fitness of SARS-CoV-2 VOCs can be analyzed in direct comparison at the nucleotide and variant level.

Here, we demonstrate a dominance of Delta over Alpha in ferrets, whereas in Syrian hamsters, Alpha dominated Delta. Moreover, we demonstrate that the advent of the Omicron VOC in the evolution of SARS-CoV-2 is a radical change from the incremental improvements in fitness observed in previous pandemic VOCs. Using a comprehensive experimental VOC competition approach against Delta, we demonstrate that the Omicron-BA.1 phenotype is characterized by (i) a reduced replication and transmission fitness in Syrian hamsters, (ii) a failure to replicate in ferrets, (iii) an accelerated growth in human epithelial cell cultures mimicking the upper respiratory tract, (iv) a reduced replication in precision-cut lung slices (PCLS) and primary human bronchial epithelial cultures, resembling conditions of the human lower respiratory tract, (v) a reduced replication fitness in naïve human ACE2 (hACE2) expressing knock-in (hACE2-KI) and transgenic (K18-hACE2) mice, and (vi) evidence of immune evasion in mRNA-vaccinated K18-hACE2 mice. Importantly, we show that the spike gene is a major determinant in the Omicron-BA.1 phenotype based on in vitro and in vivo experiments using recombinant SARS-CoV-2 clones differing only by the expression of the spike protein of the respective VOCs.

Results
Omicron-BA.1 spike enhances viral replication in the nasal but not bronchial epithelium
In order to assess the phenotypes of the VOCs Delta and Omicron-BA.1 and to evaluate the contribution of changes within the spike protein, we constructed a set of recombinant SARS-CoV-2 clones containing defined mutations in the spike gene (Fig. 1a). All constructs have an isogenic background based on the Wuhan-Hu-1 sequence and differ only in the spike gene, which was modified to contain lineage-defining spike gene mutations of the VOC Delta (SARS-CoV-2$^{S\text{-}Delta}$), VOC Omicron-BA.1 (SARS-CoV-2$^{S\text{-}Omicron}$), mutations of the Omicron-BA.1 spike N-terminal domain (NTD; SARS-CoV-2$^{NTD\text{-}Omicron}$), mutations of the Omicron-BA.1 spike receptor-binding domain (RBD; SARS-CoV-2$^{RBD\text{-}Omicron}$), or the mutations at and near the Omicron-BA.1 spike cleavage site region (CS; SARS-CoV-2$^{CS\text{-}Omicron}$). All recombinant viruses replicated but showed noticeable differences in plaque sizes (Fig. 1b). Compared to the index virus SARS-CoV-2^{D614G} (recombinant SARS-CoV-2 based on Wuhan-Hu-1 with the spike change D614G[11]), the Delta isolate showed smaller plaques, while plaques of SARS-CoV-2$^{S\text{-}Delta}$ were considerably larger. Interestingly, SARS-CoV-2$^{S\text{-}Omicron}$ displayed small plaques that were indistinguishable from the isolate of Omicron-BA.1 (EPI_ISL_7062525), but plaques of Omicron-BA.1 spike subdomain clones (SARS-CoV-2$^{NTD\text{-}Omicron}$, SARS-CoV-2$^{CS\text{-}Omicron}$, SARS-CoV-2$^{RBD\text{-}Omicron}$) differed in size (Fig. 1b), indicating possible phenotypic differences of the Omicron-BA.1 spike subdomain clones compared to the Omicron-BA.1 isolate and the full-length Omicron-BA.1 spike clone.

Next, we infected well-differentiated primary human nasal and bronchial epithelial cell cultures (hNECs and hBECs, respectively) at 33 °C for hNECs and at 37 °C for hBECs (Fig. 1c, d). Delta and the corresponding spike construct SARS-CoV-2$^{S\text{-}Delta}$ replicated with similar kinetics as wild-type SARS-CoV-2^{D614G} on both hNECs and hBECs, with SARS-CoV-2$^{S\text{-}Delta}$ reaching the highest apical titers at 72–96 h post-infection (hpi) (Fig. 1c). Strikingly, replication kinetics of Omicron-BA.1 and the corresponding spike clone SARS-CoV-2$^{S\text{-}Omicron}$ displayed accelerated growth within the first 48 hpi on hNECs. In contrast, on hBECs, Omicron-BA.1 and SARS-CoV-2$^{S\text{-}Omicron}$ did not show this early accelerated growth, and moreover, showed significantly reduced viral titers at later time points. This phenotype was confirmed by

competition assays on hNECs and hBECs using various combinations of viruses in the inoculum (Fig. 1e, f; Supplementary Fig. 1). On hNECs, the Omicron-BA.1 isolate and the corresponding SARS-CoV-2$^{S\text{-}Omicron}$ outcompeted SARS-CoV-2^{D614G}, the Delta isolate, and SARS-CoV-2$^{S\text{-}Delta}$ (Fig. 1d). In contrast, the dominance of the Omicron-BA.1 isolate, and SARS-CoV-2$^{S\text{-}Omicron}$ was reduced in hBECs (Fig. 1d). Finally, SARS-CoV-2$^{S\text{-}Delta}$ was dominant over SARS-CoV-2$^{S\text{-}Omicron}$ in an ex vivo distal precision-cut lung slices (PCLS) system (Fig. 1g).

Collectively, studies in vitro under conditions mimicking the native human upper respiratory tract epithelium (URT; hNECs at 33 °C) remarkably demonstrate that the Omicron-BA.1 spike gene (Omicron-BA.1 isolate and SARS-CoV-2$^{S\text{-}Omicron}$) confers accelerated virus replication and increased replicative fitness compared to pre-Omicron spike genes (SARS-CoV-2^{D614G}, a Delta isolate, and SARS-CoV-2$^{S\text{-}Delta}$). In contrast, under conditions resembling the human lower respiratory tract epithelium (LRT; hBECs, 37 °C; PCLS), the Omicron-BA.1 spike gene confers reduced virus replication.

Replicative fitness and transmission of VOCs Alpha, Delta, and Omicron in Syrian hamsters
To evaluate individual VOC fitness advantages in direct competition with the precursing VOC, we then turned to animal models with natural susceptibility towards SARS-CoV-2: ferrets and Syrian hamsters. Donor animals were simultaneously co-inoculated with two VOCs at iso-titer and transmission to contact animals was investigated (Supplementary Fig. 2a, b).

We investigated fitness of the VOC Delta in competition with Alpha after intranasal co-inoculation of $10^{4.625}$ TCID$_{50}$ of an Alpha-Delta mixture at a 1.95:1 ratio (Supplementary Figs. 2a and 5). For all donor and contact hamsters, Alpha showed complete dominance in nasal washings and respiratory tissues (Supplementary Figs. 5 and 8). The animals showed signs of severe disease and 10 of 12 contact hamsters reached the humane endpoint, (defined by a 20% loss of the initial body weight) (Supplementary Figs. 3a, c and 5). While Alpha was clearly dominant in all animals, sera equally neutralized Alpha and Delta VOCs (VNT$_{100}$) (Supplementary Fig. 7a).

We also tested Delta vs Omicron-BA.1 (total $10^{4.5}$ TCID$_{50}$ at a 1:2.16 ratio) in hamsters (Fig. 2a, Supplementary Fig. 2a). Upon inoculation or contact, all animals lost body weight, however, only one animal was euthanized after reaching the humane endpoint for body weight loss (Fig. 2a, Supplementary Fig. 3b, d). Although starting with a clear advantage for Omicron-BA.1 in the inoculum, Delta was immediately prevalent in nasal washings of donor hamsters with up to 10^8 genome copies per mL (GE/mL) (Fig. 2a). Remarkably, despite high genome loads of Delta, Omicron-BA.1 still replicated to 10^7 GE/mL (Fig. 2a). Nevertheless, Delta was preferentially transmitted as seen in both nasal washings and organ samples of contact animals (Fig. 2a, Supplementary Fig. 4). In tissues of donor animals at 4 dpi, mainly Delta was found in the upper (URT) and lower respiratory tract (LRT) (Fig. 2b); with highest Delta loads in the nasal concha (10^8 GE/mL). However, Omicron-BA.1 was still present in the URT of each donor animal (up to 10^7 GE/mL) (Fig. 2b). Consequently, the antibody response was mainly directed against Delta with neutralization up to a serum dilution of 1:1024, while Omicron-BA.1 was only barely neutralized (Fig. 2d). Together, we show that the Syrian hamster is highly susceptible also for the SARS-CoV-2 VOCs Alpha, Delta, and Omicron-BA.1. However, the Alpha VOC seems to be best replicating and transmitting in the Syrian hamster model associated with the highest fatality rates.

Omicron-BA.1 fails to induce productive infection in ferrets
For further characterization of the different VOCs, we also inoculated ferrets, which are known to mirror human respiratory disease. First, animals were inoculated with a Delta isolate (Supplementary Fig. 2c). All animals remained clinically healthy and did not lose body weight

Article
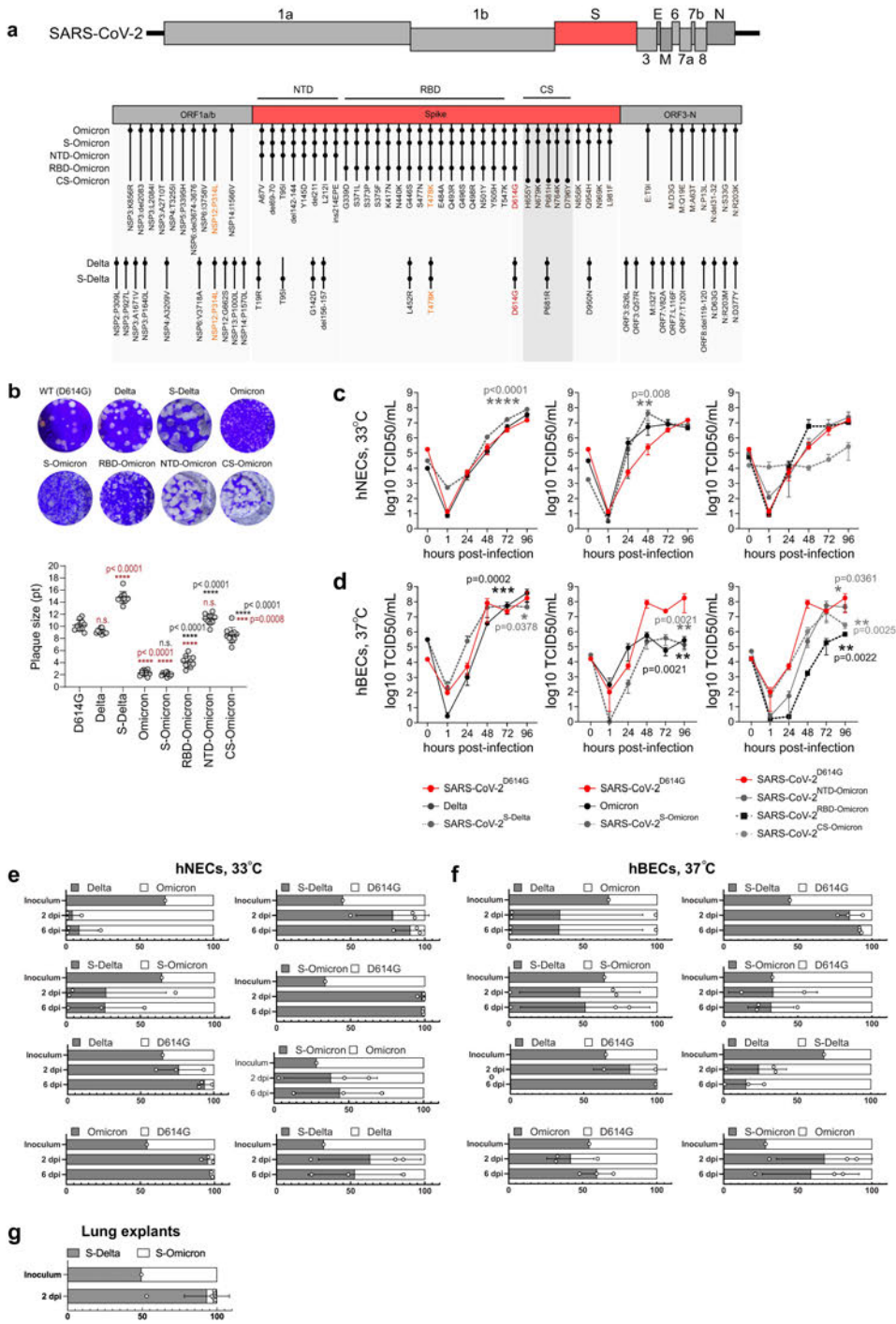
(Supplementary Fig. 3e). Viral shedding was confirmed for all donor animals by nasal washing for up to 10 days, with highest viral genome loads of up to >10^7 GE/mL at 5 and 6 dpi (Fig. 2f). Two out of three contact animals were infected by 6 days post contact (dpc) and viral loads in contacts reached up to 10^8 GE/mL (Fig. 2f). These results were also confirmed by serology (Fig. 2f).

Next, ferrets were co-inoculated with VOCs Alpha and Delta (1.33:1 ratio, 10^5 TCID$_{50}$ in total) (Supplementary Figs. 2b and 6). All ferrets remained clinically healthy throughout the animal experiment and did not lose body weight (Supplementary Fig. 3g). Within 3 days, Delta fully outcompeted Alpha in both replication and transmission (Supplementary Fig. 6), which is in line with the epidemiological situation

Article

Fig. 1 | Enhanced replication of Omicron-BA.1 in nasal but not bronchial epithelial cell cultures. a Genome sequences were compared to the SARS-CoV-2[D614G] WT virus and lineage-defining mutations (LDM) are depicted. The D614G mutation is highlighted in red, while the mutations highlighted in orange are either present in both Delta and Omicron, or in Omicron, S-Omicron, RBD-Omicron, Delta, and S-Delta, but not in SARS-CoV-2[D614G]. **b** The plaque sizes of viruses in 6-well plates 2 dpi. Sizes of 10 plaques/wells from one biological replicate were measured in Adobe Illustrator. Data are presented as mean+/−SD. Statistical significance was determined using ordinary one-way Anova and *p*-values were adjusted using Tukey's multiple-comparison test; *P < 0.05, **P < 0.01, ***P < 0.001, ****P < 0.0001. Statistical significance of the differences of each virus vs. SARS-CoV-2[D614G] WT virus are demarcated with the red asterisks, whereas the black asterisks indicate the comparison of the Omicron spike subdomain clones to Omicron. **c, d** Human nasal (NEC) (*n* = 3 donors) and bronchial epithelial cell (BEC) (*n* = 3) cultures were infected with 10⁴ TCID₅₀ of the SARS-CoV-2 variants from the apical side and

incubated at 33 °C (NECs) or 37 °C (BECs) for 1 h. Virus titers were assessed by TCID₅₀ assays on VeroE6/TMPRSS2 cells. The graph represents the titers obtained from three donors (mean+/−SD) from one biological replicate. Statistical significance was determined using two-way ANOVA and *p*-values were adjusted using Tukey's multiple-comparison test; *P < 0.05, **P < 0.01, ***P < 0.001, ****P < 0.0001. **e–g** NECs (*n* = 3), BECs (*n* = 3), or PCLS (*n* = 3) were infected with virus mixtures in a 1:1 ratio based on genome equivalents (GE) calculated by qPCR. Apical washes were collected at 2 and 6 dpi for the NECs and BECs and 2 dpi for PCLS. RNA was extracted from apical washes and sequenced on the MinION platform (Oxford Nanopore Technologies). Virus ratios were calculated for each donor based on the mean frequency of unique LDM mutations for each virus present in the mixture (for more details: Supplementary Fig. 1). Values shown represent the mean ratio/donor (circles) and the mean ratio/time point (bars) for each virus mixture (mean+/−SD). Each data point represents one biological replicate. Source data for Fig. 1 are provided as a Source Data file 1.Source Data file 1.

observed in humans. These observations were further supported by the matching serological data (Supplementary Fig. 7b).

We finally investigated the competition between Delta and Omicron-BA.1 in the ferret model by inoculating a 10^{4.75} TCID₅₀ Delta-Omicron mixture (1:1.43 ratio) (Fig. 2c, Supplementary Fig. 2B). All ferrets remained clinically healthy throughout the animal experiment and did not lose body weight (Supplementary Fig. 3h). Astonishingly, only Delta was detected in all nasal washings of the donor ferrets, starting at 1 dpi at levels of up to 10⁷ GE/mL (Fig. 2c). In addition, 5 out of 6 contact ferrets showed shedding of Delta (highest loads: 10⁷ GE/mL), starting at 2 dpc (Fig. 2c). The shedding interval lasted up to 12 days in the donor ferrets (Fig. 2c). Surprisingly, Omicron-BA.1 was not detected in any donor, hence only Delta was transmitted to contact ferrets (Fig. 2c). These results indicate a severe block of Omicron-BA.1 infection in ferrets. To confirm the unexpected observation, we inoculated ferrets with 10^{5.125} TCID50 of Omicron-BA.1 (Supplementary Fig. 2c). All ferrets remained clinically healthy throughout the study with no marked body weight changes (Supplementary Fig. 3f). Again, we detected neither shedding of Omicron-BA.1 in nasal washings, nor vRNA in the URT or LRT of ferrets euthanized at 6dpi (Fig. 2f). Serological analysis confirmed the RT-qPCR results by revealing lack of seroconversion at 21 dpi (Fig. 2f). Successful back-titration of the Omicron-BA.1 inocula for each experiment, whole-genome sequence confirmation by high-throughput sequencing and using the same virus stock for both the hamster and the ferret experiments, strongly suggest a complete replication block of VOC Omicron-BA.1 in ferrets. Therefore, the Delta variant seems to exhibit the top-level fitness in ferrets, and the vast changes in the Omicron-BA.1 sequence might be at the cost of broad host spectrum.

Delta spike mutations drive enhanced fitness in hACE2 knock-in mice

To mitigate the impact of mismatched interactions between non-human ACE2 and the Omicron-BA.1 spike/RBD, knock-in mice expressing only human ACE2 (hACE2-KI) were inoculated intranasally with 10^{4.3} TCID₅₀/mouse of Omicron-BA.1 or Delta. Infection with Delta only caused body weight loss at 4dpi. Higher virus loads and titers in the URT, LRT, and olfactory bulb were found in mice inoculated with Delta compared to Omicron-BA.1 (Fig. 3a–c, Supplementary Fig. 9a). Higher virus loads in hACE2-KI mice infected with Delta were associated with a higher pathological score in the lungs, which showed multifocal, peribronchiolar inflammatory cuffs (Fig. 3d, e, Supplementary Information Table 2). In a competition setting, Delta also dominated over Omicron-BA.1 in the URT and LRT (Fig. 3f, Supplementary Fig. 9b). To determine the importance of the spike mutations, hACE2-KI mice were inoculated with an equivalent mixture of recombinant clones only differing by the spike sequence, SARS-CoV-2[S-Delta] and SARS-CoV-2[S-Omicron]. As for the VOC isolates, SARS-CoV-2[S-Delta] fully dominated over SARS-CoV-2[S-Omicron] in the URT and LRT of hACE2-KI

mice indicating that the spike is of major importance for the phenotype of both VOCs and that spike mutations do not provide an advantage to Omicron-BA.1 over Delta in the hACE2-KI mouse model (Fig. 3g). These findings suggest that the intrinsic replicative properties of Omicron-BA.1 are unlikely to be the decisive factor for the observed replacement of Delta by Omicron-BA.1 in the human population.

Omicron-BA.1 spike confers immune escape and reduced pathogenicity

Next, we investigated the impact of prior SARS-CoV-2-specific mRNA vaccination on the replicative fitness of Omicron-BA.1 and Delta (Fig. 4a). Since current mRNA vaccines use the spike as the sole viral antigen, we focused on the impact of the spike gene on immune evasion and replication. Further, to exclude any influence of mutations outside the spike genes of the Delta and the Omicron-BA.1 VOC on replication, immune evasion, or pathogenicity, we used the isogenic viruses SARS-CoV-2[S-Delta] and SARS-CoV-2[S-Omicron] that differ only in their spike gene for infection of vaccinated and naïve mice. Transgenic K18-hACE2 were immunized (1 µg of Spikevax, Moderna) once and had detectable titers of neutralizing antibodies to the index virus SARS-CoV-2[D614G] 1 week prior to infection compared to the control groups (Fig. 4a; Supplementary Fig. 10a). Naïve and immunized mice were infected intranasally with 10⁴ TCID50/mouse of SARS-CoV-2[S-Delta], SARS-CoV-2[S-Omicron], or SARS-CoV-2[D614G].

Interestingly, only unvaccinated mice inoculated with SARS-CoV-2[S-Delta], or SARS-CoV-2[D614G] showed reduction in body weight at 6 dpi, while unvaccinated mice challenged with SARS-CoV-2[S-Omicron] and all vaccinated mice, regardless of the challenge virus, did not lose body weight (Fig. 4b, Supplementary Fig. 10b). Accordingly, clinical scores were highest for unvaccinated mice infected with SARS-CoV-2[S-Delta] (Supplementary Fig. 10c). Viral RNA loads in oropharyngeal swabs and several organs were mostly lower for SARS-CoV-2[S-Omicron]-infected mice and remained high for SARS-CoV-2[S-Delta] in the nasal cavity (Fig. 4c). Nevertheless, viral RNA loads were in most cases reduced at 6 dpi in vaccinated mice, although, as expected, reduction was less pronounced in SARS-CoV-2[S-Delta]- and SARS-CoV-2[S-Omicron]-infected mice (Fig. 4c). Strikingly, the detection of infectious virus in the nose, lung and brain of infected naïve and vaccinated mice perfectly illustrated the effect of vaccination and phenotypic differences between SARS-CoV-2[D614G], SARS-CoV-2[S-Delta] and SARS-CoV-2[S-Omicron] (Fig. 4d). Infectious wild-type SARS-CoV-2[D614G] is detected in unvaccinated mice in the nose and lung and later at 6 dpi at lower levels also in the brain. However, mRNA immunization efficiently restricted SARS-CoV-2[D614G] replication, as infectious virus was only detectable at 2 dpi in the nose and not in any other tissue. SARS-CoV-2[S-Delta] titers in unvaccinated mice were comparable to SARS-CoV-2[D614G] titers in the nose, while we observed higher titers in the lung and particularly in the brain (Fig. 4d, Supplementary Fig. 10e, f). As expected, SARS-CoV-2[S-Delta] showed some

Article https://doi.org/10.1038/s41467-022-33632-y
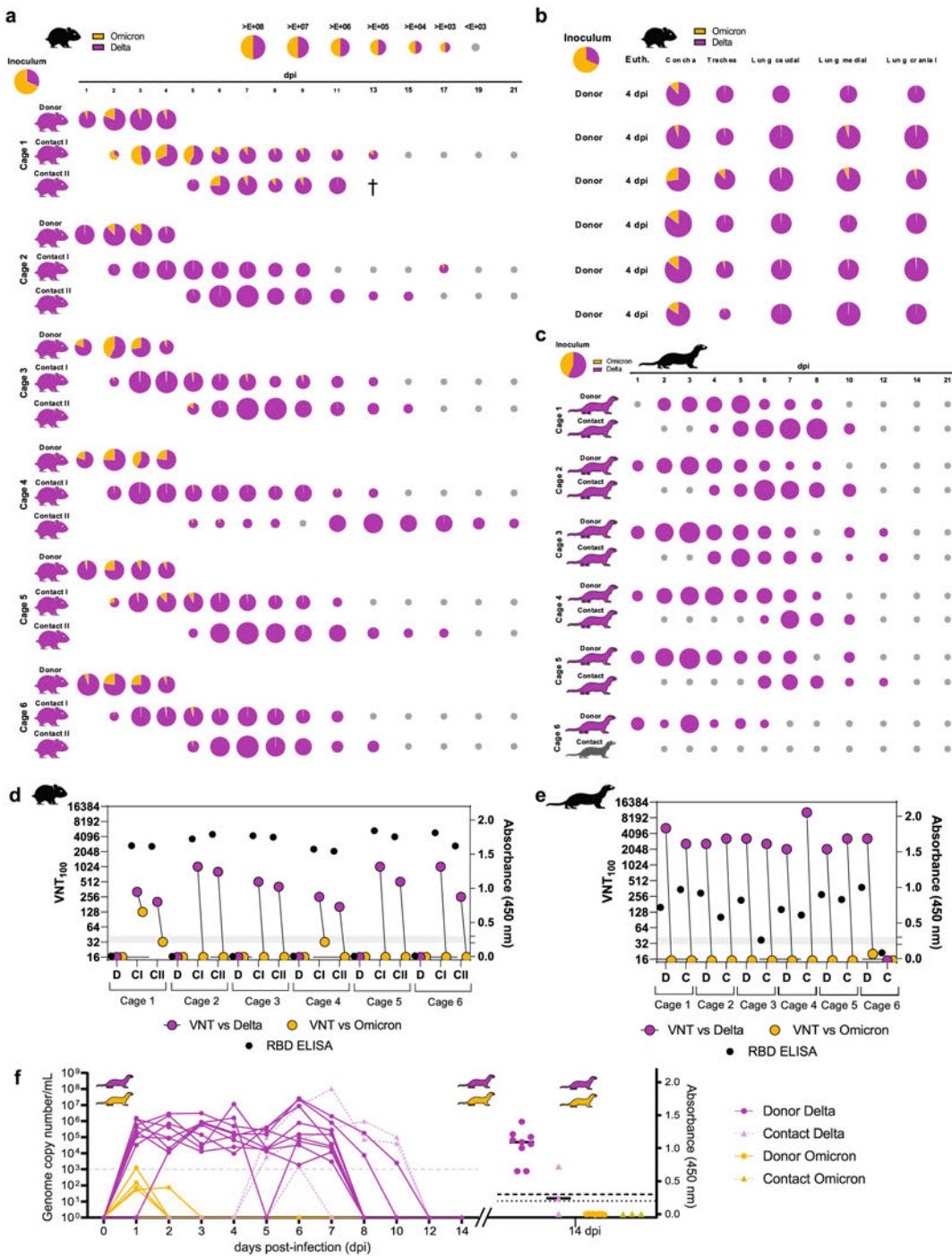
degree of immune escape as infectious virus was readily detectable at 2 dpi in the nose and lung, but eventually was cleared at 6 dpi in vaccinated mice (Fig. 4d). Finally, we detected less infectious virus of SARS-CoV-2$^{S-Omicron}$ compared to SARS-CoV-2^{D614G} and SARS-CoV-2$^{S-Delta}$ in the nose, lung and brain of unvaccinated mice, suggesting that the Omicron-BA.1 spike gene confers a less virulent phenotype than the 614G and the Delta spike gene (Fig. 4d, Supplementary Fig. 10e, f).

Moreover, the Omicron-BA.1 spike gene conferred the largest degree of immune evasion, since infectious titers were comparable between vaccinated and unvaccinated mice in the nose at 2 and 6 dpi and in the lung at 2 dpi. However, no infectious virus was detected in the brains of vaccinated mice, and titers in the lungs were reduced compared to unvaccinated mice at 6 dpi, suggesting that the mRNA vaccine is still of advantage to combat SARS-CoV-2$^{S-Omicron}$ infection in the LRT and

- 117 -

Fig. 2 | In vivo competitive co-infection and single infection studies with VOC Delta and Omicron-BA.1 in Syrian hamsters and ferrets. Simultaneous co-inoculation of six donor hamsters and ferrets each with a Delta:Omicron-BA.1 mixture (hamster, ratio of 1:2.16, total $10^{4.5}$ TCID$_{50}$/hamster and ferrets, ratio of 1:1.43, total $10^{4.75}$ TCID$_{50}$/ferret) and sequential pairwise co-housing of contact animals. All data were quantified using RT-qPCR. Pie chart size represents the total amount of viral RNA (vRNA) detected in each sample (exact vRNA equivalents are found in Source Data files and the coloring shows the individual VOC ratio). Animal silhouettes are colored according to the dominant (>66%) VOC. Limit of detection was set at 10^3 vRNA copies per mL. **a** Nasal washings of Donor and Contact I + II Syrian hamster pairs from 1 to 21 dpi. **b** vRNA in URT and LRT of donor hamsters at 4 dpi. **c** Nasal washings of Delta and Omicron-BA.1 co-inoculated Donor and

respective Contact ferrets for the 21-day infection period. **d, e** Antibody detection in hamsters (**d**) and ferrets (**e**) via VNT$_{100}$ and RBD-ELISA after simultaneous Delta and Omicron-BA.1 co-inoculation shown for donor (D), contact (C), contact I (CI), and contact II (CII) animals. Specific neutralizing capacity of sera against the Delta (pink) and Omicron-BA.1 (yellow) virus pair were analyzed. Reactivity of sera below 1:32 pre-dilution was considered negative. Generalized seroreaction was also determined by RBD-ELISA (black dots). **f** vRNA detection and seroreactivity in ferrets after infection with single virus (Delta or Omicron-BA.1); donor animals (solid line) ($n = 9$) and contact animals (dashed line) ($n = 3$). Limit of detection was set at 10^3 vRNA copies per mL and for antibody detection at >0.2 (questionable) and >0.3 (positive). Source data are provided as a Source Data file 2.Source Data file 2.

systemic dissemination (Fig. 4d, Supplementary Fig. 10e, f). The different virus phenotypes and vaccine efficiencies are corroborated by the pathological findings (Fig. 4e, Supplementary Fig. 10d; Supplementary Information Table 3). Unvaccinated mice infected with SARS-CoV-2$^{S\text{-}Delta}$ displayed severe interstitial lymphohistiocytic pneumonia with concurrent vascular inflammation and widespread nucleocapsid antigen detection in the immunohistochemical (IHC) analysis starting already at 2 dpi, while infection with SARS-CoV-2^{D614G} resulted in similarly severe pathological findings only at 6 dpi. In contrast, unvaccinated mice that were infected with SARS-CoV-2$^{S\text{-}Omicron}$ displayed milder histopathological lung lesions and less nucleocapsid antigen was detected by IHC analysis. In agreement with the observed reduced virus titers in the lungs of vaccinated mice, we observed milder lung histopathological lesions and almost no nucleocapsid antigen IHC detection in vaccinated mice with any of the viruses when compared to lungs of unvaccinated mice.

Collectively, these findings demonstrate the major impact of the Delta and Omicron-BA.1 spike genes on virus replication, immune evasion, and pathogenicity. Compared to the progenitor D614G spike gene, the Delta spike gene confers increased replication, pathogenicity, and immune escape. The Omicron-BA.1 spike gene is conferring the greatest degree of immune evasion, compared to the wild-type D614G spike and the Delta spike genes, resulting in comparable or even increased detection of infectious SARS-CoV-2$^{S\text{-}Omicron}$ compared to SARS-CoV-2^{D614G} and SARS-CoV-2$^{S\text{-}Delta}$, in several tissues and organs of vaccinated mice. Importantly, the Omicron-BA.1 spike gene also confers reduced pathogenicity, as seen in unvaccinated mice (Fig. 4b, e), suggesting that the Omicron-BA.1 spike is a major determinant of the observed milder disease in humans.

Discussion

The appearance of Omicron-BA.1 in the human population exemplified a remarkable jump in SARS-CoV-2 evolution. Omicron-BA.1 has acquired up to 50 mutations of which at least 34 are located within the spike gene[3]. Particularly, the NTD and RBD harbor many mutations that have not been seen in previous SARS-CoV-2 variants, suggesting substantial changes in spike antigenicity, receptor binding, and possibly other spike functions. Accordingly, the current experimental systems to assess phenotypic changes of SARS-CoV-2 require a revision regarding the extent to which they truly reflect epidemiological and clinical observations in humans. We and others previously showed that the Syrian hamster is a highly susceptible animal model for several SARS-CoV-2 variants and showed a great efficiency in replication and transmission[9,10,13]. Nevertheless, we show here that competitive infection and transmission experiments in the hamster model no longer reflect the human epidemiological situation. While in humans, Omicron-BA.1 rapidly became the prevailing variant over Delta, the variant that previously has outcompeted Alpha, we observed that in competitive infection experiments in the hamster model the exact opposite order of variants is dominant. Certainly, these differential observations hint to an adaptation of SARS-CoV-2

variants to the human host. Our data show that Alpha is massively replicating and dominantly transmitted with severe clinical features in the hamster model. Moreover, replicative fitness of Delta and Omicron-BA.1 decreased sequentially in direct competition with the respective earlier predominant variant in the human population[14,15]. These observations are in line with the high degree of mortality (83 % mortality) in the Delta vs Alpha compared to the Delta vs Omicron-BA.1 competition experiment (8 % mortality). A comparable high mortality rate was also seen in association with Alpha in our earlier study of paired VOC competitions including Alpha, Beta, and SARS-CoV-2^{D614G}[10], suggesting that the degree of pathogenicity in the Syrian hamster correlates with the respective replicative fitness in this model.

Another surprising finding in our study was that Omicron-BA.1 does not productively replicate in ferrets. While we see, in agreement with the epidemiological situation in humans, that the Delta variant vastly predominates over the Alpha variant in terms of early replication and especially transmission in the ferret model, we observed that Omicron-BA.1 infection is abortive. The remarkable observations of Omicron-BA.1 being outcompeted by the Delta variant in naïve Syrian hamsters and the complete block of ferret susceptibility towards Omicron-BA.1 provides further evidence to an adaptation of this variant towards humans. This also makes it rather unlikely that the Omicron variant evolved in an animal reservoir.

It was therefore important to include animal models that are based on the usage of the authentic hACE2 receptor. The hACE2 knock-in mice are a valuable model for SARS-CoV-2 replication in the URT as they show robust SARS-CoV-2 replication with only mild or sub-clinical disease[10,11]. The observation that also in this model Delta outcompeted Omicron-BA.1 and similarly, the corresponding Delta spike clone SARS-CoV-2$^{S\text{-}Delta}$ outcompeted the Omicron-BA.1 spike clone SARS-CoV-2$^{S\text{-}Omicron}$, suggests that the intrinsic replicative fitness of Delta is still higher than that of Omicron-BA.1 once a productive replication is established within the infected host and that this phenotype is mediated by the spike genes of Delta and Omicron-BA.1. Notably, the infection of hACE2-KI mice with the Delta isolate resulted for the first time in our hands in evident lung pathology and body weight loss, suggesting that this model recapitulates the increased pathogenicity of Delta in humans and that it will receive further attention in future studies that aim at assessing SARS-CoV-2 variants with high pathogenicity.

Notably, by using hNEC and hBEC cultures we were able to detect an accelerated growth of Omicron-BA.1 in hNECs within the first 48 h post infection that reflects the observed shorter incubation period of Omicron-BA.1 versus previous SARS-CoV-2 variants in humans. In contrast, in hBECs, Omicron-BA.1 replication is limited to lower peak titers, suggesting reduced replication in bronchial and lung tissue as previously demonstrated in PCLS ex vivo tissue cultures[16]. Importantly, this phenotype is also seen by infections with the Omicron-BA.1 spike clone SARS-CoV-2$^{S\text{-}Omicron}$, demonstrating that it is spike-mediated. Moreover, the reduced replication of

Article
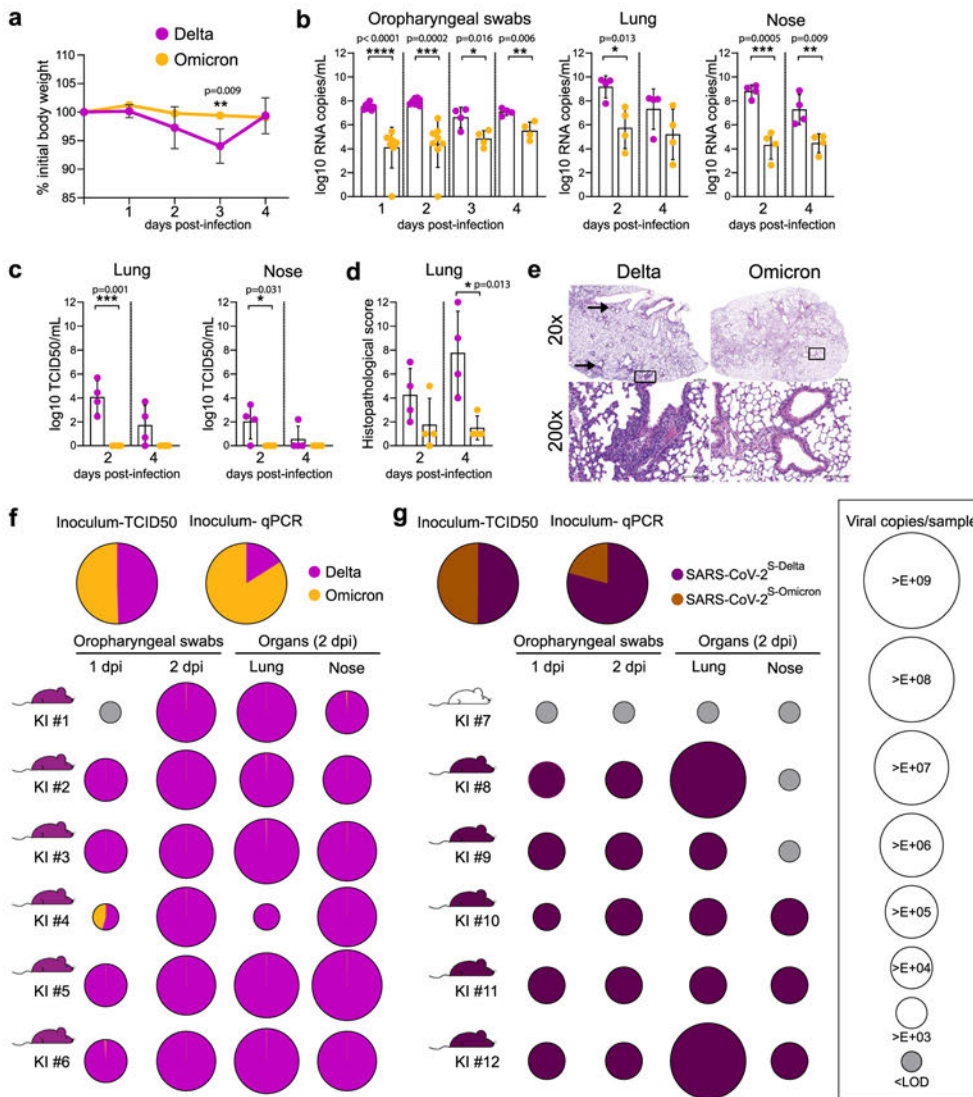
Fig. 3 | Delta spike mutations drive enhanced fitness in hACE2-knock-in mice. **a–e** hACE2-KI mice (7–16 week-old male, $n = 8$ mice/virus) were intranasally inoculated with $10^{4.3}$ TCID$_{50}$ of Delta or Omicron. **a** Average relative weight loss after infection (Relative weight loss data from each animal is given in Supplementary Fig. 9). **b** Viral copies per mL of oropharyngeal swabs or per lung and nose sample ($n = 16$ mice) quantified using E-gene probe-specific RT–qPCR. **c** Infectious virus titers from the lung and nose samples ($n = 16$ mice) determined using TCID$_{50}$ assays in VeroE6/TMPRSS2 cells. **d, e** Histopathological score and hematoxylin and eosin staining from Delta- and Omicron-infected lung sections ($n = 16$ mice) at 2 and 4 dpi. Perivascular and peribronchiolar lymphohistiocytic inflammation are highlighted with an arrow, and the higher magnification represented in the lower panel corresponds to the areas highlighted by a square in the upper panel. Scale bars, 500 (upper panel) and 100 μm (lower panel). Data are mean ± s.d. from the indicated number of biological replicates from a single experiment. The color key in a also applies to b, c and d. Statistical significance was determined using an unpaired two-

tailed Student t-test; *$P < 0.05$, **$P < 0.01$, ***$P < 0.001$, ****$P < 0.0001$. **f, g** hACE2-KI mice (7–19 week-old female, $n = 6$ mice/group) were intranasally inoculated with 10^4 TCID$_{50}$ of a 1:1 mix of **f** Delta and Omicron, or **g** SARS-CoV-2$^{S\text{-}Delta}$ and SARS-CoV-2$^{S\text{-}Omicron}$. qPCR quantification of the ratio of the two variants or recombinant viruses present in the inoculum is reported. Oropharyngeal swabs were collected 1 and 2 dpi; lung and nose tissues were collected on 2 dpi. Pie charts show the ratio of variants detected in each sample at the indicated dpi ($n = 6$ mice/group). Pie chart sizes are proportional to the total number of viral genome copies per ml (swabs) or per sample (tissues), as shown in the legend on the right. Gray pies indicate values below the LOD (i.e., 10^3 viral RNA copies per mL/sample). Mouse silhouettes are colored to indicate the dominant SARS-CoV-2 variant (>66%) in the last positive swab sample from the corresponding mouse. KI numbers 1–12 denote individual hACE2-KI mice. Data was obtained from one experiment. Source data are provided as a Source Data file 3.Source Data file 3.

SARS-CoV-2$^{S\text{-}Omicron}$ in the lungs of K18-hACE2 mice and the resulting mild pathology confirms that this phenotype is indeed spike-mediated and likely contributes to the reduced pathogenicity of Omicron-BA.1 as seen in humans. Of note, the increased replication, pathology, and clinical scores of SARS-CoV-2$^{S\text{-}Delta}$ point to the

opposite phenotype of increased pathogenicity that is according to our study also mediated by the spike gene.

Finally, our study illustrates the degree of immune evasion of Omicron-BA.1 in comparison to Delta and the index virus SARS-CoV-2^{D614G}. The mRNA vaccine is well matched to the index virus SARS-CoV-
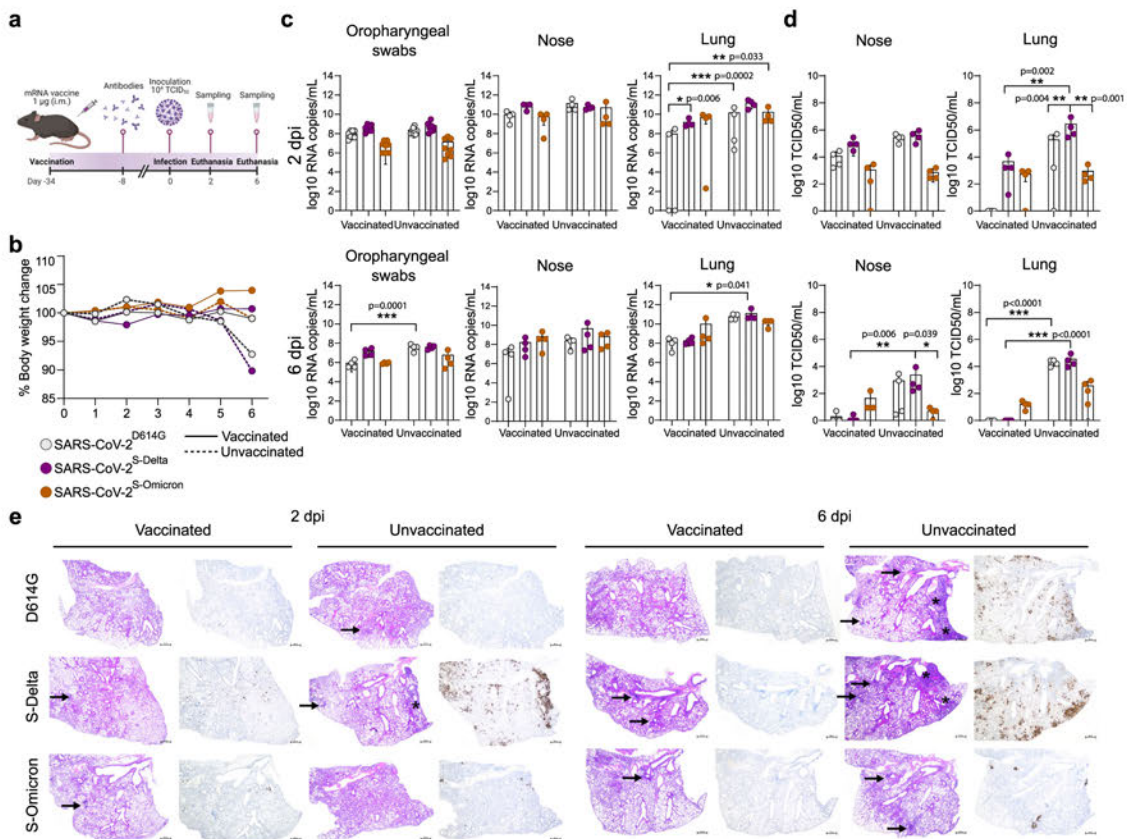
Fig. 4 | mRNA vaccine induced reduction in replication and pathogenesis of SARS-CoV-2 clones in K18-hACE2 transgenic mice. a Female K18-hACE2 transgenic mice (7–15 weeks old, $n = 8$ mice/group) were immunized intramuscularly with a single dose of 1 µg of mRNA-Vaccine Spikevax (Moderna). After 2 weeks the neutralizing antibody titers against SARS-CoV-2 were determined (Supplementary Fig. 10a). Later, mice were intranasally inoculated with 10^4 $TCID_{50}$ of SARS-CoV-2[D614G], SARS-CoV-2[S-Delta], or SARS-CoV-2[S-Omicron]. Body weight change and clinical scores of the mice were monitored daily. **b** The mean body weight change is presented (Data from individual animals are shown in Supplementary Fig. 10b). Only the unvaccinated mice infected with SARS-CoV-2[D614G] and SARS-CoV-2[S-Delta] showed noticeable weight loss. **c** Oropharyngeal swabs, lung and nose samples of the infected mice were collected at 2 or 6 days post-infection (dpi) to determine the viral load ($n = 4$ for each virus). Viral RNA-dependent RNA polymerase (RdRp) gene copies were quantified using probe-specific RT–qPCR. **d** Infectious virus titers from

the lung and nose samples ($n = 8$ mice/group) were determined using $TCID_{50}$ assays in VeroE6/TMPRSS2 cells. **e** Hematoxylin and eosin stain (left panel) and immunohistochemical analysis specific for SARS-CoV-2 nucleocapsid protein (right panel) of lung sections in vaccinated (A) and unvaccinated mice (B) at 2 and 6 dpi following infection with SARS-CoV-2[D614G] ($n = 3$), SARS-CoV-2[S-Delta] ($n = 3$), and SARS-CoV-2[S-Omicron] ($n = 4$). Consolidated lung areas are highlighted with a star, and perivascular and peribronchiolar lymphohistiocytic inflammation highlighted with an arrow. Scale bars, 500 µm. Data are mean ± s.d. from the indicated number of biological replicates. The color key in b also applies to c and d. Statistical significance was determined using two-way ANOVA (**a**–**d**) and *P*-values were adjusted using Tukey's multiple-comparison test; *$P < 0.05$, **$P < 0.01$, ***$P < 0.001$, ****$P < 0.0001$. Data were obtained from one experiment. Each data point represents one biological replicate. Source data are provided as a Source Data file 4.Source Data file 4.

2[D614G], and accordingly, vaccinated mice are well protected. Recently, it has been shown that the replicative and transmissive fitness advantage of Omicron against Delta changes in favor of Omicron when hamsters are vaccinated, highlighting the influence of Omicron-associated immune escape potential and the importance of the immune status on virus selection[17]. Our data from vaccinated mice extend this finding by using an animal model with the authentic hACE2 receptor, and by assigning this context-specific phenotypic change to the Omicron-BA.1 spike gene.

In summary, we provide here a comprehensive and comparative analysis of the Omicron-BA.1 phenotype by using several advanced in vitro and in vivo systems and different VOCs. We demonstrate that Omicron-BA.1 displays a remarkable evolutionary and phenotypic jump that impacts virus replication, host and tissue tropism, pathogenicity, and immune escape, with the spike gene being a key determinant of these phenotypic changes.

Methods
Biosafety statement
All experiments with infectious SARS-CoV-2 were performed in enhanced biosafety level 3 (BSL3) containment laboratories at Institute of Virology and Immunology, Mittelhäusern, Switzerland, and Friedrich-Loeffler-Institut, Greifswald-Insel Riems, Germany, which followed the approved standard operating procedures of BSL3 facility of relevant authorities in Switzerland and Germany. Before commencing work, all personnel received relevant training.

Cells and culture conditions
At IVI, IBSC VeroE6 (Vero C1008, ATCC) and VeroE6/TMPRSS2 cells (NIBSC Research Reagent Depository, UK) were cultured in Dulbecco's modified Eagle's medium (DMEM). BHK-SARS-N (BHK-21 cells expressing the N protein of SARS)[18] were grown in minimal essential medium (MEM). Both media were supplemented with 10% (v/v) fetal bovine

Article   https://doi.org/10.1038/s41467-022-33632-y

serum, 1% (w/v) non-essential amino acids, 100 IU/mL penicillin, 100 μg/mL streptomycin μg/ml and the cell lines maintained at 37 °C in a 5% CO_2 atmosphere.

VeroE6 cells at FLI (Collection of Cell Lines in Veterinary Medicine CCLV-RIE 0929) were cultured using a mixture of equal volumes of Eagle MEM (Hanks' balanced salts solution) and Eagle MEM (Earle's balanced salts solution) supplemented with 2 mM L-Glutamine, non-essential amino acids adjusted to 850 mg/L, $NaHCO_3$, 120 mg/L sodium pyruvate, 10% fetal bovine serum (FBS), pH 7.2.

Calu-3 cells (HTB-55, American Type Culture Collection (ATCC), Manassas, VA, USA) were propagated in Dulbecco's modified Eagle Medium−GlutaMAX, supplemented with 10% (v/v) heat-inactivated fetal bovine serum, 100 mg/mL streptomycin, 100 IU/mL penicillin, 1% (w/v) non-essential amino acids, and 15 mM 4-(2-hydroxyethyl)−1-piperazineethanesulfonic acid (HEPES, Gibco, Gaithersburg, MD, USA). Cells were maintained at 37 °C in a humidified incubator with 5% CO_2.

Viruses
Viruses are listed in Supplementary Table 1. Viruses were cultivated on VeroE6, VeroE6/TMPRSS2, or Calu-3 cells and sequence verified by performing whole-genome NGS sequencing (see below). For the hamster and ferret infection studies SARS-CoV-2 Alpha (hCoV-19/Germany/NW-RKI-I-0026/2020, L4549, SARS-CoV-2 B.1.1.7 NW-RKI-I-0026/2020 passage 3 of EPI_ISL_751799), one silent mutation in the ORF1a (sequence position 11741), SARS-CoV-2 Delta AY.127 (hCoV-19/Switzerland/BE-IFIK-918-4879/2021, L5109, passage of EPI_ISL_1760647) and SARS-CoV-2 Omicron-BA.1 (BA.1 (hCoV-19/Germany/HE-FFM-30318738/2021, passage of EPI_ISL_6959868)) were used. The Omicron-BA.1 isolate was from the Institute of Medical Virology, University Hospital Frankfurt, Goethe University, Frankfurt am Main, Germany. For the hamster and ferret competition experiments, respective Alpha, Delta or Omicron-BA.1 viruses were propagated (three passages for Alpha, two passages for Omicron-BA.1, one passage for Delta) on VeroE6 cells (Collection of Cell Lines in Veterinary Medicine CCLV-RIE 0929) using a mixture of equal volumes of Eagle MEM (Hanks' balanced salts solution) and Eagle MEM (Earle's balanced salts solution) supplemented with 2 mM L-Glutamine, nonessential amino acids adjusted to 850 mg/L, NaHCO3, 120 mg/L sodium pyruvate, 10% fetal bovine serum (FBS), pH 7.2. The virus was harvested after 72 h, titrated on VeroE6 cells and stored at −80 °C until further use.

For in vitro experiments, Delta and Omicron-BA.1 were isolated at the University of Bern. Briefly, an aliquot of 250 μl of SARS-CoV-2 nasopharyngeal swab samples from positive patients (Delta; EPI_ISL_1760647, Omicron-BA.1; EPI_ISL_7062525) were centrifuged for 5 min at room temperature at 200 × g. 200 μl of clinical material was transferred to confluent Calu-3 cells and incubated for 2–3 days at 37 °C in a humidified CO_2-incubator (5%). Virus containing supernatant was cleared from cell debris through centrifugation for 5 min at 500 × g before aliquoting and storage at −80 °C. All virus stocks were sequenced with Nanopore sequencing technology using a revised ARTIC midnight protocol (Fragment 28 update) allowing sequencing of both Delta and Omicron-BA.1 variants. Sequence verified stocks at passage 3 were used. For the experiments in hACE2-KI mice, the Delta isolate (EPI_ISL_2535433)[19] was kindly provided by Georg Kochs, Institute of Virology, Freiburg, Germany and Omicron-BA.1 was isolated at the University of Bern (EPI_ISL_7062525). The $TCID_{50}$ titers have been determined on VeroE6 and were calculated according to the Spearman-Kaerber formula.

Generation of infectious cDNA clones using transformation-associated recombination cloning and rescue of recombinant viruses
The generation of recombinant SARS-CoV-2 was approved by the Swiss Federal Office for the Environment (A202819-01). We used the in-yeast transformation-associated recombination (TAR) cloning method as

described previously with a few adaptations to generate SARS-CoV-2$^{S-Delta}$ and SARS-CoV-2$^{S-Omicron}$ [20]. Briefly, the whole SARS-CoV-2 genome was encoded in 12 overlapping DNA fragments. These so-called WU-Fragments and a TAR-vector are homologously recombined in yeast forming the yeast artificial chromosome (YAC). WU-Fragments 9 and 10 covering the spike region were replaced by newly generated and overlapping PCR products. To introduce the variant specific mutations into the spike gene, we used 50 bp primers containing the desired nucleotide changes in combination with YAC DNA templates from previously cloned viruses (Supplementary Information Table 4). Also, by using these 50 bp long primers homologous overlaps between the PCR products were created. Six PCR reactions using the Q5® High-Fidelity DNA Polymerase (NEB) were performed to replace WU-Fragment 9 and 10 to create the SARS-CoV-2$^{S-Delta}$. To create the SARS-CoV-2$^{S-Omicron}$ and its sub spike clones overlapping PCR products via RT from Omicron RNA template were done. In brief, cDNA was generated from RNA (Omicron-BA.1; EPI_ISL_7062525) by LunaScript RT SuperMix (NEB). PCR reactions using Q5® High-Fidelity DNA Polymerase were performed with the primers and templates described in Supplementary Information Table 4. The resulting PCR products were mixed and matched for Omicron-Spike, -NTD, -RBD and -CS to replace WU-Fragment 9 and 10. All PCR products were purified by the High Pure PCR Product Purification Kit (Roche) before being used for TAR cloning.

In vitro transcription was performed for EagI-cleaved YACs and PCR-amplified SARS-CoV-2 N gene using the T7 RiboMAX Large Scale RNA production system (Promega) as described previously[20]. Transcribed capped mRNA was electroporated into baby hamster kidney (BHK-21) cells expressing SARS-CoV N protein. Electroporated cells were co-cultured with susceptible VeroE6/TMPRSS2 cells to produce passage 0 (P.0) of the recombinant viruses. Subsequently, progeny viruses were used to infect fresh VeroE6/TMPRRS2 cells to generate P.1 stocks for downstream experiments.

Virus replication kinetics on human primary airway cells
hNEC and hBEC cultures were infected with 10^4 $TCID_{50}$ of the SARS-CoV-2 variants listed in the Supplementary Table 1. Viruses were diluted in HBSS (Gibco), inoculated on the apical side, and incubated for 1 h at 33 °C in case of hNECs or 37 °C in case of hBECs. Subsequently, the inoculum was removed, and the cells were washed three times with 100 μl of HBSS. The third wash was collected as the 1 hpi time point. For the duration of the experiment, hNECs and hBECs were incubated in a humidified incubator with 5% CO_2 at 33 °C or 37 °C, respectively. To measure virus progeny release, apical washes were performed every 24 h up to 96 hpi. 100 μl HBSS were incubated on the apical side for 10 min prior to the respective time point and subsequently collected, diluted 1:1 with virus transport medium (VTM), and stored at −80 °C for later analysis.

Virus titers were assessed by standard $TCID_{50}$ assays on VeroE6/TMPRSS2 cells. In short, $2 × 10^4$ cells/well were seeded in a 96-well plate 1 day before the titration and were then inoculated with a 10-fold serial dilution of the prior collected apical washes. Four technical replicates were performed for each sample. Cells were then incubated for 72 h at 37 °C in a humidified incubator with 5% CO_2. Subsequently, cells were fixed with 4% (v/v) buffered formalin (formafix) and stained with crystal violet. Infected wells were counted manually, registered in Microsoft Excel 2016 (16.0.5239.1001), and $TCID_{50}$ was calculated according to the Spearman-Kaerber formula.

Competition assay in hNEC and hBEC cultures
Inoculum mixtures were generated by mixing the respective viruses at a 1:1 ratio based on genome equivalents (GE) determined by qPCR including RNA standard. Each mixture contained $6 × 10^7$ GE of each respective virus. hNECs and hBECs were infected with inoculum mixtures apically and incubated for 1 h at 33 °C or 37 °C respectively.

Afterwards, inocula were removed and the cells were washed three times with 100 µl HBSS (Gibco). For the duration of the experiment, the hNECs and hBECs were incubated in a humidified incubator with 5% CO_2 at 33 °C or 37 °C, respectively. Apical washes were performed and collected at 2, 4 and 6 dpi. 100 µl HBSS were incubated on the apical side for 10 min prior to the respective time point and subsequently collected, mixed with 300 µl DNA/RNA Shield lysis buffer (Zymo Research) and stored at −80 °C for later analysis.

Nanopore sequencing workflow

Virus stocks, inoculum mixtures, and samples from competition assays in NECs, BECs, and lung slices were sequenced using the MinION sequencer (Oxford Nanopore Technologies) following the ARTIC nCoV-2019 sequencing protocol V3 (LoCost) (https://protocols.io/view/ncov-2019-sequencing-protocol-v3-locost-bh42j8ye) with the following modifications: the Midnight primer scheme (1200 bp amplicons) was used to perform the multiplex PCR (https://www.protocols.io/view/sars-cov2-genome-sequencing-protocol-1200bp-amplic-rm7vz8q64vx1/v6) instead of the ARTIC V3 primer scheme. In addition, two extra Omicron-specific primers (SARSCoV_1200_-Omicron_24_L: 5′-GCT GAA TAT GTC AAC AAC TCA TAT GA-3′ and SARSCoV_1200_Omicron_28_L: 5′-TTT GTG CTT TTT AGC CTT TCT GTT-3′) were added to Pool 2 of the multiplex PCR to achieve similar levels of amplification for all viruses sequenced.

RNA was extracted for all samples using either the Quick-RNA Viral Kit (Zymo Research) or the NucleoMag VET kit (Machery-Nagel) according to the manufacturer's guidelines on a Kingfisher Flex Purification system (Thermo fisher). Extracted RNA was assessed using the TaqPath COVID-19 CE-IVD RT-PCR Kit (Thermo fisher) and cDNA was prepared using the LunaScript RT SuperMix Kit (Bioconcept). Subsequently, a multiplex PCR was used to generate overlapping 1200 bp amplicons that span the length of the SARS-CoV-2 genome for all used virus VOCs. The Q5 Hot Start High-Fidelity 2X Master Mix (Bioconcept) was used for the multiplex PCR reaction. For library preparation, all samples were barcoded using the Native Barcoding Kit 96 (Oxford Nanopore Technologies, SQK-NBD112-96). Libraries were then loaded onto a R9.4.1 flow cell on a MinION sequencer (Oxford Nanopore Technologies) and monitored using the MinKNOW software (Version 21.11.9). A no-template negative control from the PCR amplification step was prepared in parallel and sequenced on each flow cell.

Live GPU basecalling was performed using Guppy v.5.1.15 (Oxford Nanopore technologies) in high-accuracy mode. Following sequencing, downstream analysis was performed using a modified version of the nCoV-2019 novel coronavirus bioinformatics protocol (ARTIC Network, https://artic.network/ncov-2019/ncov2019-bioinformatics-sop.html). The command 'artic gupplex' was used to filter "pass" reads based on length with-max-length set to 1400. The 'artic minion' command was then used to align the filtered reads to the Wuhan-Hu-1 reference genome (accession MN908947.3 [www.ncbi.nlm.nih.gov/bioproject/?term=MN908947.3]) with the 'normalize' parameter set to 500. BAM alignment files generated using the ARTIC pipeline were subsequently used as input to call variants in longshot (v.0.4.4). An input VCF file containing VOC Delta and Omicron BA.1 mutations was provided to longshot in order to genotype specific nucleotide sites. Output VCF files for each sample were used as input for downstream analysis in R v.4.1.3. Calculations were performed on UBELIX (http://www.id.unibe.ch/hpc), the HPC cluster at the University of Bern.

Downstream analysis of VCF files for each sample was performed using a custom script in R v.4.1.3. Briefly, each VCF file was first filtered to exclude mutations shared between both viruses in the mixture, non-lineage-defining mutations, sites that were difficult to call (e.g., sites with unique but overlapping mutations or with a high number of ambiguous calls), and mutations called with a depth of coverage <100. Sequencing depth across the entire genome was also checked for each

sample along with the frequency of any 'shared' mutations in each virus mixture (in these cases the frequency should be close to 1). Following filtering and quality control checks, the remaining variant calls were used to calculate the mean mutation frequencies for each virus on a per sample basis (Supplementary Fig. 1). Finally, the mean ± sd virus ratio was calculated for each virus mixture at each time point for NEC, BEC, and lung slices.

Ion torrent sequencing

Virus stocks was sequenced using a generic metagenomics sequencing workflow as described previously[21] with some modifications. For reverse-transcribing RNA into cDNA, SuperScriptIV First-Strand cDNA Synthesis System (Invitrogen, Germany) and the NEBNext Ultra II Non-Directional RNA Second Strand Synthesis Module (New England Biolabs, Germany) were used, and library quantification was done with the QIAseq Library Quant Assay Kit (Qiagen, Germany). Libraries were sequenced using an Ion 530 chip and chemistry for 400 base pair reads on an Ion Torrent S5XL instrument (Thermo Fisher Scientific, Germany).

Ethics statements for human subjects and animal experimentation

All ferret and hamster experiments were evaluated by the responsible ethics committee of the State Office of Agriculture, Food Safety, and Fishery in Mecklenburg–Western Pomerania (LALLF M-V) and gained governmental approval under registration number LVL MV TSD/7221.3-1-004/21.

Mouse studies were approved by the Commission for Animal Experimentation of the Cantonal Veterinary Office of Bern and conducted in compliance with the Swiss Animal Welfare legislation and under license BE43/20.

Lung tissue for the generation of human precision-cut lung slices (PCLSs) and human bronchial epithelial cells (hBECs) was obtained from patients undergoing pulmonary resection at the University Hospital of Bern, Inselspital, Switzerland, and the Cantonal Hospital of St. Gallen, Switzerland, respectively. Written informed consent was obtained for all the patients and the study protocols were approved by the respective local Ethics Commissions (KEK-BE_2018-01801, EKSG 11/044, and EKSG 11/103).

Hamster competition studies

The study outline for the hamster competition studies can be seen in Supplementary Fig. 2a. Six Syrian hamsters (*Mesocricetus auratus*) (Janvier Labs) were inoculated intranasally under a brief inhalation anesthesia with a 70 µl mixture of two respective SARS-CoV-2 VOC (Alpha versus Delta and Delta versus Omicron-BA.1), referred to as donor hamsters. Each inoculum, as well as the single viruses were backtitrated followed by determination of VOC ratio by dividing the $TCID_{50}$/mL values of single VOC1 by VOC2. One day following inoculation of the donor hamsters, we co-housed six naïve contact hamsters (Contact I) in a 1:1 setup, allowing direct contact of donor to contact hamster. The donor hamsters were removed from the experiment on 4 dpi for organ sampling (RT-qPCR) and have been replaced by another naïve contact hamster (Contact II).

Viral shedding was monitored by nasal washings in addition to a daily physical examination and body weighing routine. Nasal washing samples were obtained under a short-term isoflurane inhalation anesthesia from individual hamsters by administering 200 µl PBS to each nostril and collecting the reflux. Animals were sampled daily from 1 dpi to 9 dpi and afterwards every second day until 21 dpi. Under euthanasia, serum samples and an organ panel comprising representative upper (URT) and lower respiratory tract (LRT) tissues were collected from each hamster. All animals were checked daily for signs of clinical disease and weight loss. Animals reaching the humane endpoint, e.g., falling below 80% of the initial body weight relative to 0 dpi, were humanely euthanized.

Ferret competition studies

The study outline for the ferret competition studies can be seen in Supplementary Fig. 2b. Similar to the hamster study, 12 ferrets (six donor ferrets and six contact ferrets) from the FLI in-house breeding were housed pairwise in strictly separated cages to prevent spillover contamination. Of these, six ferrets were intranasally inoculated with an equal 250 µl mixture of SARS-CoV-2 Alpha and Delta or Delta and Omicron-BA.1. The inoculum of the mixture as well as from the single viruses was back titrated and the ratio of each variant was determined by dividing the $TCID_{50}$/mL values of single VOC1 by VOC2. Ferret pairs were separated for the first 24 h following inoculation. Subsequently, the ferrets were co-housed again, allowing direct contact of donor to contact ferrets. All ferrets were sampled via nasal washings with 750 µl PBS per nostril under a short-term isoflurane inhalation anesthesia. All ferrets, which were in the study group on the respective days, were sampled daily until 8 dpi and afterwards every second day until the animals were negative for SARS-CoV-2 viral genome in RT-qPCR and one last time at the study end (21 dpi). Physical condition of all animals was monitored daily throughout the experiment.

Ferret single infection studies

The study outline for the ferret single infection studies can be seen in Supplementary Fig. 2c. 12 ferrets (nine donor and three contact animals) from the FLI in-house breeding were housed in multiple connected cage units. The donor ferrets were inoculated either with 250 µl of SARS-CoV-2 Delta ($10^{4.8125}$ $TCID_{50}$/ferret, calculated from back-titration of the original material) or Omicron-BA.1 ($10^{5.125}$ $TCID_{50}$/ferret, calculated from back-titration of the original material) in two separate and independent animal trials. Contact animals were separated from the donor animals for the first 24 h, followed by co-housing again to allow direct contact of donor and contact animals. All ferrets were sampled via nasal washings with 750 µl PBS per nostril under a short-term isoflurane inhalation anesthesia. Sampling was done daily until 8 dpi and afterwards every second day until the study end at 14 dpi. For serological analysis, serum was collected at the study end (14 dpi). Physical condition of all animals was monitored daily throughout the experiment. For analysis of SARS-CoV-2 Omicron-BA.1 viral genome distribution in LRT and URT, six ferrets from the respective Omicron-BA.1-single infection trial were euthanized at 6 dpi and viral organ load was determined via Omicron-BA.1-specific RT-qPCR with Quant-Studio™ Real-Time PCR Software (v1.7.1).

Mouse studies

Mice were produced at the specific-pathogen-free facility of the Institute of Virology and Immunology (Mittelhäusern), where they were maintained in individually ventilated cages (blue line, Tecniplast), with 12-h/12-h light/dark cycle, $22 \pm 1\,°C$ ambient temperature and $50 \pm 5\%$ humidity, autoclaved food and acidified water. At least 7 days before infection, mice were placed in individually HEPA-filtered cages (IsoCage N, Tecniplast).

hACE2-KI mice (B6.Cg-$Ace2^{tm1(ACE2)Dwnt}$) and hACE2-K18Tg mice (Tg(K18-hACE2)2Prlmn) were described previously[9,22]. All mice were bred at the specific pathogen-free facility of the Institute of Virology and Immunology and housed as previously described[10]. Mice were anesthetized with isoflurane and inoculated intranasally with 20 µl per nostril. For single-infection experiments, 7–17-week-old male mice were inoculated with a dose of 2×10^4 TCD_{50}/mouse of either Delta (EPI_ISL_2535433) or Omicron-BA.1 (EPI_ISL_7062525) isolates. For competition experiments, 7–19-week-old female mice were inoculated with a mixture inoculum containing the Delta and Omicron-BA.1 isolates or a mixture of the recombinant spike clones SARS-CoV-2$^{S-Omicron}$ and SARS-CoV-2$^{S-Delta}$. Inoculum mixtures were generated by mixing the respective viruses aiming at a 1:1 ratio based $TCID_{50}$/mL titers of the single virus. The ratio of each variant in the prepared inocula was

further determined by standard RT-qPCR. At 2 or 4 dpi, mice were euthanized and organs were aseptically dissected. Systematic tissue sampling was performed as described previously[9].

K18-hACE2 mice (all female, 7–15 weeks old) were immunized intramuscularly with a single dose of 1 µg of mRNA-Vaccine Spikevax (Moderna). Five weeks after immunization, the immunized mice and a group of sex- and age-matched naïve animals were challenged intranasally with 20 µl per nostril with the virus inoculum described in the results section. Euthanasia and organ collection was performed 2 or 6 dpi as described above. All mice were monitored daily for body weight loss and clinical signs. Oropharyngeal swabs were collected daily as described before[10].

Animal specimens work up, viral RNA detection and quantification

Organ samples of about 0,1 cm^3 size from ferrets and hamsters were homogenized in a 1 mL mixture composed of equal volumes of Hank's balanced salts MEM and Earle's balanced salts MEM (containing 2 mM L-glutamine, 850 mg l − 1 NaHCO3, 120 mg l − 1 sodium pyruvate, and 1% penicillin–streptomycin) at 300 Hz for 2 min using a Tissuelyser II (Qiagen) and were then centrifuged to clarify the supernatant. Organ samples from mice were either homogenized in 0.5 mL of RA1 lysis buffer supplemented with 1% β-mercaptoethanol as described[10].

Nucleic acid was extracted from 100 µl of the nasal washes after a short centrifugation step or 100 µl of organ sample supernatant using the NucleoMag Vet kit (Macherey Nagel). Nasal washings, oropharyngeal swabs and organ samples were tested by virus-variant specific RT-qPCR to analyze the genomic ratio of the two different viruses used for inoculation.

Three specific RT-qPCR assays for SARS-CoV-2 Alpha, Delta and Omicron-BA.1 were designed based on the specific genome deletions within the ORF1 and S gene (Supplementary Information Table 5). Here, virus specific primers were used to achieve a high analytical sensitivity (<10 genome copies/µl template) of the according PCR assays, also in samples with a high genome load of the non-matching virus. For each specific RT-qPCR a dilution row of a standard with known concentration determined by digital droplet PCR was carried along to calculate the viral genome copy number per mL.

The RT-qPCR reaction was prepared using the qScript XLT One-Step RT-qPCR ToughMix (QuantaBio, Beverly, MA, USA) in a volume of 12.5 µl including 1 µl of the respective FAM mix and 2.5 µl of extracted RNA. The reaction was performed for 10 min at 50 °C for reverse transcription, 1 min at 95 °C for activation, and 42 cycles of 10 sec at 95 °C for denaturation, 10 sec at 60 °C for annealing and 20 sec at 68 °C for elongation for the Omicron-BA.1-detecting assay. For detection of Alpha and Delta, the following thermal profile was applied: 10 min at 50 °C for reverse transcription, 1 min at 95 °C for activation, and 42 cycles of 5 sec at 95 °C for denaturation, 5 sec at 62 °C for annealing and 10 sec at 68 °C for elongation. Fluorescence was measured during the annealing phase. RT-qPCRs were performed on a BioRad real-time CFX96 detection system (Bio-Rad, Hercules, USA) or with 7500 Fast System SDS (Applied Biosciences, Software Version 1.4). Statistical analysis were done in GraphPad Prism version 8.

Histopathological and immunohistochemical analysis

The left lung and the left hemisphere of the brain from K18-hACE2 mice were collected upon necropsy and immersed in 10% neutral-buffered formalin. Following fixation, both tissues were embedded in paraffin, cut at 4 µm and stained with hematoxylin and eosin (H&E) for histological evaluation. Lung tissue pathology was scored according to a previously published scoring scheme[10]. A 1:3000 dilution of a rabbit polyclonal anti-SARS-CoV nucleocapsid antibody (Rockland, 200-401-A50) was used for the immunohistochemical

Article

(IHC) analysis of the lung and the brain. Paraffin blocks were cut at 3 μm, placed in a BOND RX™ immunostainer (Leica Byosystems, Germany) and were incubated for 30 min with the first antibody at room temperature. Antigen retrieval was performed by incubating the slides with a citrate buffer for 30 min at 100 °C. Bond™ Polymer Refine Detection visualization kit (Leica Byosystems, Germany) was afterwards used for signal detection using DAB as chromogen and counterstaining with hematoxylin.

Serological tests
To evaluate the virus neutralizing potential of serum samples, we performed a live virus neutralization test following an established standard protocol as described before[23]. Briefly, sera were prediluted 1/16 in MEM and further diluted in log2 steps until a final tested dilution of 1/4096. Each dilution was evaluated for its potential to prevent 100 $TCID_{50}$ SARS-CoV-2/well of the respective VOC from inducing cytopathic effect in VeroE6 cells, giving the virus neutralization titer (VNT_{100}). Additionally, serum samples were tested by multispecies ELISA for sero-reactivity against the SARS-CoV-2 RBD domain[24]. Data is collected with Tecan i-control 2014 1.11 and analyzed with Microsoft Excel 2016 (16.0.5188.1000).

Human precision-cut lung slice cultures (PCLS)
The generation of PCLSs was done as described previously with some adaptations to human specimens[25]. Control lung tissue (preserved pulmonary architecture without emphysema or inflammation) was obtained from the distal non-tumorous areas of lung resections. Prior to processing, lung tissue was tested for SARS-CoV-2 by qPCR. After gathering, control lung tissue was maintained in DMEM (Thermo Fisher), supplemented with 1X ITS (Sigma) until further processing 2 to 5 h later. Next, lung tissue specimens were washed with PBS (Thermo Fisher) containing 1X Antibiotic-Antimycotic (Thermo Fisher), infused with 2% low-melting point agarose (Sigma) in DMEM, and subsequently put into cold PBS at 4 °C for 15 min to allow the agarose to solidify. Next, the perfused tissue was cut into small cubes of ~1 cm³, placed in the specimen tube and embedded in 2% low-melting point agarose. To generate PCLSs with a thickness of 400 μm, an automated Compresstome VF-310-0Z Vibrating Microtome (Precisionary) was used following the recommended parameters: speed of 8 mm/sec and oscillation of 27 Hz. The slices were transferred into a 12-well plate (one PCLS per well) with culture medium (DMEM, supplemented with 1% FBS, 100 units/mL of penicillin and 100 μg/mL streptomycin, and 2.5 μg/mL of Amphotericin B (all from Thermo Fisher)). Cultures were maintained at 37 °C, 5% CO_2 and culture medium changed every 24 h for 2–3 days prior infection.

Infection of human precision-cut lung slice cultures
PCLS cultures were infected with a 1:1 mixture of SARS-CoV-2[S-Delta] and SARS-CoV-2[S-Omicron] in 0.5 mL DMEM, supplemented with 0.1% FBS, 100 units/mL of penicillin and 100 μg/mL streptomycin, and 2.5 μg/mL of Amphotericin B for 2–4 h. Next, the inoculum was removed, PCLSs were washed twice with pre-warmed PBS, and 2 mL of culture medium were added per well. Medium was changed after 24 h. Fourty eight hpi, PCLSs were washed and transferred into cold TRIzol reagent (Thermo Fisher) and kept at −70 °C until further processing.

RNA isolation of human PCLS
Total RNA was extracted from PCLS cultures using TRIzol reagent in combination with the RNA Clean & Concentrator Kit (Zymo Research). Briefly, Tissue slices were homogenized using MagNA Lyser Green Beads (Roche diagnostics) in combination with a tissue homogenizer (MP Biomedicals) and lysed with 700 μl of cold TRIzol reagent per PCLS. Two hundred mL of chloroform was added to the TRIzol lysate, the samples were mixed vigorously, and then incubated for 2–3 min at room temperature. Next, the extractions were centrifuged at 12,000 g

for 15 min at 4 °C. The aqueous phase was then collected, mixed 1:1 with 75% ethanol, and incubated for 10 min at room temperature to let RNA precipitate. The RNA precipitate was further purified with the RNA Clean & Concentrator Kit according to the manufacturer's instructions.

Well-differentiated primary nasal and bronchial epithelial cells
Primary human nasal epithelial cell cultures (hNECs) were obtained commercially (Epithelix Sàrl) and primary human bronchial epithelial cell cultures (hBECs) were isolated from lung slices. The generation of well-differentiated (WD)-hNECs and WD-hBECs at the air-liquid interface (ALI) was described previously with minor adjustments[26,27]. For expansion, hNECs and hBECs were cultured in collagen-coated (Sigma) cell culture flasks (Costar) in PneumaCult Ex Plus medium, supplemented with 1 μM hydrocortisone, 5 μM Y-27632 (Stem Cell Technologies), 1 μM A-83-01 (Tocris), 3 μM isoproterenol (abcam), and 100 μg/mL primocin (Invivogen) and maintained in a humidified atmosphere at 37 °C, 5% CO_2. Next, the expanded cells were seeded at a density of 50,000 cells per insert onto collagen-coated (Sigma) 24-well plate inserts with a pore size of 0.4 μm (Greiner Bio-One) and grown under submerged conditions with 200 μl of supplemented PneumaCult ExPlus medium on the apical side and 500 μl in the basolateral chamber. When cells reached confluence, as assessed by measuring the trans-epithelial electrical resistance (TEER) using a Volt/Ohm Meter (EVOM²/STX2, World Precision Instruments) and microscopical evaluation, the apical medium was removed, cells were washed with pre-warmed Hank's balanced salt solution (HBSS, Thermo Fisher), and then exposed to the air. PneumaCult ALI medium supplemented with 4 μg/mL heparin (Stem Cell Technologies), 5 μM hydrocortisone, and 100 μg/mL primocin was added to the basolateral chamber to induce differentiation of the cells. Every 2–3 days, the basal medium was changed and cultures maintained at 37 °C, 5% CO_2 until the appearance of ciliated cells and mucus production. The cell layer was washed once a week with 250 μL of pre-warmed HBSS for 20 min at 37 °C to get rid of mucus. The hNEC and hBEC cultures were considered well-differentiated 3 weeks post-exposure to ALI.

Statistical analysis
Statistical analysis was performed using GraphPad Prism 8. Unless noted otherwise, the results are expressed as mean ± s.d. Specific tests are indicated in the main text or the figure legends.

Figures
Cartoon figures for animal experimentations were created with BioRender.com.

Data availability
All data are available in the main text or the supplementary materials. Source data are provided with this paper. The project information is accessible with the BioProject ID PRJNA868423. Source data are provided with this paper.

References
1. Motozono, C. et al. SARS-CoV-2 spike L452R variant evades cellular immunity and increases infectivity. *Cell Host Microbe* **29**, 1124–1136 e11 (2021).
2. Liu, Y. et al. Delta spike P681R mutation enhances SARS-CoV-2 fitness over Alpha variant. *Cell Rep.* **39**, 110829 (2022).
3. ECDC. *Implications of the Emergence and Spread of the SARSCoV-2 B.1.1. 529 Variant of Concern (Omicron), for the EU/EEA* (ECDC, 2021).
4. Cele, S. et al. Omicron extensively but incompletely escapes Pfizer BNT162b2 neutralization. *Nature* **602**, 654–656 (2022).
5. Wilhelm, A. et al. Reduced neutralization of SARS-CoV-2 Omicron variant by vaccine sera and monoclonal antibodies. *medRxiv* https://doi.org/10.1101/2021.12.07.21267432 (2021).

Article

6. CoVariants. *Overview of Variants in Countries* https://covariants.org/per-country (2022).

7. Gu, H. et al. Recombinant BA.1/BA.2 SARS-CoV-2 virus in arriving travelers, Hong Kong, February 2022. *Emerg. Infect. Dis.* **28**, 1276–1278 (2022).

8. de Vries, R. D. et al. Animal models of SARS-CoV-2 transmission. *Curr. Opin. Virol.* **50**, 8–16 (2021).

9. Zhou, B. et al. SARS-CoV-2 spike D614G change enhances replication and transmission. *Nature* **592**, 122–127 (2021).

10. Ulrich, L. et al. Enhanced fitness of SARS-CoV-2 variant of concern Alpha but not Beta. *Nature* **602**, 307–313 (2022).

11. Plante, J. A. et al. Spike mutation D614G alters SARS-CoV-2 fitness. *Nature* **592**, 116–121 (2021).

12. Touret, F. et al. Replicative fitness of a SARS-CoV-2 20I/501Y.V1 variant from lineage B.1.1.7 in human reconstituted bronchial epithelium. *mBio* **12**, e0085021 (2021).

13. Port, J. R. et al. Increased small particle aerosol transmission of B.1.1.7 compared with SARS-CoV-2 lineage A in vivo. *Nat. Microbiol.* **7**, 213–223 (2022).

14. McMahan, K. et al. Reduced pathogenicity of the SARS-CoV-2 omicron variant in hamsters. *Med* **3**, 262–268.e4 (2022).

15. Abdelnabi, R. et al. The omicron (B. 1.1. 529) SARS-CoV-2 variant of concern does not readily infect Syrian hamsters. *Antivir. Res.* **198**, 105253 (2022).

16. Hui, K. P. Y. et al. SARS-CoV-2 Omicron variant replication in human bronchus and lung ex vivo. *Nature* **603**, 715–720 (2022).

17. Yuan, S. et al. The SARS-CoV-2 Omicron (B.1.1.529) variant exhibits altered pathogenicity, transmissibility, and fitness in the golden Syrian hamster model. *bioRxiv* https://doi.org/10.1101/2022.01.12.476031 (2022).

18. van den Worm, S. H. et al. Reverse genetics of SARS-related coronavirus using vaccinia virus-based recombination. *PLoS One* **7**, e32857 (2012).

19. Kaleta, T. et al. Antibody escape and global spread of SARS-CoV-2 lineage A.27. *Nat. Commun.* **13**, 1152 (2022).

20. Thi Nhu Thao, T. et al. Rapid reconstruction of SARS-CoV-2 using a synthetic genomics platform. *Nature* **582**, 561–565 (2020).

21. Wylezich, C. et al. A versatile sample processing workflow for metagenomic pathogen detection. *Sci. Rep.* **8**, 13108 (2018).

22. McCray, P. B. Jr. et al. Lethal infection of K18-hACE2 mice infected with severe acute respiratory syndrome coronavirus. *J Virol* **81**, 813–821 (2007).

23. Schlottau, K. et al. SARS-CoV-2 in fruit bats, ferrets, pigs, and chickens: an experimental transmission study. *The Lancet Microbe* **1**, e218-e225 (2020).

24. Wernike, K. et al. Multi-species ELISA for the detection of antibodies against SARS-CoV-2 in animals. *Transbound Emerg. Dis.* **68**, 1779–1785 (2021).

25. Brügger, M. et al. Pulmonary mesenchymal stem cells are engaged in distinct steps of host response to respiratory syncytial virus infection. *PLoS Pathog.* **17**, e1009789 (2021).

26. Fahmi, A. et al. SARS-CoV-2 can infect and propagate in human placenta explants. *Cell. Rep. Med.* **2**, 100456 (2021).

27. Tyson, J.R. et al. Improvements to the ARTIC multiplex PCR method for SARS-CoV-2 genome sequencing using nanopore. *bioRxiv* https://doi.org/10.1101/2020.09.04.283077 (2020).

Author contributions

G.T.B., N.J.H., A.T., J.N.K., J.S., N.E., L.U., R.D., D.H., M.P.A., C.B., M.Be., V.T. conceived the study; G.T.B., N.J.H., A.T., J.S., N.E., L.U., C.D., S.S., B.S.T., I.B.V., D.H. performed most of the experiments; B.H., N.G.F.L., E.A.M., A.B., C.W., D.H., K.W., A.G., L.T., V.F., H.S., M.Br., B.I.O.E., B.Z., G.B., A.K., K.S., S.O., R.M.L., Man.W., C.M., P.D., T.M.M., M.F.-C., A.R., Mar.W., S.C. did experimental work and/or provided essential experimental systems and reagents; J.N.K., C.W. performed sequencing including computational analyses; G.T.B., N.J.H., A.T., J.N.K., J.S., N.E., L.U., D.H., M.P.A., C.B., M.Be., V.T. wrote the manuscript and made the figures. All authors read and approved the final manuscript.

Competing interests

Authors declare that they have no competing interests.

Additional information

Supplementary information The online version contains supplementary material available at https://doi.org/10.1038/s41467-022-33632-y.

Correspondence and requests for materials should be addressed to Marco P. Alves, Charaf Benarafa, Martin Beer or Volker Thiel.

Peer review information *Nature Communications* thanks Claudia Thompson and the other, anonymous, reviewer(s) for their contribution to the peer review of this work. Peer reviewer reports are available.

Reprints and permission information is available at http://www.nature.com/reprints

Publisher's note Springer Nature remains neutral with regard to jurisdictional claims in published maps and institutional affiliations.

Article https://doi.org/10.1038/s41467-022-33632-y

G. Tuba Barut [1,2,15], Nico Joel Halwe [3,15], Adriano Taddeo [1,2,15], Jenna N. Kelly [1,2,4,5,15], Jacob Schön[3], Nadine Ebert[1,2], Lorenz Ulrich [3], Christelle Devisme[1,2], Silvio Steiner [1,2], Bettina Salome Trüeb[1,2], Bernd Hoffmann [3], Inês Berenguer Veiga [1,2], Nathan Georges François Leborgne[1,2], Etori Aguiar Moreira[1,2], Angele Breithaupt [6], Claudia Wylezich [3], Dirk Höper [3], Kerstin Wernike [3], Aurélie Godel[1,2], Lisa Thomann [1,2], Vera Flück[1,2], Hanspeter Stalder [1,2], Melanie Brügger[1,2], Blandina I. Oliveira Esteves[1,2], Beatrice Zumkehr[1,2], Guillaume Beilleau [1,2,7], Annika Kratzel [1,2], Kimberly Schmied [1,2], Sarah Ochsenbein[1,2], Reto M. Lang[1,2,7], Manon Wider[8], Carlos Machahua[9,10], Patrick Dorn[11,12], Thomas M. Marti [11,12], Manuela Funke-Chambour[9,10], Andri Rauch [4,13], Marek Widera [14], Sandra Ciesek [14], Ronald Dijkman [4,5,8], Donata Hoffmann [3], Marco P. Alves [1,2,4,16] ✉, Charaf Benarafa [1,2,4,16] ✉, Martin Beer [3,5,16] ✉ & Volker Thiel [1,2,4,5,16] ✉

[1]Institute of Virology and Immunology, Bern and Mittelhäusern, Bern, Switzerland. [2]Department of Infectious Diseases and Pathobiology, Vetsuisse Faculty, University of Bern, Bern, Switzerland. [3]Institute of Diagnostic Virology, Friedrich-Loeffler-Institut, Greifswald-Insel Riems, Greifswald, Germany . [4]Multidisciplinary Center for Infectious Diseases, University of Bern, Bern, Switzerland. [5]European Virus Bioinformatics Center, Jena, Germany. [6]Department of Experimental Animal Facilities and Biorisk Management, Friedrich-Loeffler-Institut, Greifswald-Insel Riems, Greifswald, Germany. [7]Graduate School for Cellular and Biomedical Sciences, University of Bern, Bern, Switzerland. [8]Institute for Infectious Diseases, University of Bern, Bern, Switzerland. [9]Department of Pulmonary Medicine, Inselspital, Bern University Hospital, University of Bern, Bern, Switzerland. [10]Department for Pulmonary Medicine, BioMedical Research, University of Bern, Bern, Switzerland. [11]Division of General Thoracic Surgery, Inselspital, Bern University Hospital, University of Bern, Bern, Switzerland. [12]Department for BioMedical Research, Inselspital, Bern University Hospital, University of Bern, Bern, Switzerland. [13]Department of Infectious Diseases, Inselspital, Bern University Hospital, University of Bern, Bern, Switzerland. [14]Institute of Medical Virology, University Hospital Frankfurt, Goethe University, Frankfurt am Main, Germany. [15]These authors contributed equally: G. Tuba Barut, Nico Joel Halwe, Adriano Taddeo, Jenna N. Kelly. [21]These authors jointly supervised this work: Marco P. Alves, Charaf Benarafa, Martin Beer, Volker Thiel. ✉e-mail: marco.alves@vetsuisse.unibe.ch; charaf.benarafa@vetsuisse.unibe.ch; martin.beer@fli.de; volker.thiel@vetsuisse.unibe.ch

Supplementary Figure 1
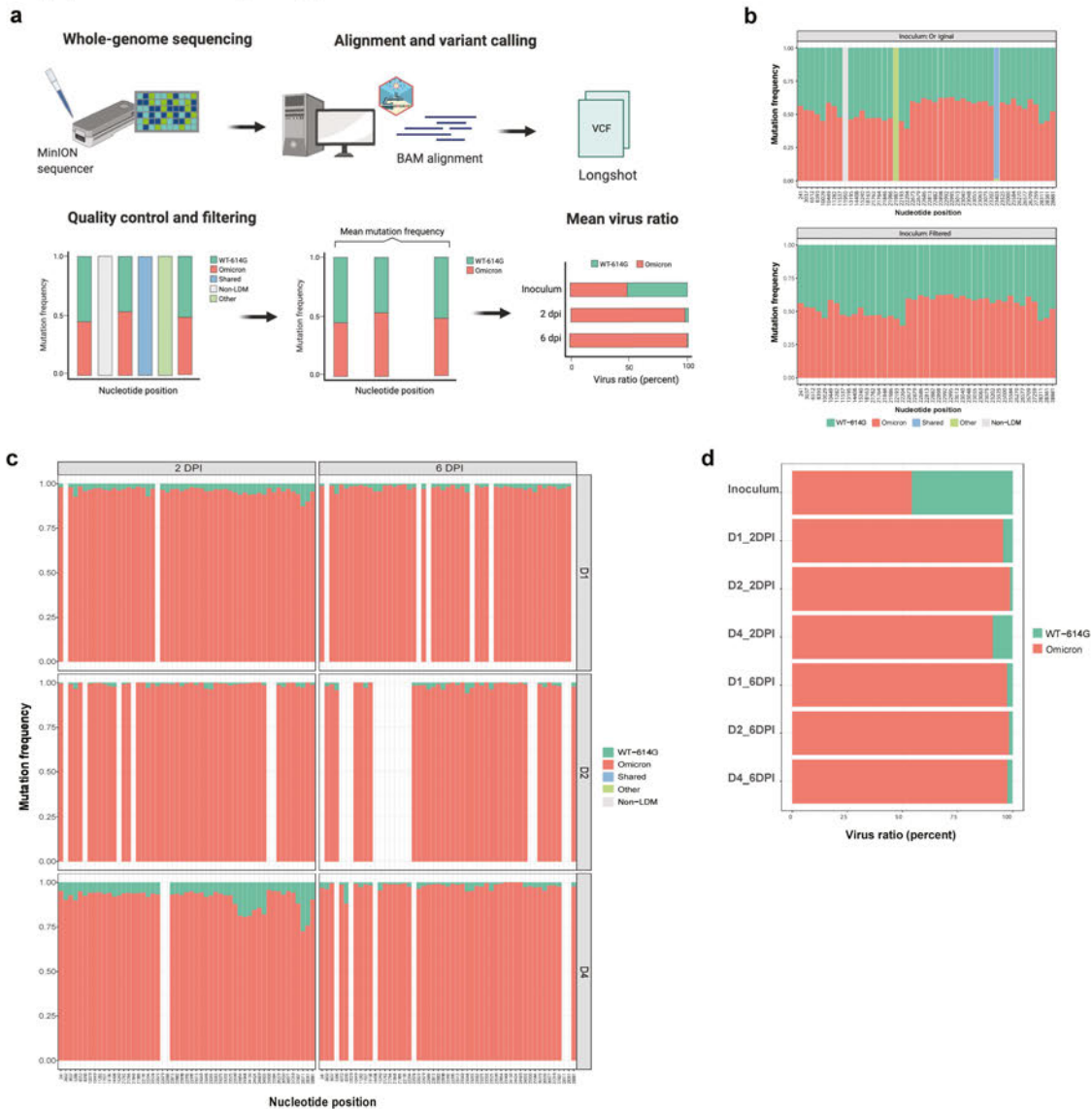
Supplementary Fig. 1: Sequencing data analysis. a) Schematic illustrating the general sequencing and bioinformatics workflow used to determine the virus ratios in Fig. 1e-g. For each virus mixture in the NEC, BEC, and lung explants samples, RNA was extracted from apical washes at 2 and/or 6 dpi and sequenced on the MinION sequencer using a modified version of the ARTIC protocol for SARS-CoV-2 sequencing (1200 bp amplicons with the midnight primer scheme, see methods for specific modifications)[26]. Live GPU basecalling was performed using Guppy v.5.1.15 (Oxford Nanopore technologies) in high-accuracy mode and the downstream analysis was performed using a modified version of the ARTIC bioinformatics pipeline (https://artic.network/ncov-2019/ncov2019-bioinformatics-sop.html). Briefly, input reads were filtered based on read length and then mapped to the Wuhan-Hu-1 reference genome (accession MN908947.3 [www.ncbi.nlm.nih.gov/bioproject/?term=MN908947.3]) using the 'artic minion' command. BAM alignment files from the ARTIC pipeline were then used for variant calling in longshot (v.0.4.4) with an input VCF file containing VOC Delta and Omicron-BA.1 mutations provided to call variants at specific nucleotide sites. The downstream analysis of VCF files was performed in R v.4.1.3 and involved filtering the VCF file for each sample to exclude mutations shared between both viruses in the mixture (shared, blue), non-lineage-defining mutations (non-LDM, grey), and any sites with overlapping mutations in both viruses that were difficult to call (other, green). Mutations called with a depth of coverage lower than 100 were also excluded from the downstream analysis (bottom left panel). Mutations in filtered VCF files (bottom middle panel) were then used to calculate the mean mutation frequency for each virus per sample. Finally, the mean ± sd virus ratio was calculated for each time point (bottom right panel). **b)** Stacked bar plot showing the frequency of individual mutations called in the VCF file for the WT-614G and Omicron inoculum before (top) and after (bottom) filtering. **c)** Stacked bar plot showing the frequency of individual mutations in the filtered VCF files for all WT-614G and Omicron NEC samples (3 donors, 2 and 6 dpi). These values were used to calculate a mean mutation frequency for each virus per sample, which is shown in **d)**.

Supplementary Figure 2
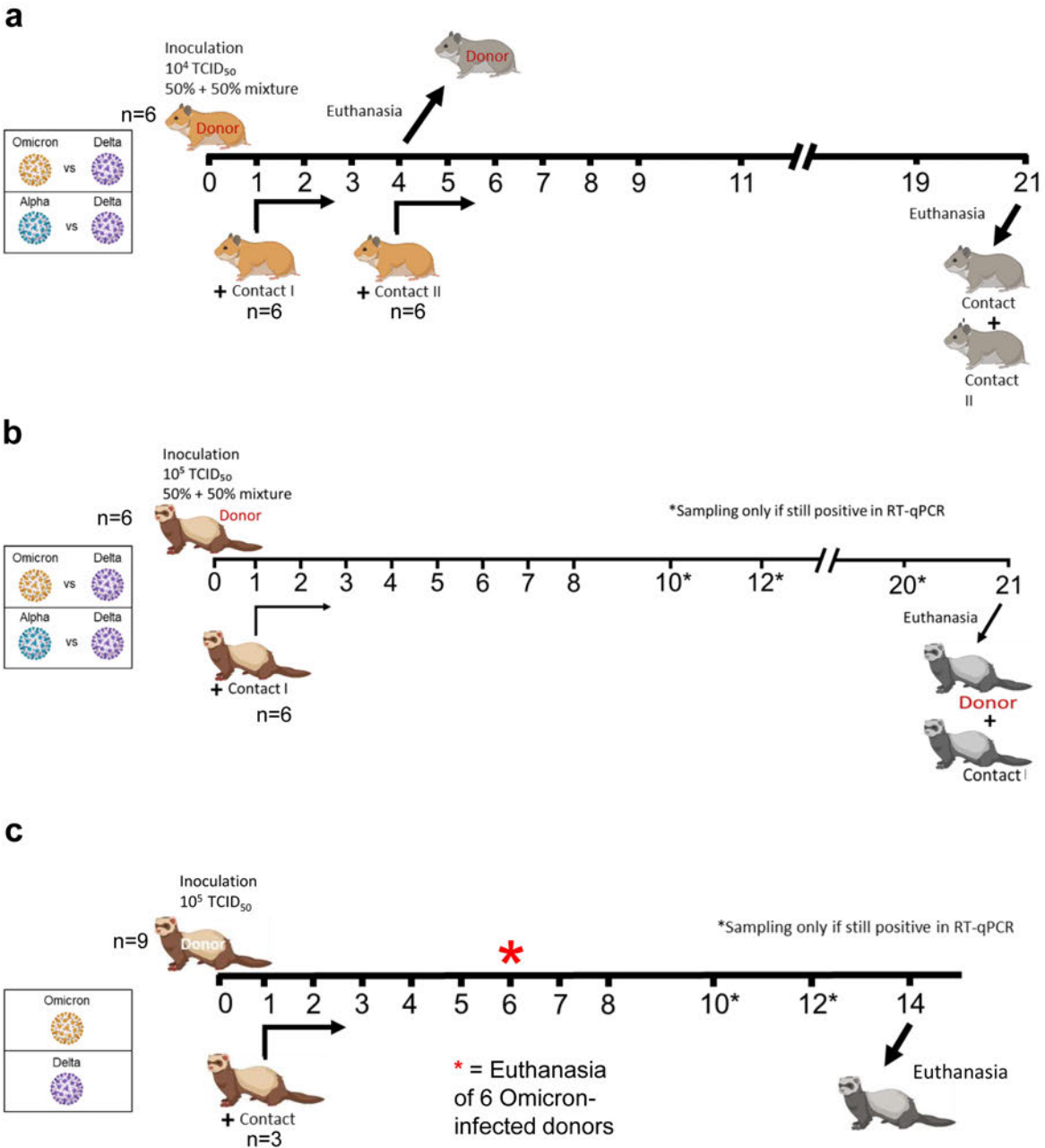
Supplementary Fig. 2: Experimental outline for studies with Syrian hamsters and ferrets. Donor hamsters (n=6) were intranasally inoculated with either an Omicron-BA.1, -Delta or an Alpha-Delta mixture at iso-titer. A Competition studies in hamsters. Each donor was co-housed with one contact I hamster 1dpi. 4dpi after euthanasia of the donors, one contact II hamster was introduced to each contact I hamster. B Study outline for the ferret competition studies with Omicron-BA.1-Delta and Alpha-Delta mixtures. C Timeline for the ferret study with single-variant-inocula (either Omicron-BA.1 or Delta). 6dpi six donor animals, which were inoculated with Omicron-BA.1, were euthanized for determination of viral organ load in URT and LRT.

Supplementary Figure 3
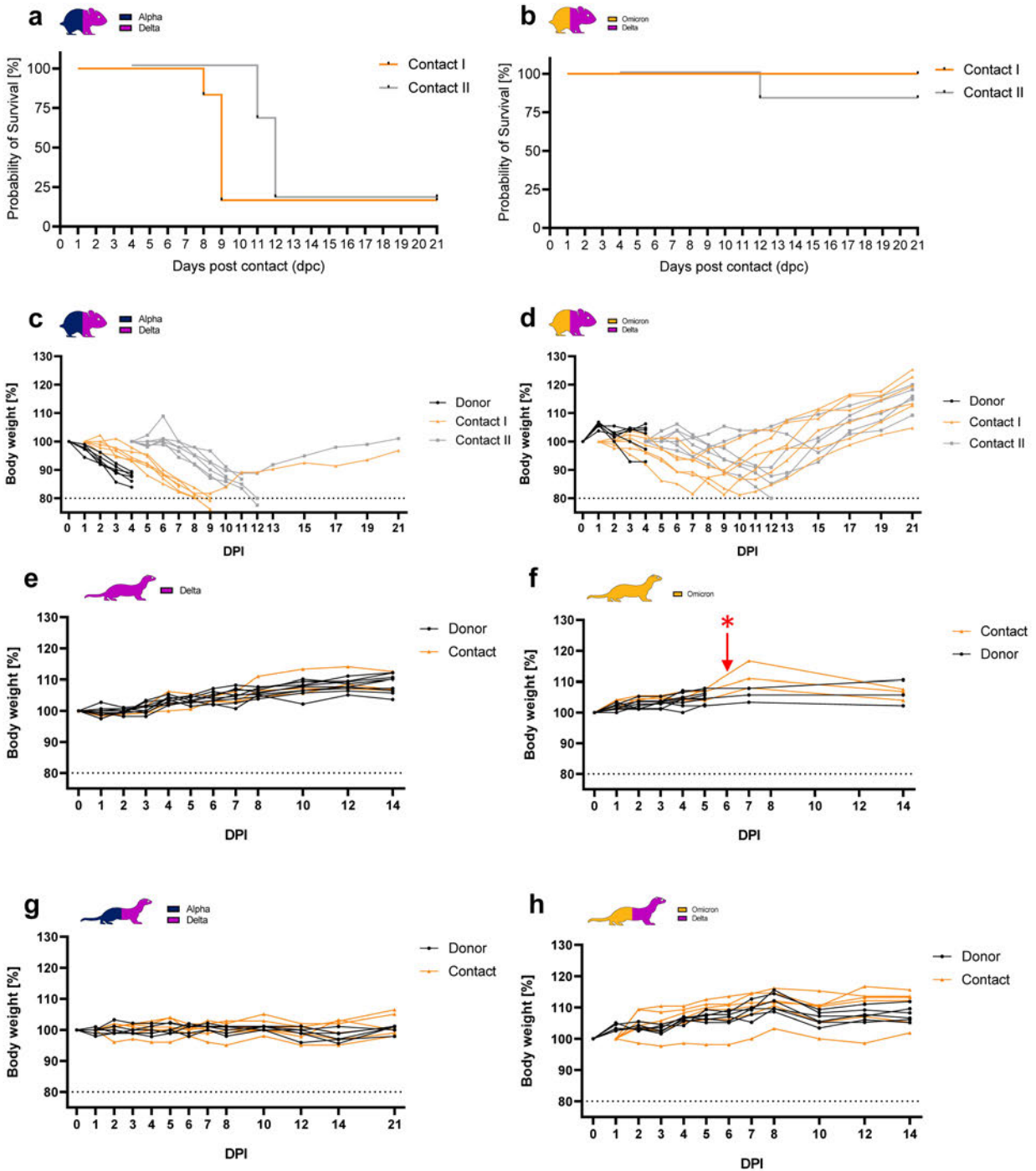
Supplementary Fig. 3: Body weight changes and survival rate of hamsters/ferrets in the competitive infection and transmission experiments. a) Survival of Syrian hamsters during competitive infection and transmission experiment between Alpha and Delta VOC. b) Survival of Syrian hamsters during competitive infection and transmission experiment between Delta and Omicron-BA.1 VOC. c) Percentages of body weight change in Syrian hamsters competitively inoculated with Alpha and Delta VOC. d) Percentages of body weight change in Syrian hamsters competitively inoculated with Delta and Omicron-BA.1 VOC. e) Percentages of body weight change in ferrets during single infection study with Delta VOC. f) Percentages of body weight change in ferrets during single infection study with Omicron-BA.1 VOC. Red star and arrow show timepoint of euthanasia (6 dpi) for six ferrets to analyze viral load distribution in organs. g) Percentages of body weight change in ferrets competitively inoculated with Alpha and Delta VOC. h) Percentages of body weight change in ferrets competitively inoculated with Delta and Omicron-BA.1 VOC.

Supplementary Figure 4
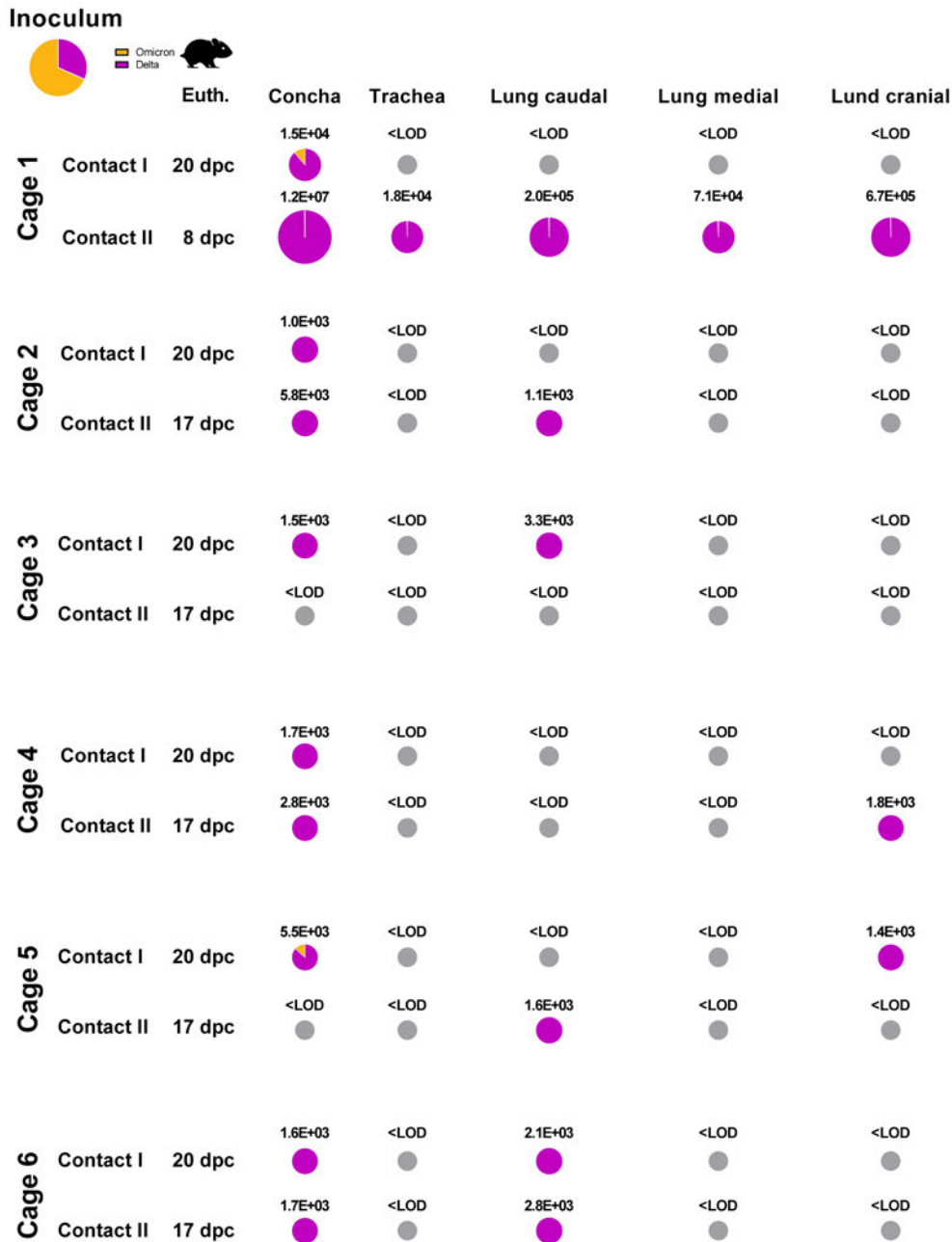
Supplementary Fig. 4: Viral load in organs of Contact I and Contact II hamsters competitively inoculated with Delta and Omicron-BA.1 VOC at respective euthanasia timepoints Viral genome load in upper (URT) and lower (LRT) respiratory tract tissues of Syrian hamsters in the competitive transmission experiment between SARS-CoV-2 VOCs Delta and Omicron-BA.1. Syrian hamsters were inoculated with comparable genome equivalent mixture of Delta and Omicron-BA.1 VOC. Absolute quantification was performed by RT–qPCR analysis of tissue homogenates of Contact I and Contact II hamsters in relation to a set of defined standards. Tissue samples were collected at euthanasia (Euth.). Pie chart colors illustrate the ratio of variants detected in each sample at the indicated dpi or days post contact (dpc). Pie chart sizes are proportional to the total viral genome copies reported above. Grey pies indicate values below the LOD ($<10^3$ viral genome copies per mL).

Supplementary Figure 5
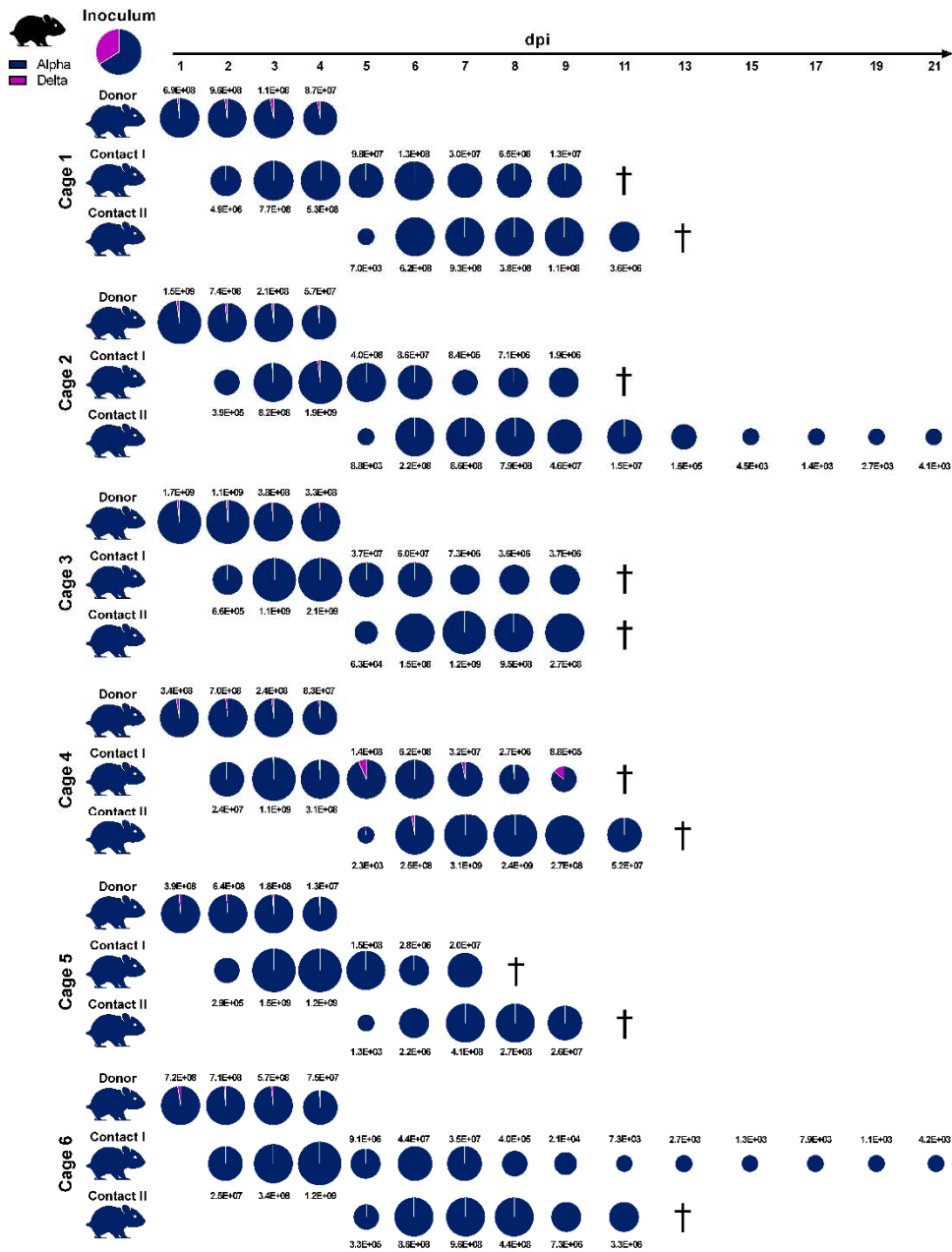
Supplementary Fig. 5: Competitive infection of hamsters with SARS-CoV-2 Delta and Alpha Six donor hamsters were each inoculated intranasally with $10^{4.625}$ TCID$_{50}$ determined by back titration and composed of a mixture of SARS-CoV-2 Alpha (dark blue) and Delta (purple) at 1.95:1 ratio determined by back-titration of the original single virus amounts used in the experiment. Donor hamsters, contact I and II hamsters were co-housed sequentially as shown in Supplementary Data Fig.2. Nasal washings were performed daily from 1-9 dpi and afterwards every two days until 21 dpi. Each pie chart illustrates the ratio of the respective viruses in nasal washings for each sampling day. Total genome copies/mL are indicated above or below the respective pies. Hamster silhouettes are colored according to the dominant variant (>66%) detected in the latest sample of each animal. Black crosses indicate the respective animal was already dead.

Supplementary Figure 6
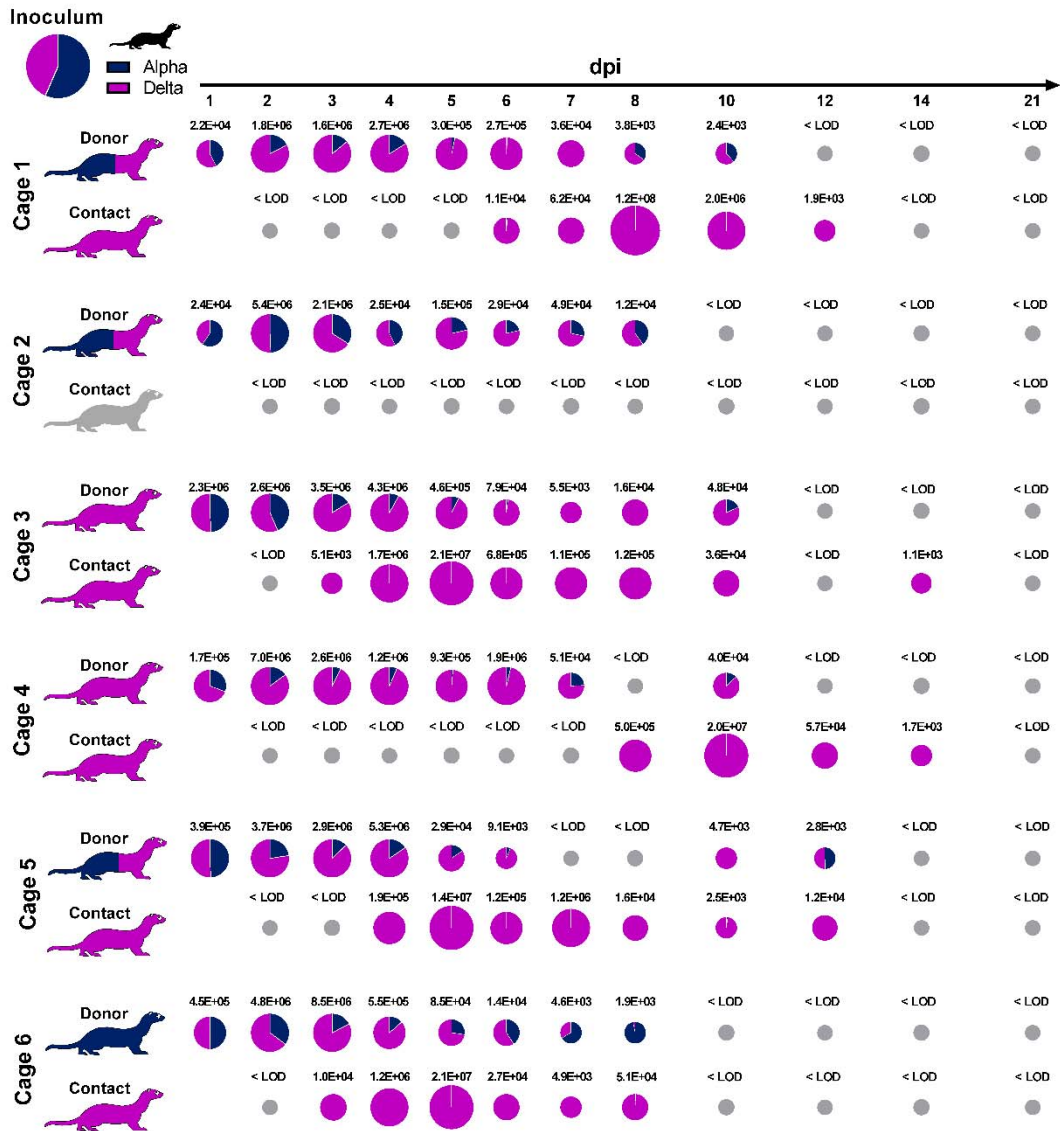
Supplementary Fig. 6: Competitive infection of ferrets with SARS-CoV-2 Alpha and Delta
Six donor ferrets were each inoculated with 10^5 TCID$_{50}$ determined by back titration and composed of a mixture of Alpha (dark blue) and SARS-CoV-2 Delta (purple) at a 1.33:1 ratio determined by back-titration of the original single virus amounts used in the experiment. Donor and Contact ferrets were co-housed sequentially as shown in Supplementary Data Fig.2. Pie charts illustrate the ratio of either SARS-CoV-2 Alpha or SARS-CoV-2 Delta detected in nasal washings of the donor or contact ferrets in the respective ferret groups at indicated dpi. Viral genome copies/mL are shown above or below respective pie charts; Grey pies indicate values below the LOD ($<10^3$ viral genome copies per mL). Coloring of the ferret silhouettes refers to the predominant SARS-CoV-2 variant ($>66\%$) detected in the latest sample of the respective animal.

Supplementary Figure 7
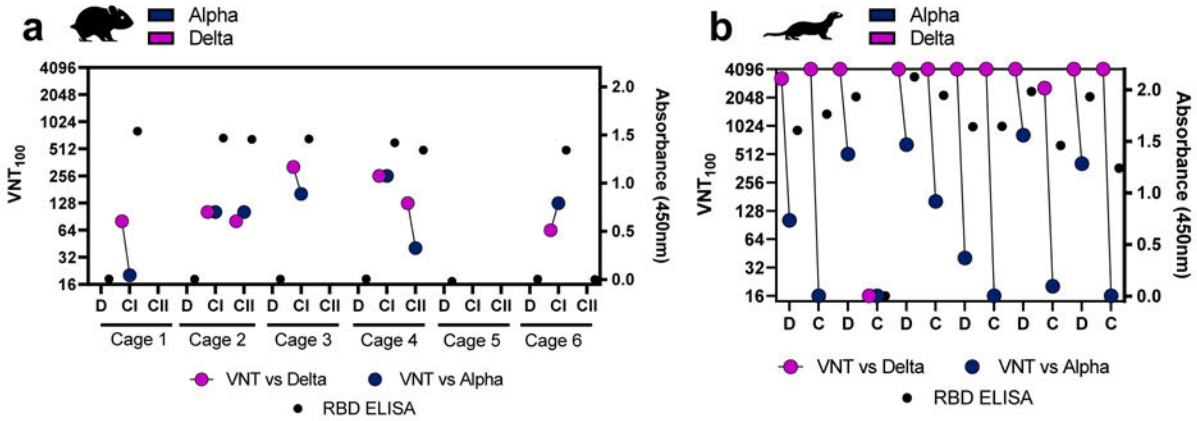
Supplementary Fig. 7: ELISA and VNT100 of sera received from competitive infection experiments with Alpha and Delta in hamsters/ferrets. Blue dots represent neutralization of Alpha variant, purple dots represent neutralization of the Delta variant in the respective animal according to the highest dilution where virus neutralization was visible (left Y-Axis). Black dots show RBD-ELISA-reactivity of animal sera at respective euthanasia timepoint (right Y-Axis) (a) VNT100 and RBD-ELISA from animal sera of the Alpha vs Delta competitive infection and transmission experiment in hamsters (b) VNT100 and RBD-ELISA from animal sera of the competitive infection and transmission experiment with Delta and Alpha VOC in ferrets.

Supplementary Figure 8
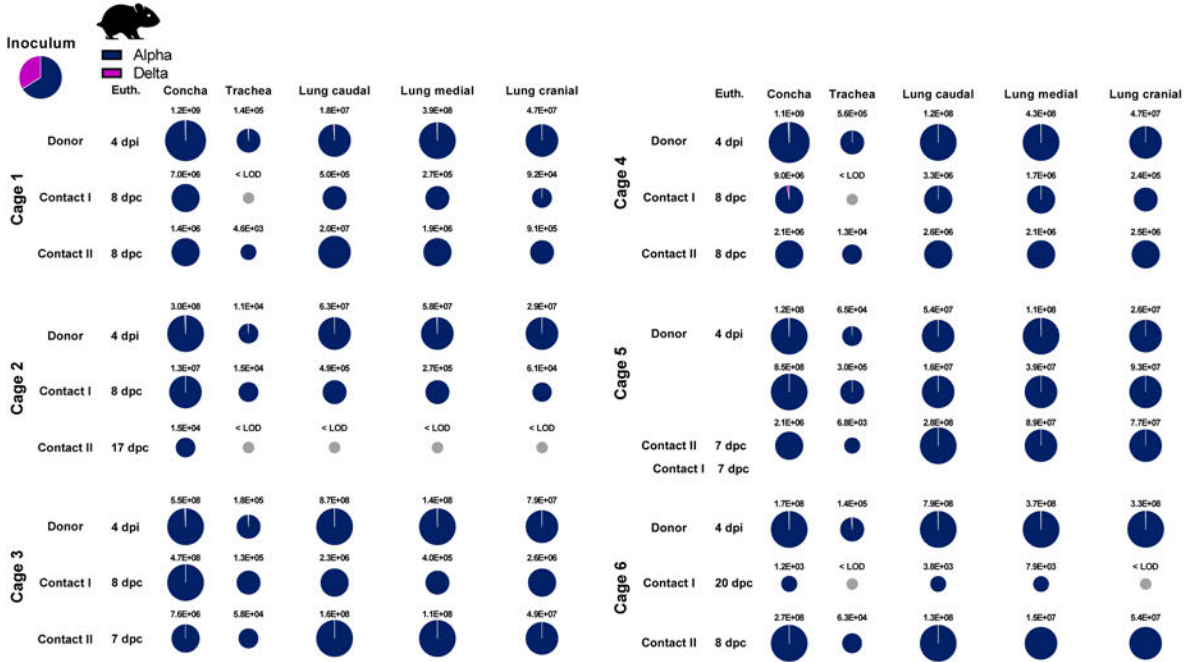
Supplementary Fig. 8: Viral load in organs of Donor, Contact I and Contact II hamsters competitively inoculated with Alpha and Delta VOC at respective euthanasia timepoints. Viral genome load in upper (URT) and lower (LRT) respiratory tract tissues of Syrian hamsters in the competitive transmission experiment between SARS-CoV-2 VOCs Alpha and Delta. Syrian hamsters were inoculated with comparable genome equivalent mixture of either Alpha or Delta VOC. Absolute quantification was performed by RT–qPCR analysis of tissue homogenates of donor, contact I and contact II hamsters in relation to a set of defined standards. Tissue samples were collected at euthanasia (Euth.). Pie chart colors illustrate the ratio of variants detected in each sample at the indicated dpi or days post contact (dpc). Pie chart sizes are proportional to the total viral genome copies reported above. Grey pies indicate values below the LOD (<10^3 viral genome copies per mL).

Supplementary Figure 9

a   Single infections with Delta and Omicron
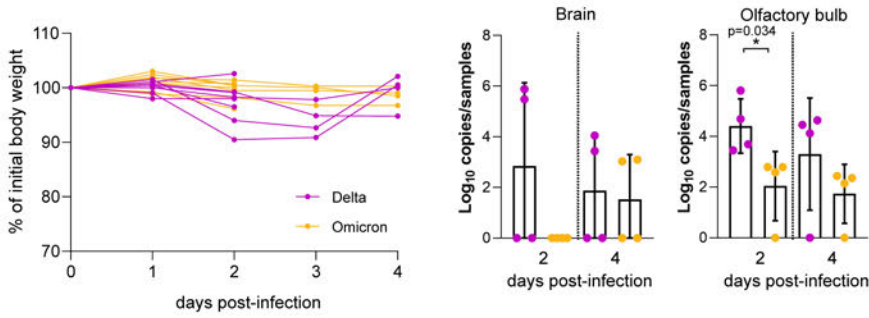
b   Competition experiments with Delta, Omicron, S-Delta and S-Omicron
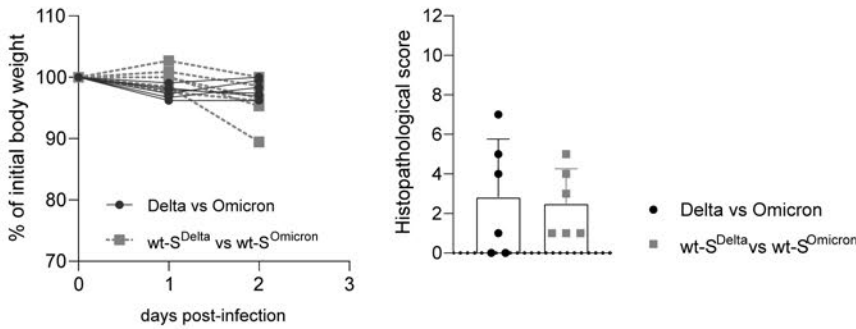
Supplementary Fig. 9: Delta spike mutations drive enhanced fitness in humanized mice. a) hACE2-KI mice (7 to 16 week-old male) were intranasally inoculated with $10^{4.3}$ tissue culture infectious dose 50 ($TCID_{50}$) of Delta or Omicron isolates. The left graph reports the body weight loss for each of the hACE2-KI in Fig. 3a. The right graph depicts the viral copies in brain and olfactory bulb samples quantified using E-gene probe-specific RT–qPCR. Data are mean ± s.d. from the indicated number of biological replicates from a single experiment. Statistical significance was determined using an unpaired two-tailed Student t-test; **P < 0.01. **b)** hACE2-KI mice (7 to 19 week-old female, n=6/group) were intranasally inoculated with 10^4 TCID50 of a 1:1 mix of Delta and Omicron or SARS-CoV-2$^{S\text{-}Delta}$ and SARS-CoV-2$^{S\text{-}Omicron}$. The graph on the left shows the body weight loss for each of the inoculated animal. The graph on the right shows the histopathological score in these mice. Data are mean ± s.d. from the indicated number of biological replicates from a single experiment.

Supplementary Figure 10
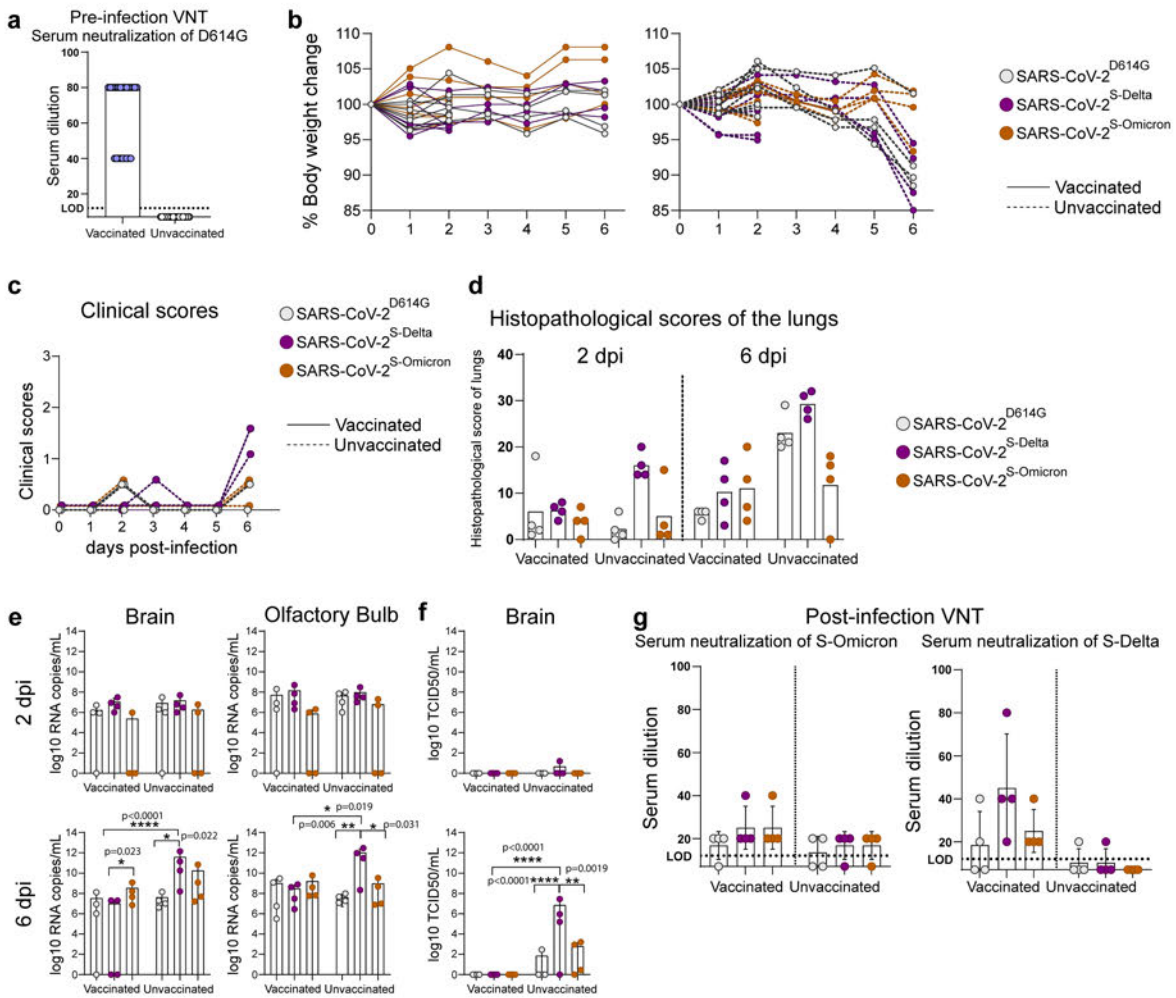
Supplementary Fig. 10: mRNA vaccine induced reduction in replication and pathogenesis of SARS-CoV-2 clones in K18-hACE2 transgenic mice. a) Female K18-hACE2 transgenic mice (7 to 15 weeks old, n=16 mice) were immunized intramuscularly with a single dose of 1 µg of mRNA-Vaccine Spikevax (Moderna). After two weeks the neutralizing antibody titers against SARS-CoV-2^{D614G} were determined. Later, mice were (n=8 mice/group) intranasally inoculated with 10^4 tissue culture infectious dose 50 ($TCID_{50}$) of SARS-CoV-2^{D614G}, SARS-CoV-2$^{S-Delta}$ and SARS-CoV-2$^{S-Omicron}$. **b)** The body weight change and **c)** the clinical scores of the mice were monitored daily. **d)** Histopathological scores were given to evaluate the severity of the lung pathology. **e)** Brain and olfactory bulb samples of the infected mice were collected at 2 or 6 days post-infection (dpi) to determine the viral load (n = 4 for each group). Viral RNA-dependent RNA polymerase (RdRp) gene copies of brain and olfactory bulb tissues were quantified using probe-specific RT–qPCR. **f)** Infectious virus titers from the brain samples were determined using $TCID_{50}$ assays in VeroE6/TMPRSS2 cells. **g)** Virus neutralization capacities of the serum collected from infected mice at 6 dpi are tested against SARS-CoV-2$^{S-Delta}$ and SARS-CoV-2$^{S-Omicron}$ clones. Each dot in the graphs represents one animal, and the bars show mean values +/- SD. The color key in b also applies to c, d, e and f. Statistical significance was determined using ordinary two-way ANOVA (a–d) and P values were adjusted using Tukey's multiple-comparison test; *P < 0.05, **P < 0.01, ***P < 0.001, ****P < 0.0001. Data were obtained from one experiment. Each data point represents one biological replicate.

Supplementary Information Guide

1. **Supplementary Information Table 1:** List of the viruses used in the experiments.
2. **Supplementary Information Table 2:** Histopathological characterization of hACE-2-KI mice infected with Delta or Omicron-BA.1 isolates
3. **Supplementary Information Table 3:** Histopathological characterization of K18-hACE2 mice infected with SARS-CoV-2$^{S\text{-}Delta}$ or SARS-CoV-2$^{S\text{-}Omicron}$

4. **Supplementary Information Table 4:** Primer Pairs for Delta and Omicron.
5. **Supplementary Information Table 5:** Primers and probes for viral RNA detection via RT-qPCR.

Supplementary Information Table 1

SARS-CoV-2	Reference	Model	Inocula
SARS-CoV-2^{D614G}	https://doi.org/10.1038/s41586-021-03361-1	hACE2-K18 mice	SARS-CoV-2^{D614G} Single
		hNEC/hBEC	SARS-CoV-2^{D614G} Single
			SARS-CoV-2^{D614G} vs Delta
			SARS-CoV-2^{D614G} vs Omicron-BA.1
			SARS-CoV-2^{D614G} vs SARS-CoV-2$^{S-Delta}$
			SARS-CoV-2^{D614G} vs SARS-CoV-2$^{S-Omicron}$
Alpha	EPI_ISL_751799	Hamster and ferret	Alpha vs Delta
Delta	EPI_ISL_1760647	Ferret	Delta Single
		Hamster and ferret	Alpha vs Delta
			Delta vs Omicron-BA.1
		hNEC/hBEC	Delta Single
			SARS-CoV-2^{D614G} vs Delta
			Delta vs Omicron-BA.1
			Delta vs SARS-CoV-2$^{S-Delta}$
	EPI_ISL_2535433	hACE2-KI mice	Delta Single
			Delta vs Omicron-BA.1
Omicron-BA.1	EPI_ISL_6959868	Ferret	Omicron-BA.1 Single
		Hamster and ferret	Delta vs Omicron-BA.1
	EPI_ISL_7062525	hACE2-KI mice	Omicron-BA.1 Single
			Delta vs Omicron-BA.1
		hNEC/hBEC	Omicron-BA.1 Single
			SARS-CoV-2^{D614G} vs Omicron-BA.1
			Delta vs Omicron-BA.1
			Omicron-BA.1 vs SARS-CoV-2$^{S-Omicron}$
SARS-CoV-2$^{S-Delta}$	Backbone: NCBI Reference Sequence: Wuhan-Hu-1 NC_045512.2 Spike: EPI_ISL_5769545	hACE2-KI mice	SARS-CoV-2$^{S-Delta}$ vs SARS-CoV-2$^{S-Omicron}$
		NEC/BEC	SARS-CoV-2$^{S-Delta}$ Single
			SARS-CoV-2^{D614G} vs SARS-CoV-2$^{S-Delta}$
			Delta vs SARS-CoV-2$^{S-Delta}$
			SARS-CoV-2$^{S-Delta}$ vs SARS-CoV-2$^{S-Omicron}$
		PCLS	SARS-CoV-2$^{S-Delta}$ vs SARS-CoV-2$^{S-Omicron}$
SARS-CoV-2$^{S-Omicron}$	Backbone: NCBI Reference Sequence: Wuhan-Hu-1 NC_045512.2 Spike: EPI_ISL_7062525	hACE2-KI mice	SARS-CoV-2$^{S-Delta}$ vs SARS-CoV-2$^{S-Omicron}$
		hNEC/hBEC	SARS-CoV-2$^{S-Omicron}$ Single
			SARS-CoV-2^{D614G} vs SARS-CoV-2$^{S-Omicron}$
			Omicron-BA.1 vs SARS-CoV-2$^{S-Omicron}$
			SARS-CoV-2$^{S-Delta}$ vs SARS-CoV-2$^{S-Omicron}$
		PCLS	SARS-CoV-2$^{S-Delta}$ vs SARS-CoV-2$^{S-Omicron}$

Supplementary Information Table 2

Delta-infection

	dpl 2				dpl 4			
Days post-infection								
Mouse	KI #13	KI #14	KI #15	KI #16	KI #17	KI #18	KI #19	KI #20
Overview								
Alveolar edema	0	0	0	0	0	0	0	0
Emphysema	0	0	0	0	0	0	0	0
Atelectasis	0	0	0	0	0	0	0	0
Higher magnification								
Inflammation score								
Alveolar infiltrates	0	0	0	0	0	0	0	0
Grade	0	0	0	0	0	0	0	0
Predominant inflammatory cell type	0	0	0	0	0	0	0	0
Interstitial infiltrates	0	0	0	0	0	1	0	0
Grade	0	0	0	0	0	4	0	0
Predominant inflammatory cell type	0	0	0	0	0	M + L	0	0
Peribronchial infiltrates	0	1	1	0	3	1	1	0
Grade	0	1	1	0	2	2	2	0
Predominant inflammatory cell type	0	M + L	M + L	0	M + L	M + L	M + L	0
Necrotising bronchitis	0	1	1	0	1	0	1	0
Grade	1	2	2	0	2	1	2	2
Predominant inflammatory cell type	M	M	M + L	0	M	M	M	M
Intrabronchial mucus increase	0	0	0	0	0	0	0	0
Perivascular infiltrates	1	0	0	1	0	0	0	1
Grade	1	0	0	1	0	0	0	1
Predominant inflammatory cell type	M + L	0	0	M + L	0	0	0	M + L
Vascular lesions								
Intravascular rolling inflammatory cells	0	0	0	0	1	0	0	0
Endothelitis	0	0	0	0	1	0	0	0
Vasculitis	0	0	0	0	0	0	0	0
Hyaline thrombi	0	0	0	0	0	0	0	0
Hemosiderin	0	0	0	0	0	0	0	0
Arterial media hypertrophy/ hyperplasia	0	0	0	0	0	0	0	0
Vascular occlusion	0	0	0	0	0	0	0	0
Diffuse alveolar damage (DAD)/Necrosis								
Necrosis alveolar epithelial cells (AEC)	0	0	0	0	0	0	0	0
DAD	0	0	0	0	0	0	0	0
Intraalveolar fibrin	0	0	0	0	0	0	0	0
Varia								
Hypertrophy/hyperplasia bronchiolar epithelium	0	0	0	0	0	0	0	0
Hyperplasia /hypertrophy type II pneumocytes	0	0	0	0	0	0	0	0
Atypical cells/syncytia	0	0	0	0	0	0	0	0
Pleura	0	0	0	0	0	0	0	0
BALT	0	0	0	0	0	0	0	0
TOTAL SCORE	3	7	5	2	12	9	6	4

Omicron infection

	dpl 2				dpl 4			
Mouse	KI #21	KI #22	KI #23	KI #24	KI #25	KI #26	KI #27	KI #28
Alveolar edema	0	0	0	0	0	0	0	0
Emphysema	0	0	0	0	0	0	0	0
Atelectasis	0	0	0	0	0	0	0	0
Alveolar infiltrates	0	0	0	0	0	0	0	0
Grade	0	0	0	0	0	0	0	0
Predominant inflammatory cell type	0	0	0	0	0	0	0	0
Interstitial infiltrates	0	0	0	0	0	0	0	0
Grade	0	0	0	0	0	0	0	0
Predominant inflammatory cell type	0	0	0	0	0	0	0	0
Peribronchial infiltrates	0	1	0	0	0	0	0	0
Grade	0	1	0	0	0	0	0	0
Predominant inflammatory cell type	0	M + L + N	0	0	0	0	0	0
Necrotising bronchitis	0	0	0	0	0	1	0	0
Grade	1	1	1	0	1	1	1	1
Predominant inflammatory cell type	M	M	M	0	M	M	M	M
Intrabronchial mucus increase	0	0	0	0	0	0	0	0
Perivascular infiltrates	0	1	0	0	0	1	0	0
Grade	0	1	0	0	0	1	0	0
Predominant inflammatory cell type	0	M + L	0	0	0	L	0	0
Intravascular rolling inflammatory cells	0	0	0	0	0	0	0	0
Endothelitis	0	0	0	0	0	0	0	0
Vasculitis	0	0	0	0	0	0	0	0
Hyaline thrombi	0	0	0	0	0	0	0	0
Hemosiderin	0	0	0	0	0	0	0	0
Arterial media hypertrophy/ hyperplasia	0	0	0	0	0	0	0	0
Vascular occlusion	0	0	0	0	0	0	0	0
Necrosis alveolar epithelial cells (AEC)	0	0	0	0	0	0	0	0
DAD	0	0	0	0	0	0	0	0
Intraalveolar fibrin	0	0	0	0	0	0	0	0
Hypertrophy/hyperplasia bronchiolar epithelium	0	0	0	0	0	0	0	0
Hyperplasia /hypertrophy type II pneumocytes	0	0	0	0	0	0	0	0
Atypical cells/syncytia	0	0	0	0	0	0	0	0
Pleura	0	0	0	0	0	0	0	0
BALT	0	0	0	0	0	0	0	0
TOTAL SCORE	1	5	1	0	1	3	1	1

Delta / Omicron Mix

	dpl 2					
Mouse	KI #1	KI #2	KI #3	KI #4	KI #5	KI #6
Alveolar edema	0	0	0	0	0	0
Emphysema	0	0	0	0	0	0
Atelectasis	0	0	0	0	0	0
Alveolar infiltrates	0	0	0	0	0	0
Grade	0	0	0	0	0	0
Predominant inflammatory cell type	0	0	0	0	0	0
Interstitial infiltrates	0	0	0	1	0	0
Grade	0	0	0	2	0	0
Predominant inflammatory cell type	0	0	0	M	0	0
Peribronchial infiltrates	0	1	1	0	0	0
Grade	0	1	1	0	0	0
Predominant inflammatory cell type	0	M + L	M + L + N	0	0	0
Necrotising bronchitis	0	1	1	1	0	0
Grade	0	1	2	1	0	1
Predominant inflammatory cell type	0	M	M	M	0	M
Intrabronchial mucus increase	0	0	0	0	0	0
Perivascular infiltrates	0	0	0	0	0	0
Grade	0	1	0	0	0	0
Predominant inflammatory cell type	0	L	0	0	0	0
Intravascular rolling inflammatory cells	0	0	0	0	0	0
Endothelitis	0	0	0	0	0	0
Vasculitis	0	0	0	0	0	0
Hyaline thrombi	0	0	0	0	0	0
Hemosiderin	0	0	0	0	0	0
Arterial media hypertrophy/ hyperplasia	0	0	0	0	0	0
Vascular occlusion	0	0	0	0	0	0
Necrosis alveolar epithelial cells (AEC)	0	0	0	0	0	0
DAD	0	0	0	0	0	0
Intraalveolar fibrin	0	0	0	0	0	0
Hypertrophy/hyperplasia bronchiolar epithelium	0	0	0	0	0	0
Hyperplasia /hypertrophy type II pneumocytes	0	0	0	0	0	0
Atypical cells/syncytia	0	0	0	0	0	0
Pleura	0	0	0	0	0	0
BALT	0	0	0	0	0	0
TOTAL SCORE	0	4	7	5	0	1

SARS-CoV-2 Delta / SARS-CoV-2 Omicron Mix

	dpl 2					
Mouse	KI #7	KI #8	KI #9	KI #10	KI #11	KI #12
Alveolar edema	0	0	0	0	0	0
Emphysema	0	0	0	0	0	0
Atelectasis	0	0	0	0	0	0
Alveolar infiltrates	0	0	0	0	0	0
Grade	0	0	0	0	0	0
Predominant inflammatory cell type	0	0	0	0	0	0
Interstitial infiltrates	0	0	0	0	0	0
Grade	0	0	0	0	0	0
Predominant inflammatory cell type	0	0	0	0	0	0
Peribronchial infiltrates	0	0	0	0	0	M + L
Grade	0	0	0	0	0	1
Predominant inflammatory cell type	0	0	0	0	0	0
Necrotising bronchitis	1	1	1	1	1	1
Grade	1	1	1	0	1	0
Predominant inflammatory cell type	M	M	M	M	M	M
Intrabronchial mucus increase	0	0	0	0	0	0
Perivascular infiltrates	0	1	1	0	0	1
Grade	0	1	2	0	0	1
Predominant inflammatory cell type	0	M + L	M + L	0	0	M + L + N
Intravascular rolling inflammatory cells	0	0	0	0	0	0
Endothelitis	0	0	0	0	0	0
Vasculitis	0	0	0	0	0	0
Hyaline thrombi	0	0	0	0	0	0
Hemosiderin	0	0	0	0	0	0
Arterial media hypertrophy/ hyperplasia	0	0	0	0	0	0
Vascular occlusion	0	0	0	0	0	0
Necrosis alveolar epithelial cells (AEC)	0	0	0	0	0	0
DAD	0	0	0	0	0	0
Intraalveolar fibrin	0	0	0	0	0	0
Hypertrophy/hyperplasia bronchiolar epithelium	0	0	0	0	0	0
Hyperplasia /hypertrophy type II pneumocytes	0	0	0	0	0	0
Atypical cells/syncytia	0	0	0	0	0	0
Pleura	0	0	0	0	0	0
BALT	0	0	0	0	0	0
TOTAL SCORE	1	3	4	1	1	5

Supplementary Information Table 3

Supplementary Information Table 4

Spike-Variant	Primer name	Primer sequence (5' to 3')	Amplification product (bp)	PCR Template (cDNA or YAC from previous clones)
SARS-CoV-2S-Delta	WU-19-F	GGAGTCACATTAATTGGAGAAGC	1537	SpD614G
	CoV2-Sp-T19R-R	GTATGCAGGGGGTAATTGAGTTCTGGTTcTAAGATTAACACACTGACTAG		
	CoV2-Sp-T19R-F	CTAGTCAGTGTGTTAATCTTAgAACCAGAACTCAATTACCCCCTGCATAC	269	SpD614G
	CoV2-Sp-T95I-R	TATTATGTTAGACTTCTCAaTGGAAGCAAAATAAACACCATCATTAAATG		
	CoV2-Sp-T95I-F	TTTAATGATGGTGTTTATTTTGCTTCCAtTGAGAAGTCTAACATAATAAG	234	SpG142D
	CoV2-Sp-E156d-E157d-R158G-R1+R2	GCAATTATTCGCACTAGAATAAACTCcACTTTCCATCCAACTTTTGTTG		
	CoV2-Sp-E156d-E157d-R158G-F1+F2	CAAAAACAACAAAAGTTGGATGGAAAGTgGAGTTTATTCTAGTGCG	1199	SpL452R
	CoV2-Sp-T478K-R	CCTTCAACACCATTACAAGGTtTGCTACCGGCCTGATAGATTTCAGTTG		
	CoV2-Sp-T478K-F	CAACTGAAATCTATCAGGCCGGTAGCAaACCTTGTAATGGTGTTGAAGG	1468	SpD614G
	CoV2-Sp-D950N-R	GCTTGTGCATTTTGGTTGACCACATtTTGAAGTTTTCCAAGTGCACTTGC		
	CoV2-Sp-D950N-F	GCAAGTGCACTTGGAAAACTTCAAaATGTGGTCAACCAAAATGCACAAGC	1555	SpD614G
	WU-22-R	TCATGTTCAGAAATAGGACTTGTTG		
SARS-CoV-2S-Omicron	WU-19-F	GGAGTCACATTAATTGGAGAAGC	1203	SpD614G
	WU-60-R	TTGTTCGCGTGGTTTGCCAAG		
	WU-61-F	CTTGGAATGCTGATCTTTATAAGC	1221	cDNA of Omicron for Omicron spike and OmNTD; SpD614G for OmRBD and OmCS
	WU-62-R	TAGAAAAGTCCTAGGTTGAAGATAAC		
	WU-63-F	TTCGGCTTTAGAACCATTGGTAG	1209	cDNA of Omicron for Omicron spike and OmRBD; SpD614G for OmNTD and OmCS
	CoV2-D614G-R	GCAACAGGGACTTCTGTGCAGTTAACACCCTGATAAAGAACAGCAACCTG		
	CoV2-D614G-F	CAGGTTGCTGTTCTTTATCAGGGTGTTAACTGCACAGAAGTCCCTGTTGC	815	cDNA of Omicron for Omicron spike and OmCS ; SpD614G for OmNTD and OmRBD
	WU-64-R	AACAGTGCAGAAGTGTATTGAGC		
	WU-65-F	TGATTGCCTTGGTGATATTGCTG	1206	cDNA of Omicron for Omicron spike; SpD614G for OmNTD, OmRBD, OmCS
	WU-66-R	CAACTGGTCATACAGCAAAGCAT		
	WU-67-F	GACATCTCTGGCATTAATGCTTC	877	SpD614G
	WU-22-R	TCATGTTCAGAAATAGGACTTGTTG		

Supplementary Information Table 5

Assay Name	Oligo name	Sequence (5´- 3´)	Conc.	Position
SARS-CoV-2-Alpha-S assay	Alpha-S-22011-F	AAA GTT GGA TGG AAA GTG AGT TCA	10 µM	22011
	SARS2-S-22132R	CCT AAG ATT TTT GAA ATT ACC CTG T	10 µM	22132
	SARS2-S-22074FAM	FAM- TCT CTC AGC CTT TTC TTA TGG ACC T -BHQ1	5 µM	22074
SARS-CoV-2-Delta-S assay	Delta-S-22011-F	AAA GTT GGA TGG AAA GTG GAG	10 µM	22011
	SARS2-S-22132R	CCT AAG ATT TTT GAA ATT ACC CTG T	10 µM	22132
	SARS2-S-22074FAM	FAM- TCT CTC AGC CTT TTC TTA TGG ACC T -BHQ1	5 µM	22074
SARS-CoV-2-Omicron-BA.1-S assay	O-S22172-F	TATTCTAAGCACACGCCTATTATAG	10 µM	22172
	O-S22280-R	TAGTGATGTTAATACCTATTGGCAAATC	10 µM	22280
	O-S22202-FAM	FAM-CGTGAGCCAGAAGATCTCCCTC-BHQ1	5 µM	22202

4   Own Contributions

Publication I

<u>Egyptian Fruit Bats (*Rousettus aegyptiacus*) Were Resistant to Experimental Inoculation with Avian-Origin Influenza A Virus of Subtype H9N2, But Are Susceptible to Experimental Infection with Bat-Borne H9N2 Virus</u>

Nico Joël Halwe, Marco Gorka, Bernd Hoffmann, Melanie Rissmann, Angele Breithaupt, Martin Schwemmle, Martin Beer, Ahmed Kandeil, Mohamed A. Ali, Ghazi Kayali, Donata Hoffmann, Anne Balkema-Buschmann

Contributions – Publication I

Nico Joël Halwe:	Methodology, formal analysis, investigation, writing – original draft preparation
Marco Gorka:	Methodology, investigation, writing – original draft preparation
Bernd Hoffmann:	Methodology, formal analysis, supervision
Melanie Rissmann:	Methodology, investigation
Angele Breithaupt:	Methodology, formal analysis
Martin Schwemmle:	Writing – review and editing
Martin Beer:	Conceptualization, writing – review and editing, funding acquisition

Ahmed Kandeil:	Writing – review and editing
Mohamed A. Ali:	Writing – review and editing
Ghazi Kayali:	Writing – review and editing
Donata Hoffmann:	Conceptualization, data curation, writing – review and editing, project administration
Anne Balkema-Buschmann:	Conceptualization, data curation, funding acquisition

Contributions – Publication I

Publication II

<u>The bat-borne influenza A virus H9N2 exhibits a set of unexpected pre-pandemic features</u>

*Submitted to **Nature Medicine, 2023***

<u>Nico Joël Halwe,</u> Lea Hamberger, Julia Sehl-Ewert, Christin Mache, Jacob Schön, Lorenz Ulrich, Sten Calvelage, Mario Tönnies, Jonas Fuchs, Pooja Bandawane, Madhumathi Loganathan, Anass Abbad, Juan Manuel Carreño, Maria C Bermúdez-González, Viviana Simon, Ahmed Kandeil, Rabeh El-Shesheny, Mohamed A. Ali, Ghazi Kayali, Matthias Budt, Stefan Hippenstiel, Andreas C. Hocke, Florian Krammer, Thorsten Wolff, Martin Schwemmle, Kevin Ciminski*, Donata Hoffmann*, Martin Beer*

<u>Contributions – Publication II</u>

<u>Nico Joël Halwe:</u>	Conceptualization, design and performance of turkey, chicken and ferret experiments, writing – original draft preparation, writing – review and editing
Lea Hamberger:	Design and performance of mouse experiments
Julia Sehl-Ewert:	Ferret pathology, writing – review and editing
Christin Mache:	Design and performance of human lung explant infection experiments
Jacob Schön:	Design and performance of turkey, chicken and ferret experiments
Lorenz Ulrich:	Design and performance of turkey, chicken and ferret experiments, ferret pathology, writing – review and editing
Sten Calvelage:	Computational analysis
Mario Tönnies:	Design and performance of human lung explant infection experiments

Jonas Fuchs: Design and performance of mouse experiments

Pooja Bandawane: Collection of serum samples, design and performance of serological analysis

Madhumathi Loganathan: Collection of serum samples, design and performance of serological analysis

Anass Abbad: Collection of serum samples, design and performance of serological analysis

Juan Manuel Carreño: Collection of serum samples, design and performance of serological analysis

Maria C Bermúdez-González: Collection of serum samples, design and performance of serological analysis

Viviana Simon: Collection of serum samples, design and performance of serological analysis

Ahmed Kandeil: Provision of reagents

Rabeh El-Shesheny: Provision of reagents

Mohamed A. Ali: Provision of reagents

Ghazi Kayali: Provision of reagents

Matthias Budt: Design and performance of human lung explant infection experiments

Stefan Hippenstiel: Design and performance of human lung explant infection experiments

Andreas C. Hocke: Design and performance of human lung explant infection experiments

Florian Krammer: Collection of serum samples, design and performance of serological analysis, writing – review and editing

Thorsten Wolff: Design and performance of human lung explant infection experiments, funding acquisition

Martin Schwemmle: Writing – original draft, writing – review and editing, funding acquisition

Kevin Ciminski:

Design and performance of mouse experiments, writing – original draft preparation, writing – review and editing, funding acquisition

Donata Hoffmann:

Conceptualization, design and performance of turkey, chicken and ferret experiments, writing – review and editing

Martin Beer:

Conceptualization, writing – original draft, writing – review and editing, funding acquisition

Contributions – Publication II

Publication III

Enhanced fitness of SARS-CoV-2 variant of concern Alpha but not Beta

Nature, 2022

Lorenz Ulrich*, **Nico Joël Halwe***, Adriano Taddeo*, Nadine Ebert*, Jacob Schön, Christelle Devisme, Bettina Salome Trüeb, Bernd Hoffmann, Manon Wider, Xiaoyu Fan, Meriem Bekliz, Manel Essaidi-Laziosi, Marie Luisa Schmidt, Daniela Niemeyer, Victor Max Corman, Anna Kraft, Aurélie Godel, Laura Laloli, Jenna N. Kelly, Brenda M. Calderon, Angele Breithaupt, Claudia Wylezich, Inês Berenguer Veiga, Mitra Gultom, Sarah Osman, Bin Zhou, Kenneth Adea, Benjamin Meyer, Christiane S. Eberhardt, Lisa Thomann, Monika Gsell, Fabien Labroussaa, Jörg Jores, Artur Summerfield, Christian Drosten, Isabella Anne Eckerle, David E. Wentworth, Ronald Dijkman, Donata Hoffmann[†], Volker Thiel[†], Martin Beer[†] & Charaf Benarafa[†]

Contributions – Publication III

Lorenz Ulrich:	Data curation, investigation, visualization, writing – original draft, writing – review and editing
Nico Joël Halwe:	Data curation, investigation, visualization, writing – original draft, writing – review and editing
Adriano Taddeo:	Data curation, investigation, visualization, writing – original draft,
Nadine Ebert:	Data curation, investigation
Jacob Schön:	Data curation, investigation, visualization

Christelle Devisme:	Data curation, Investigation, visualization
Bettina Salome Trüeb:	Investigation
Bernd Hoffmann:	Investigation, Methodology
Manon Wider:	Investigation
Xiaoyu Fan:	Investigation
Meriem Bekliz:	Investigation
Manel Essaidi-Laziosi:	Investigation
Marie Luisa Schmidt:	Investigation
Daniela Niemeyer:	Investigation
Victor Max Corman:	Investigation
Anna Kraft:	Investigation
Aurélie Godel:	Investigation
Laura Laloli:	Investigation
Jenna N. Kelly:	Investigation
Brenda M. Calderon:	Investigation
Angele Breithaupt:	Investigation, Methodology, Writing – review and editing
Claudia Wylezich:	Investigation
Inês Berenguer Veiga:	Investigation
Mitra Gultom:	Investigation
Sarah Osman:	Investigation
Bin Zhou:	Investigation
Kenneth Adea:	Investigation
Benjamin Meyer:	Investigation
Christiane S. Eberhardt:	Investigation
Lisa Thomann:	Investigation, writing - review and editing

Monika Gsell: Investigation

Fabien Labroussaa: Investigation

Jörg Jores: Investigation

Artur Summerfield: Funding acquisition

Christian Drosten: Supervision

Isabella Anne Eckerle: Funding acquisition, supervision

David E. Wentworth: Funding acquisition

Ronald Dijkman: Data curation, funding acquisition, investigation, visualization, writing – original draft, writing – review and editing

Donata Hoffmann: Conceptualization, investigation, supervision, writing – original draft, writing – review and editing

Volker Thiel: Conceptualization, funding acquisition, supervision, writing – review and editing

Martin Beer: Conceptualization, funding acquisition, supervision, writing – original draft, writing – review and editing

Charaf Benarafa: Conceptualization, funding acquisition, supervision, writing – original draft, writing – review and editing

Contributions – Publication III

Publication IV

The spike gene is a major determinant for the SARS-CoV-2 Omicron-BA.1 phenotype

Nature Communications, 2022

G. Tuba Barut*, **Nico Joël Halwe***, Adriano Taddeo*, Jenna N. Kelly*, Jacob Schön, Nadine Ebert, Lorenz Ulrich, Christelle Devisme, Silvio Steiner, Bettina Salome Trüeb, Bernd Hoffmann, Inês Berenguer Veiga, Nathan Georges François Leborgne, Etori Aguiar Moreira, Angele Breithaupt, Claudia Wylezich, Dirk Höper, Kerstin Wernike, Aurélie Godel, Lisa Thomann, Vera Flück, Hanspeter Stalder, Melanie Brügger, Blandina I. Oliveira Esteves, Beatrice Zumkehr, Guillaume Beilleau, Annika Kratzel, Kimberly Schmied, Sarah Ochsenbein, Reto M. Lang, Manon Wider, Carlos Machahua, Patrick Dorn, Thomas M. Marti, Manuela Funke-Chambour, Andri Rauch, Marek Widera, Sandra Ciesek, Ronald Dijkman, Donata Hoffmann, Marco P. Alves†, Charaf Benarafa†, Martin Beer† & Volker Thiel†

Contributions – Publication IV

G. Tuba Barut:	Conceptualization, performed most of the experiments, wrote the manuscript and made the figures
Nico Joël Halwe:	Conceptualization, performed most of the experiments, wrote the manuscript and made the figures
Adriano Taddeo:	Conceptualization, performed most of the experiments, wrote the manuscript and made the figures

Jenna N. Kelly:	Conceptualization, performed sequencing including computational analyses, wrote the manuscript and made the figures
Jacob Schön:	Conceptualization, performed most of the experiments, wrote the manuscript and made the figures
Nadine Ebert:	Conceptualization, performed most of the experiments, wrote the manuscript and made the figures
Lorenz Ulrich:	Conceptualization, performed most of the experiments, wrote the manuscript and made the figures
Christelle Devisme:	Performed most of the experiments
Silvio Steiner:	Performed most of the experiments
Bettina Salome Trüeb:	Performed most of the experiments
Bernd Hoffmann:	Experimental work and provided essential experimental systems and reagents
Inês Berenguer Veiga:	Performed most of the experiments
Nathan G. F. Leborgne:	Experimental work
Etori Aguiar Moreira:	Experimental work
Angele Breithaupt:	Experimental work
Claudia Wylezich:	Experimental work and provided essential experimental systems and reagents, performed sequencing including computational analyses
Dirk Höper:	Provided essential experimental systems and reagents
Kerstin Wernike:	Experimental work and provided essential experimental systems and reagents
Aurélie Godel:	Experimental work

Lisa Thomann:	Experimental work
Vera Flück:	Experimental work
Hanspeter Stalder:	Experimental work
Melanie Brügger:	Experimental work
Blandina I. Oliveira Esteves:	Experimental work
Beatrice Zumkehr:	Experimental work
Guillaume Beilleau:	Experimental work
Annika Kratzel:	Experimental work
Kimberly Schmied:	Experimental work
Sarah Ochsenbein:	Experimental work
Reto M. Lang:	Experimental work
Manon Wider:	Experimental work
Carlos Machahua:	Experimental work
Patrick Dorn:	Experimental work
Thomas M. Marti:	Experimental work
Manuela Funke-Chambour:	Experimental work
Andri Rauch:	Experimental work
Marek Widera:	Provided essential experimental systems and reagents
Sandra Ciesek:	Provided essential experimental systems and reagents
Ronald Dijkman:	Conceptualization
Donata Hoffmann:	Conceptualization, performed most of the experiments, provided essential experimental systems and reagents, wrote the manuscript and made the figures
Marco P. Alves:	Conceptualization, wrote the manuscript and made the figures

Charaf Benarafa: Conceptualization, wrote the manuscript and
                          made the figures

Martin Beer: Conceptualization, wrote the manuscript and
                          made the figures

Volker Thiel: Conceptualization, wrote the manuscript and
                          made the figures

In Agreement (Publication I to IV)

—————————————————　　　　　　　　　—————————————————
　　　　　Place, Date　　　　　　　　　　　　　　　　Nico Joël Halwe

—————————————————　　　　　　　　　—————————————————
　　Prof. Dr. Stefan Finke　　　　　　　　　　　　Prof. Dr. Martin Beer

5   Discussion

5.1   The Egyptian fruit bat model for bat H9N2 – possibilities and limitations – Publication I

The bat-borne influenza A virus of subtype H9N2 was discovered in 2019 and isolated from fecal samples of Egyptian fruit bats (*Rousettus aegyptiacus*) (Kandeil et al. 2019). Back then, researchers identified high phylogenetic similarities of the bat H9N2 gene segments encoding the HA and NA proteins with other avian H9N2 IAVs, suggesting reassortment events between an ancestral backbone and avian IAVs (Ciminski et al. 2020). Interestingly, the bat H9N2 does not replicate in adult white leghorn chicken, although it still initiates a productive replication in embryonated chicken eggs. This was first reported by Kandeil et al. 2019 and the efficient replication of bat H9N2 in embryonated chicken eggs could be confirmed in **Publication I**. To get a further overview about the pathogenicity, transmissibility and host organ tropism of the new bat H9N2 virus, we performed an infection study with bat H9N2 in their natural hosts, the Egyptian fruit bats **(Publication I)**. Interestingly, these animals revealed only a low-level replication with highest genome copy numbers in the upper respiratory tract (URT), as demonstrated by RT-qPCR results from oral swabs. This finding was surprising, as the virus was originally isolated from fecal samples in the same species back in 2019. However, RT-qPCR analysis of rectal swabs from the inoculated fruit bats revealed only marginal viral genome copies per mL ($<10^2$). These observations show clear limitations of the Egyptian fruit bat as animal model and future studies have to define necessary prerequisites for a bat H9N2 circulation in these fruit bats in the field. This could be age-related issues, simply the route of infection or other yet unknown factors. Nonetheless, it has just recently been demonstrated that there are marked differences in the immune system of adult and juvenile *Rousettus aegyptiacus* bats, and immune maturation might be an important factor in exhibiting disease tolerance over specific viruses (Friedrichs et al. 2022). In line with that, it is generally assumed that bats can be persistently infected with viral pathogens, for example during hibernation (Subudhi et al. 2017). Therefore, adult bats may be able to exhibit disease tolerance by limiting virus replication, though prolonged shedding periods, while juvenile bats may exhibit a higher level of viral replication and thereby may represent the driving force in the maintenance of viral transmission chains in wildlife (Mandl et al. 2018; Storm et al. 2018; Guito et al. 2021; Friedrichs et al. 2022). Indeed, general susceptibility of *Rousettus aegyptiacus* bats to bat H9N2 was confirmed also through positive seroconversion of directly inoculated animals euthanized

at 21 dpi and virus was efficiently isolated and productively replicated in embryonated chicken eggs originating from multiple organ or swab samples. In contrast, no viral RNA was found in swab samples and no seroconversion was observed in serum samples of Egyptian fruit bats inoculated with an avian H9N2 strain. Conclusively, it was assumed that bat-IAVs in general might be highly adapted to specific bat species and non-bat IAVs may require further adaptation or reassortment to establish a productive infection in a bat-host.

Nevertheless, these adaptation processes between bat H9N2 and avian or mammalian IAVs are considered to be possible. Especially, because of similar packaging sequences of bat H9N2 and AIVs gene segments that even might have recently led to the already mentioned reassortment events between bat H9N2 and AIVs (Gerber et al. 2014; Kandeil et al. 2019; Ciminski et al. 2020). In contrast, the incompatible segment ends of the two other known bat IAVs (H17 and H18), renders reassortment events for these viruses very unlikely (Juozapaitis et al. 2014; Zhou et al. 2014).

Importantly, it has to be kept in mind that the bat H9N2 has only been found in *Rousettus* bat species, which is a mammalian species. It therefore has to be assumed that this virus is already highly adapted to mammals, which can be interpreted as a highly relevant risk factor increasing its spillover potential. Furthermore, the natural food searching strategies of Egyptian fruit bats encompass looting of different fruit tree leftovers from family households (Centeno-Cuadros et al. 2017). Additionally, these fruit tree leftovers may likewise serve as poultry feed, and backyard poultry in Egypt is a highly common source to pay for living expenses (Gharib et al. 2012; Hosny 2016). Through this interface, fruit bats may frequently come in contact with humans and/or poultry species and thereby may accomplish spillover infections. The spillover risk is even more enhanced by the fact that the Egyptian fruit bat is a migratory species and a recent publication has detected the bat H9N2 virus even in a region in South Africa, assuming that this virus is already widespread over the African continent (Rademan et al. 2023). Conclusively, these observations and hypotheses highlight the necessity for a zoonotic risk assessment of bat H9N2 in highly susceptible and prominent mammalian and poultry animal models of IAV-research, which was therefore investigated in **Publication II**.

5.2 Bat H9N2 exhibits concerning zoonotic and potentially pre-pandemic characteristics – Publication II

The Egyptian fruit bat experiment did not prove this animal species as a high-level replication animal model for bat H9N2, as well as its pathogenicity and disease progression. In **Publication II**, firstly, the susceptibility of day-old chicks and day-old turkeys to bat H9N2 was examined,

especially since the first H9N2 IAV of avian origin was isolated from a turkey in 1966 (Homme and Easterday 1970). Considerably, repeated outbreaks of avian H9N2 IAVs in turkey-based poultry farms over the globe are frequently reported (Jiang et al. 2012; Afifi et al. 2013; Li et al. 2017). Interestingly, while chicken hatchlings were not susceptible to bat H9N2 infection, turkey hatchlings productively replicated bat H9N2 with clear seroconversion of all inoculated animals. These results firstly support the results of an abortive bat H9N2 replication in adult chickens from Kandeil et al. 2019 and moreover suggest important species-specific differences between these poultry species that may or may not allow bat H9N2 replication in the respective species. Now, based on the data gained in **Publication II**, a potential introduction of bat H9N2 into this animal species cannot be excluded anymore and further studies are required to investigate the likelihood for such an event, paralleled by surveillance studies in turkey populations in Africa. However, apart from poultry susceptibility, the most important goal of **Publication II** was to unravel the zoonotic potential of bat H9N2. Especially, since this virus has been isolated from and is probably already well adapted to mammalian species (Kandeil et al. 2019). Therefore, the ferret and the MxA transgenic mouse model were used to examine the susceptibility to bat H9N2. Surprisingly, ferrets were highly susceptible, efficiently transmitted the virus to direct contact animals, and histological analysis revealed a severe rhinitis with obvious IAV-antigen in the olfactory epithelium of the ferret nose. It was thereby demonstrated that bat H9N2 is able to efficiently replicate in and transmit between ferrets without further genetic adaptation, strongly indicating that this virus is already well adapted to mammalian rather than avian species. Moreover, since the Egyptian fruit bats as potential natural hosts of the bat H9N2 IAV were only moderately susceptible to experimental bat H9N2 infection as seen in **Publication I**, this bat species can be questioned again as singular natural host of this virus. The effective replication and transmission capacity in ferrets, one of the most valuable models to mimic IAV infections in humans (Maher and DeStefano 2004), opens more questions concerning the pre-pandemic potential of bat H9N2.

An important and often underestimated prerequisite for IAVs establishing either pandemic or larger seasonal outbreaks relies in their escape from antiviral MxA restriction factor (Dittmann et al. 2008; Götz et al. 2016). In combination with specific, yet unidentified interferon-induced factors, the MxA protein inhibits the transport of IAV vRNPs into the cellular nucleus, thereby strongly interfering with IAV replication (Pavlovic et al. 1990; Xiao et al. 2013; Haller and Kochs 2020). To date, the identified escape mechanism of IAVs from human MxA is mainly based on specific amino acid substitutions within the NP gene segment sequence, for example the E53D, L283P or the F313Y/V substitution (Dornfeld et al. 2019; Haller and Kochs 2020).

The bat H9N2 NP sequence lacks these specific mutations, which should in principle prevent escape from human MxA interventions. In **Publication II**, bat H9N2 replication is diminished *in vitro* using cells lines expressing an active MxA protein, while the polymerase activity of bat H9N2 is less affected from the MxA based inhibitory function than the polymerase activity of avian IAVs. Contrastingly, comparative experimental infection of C57/Bl6 and hMxA transgenic mice revealed comparable lung titers of bat H9N2 replication in both mice models, with no initiation of hMxA-expression in the transgenic hMxA-mice. These observations strongly suggest an alternative pathway of bat H9N2-associated MxA-escape by potentially suppressing hMxA-expression *in vivo* after infection.

An additional pre-pandemic feature of zoonotic IAVs, such as bat H9N2, encompasses their antigenic diversity to circulating IAV-strains in humans. **Publication II** clearly revealed that individual humans vaccinated against circulating H1N1 and H3N2 strains were serologically naïve towards the bat-N2, although strong antibody responses were observed against the N2 of avian IAV origin. If the bat H9N2 virus thereby would finally accomplish spillover infection to humans, it would likely be introduced in an immunologically naïve population, a further concerning pre-pandemic characteristic of bat H9N2. In addition to that, the *ex vivo* growth kinetics approach in human lung transplant cultures in **Publication II** revealed that the bat H9N2 replicated highly efficient and significantly stronger compared to a seasonal H3N2 IAV isolate in these human lung tissues. These results thereby suggest an already advanced adaptation of the bat H9N2 to the human alveolar tissue, which markedly increases the possibility of humans being susceptible to bat H9N2.

The **Publications I and II** summarize and elucidate that while a virus does not exhibit severe disease progression in its potentially natural host, this does not hold true for a different host that might be infected by a viral spillover event from the natural host. It is therefore of indispensable interest to characterize emerging and newly discovered viruses in a variety of animal models, including livestock animals that might function as intermediate host, to fully elucidate its host range, virulence and transmissive potential. As the bat H9N2 example shows, this virus unexpectedly exhibited pre-pandemic features, which would have remained unnoticed in case this virus would not have been characterized further. Therefore, **Publications I and II** in this dissertation demonstrate the strong relevance of profound *in vivo* characterization of newly emerging viruses in advance to identify their pre-pandemic potential, exemplified by the bat H9N2 virus.

Missing a newly emerging zoonotic virus and lack of deep characterization in terms of its pandemic potential will sooner or later confront the global population with a pandemic virus. Exactly this scenario happened in December 2019, when the SARS-CoV-2 virus established spillover infections from unknown hosts to humans (Zhou et al. 2020). Consequently, this virus rapidly spread over the globe, while likewise evolving into more serious VOCs, in the end infecting and killing millions of people (WHO as of 1st december 2022). While **Publications I and Publication II** provide useful modes of action in order to characterize potential pre-pandemic viruses, **Publication III and Publication IV** in this dissertation basically focus on substantial characterization in case a pathogen has already accomplished pandemic outbreaks, here exemplified by SARS-CoV-2 via *in vivo* characterization in multiple animal models.

5.3   *In vivo* competitions of SARS-CoV-2 VOCs as main approach to determine variant fitness – Publication III

SARS-CoV-2, which emerged in 2019, has evolved multiple times throughout the still ongoing pandemic, generating multiple different VOCs with specific fitness advantages over their respective precursory prevailing VOC (Korber et al. 2020; WHO as of 1st december 2022). These SARS-CoV-2 variants may outcompete currently dominating strains due to either replication and transmission advantages, enhanced virulence or stronger immune escape properties based on amino acid mutations throughout the viral genome (Zhou et al. 2021; Liu et al. 2022b). Therefore, *in vitro* and *in vivo* infection and transmission competitions between VOCs performed firstly in the precursory publication from Zhou et al. 2021 were hypothesized to allow the prediction of future prevailing VOCs and their genetic determinants for predominance. The goal of the studies in **Publication III** was basically to lay the cornerstone for rapid risk assessments in conformity with respective counteracting measures to prevent spread or promote adapted vaccine development against the respective SARS-CoV-2 VOCs. During the time of conducting these studies, SARS-CoV-2 Alpha and Beta VOCs were dominating in different parts of the world (Fujino et al. 2021; Tegally et al. 2021; Washington et al. 2021) and especially the spike-associated mutations were hypothesized to be the main cause (Liu et al. 2022c). In **Publication III** of this dissertation, the competitive (dis-)advantages of the emerging Alpha and Beta VOC were investigated *in vitro* and in a multi-species approach including the ferret, the Syrian hamster, as well as the transgenic (tg) K18-hACE2 and hACE2-KI mice models. The *in vitro* studies gave a first hint of specific VOC fitness advantages, but a full picture of these variants could only be achieved by *in vivo* experiments. More precisely, in the Syrian hamster model, Alpha was able to prevail in terms of replicative and transmissive

fitness over Beta, but demonstrates equal fitness as the SARS-CoV-2 WT. These observations deviate from human epidemiological data insofar as the Alpha VOC fully predominated over Beta VOC and WT SARS-CoV-2 in the human population at that time (RKI 2021), thereby necessitating the use of a another animal model to either validate or rather debilitate the results obtained through the hamster experiments. However, Beta replicated to a substantial amount in donor hamster lungs of the lower respiratory tract (LRT) in competition with Alpha, although URT replication in hamsters was dominated by Alpha. Thereby, the here described competitive infection and transmission approach in hamsters nevertheless suits for the investigation of SARS-CoV-2 VOC tissue tropism and highly suggests that a URT replication advantage of a specific VOC determines which variant will be transferred to contact animals. This is even in accordance with human epidemiological data again, stating an increased hospitalization risk for patients infected with the Beta variant compared to WT, but also Alpha (Funk et al. 2021; Veneti et al. 2021). The hamster model thereby still stands out as a useful model to deliver first hints in the anticipation of SARS-CoV-2 VOC disease severity, which may be largely dependent on LRT replication efficacy of respective VOCs, although the data on transmission between hamsters did not match the epidemiological data in humans. The hamster may also represent a so called "super spreader" model, since this animal highly efficiently transmitted all used variants rapidly to their contacts and is even able to keep these transmission chains up via a second contact round. These scenarios have also been observed in humans from time to time (Lemieux et al. 2020; Wei et al. 2020; Edwards et al. 2021).

Contrastingly, the ferret revealed total replication and transmission predominance of Alpha over WT SARS-CoV-2 in **Publication III**, without replication in the LRT and without showing any clinical symptoms. Further observations in the genetically modified K18-hACE2 and hACE2-KI mouse models used in **Publication III** also demonstrate predominance of Alpha over WT SARS-CoV-2 and Beta, which is in accordance with the ferret model. Importantly, the mouse models both contain the ACE2-receptor from humans, making a SARS-CoV-2 phenotype translation from these mice models to humans more credible. In the thereof following experiment in **Publication III**, a recombinant clone expressing the spike mutations of the Alpha VOC in a SARS-CoV-2 WT backbone (wt-S^{Alpha}) was tested in the hACE2-KI mouse model, addressing the interplay of these mutations in achieving global predominance. Here, the spike mutations of Alpha VOC alone were sufficient to achieve predominance over WT SARS-CoV-2 in these animals. These results highlight not only the importance of these spike protein mutations for viral fitness, but also the relevance and the adaptation of SARS-CoV-2 VOCs to the human ACE2 receptor and therefore to humans in general. Apparently, the

ferret and both mouse models seem to mimic the epidemiological situation in humans concerning SARS-CoV-2 VOC dominance equally well and better than the Syrian hamster. Therefore, the combination of all these models hereafter gained high relevance in the characterization of future arising SARS-CoV-2 VOCs, also in analogy to humans. As an initial preselection method, the use of organoids in terms of growth kinetics and viral distribution may be also helpful to get a first insight in the characteristics of these viruses, also in the interest of saving animal lives (Kim et al. 2020; Chen et al. 2022; Han et al. 2022).

Being reminiscent of **Publication I and II** in this dissertation, the bat H9N2 virus also demonstrated a great adaptation to mammalian species, which was proven by *in vivo* experiments in the ferret model. The ferret thereby again stands out as one of the most valuable animal models in translating the disease phenotype of emerging viruses from ferrets to humans and should be kept in mind for an urgent characterization of newly emerging zoonotic and potentially pandemic viruses.

Referring again to **Publication III**, all of the used animal models nevertheless are delivering different kinds of information and consolidating all this information eventually revealed a full picture about the threat of emerging SARS-CoV-2 variants. Competitive infection and transmission experiments in a multi-species approach can therefore not only be used as an "early-warning system" for potentially prevailing virus variants in the human population (ferrets and mouse models), but also to estimate the potential disease severity induced by an infection with and the transmissive fitness outgoing from the respective VOC (Syrian hamster model). However, it has to be considered that SARS-CoV-2 VOCs are evolving at an astonishing speed, as multiple different VOCs were discovered rapidly after Alpha and Beta VOC just prevailed over the globe, among which Omicron VOC was the latest variant predominating in humans at the time of writing this dissertation (RKI 2021; WHO as of 1st december 2022). Therefore, the discussed experiments, especially in the context of SARS-CoV-2, have to be carried out in a relatively short time frame after a new VOC is discovered to allow major influence on counteracting measures to prevent the spread of this respective VOC. If done so, these experiments can be extremely helpful in the fight against the SARS-CoV-2 pandemic.

In summary, the experiments in **Publication III** elucidate the importance of using multiple test systems including several different animal models for experimental *in vivo* studies to receive a full picture about the diverse fitness benefits of SARS-CoV-2 VOCs. In line with that, the advantage of using multiple animal models to fully characterize emerging viruses was also already mentioned in **Publication I and II**. At this point, it is therefore noteworthy again to

strongly support the use of a variety of animal models for *in vivo* characterization of emerging viruses not only in the matter of pandemic preparedness, but also pandemic spread precautions.

5.4   Identifying the fitness providing genetic determinants of the VOC Omicron requires *in vivo* characterization - Publication IV

The tremendous amount of results obtained in **Publication III** laid the cornerstone to rapidly evaluate the threat of emerging SARS-CoV-2 VOCs by performing competitive and single infection and transmission experiments of these VOCs in the best fitting animal models. **Publication IV** basically uses the same methods as **Publication III** to characterize the newly emerged SARS-CoV-2 VOC Omicron BA.1 in comparison with its precursory prevailing VOC Delta. This time though, the methods could be more finetuned by taking into consideration the overall immunity of the global population at the time of conducting the studies. This was not only because commercially available vaccines have been licensed, but also because the majority of the even unvaccinated human population already had been infected with SARS-CoV-2 and thus revealed a serological response against the virus (Sallam 2021; Bergeri et al. 2022). However, the antigenic distance of Omicron from all other SARS-CoV-2 variants is quite large and a dramatic decrease in neutralizing antibody titers elicited by SARS-CoV-2 WT-based mRNA vaccination against Omicron VOC are proven (Cele et al. 2022; Xie et al. 2022). Accordingly, several breakthrough infections with this variant have been confirmed (Tan et al. 2023).

As it is not feasible to vaccinate cell cultures, animal models are the only way to receive a full picture about specific SARS-CoV-2 variant fitness as compared to *in vitro* studies until the time of writing this dissertation. Keeping this in mind, the studies in **Publication IV** of this dissertation, aside from a set of *in vitro* experiments, focused largely on a general characterization of Delta and Omicron BA.1 VOCs in naïve Syrian hamsters, ferrets and hACE2-KI mice, followed by single or competitive infection studies with Delta and Omicron BA.1 spike-clones (SARS-CoV-2$^{\text{S-Delta}}$ and SARS-CoV-2$^{\text{S-Omicron BA.1}}$) in unvaccinated hACE2-KI, as well as in vaccinated and unvaccinated K18-hACE2 mice. The individual recombinant SARS-CoV-2 VOC Delta or Omicron BA.1 viruses with a specific set of S-protein mutations were used to identify the genetic determinants responsible for the VOC-specific fitness advantages. While *in vitro* competitions between isolates and spike recombinants of Delta and Omicron-BA.1 demonstrated spike-associated predominance of Omicron BA.1 over SARS-CoV-2 WT and Delta, Delta fully predominated over an Omicron BA.1 isolate in competitive

infection and transmission experiments in naïve Syrian hamsters, hACE2-KI mice and ferrets. Most surprisingly, an approach to infect the naïve ferret model only with Omicron BA.1 VOC led to an abortion of replication.

Conclusively, marked differences become apparent when comparing the results from the *in vitro* experiments to the *in vivo* experiments with the naïve animal models. Although Omicron BA.1 outperformed Delta *in vitro*, it was not able to verify these results in all tested naïve animal models, even not in the ferret or the hACE2-KI mice. Based on the results from **Publication III**, ferrets were hypothesized to be well translational models for SARS-CoV-2 infections in humans. However, the fact that Omicron BA.1 is not able to infect ferrets anymore strongly supports the theory that this VOC has adapted to humans perfectly well, which is also in accordance to human epidemiological data. Supportive to that theory, **Publication IV** and also other researchers could show that the virulence of VOC Omicron has decreased, visible for example in case of the physiological parameters of Syrian hamsters or in the different mice models (lower body weight loss etc.) (Halfmann et al. 2022; Yuan et al. 2022). These results highly emphasize again the necessity of multiple animal models for full characterization of emerging viruses, such as SARS-CoV-2 VOCs, as only the whole organism can provide a realistic physiological platform for that purpose. Importantly, this also includes the immunological parameters. In **Publication IV**, comparative single infection of vaccinated or unvaccinated K18-hACE2 mice with SARS-CoV-2$^{\text{S-Delta}}$ and SARS-CoV-2$^{\text{S-Omicron}}$ indeed revealed that mRNA-based vaccination against SARS-CoV-2 WT efficiently prevented body weight loss and decreased (infectious) viral load in swabs and organ samples after infection with SARS-CoV-2$^{\text{S-Delta}}$. In contrast, a decrease in (infectious) viral load in oropharyngeal swabs, as well as nose or lung organ samples was only marginally detectable for mRNA vaccinated compared to non-vaccinated animals challenged with SARS-CoV-2$^{\text{S-Omicron}}$. As the earlier mentioned human breakthrough infections and drop in virus neutralizing antibody titers had assumed, the collective *in vitro* and especially *in vivo* studies in **Publication IV** clearly demonstrate a spike-dependent immune escape advantage of SARS-CoV-2 Omicron BA.1 over Delta, which thereby likely contributed to the SARS-CoV-2 Omicron BA.1 predominance in the human population. In line with that, other researchers performed a competitive infection and transmission study with SARS-CoV-2 Omicron BA.1 and Delta VOC in vaccinated and unvaccinated Syrian hamsters and could indeed confirm that Omicron BA.1 VOC had transmissive and replicative advantages over Delta VOC in vaccinated animals (Yuan et al. 2022). These observations further substantiate the results from **Publication IV**.

In summary, **Publication III and IV** provide useful, comprehensive and detailed methods to rapidly identify and classify newly emerging virus variants that may gain the mastery over previously prevailing variants of the respective virus, here exemplified for SARS-CoV-2. Importantly, several lessons can be learned from these approaches: Firstly, *in vitro* characterization alone might be not sufficient to reveal all fitness advantages of a specific virus or virus variant. Secondly, experimental single and competitive infection studies of virus variants in a multi-species approach are necessary, since each animal model will provide different kinds of important information about the specific virus variant. **Publication III and IV** show that for SARS-CoV-2, the ferret and the genetically modified mouse models harboring the hACE2-receptor are good animal models in mimicking the human epidemiological SARS-CoV-2 prevalence situation at least until VOC Omicron BA.1, while the Syrian hamster is a useful model to study SARS-CoV-2 VOC tissue tropism, disease severity and transmission capacity. Thirdly, the use of recombinant viruses expressing specific potentially fitness providing amino acid mutations helps to identify the cause for a global predominance on a molecular level. Lastly, the overall immunity of the global population has to be considered at the time of conducting such studies, as increasing vaccination and re-convalescence of the global population will clearly lead to the emergence of virus variants exhibiting fitness advantages through immune escape mechanisms, as seen for SARS-CoV-2 Omicron BA.1 in **Publication IV**.

Most importantly though, these approaches are not restricted to SARS-CoV-2 at all, but could also be used for future pandemic viruses. If a future pandemic virus is infecting as much people as SARS-CoV-2 has accomplished until now, there is a great potential of this hypothetic virus to develop equally high fitness providing mutation rates. In turn, competitive infection and transmission studies in animal models with emerging variants of this specific virus will be a useful tool to predict their dominance and subsequent prevalence. Additionally, the use of not only pre-immunized donor animals, but also pre-immunized contact animals will likely be of importance to simulate the human situation at specific timepoints in a potential pandemic.

In conclusion of **Publication I** to **Publication IV**, this dissertation provides a sequence of useful studies to firstly characterize a newly discovered, emerging and potentially zoonotic respiratory virus from its discovery to a potentially pandemic virus. The first steps after discovery include a rapid characterization of this emerging virus in its natural host, exemplified by the bat H9N2 IAV **(Publication I)**. Secondly, it is important to identify the spillover potential to humans and other (domestic) species by inoculation of a variety of animal models,

infection of human lung explants and antigenic diversity analysis to related virus strains, also exemplified by the bat H9N2 virus **(Publication II)**. These methods are of utmost importance in the interest of pandemic preparedness. If such a virus nevertheless accomplishes a spillover infection to and consequently efficient spread within humans, this virus may acquire fitness providing mutations, eventually leading to the emergence of different virus variants. Thereafter, the interest of pandemic preparedness will change to the interest of pandemic spread prevention and precautionary measures. These points can be addressed by rapidly assessing the replicative and transmissive fitness advantages of such virus variants and their genetic determinants by competitive inoculation. Such experiments were performed in a multi-species approach to fully characterize viral host range, replicative and transmissive fitness advantages, pathogenicity, disease severity, as well as specific tissue tropism in **Publication III**. The method herein was performed with the pandemic SARS-CoV-2 virus and its different VOCs, and has to be performed with future viruses of concerning zoonotic potential, such as bat H9N2. After identification of the potential fitness pandemic virus variant, the overall evolution of the pandemic pathogens - especially in respect of global vaccination - has to be considered. Dominant virus variants with a potential immune escape fitness advantage can only be identified via using experimental competitive and single infection studies with vaccinated and unvaccinated animal models, which was done in case of SARS-CoV-2 Omicron and Delta in **Publication IV**. These results finally are necessary to confirm an immune escape-dependent fitness advantage of a specific virus variant that could become predominant in a pandemic situation, which also might lead to the rapid production of virus variant adapted vaccines as it is currently for the SARS-CoV-2 Omicron adapted vaccine (Muik et al. 2022).

The SARS-CoV-2 pandemic, as well as the discovery of the potentially pre-pandemic bat H9N2, assume that there might be multiple other so far undiscovered and potentially zoonotic and pre-pandemic viruses around. Using the appropriate methods for virus characterization, as exemplified by **Publication I** to **Publication IV** of this dissertation, will help to prepare for and fight against the next pandemic.

6   Summary

As the animal-to-human interface becomes increasingly narrow, transmission events of zoonotic pathogens between animals and humans become more and more probable. While SARS-CoV-2 already accomplished a spillover infection to humans and is responsible for the current pandemic, the bat H9N2 IAV with so far unknown zoonotic potential was only recently discovered. In order to identify I) the role and potential of a newly discovered, potentially pre-pandemic virus, such as the bat H9N2, or II) possible future prevailing virus mutant variants of an already known pandemic virus, such as SARS-CoV-2, it is important to characterize these emerging viruses *in vivo* as soon and as good as possible.

The first objective in this dissertation **(Publications I and II)** therefore deals with the characterization of bat H9N2 and the estimation of its zoonotic or even pandemic potential.

In **Publication I**, a general susceptibility of directly inoculated Egyptian fruit bats to bat H9N2 was confirmed by successful seroconversion, although exhibiting only moderate viral shedding. All three contact animals remained seronegative, though one contact bat showed slight lesions in the histopathological analysis.

Publication II further addressed the question of the zoonotic potential of this virus. Inoculation of day-old turkey hatchlings demonstrated moderate susceptibility to bat H9N2 infection with a measurable seroconversion, while day-old chicken hatchlings were not susceptible to bat H9N2. Ferrets proved to be highly susceptible to bat H9N2 with high viral shedding, a transmission efficiency rate of 100% to direct contact animals at 2 days post contact, but with only minimal clinical signs. Importantly, the virus demonstrated the ability to evade the MxA-restriction factor and to replicate efficiently in human lung tissue explants. Furthermore, seasonal IAV- and standard IAV-vaccines showed no cross reactivity against the bat-N2 protein in humans. Therefore, further research on such viruses is urgently needed in order to prevent a renewed pandemic situation in the future as caused by SARS-CoV-2.

The second objective in this dissertation dealt with the identification and characterization of emerging SARS-CoV-2 Variants of Concern (VOCs).

Therefore, in **Publication III**, competitive infection experiments were performed using the Syrian golden hamster, the ferret, and transgenic mouse models (K18-hACE2 and hACE2-KI). These studies revealed replicative and transmissive predominance of Alpha VOC over Beta VOC, but not over SARS-CoV-2 WT in the hamster model, although Beta VOC substantially replicated in the lungs of donor animals. In contrast, the Alpha VOC had an unambiguous replication and transmission advantage over WT SARS-CoV-2 in the ferret and both mouse

models. A recombinant SARS-CoV-2 WT-S^{Alpha} virus helped to assign the fitness advantage of this variant particularly to the spike protein-associated mutations.

In **Publication IV,** *in vitro* results inferred an early replicative fitness advantage of Omicron BA.1 over Delta VOC, although the opposite was observed in competitively inoculated hamsters, ferrets and naive hACE2-KI mice. In addition, **Publication IV** demonstrated a disadvantage in transmission for the VOC Omicron BA.1 over the Delta VOC and a lack of susceptibility of ferrets after a single infection with the VOC Omicron BA.1. An mRNA vaccination of K18-hACE2 mice caused a drastic reduction of infectious virus particles in organ material following an infection with a recombinant SARS-CoV-2 WT-S^{Delta}, but not when challenged with the SARS-CoV-2 S$^{Omicron\ BA.1}$ clone.

This dissertation includes numerous, comprehensive experimental studies that are generally important for the characterization of emerging, potentially pre-pandemic viruses and may provide crucial information about the future dominance of certain virus variants in an ongoing pandemic. Here, the need for the use of a variety of animal models becomes apparent. By characterizing and classifying potentially zoonotic strains, these methods will help to better prepare for potentially upcoming pandemics and, in the case of a zoonotic or even pandemic event, to better detect and understand the circulating strains and their evolution.

7   Zusammenfassung

Da die Schnittstelle zwischen Menschen und Tieren immer enger wird, ist in der Folge die Übertragungswahrscheinlichkeit eines Erregers von Tier zu Mensch unter Umständen deutlich erhöht. Während SARS-CoV-2 bereits erfolgreich eine Übertragung auf den Menschen realisierte und dadurch verantwortlich für die aktuelle Pandemie ist, wurde das Fledertier-assoziierte H9N2 IAV (bat H9N2) mit aktuell unbekanntem, zoonotischem Potential neu entdeckt. Um nun I) die Rolle und das Potential eines neuen, eventuell prä-pandemischen Virus', wie des bat H9N2, oder II) zukünftig vorherrschende Virusvarianten eines bereits bekannten, pandemischen Virus', wie z.B. des SARS-CoV-2, zu identifizieren, ist es nötig, diese Viren so schnell und gut wie möglich auch *in vivo* zu charakterisieren

Die erste Fragestellung dieser Dissertation **(Publikationen I und II)** befasst sich daher mit der Charakterisierung des bat H9N2 und die Abschätzung seines pandemischen Potentials.

In **Publikation I** wurde eine generelle Empfänglichkeit der inokulierten Nilflughunde als natürlicher Wirt für bat H9N2 über die erfolgte Serokonversion bestätigt, obwohl die Tiere nur moderate Viruslasten ausschieden. Alle drei Kontakttiere blieben allerdings seronegativ, obwohl ein Kontakttier leichte Läsionen in der histologischen Analyse zeigte.

Publikation II befasste sich ebenfalls mit der Frage des zoonotischen Potentials dieses Virus. Die Inokulation von Eintags-Putenküken bewies eine moderate Empfänglichkeit mit messbarer Serokonversion dieser Tiere, während Eintags-Hühnerküken nicht für bat H9N2 empfänglich waren. Frettchen erwiesen sich als sehr gut mit bat H9N2 infizierbar, mit einer sehr hohen Virusausscheidung, einer effizienten Transmissionsrate von 100% zu direkten Kontakttieren an Tag 2 nach Erstkontakt, aber nur minimaler Klinik. Das Virus bewies ebenso die Fähigkeit dem MxA-Restriktionsfaktor auszuweichen und in humanen Lungengewebsexplanaten effizient zu replizieren. Weiterhin konnte gezeigt werden, dass saisonale IAV und die Standard IAV-Vakzinen keine Kreuzreaktivität gegen das N2-Protein des bat H9N2 Virus im Menschen induzieren. Daher ist eine weitergehende Erforschung solcher Viren dringend notwendig, um zukünftig eine erneute pandemische Situation wie durch SARS-CoV-2 hervorgerufen, zu verhindern.

Die zweite Fragestellung dieser Dissertation beschäftigt sich mit der Identifikation und Charakterisierung von neu auftretenden SARS-CoV-2 Variants of Concern (VOCs).

In **Publikation III** wurden daher kompetitive Infektionsversuche mit dem syrischen Goldhamster, dem Frettchen, sowie transgenen Mausmodellen (K18-hACE2 und hACE2-KI) durchgeführt. Diese Studien konnten einen deutlichen, replikativen und transmissiven Vorteil

der VOC Alpha über VOC Beta, nicht aber gegenüber dem WT SARS-CoV-2 im Hamstermodell darlegen, obwohl VOC Beta substantiell in der Lunge von Donor-Tieren replizierte. Im Gegensatz hierzu erwies sich die Replikation und Transmission der VOC Alpha als deutlich im Vorteil gegenüber WT SARS-CoV-2 im Frettchen und in beiden Mausmodellen. Ein rekombinantes SARS-CoV-2 WT-S^{Alpha} Virus half, den Fitnessvorteil dieser Variante besonders den Spike-Protein-assoziierten Mutationen zuzuordnen.

In **Publikation IV** zeigten *in vitro* Ergebnisse einen frühen, replikativen Vorteil der VOC Omikron BA.1 gegenüber der VOC Delta, obwohl im kompetitiv inokulierten Hamster-, Frettchen- und naivem K18-hACE2-Mausmodell stets ein Vorteil der VOC Delta beobachtet werden konnte. Außerdem wurde in **Publikation IV** ein transmissiver Nachteil der VOC Omikron BA.1 gegenüber VOC Delta und eine fehlende Empfänglichkeit des Frettchens nach einer Einzelinfektion mit der VOC Omikron BA.1 nachgewiesen. Eine mRNA-Vakzinierung bewirkte eine drastische Reduktion infektiöser Viruspartikel in Organmaterial von K18-hACE2 Mäusen in Folge einer Belastungsinfektion mit einem rekombinanten SARS-CoV-2 WT-S^{Delta} Virus, nicht jedoch in Folge einer SARS-CoV-2 WT-S$^{Omikron\ BA.1}$Infektion.

Diese Dissertation umfasst zahlreiche, detaillierte experimentelle Studien, die einerseits generell für die Charakterisierung von neu auftretenden, möglicherweise prä-pandemischen Viren von Bedeutung sind, andererseits aber auch entscheidende Hinweise über die zukünftige Dominanz bestimmter Virusvarianten in einer laufenden Pandemie liefern können. Hierbei wird die Notwendigkeit der Verwendung von unterschiedlichen Tiermodellen deutlich. Diese Methoden werden durch die Charakterisierung und Klassifizierung möglicherweise zoonotischer Virusstämme dabei helfen, sich besser auf bevorstehende potentielle Pandemien vorzubereiten und im Falle eines zoonotischen oder gar pandemischen Geschehens die zirkulierenden Stämme und deren Evolution besser zu erfassen und zu verstehen.

8   References

Adlhoch, Cornelia; Fusaro, Alice; Gonzales, José L.; Kuiken, Thijs; Marangon, Stefano; Niqueux, Éric et al. (2022): Avian influenza overview December 2021 – March 2022. In *EFSA Journal* 20 (4). DOI: 10.2903/j.efsa.2022.7289.

Afifi, Manal A. A.; El-Kady, Magdy F.; Zoelfakar, Sahar A.; Abdel-Moneim, Ahmed Sayed (2013): Serological surveillance reveals widespread influenza A H7 and H9 subtypes among chicken flocks in Egypt. In *Tropical animal health and production* 45 (2), pp. 687–690. DOI: 10.1007/s11250-012-0243-9.

Akarsu, Hatice; Burmeister, Wilhelm P.; Petosa, Carlo; Petit, Isabelle; Müller, Christoph W.; Ruigrok, Rob W.H.; Baudin, Florence (2003): Crystal structure of the M1 protein-binding domain of the influenza A virus nuclear export protein (NEP/NS2). In *The EMBO Journal* 22 (18), pp. 4646–4655. DOI: 10.1093/emboj/cdg449.

Aldous, E. W.; Seekings, J. M.; McNally, A.; Nili, H.; Fuller, C. M.; Irvine, R. M. et al. (2010): Infection dynamics of highly pathogenic avian influenza and virulent avian paramyxovirus type 1 viruses in chickens, turkeys and ducks. In *Avian pathology : journal of the W.V.P.A* 39 (4), pp. 265–273. DOI: 10.1080/03079457.2010.492825.

Aleem, Abdul; Akbar Samad, Abdul Bari; Slenker, Amy K. (2022): StatPearls. Emerging Variants of SARS-CoV-2 And Novel Therapeutics Against Coronavirus (COVID-19). Treasure Island (FL).

Almayahi, Zayid K.; Al Kindi, Hanan; Davies, C. Todd; Al-Rawahi, Bader; Al-Jardani, Amina; Al-Yaqoubi, Fatma et al. (2020): First report of human infection with avian influenza A(H9N2) virus in Oman: The need for a One Health approach. In *International journal of infectious diseases : IJID : official publication of the International Society for Infectious Diseases* 91, pp. 169–173. DOI: 10.1016/j.ijid.2019.11.020.

An, Dong; Li, Kun; Rowe, Dawne K.; Diaz, Maria Cristina Huertas; Griffin, Emily F.; Beavis, Ashley C. et al. (2021): Protection of K18-hACE2 mice and ferrets against SARS-CoV-2 challenge by a single-dose mucosal immunization with a parainfluenza virus 5-based COVID-19 vaccine. In *Science advances* 7 (27). DOI: 10.1126/sciadv.abi5246.

Andeweg, Stijn P.; Vennema, Harry; Veldhuijzen, Irene; Smorenburg, Naomi; Schmitz, Dennis; Zwagemaker, Florian et al. (2022): Elevated risk of infection with SARS-CoV-2 Beta, Gamma, and Delta variant compared to Alpha variant in vaccinated individuals. In *Science translational medicine*, eabn4338. DOI: 10.1126/scitranslmed.abn4338.

Anti, Priscilla; Owusu, Michael; Agbenyega, Olivia; Annan, Augustina; Badu, Ebenezer Kofi; Nkrumah, Evans Ewald et al. (2015): Human–Bat Interactions in Rural West Africa. In *Emerging Infectious Diseases* 21 (8), pp. 1418–1421. DOI: 10.3201/eid2108.142015.

Arora, Prerna; Zhang, Lu; Rocha, Cheila; Graichen, Luise; Nehlmeier, Inga; Kempf, Amy et al. (2022): The SARS-CoV-2 Delta-Omicron Recombinant Lineage (XD) Exhibits Immune-Escape Properties Similar to the Omicron (BA.1) Variant. In *International journal of molecular sciences* 23 (22). DOI: 10.3390/ijms232214057.

Artois, Jean; Ippoliti, Carla; Conte, Annamaria; Dhingra, Madhur S.; Alfonso, Pastor; Tahawy, Abdelgawad El et al. (2018): Avian influenza A (H5N1) outbreaks in different poultry farm types in Egypt: the effect of vaccination, closing status and farm size. In *BMC Veterinary Research* 14. DOI: 10.1186/s12917-018-1519-8.

Bayati, Armin; Kumar, Rahul; Francis, Vincent; McPherson, Peter S. (2021): SARS-CoV-2 infects cells after viral entry via clathrin-mediated endocytosis. In *The Journal of biological chemistry* 296, p. 100306. DOI: 10.1016/j.jbc.2021.100306.

Becker, Daniel J.; Albery, Gregory F.; Kessler, Maureen K.; Lunn, Tamika J.; Falvo, Caylee A.; Czirják, Gábor Á. et al. (2020): Macroimmunology: the drivers and consequences of spatial patterns in wildlife immune defense. In *The Journal of animal ecology* 89 (4), pp. 972–995. DOI: 10.1111/1365-2656.13166.

Belser, Jessica A.; Barclay, Wendy; Barr, Ian; Fouchier, Ron A.M.; Matsuyama, Ryota; Nishiura, Hiroshi et al. (2018): Ferrets as Models for Influenza Virus Transmission Studies and Pandemic Risk Assessments. In *Emerging Infectious Diseases* 24 (6), pp. 965–971. DOI: 10.3201/eid2406.172114.

Belser, Jessica A.; Eckert, Alissa M.; Huynh, Thanhthao; Gary, Joy M.; Ritter, Jana M.; Tumpey, Terrence M.; Maines, Taronna R. (2020): A Guide for the Use of the Ferret Model for Influenza Virus Infection. In *The American journal of pathology* 190 (1), pp. 11–24. DOI: 10.1016/j.ajpath.2019.09.017.

Belser, Jessica A.; Katz, Jacqueline M.; Tumpey, Terrence M. (2011): The ferret as a model organism to study influenza A virus infection. In *Disease Models & Mechanisms* 4 (5), pp. 575–579. DOI: 10.1242/dmm.007823.

Bergeri, Isabel; Whelan, Mairead G.; Ware, Harriet; Subissi, Lorenzo; Nardone, Anthony; Lewis, Hannah C. et al. (2022): Global SARS-CoV-2 seroprevalence from January 2020 to April 2022: A systematic review and meta-analysis of standardized population-based studies. In *PLoS Medicine* 19 (11), e1004107. DOI: 10.1371/journal.pmed.1004107.

Berhane, Y.; Ojkic, D.; Pople, N.; Lung, O.; Pasick, J. (2016): Reoccurrence of Suspected Human-to-Turkey Transmission of H1N1 Pandemic 2009 Virus in Turkey Breeder Flocks in Ontario and Manitoba, 2016. In *Transboundary and emerging diseases* 63 (6), pp. 590–594. DOI: 10.1111/tbed.12566.

Berhane, Yohannes; Suderman, Matthew; Babiuk, Shawn; Pickering, Bradley (2021): Susceptibility of turkeys, chickens and chicken embryos to SARS-CoV-2. In *Transboundary and emerging diseases* 68 (6), pp. 3038–3042. DOI: 10.1111/tbed.13970.

Bertram, Stephanie; Dijkman, Ronald; Habjan, Matthias; Heurich, Adeline; Gierer, Stefanie; Glowacka, Ilona et al. (2013): TMPRSS2 Activates the Human Coronavirus 229E for Cathepsin-Independent Host Cell Entry and Is Expressed in Viral Target Cells in the Respiratory Epithelium. In *Journal of Virology* 87 (11), pp. 6150–6160. DOI: 10.1128/JVI.03372-12.

Bickley, Steve J.; Chan, Ho Fai; Skali, Ahmed; Stadelmann, David; Torgler, Benno (2021): How does globalization affect COVID-19 responses? In *Globalization and health* 17 (1), p. 57. DOI: 10.1186/s12992-021-00677-5.

Blackwood, Julie C.; Streicker, Daniel G.; Altizer, Sonia; Rohani, Pejman (2013): Resolving the roles of immunity, pathogenesis, and immigration for rabies persistence in vampire bats. In *Proceedings of the National Academy of Sciences of the United States of America* 110 (51), pp. 20837–20842. DOI: 10.1073/pnas.1308817110.

Blaurock, Claudia; Pfaff, Florian; Scheibner, David; Hoffmann, Bernd; Fusaro, Alice; Monne, Isabella et al. (2022): Evidence for Different Virulence Determinants and Host Response after Infection of Turkeys and Chickens with Highly Pathogenic H7N1 Avian Influenza Virus. In *Journal of Virology* 96 (17), e0099422. DOI: 10.1128/jvi.00994-22.

Bleul, Tim; Zhuang, Xinyu; Hildebrand, Antonia; Lange, Clemens; Böhringer, Daniel; Schlunck, Günther et al. (2020): Different Innate Immune Responses in BALB/c and C57BL/6 Strains following Corneal Transplantation. In *Journal of Innate Immunity* 13 (1), pp. 49–59. DOI: 10.1159/000509716.

Boley, Patricia A.; Lee, Carolyn M.; Schrock, Jennifer; Yadav, Kush Kumar; Patil, Veerupaxagouda; Suresh, Raksha et al. (2023): Enhanced mucosal immune responses and reduced viral load in the respiratory tract of ferrets to intranasal lipid nanoparticle-based SARS-CoV-2 proteins and mRNA vaccines. In *Journal of nanobiotechnology* 21 (1), p. 60. DOI: 10.1186/s12951-023-01816-3.

Bonanad, Clara; García-Blas, Sergio; Tarazona-Santabalbina, Francisco; Sanchis, Juan; Bertomeu-González, Vicente; Fácila, Lorenzo et al. (2020): The Effect of Age on Mortality in Patients With COVID-19: A Meta-Analysis With 611,583 Subjects. In *Journal of the American Medical Directors Association* 21 (7), pp. 915–918. DOI: 10.1016/j.jamda.2020.05.045.

Borremans, Benny; Faust, Christina; Manlove, Kezia R.; Sokolow, Susanne H.; Lloyd-Smith, James O. (2019): Cross-species pathogen spillover across ecosystem boundaries: mechanisms and theory. In *Philosophical Transactions of the Royal Society B: Biological Sciences* 374 (1782). DOI: 10.1098/rstb.2018.0344.

Böttcher-Friebertshäuser, Eva; Garten, Wolfgang; Matrosovich, Mikhail; Klenk, Hans Dieter (2014): The hemagglutinin: a determinant of pathogenicity. In *Current topics in microbiology and immunology* 385, pp. 3–34. DOI: 10.1007/82_2014_384.

Bouvenot, Typhanie; Dewitte, Amélie; Bennaceur, Nadia; Pradel, Elizabeth; Pierre, François; Bontemps-Gallo, Sébastien; Sebbane, Florent (2021): Interplay between Yersinia pestis and its flea vector in lipoate metabolism. In *The ISME journal* 15 (4), pp. 1136–1149. DOI: 10.1038/s41396-020-00839-0.

Burgin, Connor J.; Colella, Jocelyn P.; Kahn, Philip L.; Upham, Nathan S. (2018): How many species of mammals are there? In *Journal of Mammalogy* 99 (1), pp. 1–14. DOI: 10.1093/jmammal/gyx147.

Burnet, F. M.; Bull, Diana H. (1943): CHANGES IN INFLUENZA VIRUS ASSOCIATED WITH ADAPTATION TO PASSAGE IN CHICK EMBRYOS. In *Aust J Exp Biol Med* 21 (2), pp. 55–69. DOI: 10.1038/icb.1943.7.

Butt, Adeel A.; Dargham, Soha R.; Chemaitelly, Hiam; Al Khal, Abdullatif; Tang, Patrick; Hasan, Mohammad R. et al. (2021): Severity of Illness in Persons Infected With the SARS-CoV-2 Delta Variant vs Beta Variant in Qatar. In *JAMA Internal Medicine* 182 (2), pp. 1–9. DOI: 10.1001/jamainternmed.2021.7949.

Calisher, Charles H.; Childs, James E.; Field, Hume E.; Holmes, Kathryn V.; Schountz, Tony (2006): Bats: important reservoir hosts of emerging viruses. In *Clinical microbiology reviews* 19 (3), pp. 531–545. DOI: 10.1128/CMR.00017-06.

Campbell, Lee K.; Fleming-Canepa, Ximena; Webster, Robert G.; Magor, Katharine E. (2021): Tissue Specific Transcriptome Changes Upon Influenza A Virus Replication in the Duck. In *Frontiers in immunology* 12. DOI: 10.3389/fimmu.2021.786205.

Campbell, Lee K.; Magor, Katharine E. (2020): Pattern Recognition Receptor Signaling and Innate Responses to Influenza A Viruses in the Mallard Duck, Compared to Humans and Chickens. In *Frontiers in cellular and infection microbiology* 10, p. 209. DOI: 10.3389/fcimb.2020.00209.

Cao, Yunlong; Yisimayi, Ayijiang; Jian, Fanchong; Song, Weiliang; Xiao, Tianhe; Wang, Lei et al. (2022): BA.2.12.1, BA.4 and BA.5 escape antibodies elicited by Omicron infection. In *Nature* 608 (7923), pp. 593–602. DOI: 10.1038/s41586-022-04980-y.

Cappelle, Julien; Hoem, Thavry; Hul, Vibol; Furey, Neil; Nguon, Kunthy; Prigent, Steven et al. (2020): Nipah virus circulation at human-bat interfaces, Cambodia. In *Bulletin of the World Health Organization* 98 (8), pp. 539–547. DOI: 10.2471/BLT.20.254227.

CDC (2022): Estimated Flu-Related Illnesses, Medical visits, Hospitalizations, and Deaths in the United States — 2019–2020 Flu Season. Available online at https://www.cdc.gov/flu/about/burden/2019-2020.html.

Cele, Sandile; Jackson, Laurelle; Khoury, David S.; Khan, Khadija; Moyo-Gwete, Thandeka; Tegally, Houriiyah et al. (2022): Omicron extensively but incompletely escapes Pfizer BNT162b2 neutralization. In *Nature* 602 (7898), pp. 654–656. DOI: 10.1038/s41586-021-04387-1.

Centeno-Cuadros, A.; Hulva, P.; Romportl, D.; Santoro, S.; Stříbná, T.; Shohami, D. et al. (2017): Habitat use, but not gene flow, is influenced by human activities in two ecotypes of Egyptian fruit bat (Rousettus aegyptiacus). In *Molecular ecology* 26 (22), pp. 6224–6237. DOI: 10.1111/mec.14365.

Chan, Jasper Fuk-Woo; Hu, Bingjie; Chai, Yue; Shuai, Huiping; Liu, Huan; Shi, Jialu et al. (2022): Virological features and pathogenicity of SARS-CoV-2 Omicron BA.2. In *Cell reports. Medicine* 3 (9), p. 100743. DOI: 10.1016/j.xcrm.2022.100743.

Chauhan, Ravendra P.; Gordon, Michelle L. (2022): An overview of influenza A virus genes, protein functions, and replication cycle highlighting important updates. In *Virus genes* 58 (4), pp. 255–269. DOI: 10.1007/s11262-022-01904-w.

Chen, Dong; Su, Xi; Chen, Haibo; Chen, Siyan; Zhao, Yongsheng; Wei, Wei (2022): Human Organoids as a Promising Platform for Fighting COVID-19. In *International Journal of Biological Sciences* 18 (3), pp. 901–910. DOI: 10.7150/ijbs.64993.

Chen, Lihong; Liu, Bo; Yang, Jian; Jin, Qi (2014): DBatVir: the database of bat-associated viruses. In *Database : the journal of biological databases and curation* 2014, bau021. DOI: 10.1093/database/bau021.

Cherian, Sarah; Potdar, Varsha; Jadhav, Santosh; Yadav, Pragya; Gupta, Nivedita; Das, Mousumi et al. (2021): SARS-CoV-2 Spike Mutations, L452R, T478K, E484Q and P681R, in the Second Wave of COVID-19 in Maharashtra, India. In *Microorganisms* 9 (7). DOI: 10.3390/microorganisms9071542.

Cherry, James. D. (2004): The chronology of the 2002–2003 SARS mini pandemic. In *Paediatric Respiratory Reviews* 5 (4), pp. 262–269. DOI: 10.1016/j.prrv.2004.07.009.

Chlanda, Petr; Zimmerberg, Joshua (2016): Protein-lipid interactions critical to replication of the influenza A virus during infection. In *FEBS letters* 590 (13), pp. 1940–1954. DOI: 10.1002/1873-3468.12118.

Chu, Daniel K. W.; Poon, Leo L. M.; Gomaa, Mokhtar M.; Shehata, Mahmoud M.; Perera, Ranawaka A. P. M.; Abu Zeid, Dina et al. (2014): MERS coronaviruses in dromedary camels, Egypt. In *Emerging Infectious Diseases* 20 (6), pp. 1049–1053. DOI: 10.3201/eid2006.140299.

Ciminski, Kevin; Pfaff, Florian; Beer, Martin; Schwemmle, Martin (2020): Bats reveal the true power of influenza A virus adaptability. In *PLoS pathogens* 16 (4), e1008384. DOI: 10.1371/journal.ppat.1008384.

Ciminski, Kevin; Ran, Wei; Gorka, Marco; Lee, Jinhwa; Malmlov, Ashley; Schinköthe, Jan et al. (2019): Bat influenza viruses transmit among bats but are poorly adapted to non-bat species. In *Nature microbiology* 4 (12), pp. 2298–2309. DOI: 10.1038/s41564-019-0556-9.

Claire, Marisa C. St; Ragland, Dan R.; Bollinger, Laura; Jahrling, Peter B. (2017): Animal Models of Ebolavirus Infection. In *Comparative Medicine* 67 (3), pp. 253–262.

Cohen, Miriam; Zhang, Xing-Quan; Senaati, Hooman P.; Chen, Hui-Wen; Varki, Nissi M.; Schooley, Robert T.; Gagneux, Pascal (2013): Influenza A penetrates host mucus by cleaving sialic acids with neuraminidase. In *Virology Journal* 10, p. 321. DOI: 10.1186/1743-422X-10-321.

Cortese, Mirko; Lee, Ji-Young; Cerikan, Berati; Neufeldt, Christopher J.; Oorschot, Viola M. J.; Köhrer, Sebastian et al. (2020): Integrative Imaging Reveals SARS-CoV-2-Induced Reshaping of Subcellular Morphologies. In *Cell host & microbe* 28 (6), 853-866.e5. DOI: 10.1016/j.chom.2020.11.003.

Cox, Nancy J.; Trock, Susan C.; Burke, Stephen A. (2014): Pandemic preparedness and the Influenza Risk Assessment Tool (IRAT). In *Current topics in microbiology and immunology* 385, pp. 119–136. DOI: 10.1007/82_2014_419.

Cui, Jie; Li, Fang; Shi, Zheng-Li (2019): Origin and evolution of pathogenic coronaviruses. In *Nature reviews. Microbiology* 17 (3), pp. 181–192. DOI: 10.1038/s41579-018-0118-9.

Damas, Joana; Hughes, Graham M.; Keough, Kathleen C.; Painter, Corrie A.; Persky, Nicole S.; Corbo, Marco et al. (2020): Broad host range of SARS-CoV-2 predicted by comparative and structural analysis of ACE2 in vertebrates. In *Proceedings of the National Academy of Sciences of the United States of America* 117 (36), pp. 22311–22322. DOI: 10.1073/pnas.2010146117.

Davidson, Andrew D.; Williamson, Maia Kavanagh; Lewis, Sebastian; Shoemark, Deborah; Carroll, Miles W.; Heesom, Kate J. et al. (2020): Characterisation of the transcriptome and proteome of SARS-CoV-2 reveals a cell passage induced in-frame deletion of the furin-like cleavage site from the spike glycoprotein. In *Genome medicine* 12 (1), p. 68. DOI: 10.1186/s13073-020-00763-0.

Dawood, Fatimah S.; Iuliano, A. Danielle; Reed, Carrie; Meltzer, Martin I.; Shay, David K.; Cheng, Po-Yung et al. (2012): Estimated global mortality associated with the first 12 months of 2009 pandemic influenza A H1N1 virus circulation: a modelling study. In *The Lancet. Infectious diseases* 12 (9), pp. 687–695. DOI: 10.1016/S1473-3099(12)70121-4.

Deeg, Christoph M.; Hassan, Ebrahim; Mutz, Pascal; Rheinemann, Lara; Götz, Veronika; Magar, Linda et al. (2017): In vivo evasion of MxA by avian influenza viruses requires human signature in the viral nucleoprotein. In *The Journal of Experimental Medicine* 214 (5), pp. 1239–1248. DOI: 10.1084/jem.20161033.

Di Chen; Zheng, Qiaoxia; Sun, Long; Ji, Mingming; Li, Yan; Deng, Hongyu; Zhang, Hong (2021): ORF3a of SARS-CoV-2 promotes lysosomal exocytosis-mediated viral egress. In *Developmental Cell* 56 (23), 3250-3263.e5. DOI: 10.1016/j.devcel.2021.10.006.

Dittmann, Jan; Stertz, Silke; Grimm, Daniel; Steel, John; García-Sastre, Adolfo; Haller, Otto; Kochs, Georg (2008): Influenza A Virus Strains Differ in Sensitivity to the Antiviral Action of Mx-GTPase▿. In *Journal of Virology* 82 (7), pp. 3624–3631. DOI: 10.1128/JVI.01753-07.

Dong, Wenjuan; Mead, Heather; Tian, Lei; Park, Jun-Gyu; Garcia, Juan I.; Jaramillo, Sierra et al. (2022): The K18-Human ACE2 Transgenic Mouse Model Recapitulates Non-severe and Severe COVID-19 in Response to an Infectious Dose of the SARS-CoV-2 Virus. In *Journal of Virology* 96 (1), e0096421. DOI: 10.1128/JVI.00964-21.

Dornfeld, Dominik; Petric, Philipp P.; Hassan, Ebrahim; Zell, Roland; Schwemmle, Martin (2019): Eurasian Avian-Like Swine Influenza A Viruses Escape Human MxA Restriction through Distinct Mutations in Their Nucleoprotein. In *Journal of Virology* 93 (2). DOI: 10.1128/JVI.00997-18.

Dou, Dan; Revol, Rebecca; Östbye, Henrik; Wang, Hao; Daniels, Robert (2018): Influenza A Virus Cell Entry, Replication, Virion Assembly and Movement. In *Frontiers in immunology* 9, p. 1581. DOI: 10.3389/fimmu.2018.01581.

Duerr, Ralf; Dimartino, Dacia; Marier, Christian; Zappile, Paul; Levine, Samuel; Francois, Fritz et al. (2022): Clinical and genomic signatures of SARS-CoV-2 Delta breakthrough infections in New York. In *EBioMedicine* 82, p. 104141. DOI: 10.1016/j.ebiom.2022.104141.

Duerrwald, Ralf; Schlegel, Michael; Bauer, Katja; Vissiennon, Théophile; Wutzler, Peter; Schmidtke, Michaela (2013): Efficacy of influenza vaccination and tamiflu® treatment--comparative studies with Eurasian Swine influenza viruses in pigs. In *PloS one* 8 (4), e61597. DOI: 10.1371/journal.pone.0061597.

Eby, Peggy; Peel, Alison J.; Hoegh, Andrew; Madden, Wyatt; Giles, John R.; Hudson, Peter J.; Plowright, Raina K. (2022): Pathogen spillover driven by rapid changes in bat ecology. In *Nature*, pp. 1–5. DOI: 10.1038/s41586-022-05506-2.

ECDC (as of 2023): SARS-CoV-2 variants of concern as of 23 March 2023. Available online at https://www.ecdc.europa.eu/en/covid-19/variants-concern.

Edwards, David A.; Ausiello, Dennis; Salzman, Jonathan; Devlin, Tom; Langer, Robert; Beddingfield, Brandon J. et al. (2021): Exhaled aerosol increases with COVID-19 infection, age, and obesity. In *Proceedings of the National Academy of Sciences of the United States of America* 118 (8). DOI: 10.1073/pnas.2021830118.

Eisfeld, Amie J.; Neumann, Gabriele; Kawaoka, Yoshihiro (2014): At the centre: influenza A virus ribonucleoproteins. In *Nature reviews. Microbiology* 13 (1), pp. 28–41. DOI: 10.1038/nrmicro3367.

Ellwanger, Joel Henrique; Chies, José Artur Bogo (2021): Zoonotic spillover: Understanding basic aspects for better prevention. In *Genetics and Molecular Biology* 44 (1 Suppl 1). DOI: 10.1590/1678-4685-GMB-2020-0355.

Elton, Debra; Simpson-Holley, Martha; Archer, Kate; Medcalf, Liz; Hallam, Roger; McCauley, John; Digard, Paul (2001): Interaction of the Influenza Virus Nucleoprotein with the Cellular CRM1-Mediated Nuclear Export Pathway. In *Journal of Virology* 75 (1), pp. 408–419. DOI: 10.1128/JVI.75.1.408-419.2001.

Elviss, Nicola C.; Allen, David J.; Kelly, Daniel; Akello, Joyce Odeke; Hau, Sarah; Fox, Andrew J. et al. (2022): Norovirus attribution study: Detection of norovirus from the commercial food preparation environment in outbreak and non-outbreak premises. In *Journal of applied microbiology* 133 (6), pp. 3391–3403. DOI: 10.1111/jam.15761.

Esper, Frank P.; Adhikari, Thamali M.; Tu, Zheng Jin; Cheng, Yu Wei; El-Haddad, Kim; Farkas, Daniel H. et al. (2022): Alpha to Omicron: Disease Severity and Clinical Outcomes of Major SARS-CoV-2 Variants. In *The Journal of Infectious Diseases*. DOI: 10.1093/infdis/jiac411.

Fan, Shufang; Gu, Chunyang; Kong, Huihui; Guan, Lizheng; Neumann, Gabriele; Kawaoka, Yoshihiro (2022): Influenza Viruses Suitable for Studies in Syrian Hamsters. In *Viruses* 14 (8). DOI: 10.3390/v14081629.

Faria, Nuno R.; Mellan, Thomas A.; Whittaker, Charles; Claro, Ingra M.; Da Candido, Darlan S.; Mishra, Swapnil et al. (2021): Genomics and epidemiology of the P.1 SARS-CoV-2 lineage in Manaus, Brazil. In *Science (New York, N.Y.)* 372 (6544), pp. 815–821. DOI: 10.1126/science.abh2644.

Feikin, Daniel R.; Higdon, Melissa M.; Andrews, Nick; Collie, Shirley; Deloria Knoll, Maria; Kwong, Jeffrey C. et al. (2023): Assessing COVID-19 vaccine effectiveness against Omicron subvariants: Report from a meeting of the World Health Organization. In *Vaccine* 41 (14), pp. 2329–2338. DOI: 10.1016/j.vaccine.2023.02.020.

Feng, Wenjing; Sun, Xiaoning; Shi, Ning; Zhang, Maolin; Guan, Zhenhong; Duan, Ming (2017): Influenza a virus NS1 protein induced A20 contributes to viral replication by suppressing interferon-induced antiviral response. In *Biochemical and biophysical research communications* 482 (4), pp. 1107–1113. DOI: 10.1016/j.bbrc.2016.11.166.

Flerlage, Tim; Boyd, David F.; Meliopoulos, Victoria; Thomas, Paul G.; Schultz-Cherry, Stacey (2021): Influenza virus and SARS-CoV-2: pathogenesis and host responses in the respiratory tract. In *Nature reviews. Microbiology* 19 (7), pp. 425–441. DOI: 10.1038/s41579-021-00542-7.

Freidl, Gudrun Stephanie; Binger, Tabea; Müller, Marcel Alexander; Bruin, Erwin de; van Beek, Janko; Corman, Victor Max et al. (2015): Serological evidence of influenza A viruses in frugivorous bats from Africa. In *PloS one* 10 (5), e0127035. DOI: 10.1371/journal.pone.0127035.

Freuling, Conrad M.; Breithaupt, Angele; Müller, Thomas; Sehl, Julia; Balkema-Buschmann, Anne; Rissmann, Melanie et al. (2020): Susceptibility of Raccoon Dogs for Experimental SARS-CoV-2 Infection. In *Emerging Infectious Diseases* 26 (12), pp. 2982–2985. DOI: 10.3201/eid2612.203733.

Friedrichs, Virginia; Toussaint, Christophe; Schäfer, Alexander; Rissmann, Melanie; Dietrich, Oliver; Mettenleiter, Thomas C. et al. (2022): Landscape and age dynamics of immune cells in the Egyptian rousette bat. In *Cell reports* 40 (10), p. 111305. DOI: 10.1016/j.celrep.2022.111305.

Frost, Simon D. W.; Magalis, Brittany Rife; Kosakovsky Pond, Sergei L. (2018): Neutral Theory and Rapidly Evolving Viral Pathogens. In *Molecular Biology and Evolution* 35 (6), pp. 1348–1354. DOI: 10.1093/molbev/msy088.

Fujino, Takahisa; Nomoto, Hidetoshi; Kutsuna, Satoshi; Ujiie, Mugen; Suzuki, Tetsuya; Sato, Rubuna et al. (2021): Novel SARS-CoV-2 Variant in Travelers from Brazil to Japan. In *Emerging Infectious Diseases* 27 (4), pp. 1243–1245. DOI: 10.3201/eid2704.210138.

Fumagalli, Valeria; Ravà, Micol; Marotta, Davide; Di Lucia, Pietro; Laura, Chiara; Sala, Eleonora et al. (2022): Administration of aerosolized SARS-CoV-2 to K18-hACE2 mice uncouples respiratory infection from fatal neuroinvasion. In *Science immunology* 7 (67), eabl9929. DOI: 10.1126/sciimmunol.abl9929.

Funk, Tjede; Pharris, Anastasia; Spiteri, Gianfranco; Bundle, Nick; Melidou, Angeliki; Carr, Michael et al. (2021): Characteristics of SARS-CoV-2 variants of concern B.1.1.7, B.1.351 or P.1: data from seven EU/EEA countries, weeks 38/2020 to 10/2021. In *Euro surveillance : bulletin Europeen sur les maladies transmissibles = European*

communicable disease bulletin 26 (16). DOI: 10.2807/1560-7917.ES.2021.26.16.2100348.

Ganti, Ketaki; Bagga, Anish; DaSilva, Juliana; Shepard, Samuel S.; Barnes, John R.; Shriner, Susan et al. (2021): Avian Influenza A Viruses Reassort and Diversify Differently in Mallards and Mammals. In *Viruses* 13 (3). DOI: 10.3390/v13030509.

Gao, Shijuan; Song, Liping; Li, Jiandong; Zhang, Zhenzhu; Peng, Haiyan; Jiang, Wei et al. (2012): Influenza A virus-encoded NS1 virulence factor protein inhibits innate immune response by targeting IKK. In *Cellular microbiology* 14 (12), pp. 1849–1866. DOI: 10.1111/cmi.12005.

Gao, Ya; Chen, Yamin; Liu, Ming; Shi, Shuzhen; Tian, Jinhui (2020): Impacts of immunosuppression and immunodeficiency on COVID-19: A systematic review and meta-analysis. In *The Journal of Infection* 81 (2), e93-5. DOI: 10.1016/j.jinf.2020.05.017.

García-Sastre, Adolfo (2012): The neuraminidase of bat influenza viruses is not a neuraminidase. In *Proceedings of the National Academy of Sciences of the United States of America* 109 (46), pp. 18635–18636. DOI: 10.1073/pnas.1215857109.

Geiser, Fritz; Stawski, Clare (2011): Hibernation and torpor in tropical and subtropical bats in relation to energetics, extinctions, and the evolution of endothermy. In *Integrative and comparative biology* 51 (3), pp. 337–348. DOI: 10.1093/icb/icr042.

George, Dylan B.; Webb, Colleen T.; Farnsworth, Matthew L.; O'Shea, Thomas J.; Bowen, Richard A.; Smith, David L. et al. (2011): Host and viral ecology determine bat rabies seasonality and maintenance. In *Proceedings of the National Academy of Sciences of the United States of America* 108 (25), pp. 10208–10213. DOI: 10.1073/pnas.1010875108.

Gerber, Marie; Isel, Catherine; Moules, Vincent; Marquet, Roland (2014): Selective packaging of the influenza A genome and consequences for genetic reassortment. In *Trends in microbiology* 22 (8), pp. 446–455. DOI: 10.1016/j.tim.2014.04.001.

Gharib, H.; Abdel-Aziz, Y. A.; El-menawey, M. A.; Hamouda, R. (2012): CHARACTERIZATION OF FAMILY POULTRY PRODUCTION SYSTEM IN THE RURAL SECTOR OF AL-SHARKIA GOVERNORATE, EGYPT. In *Egyptian Journal of Animal Production* 49 (2), pp. 195–205. DOI: 10.21608/ejap.2012.94336.

Ghosh, Sourish; Dellibovi-Ragheb, Teegan A.; Kerviel, Adeline; Pak, Eowyn; Qiu, Qi; Fisher, Matthew et al. (2020): β-Coronaviruses Use Lysosomes for Egress Instead of the Biosynthetic Secretory Pathway. In *Cell* 183 (6), 1520-1535.e14. DOI: 10.1016/j.cell.2020.10.039.

Gibb, Rory; Redding, David W.; Chin, Kai Qing; Donnelly, Christl A.; Blackburn, Tim M.; Newbold, Tim; Jones, Kate E. (2020): Zoonotic host diversity increases in human-dominated ecosystems. In *Nature* 584 (7821), pp. 398–402. DOI: 10.1038/s41586-020-2562-8.

Gorbunova, Vera; Seluanov, Andrei; Kennedy, Brian K. (2020): The World Goes Bats: Living Longer and Tolerating Viruses. In *Cell metabolism* 32 (1), pp. 31–43. DOI: 10.1016/j.cmet.2020.06.013.

Götz, Veronika; Magar, Linda; Dornfeld, Dominik; Giese, Sebastian; Pohlmann, Anne; Höper, Dirk et al. (2016): Corrigendum: Influenza A viruses escape from MxA restriction at the expense of efficient nuclear vRNP import. In *Scientific reports* 6, p. 25428. DOI: 10.1038/srep25428.

GOV.UK (2020): Regulatory approval of Pfizer/BioNTech vaccine for COVID-19. Available online at https://www.gov.uk/government/publications/regulatory-approval-of-pfizer-biontech-vaccine-for-covid-19.

Graham, Flora (2022): Daily briefing: World population estimated to reach eight billion today. In *Nature*. DOI: 10.1038/d41586-022-03739-9.

Graham, Jay P.; Leibler, Jessica H.; Price, Lance B.; Otte, Joachim M.; Pfeiffer, Dirk U.; Tiensin, T.; Silbergeld, Ellen K. (2008): The Animal-Human Interface and Infectious Disease in Industrial Food Animal Production: Rethinking Biosecurity and Biocontainment. In *Public Health Reports* 123 (3), pp. 282–299.

Gram, Mie Agermose; Emborg, Hanne-Dorthe; Schelde, Astrid Blicher; Friis, Nikolaj Ulrik; Nielsen, Katrine Finderup; Moustsen-Helms, Ida Rask et al. (2022): Vaccine effectiveness against SARS-CoV-2 infection or COVID-19 hospitalization with the Alpha, Delta, or Omicron SARS-CoV-2 variant: A nationwide Danish cohort study. In *PLoS Medicine* 19 (9). DOI: 10.1371/journal.pmed.1003992.

Grange, Zoë L.; Goldstein, Tracey; Johnson, Christine K.; Anthony, Simon; Gilardi, Kirsten; Daszak, Peter et al. (2021): Ranking the risk of animal-to-human spillover for newly discovered viruses. In *Proceedings of the National Academy of Sciences of the United States of America* 118 (15). DOI: 10.1073/pnas.2002324118.

Groff, Destin; Sun, Ashley; Ssentongo, Anna E.; Ba, Djibril M.; Parsons, Nicholas; Poudel, Govinda R. et al. (2021): Short-term and Long-term Rates of Postacute Sequelae of SARS-CoV-2 Infection: A Systematic Review. In *JAMA Network Open* 4 (10). DOI: 10.1001/jamanetworkopen.2021.28568.

Grund, Christian; Hoffmann, Donata; Ulrich, Reiner; Naguib, Mahmoud; Schinköthe, Jan; Hoffmann, Bernd et al. (2018): A novel European H5N8 influenza A virus has increased virulence in ducks but low zoonotic potential. In *Emerging Microbes & Infections* 7. DOI: 10.1038/s41426-018-0130-1.

Guan, Y.; Peiris, J. S. M.; Lipatov, A. S.; Ellis, T. M.; Dyrting, K. C.; Krauss, S. et al. (2002): Emergence of multiple genotypes of H5N1 avian influenza viruses in Hong Kong SAR. In *Proceedings of the National Academy of Sciences of the United States of America* 99 (13), pp. 8950–8955. DOI: 10.1073/pnas.132268999.

Guito, Jonathan C.; Prescott, Joseph B.; Arnold, Catherine E.; Amman, Brian R.; Schuh, Amy J.; Spengler, Jessica R. et al. (2021): Asymptomatic Infection of Marburg Virus Reservoir Bats Is Explained by a Strategy of Immunoprotective Disease Tolerance. In *Current biology : CB* 31 (2), 257-270.e5. DOI: 10.1016/j.cub.2020.10.015.

Gunther, Randall C.; Bharathi, Vanthana; Miles, Stephen D.; Tumey, Lauryn R.; Schmedes, Clare M.; Tatsumi, Kohei et al. (2021): Myeloid Protease-Activated Receptor-2 Contributes to Influenza A Virus Pathology in Mice. In *Frontiers in immunology* 12, p. 791017. DOI: 10.3389/fimmu.2021.791017.

Hachmann, Nicole P.; Miller, Jessica; Collier, Ai-Ris Y.; Ventura, John D.; Yu, Jingyou; Rowe, Marjorie et al. (2022): Neutralization Escape by SARS-CoV-2 Omicron Subvariants BA.2.12.1, BA.4, and BA.5. In *The New England journal of medicine* 387 (1), pp. 86–88. DOI: 10.1056/nejmc2206576.

Halfmann, Peter J.; Iida, Shun; Iwatsuki-Horimoto, Kiyoko; Maemura, Tadashi; Kiso, Maki; Scheaffer, Suzanne M. et al. (2022): SARS-CoV-2 Omicron virus causes attenuated disease in mice and hamsters. In *Nature* 603 (7902), pp. 687–692. DOI: 10.1038/s41586-022-04441-6.

Haller, Otto; Kochs, Georg (2020): Mx genes: host determinants controlling influenza virus infection and trans-species transmission. In *Human genetics* 139 (6-7), pp. 695–705. DOI: 10.1007/s00439-019-02092-8.

Han, Yuling; Yang, Liuliu; Lacko, Lauretta A.; Chen, Shuibing (2022): Human organoid models to study SARS-CoV-2 infection. In *Nature methods* 19 (4), pp. 418–428. DOI: 10.1038/s41592-022-01453-y.

He, Ping; Wang, Guojun; Mo, Yanning; Yu, Qingxiong; Xiao, Xiong; Yang, Wenjuan et al. (2018): Novel triple-reassortant influenza viruses in pigs, Guangxi, China. In *Emerging Microbes & Infections* 7. DOI: 10.1038/s41426-018-0088-z.

Hefti, H. P.; Frese, M.; Landis, H.; Di Paolo, C.; Aguzzi, A.; Haller, O.; Pavlovic, J. (1999): Human MxA protein protects mice lacking a functional alpha/beta interferon system against La crosse virus and other lethal viral infections. In *Journal of Virology* 73 (8), pp. 6984–6991. DOI: 10.1128/JVI.73.8.6984-6991.1999.

Hemmink, Johanneke D.; Morgan, Sophie B.; Aramouni, Mario; Everett, Helen; Salguero, Francisco J.; Canini, Laetitia et al. (2016): Distinct immune responses and virus shedding in pigs following aerosol, intra-nasal and contact infection with pandemic swine influenza A virus, A(H1N1)09. In *Veterinary Research* 47. DOI: 10.1186/s13567-016-0390-5.

Hemmink, Johanneke D.; Whittaker, Catherine J.; Shelton, Holly A. (2018): Animal Models in Influenza Research. In *Methods in molecular biology (Clifton, N.J.)* 1836, pp. 401–430. DOI: 10.1007/978-1-4939-8678-1_20.

Hennig, Christin; Graaf, Annika; Petric, Philipp P.; Graf, Laura; Schwemmle, Martin; Beer, Martin; Harder, Timm (2022): Are pigs overestimated as a source of zoonotic influenza viruses? In *Porcine Health Management* 8. DOI: 10.1186/s40813-022-00274-x.

Henritzi, Dinah; Petric, Philipp Peter; Lewis, Nicola Sarah; Graaf, Annika; Pessia, Alberto; Starick, Elke et al. (2020): Surveillance of European Domestic Pig Populations Identifies an Emerging Reservoir of Potentially Zoonotic Swine Influenza A Viruses. In *Cell host & microbe* 28 (4), 614-627.e6. DOI: 10.1016/j.chom.2020.07.006.

Hill, Nichola J.; Bishop, Mary Anne; Trovão, Nídia S.; Ineson, Katherine M.; Schaefer, Anne L.; Puryear, Wendy B. et al. (2022): Ecological divergence of wild birds drives avian influenza spillover and global spread. In *PLoS pathogens* 18 (5), e1010062. DOI: 10.1371/journal.ppat.1010062.

Hoffmann, Donata; Corleis, Björn; Rauch, Susanne; Roth, Nicole; Mühe, Janine; Halwe, Nico Joel et al. (2021): CVnCoV and CV2CoV protect human ACE2 transgenic mice from ancestral B BavPat1 and emerging B.1.351 SARS-CoV-2. In *Nature communications* 12 (1), p. 4048. DOI: 10.1038/s41467-021-24339-7.

Hoffmann, Markus; Kleine-Weber, Hannah; Pöhlmann, Stefan (2020): A Multibasic Cleavage Site in the Spike Protein of SARS-CoV-2 Is Essential for Infection of Human Lung Cells. In *Molecular Cell* 78 (4), 779-784.e5. DOI: 10.1016/j.molcel.2020.04.022.

Hoffmann, Markus; Zhang, Lu; Pöhlmann, Stefan (2022): Omicron: Master of immune evasion maintains robust ACE2 binding. In *Signal transduction and targeted therapy* 7 (1), p. 118. DOI: 10.1038/s41392-022-00965-5.

Homme, P. J.; Easterday, B. C. (1970): Avian Influenza Virus Infections. I. Characteristics of Influenza A/Turkey/Wisconsin/1966 Virus. In *Avian diseases* 14 (1), p. 66. DOI: 10.2307/1588557.

Horimoto, T.; Nakayama, K.; Smeekens, S. P.; Kawaoka, Y. (1994): Proprotein-processing endoproteases PC6 and furin both activate hemagglutinin of virulent avian influenza viruses. In *Journal of Virology* 68 (9), pp. 6074–6078. DOI: 10.1128/JVI.68.9.6074-6078.1994.

Hosny, Farid A. (2016): Poultry sector country review. With assistance of FAO Animal Production and Health Division. Available online at https://www.fao.org/3/ai355e/ai355e.pdf.

Hou, Yixuan J.; Chiba, Shiho; Halfmann, Peter; Ehre, Camille; Kuroda, Makoto; Dinnon, Kenneth H. et al. (2020): SARS-CoV-2 D614G variant exhibits efficient replication ex vivo and transmission in vivo. In *Science (New York, N.Y.)* 370 (6523), pp. 1464–1468. DOI: 10.1126/science.abe8499.

Hu, Ben; Zeng, Lei-Ping; Yang, Xing-Lou; Ge, Xing-Yi; Zhang, Wei; Li, Bei et al. (2017): Discovery of a rich gene pool of bat SARS-related coronaviruses provides new insights into the origin of SARS coronavirus. In *PLoS pathogens* 13 (11), e1006698. DOI: 10.1371/journal.ppat.1006698.

Huang, Yuan; Yang, Chan; Xu, Xin-Feng; Xu, Wei; Liu, Shu-Wen (2020): Structural and functional properties of SARS-CoV-2 spike protein: potential antivirus drug development for COVID-19. In *Acta pharmacologica Sinica* 41 (9), pp. 1141–1149. DOI: 10.1038/s41401-020-0485-4.

Huson, Daniel H.; Bryant, David (2006): Application of phylogenetic networks in evolutionary studies. In *Molecular Biology and Evolution* 23 (2), pp. 254–267. DOI: 10.1093/molbev/msj030.

Hussein, Nur Ahmed; Ismail, Abdiwahid Mohamed; Jama, Saaid Said (2022): Assessment of Hepatitis B Vaccination Status and Associated Factors among Healthcare Workers in Bosaso, Puntland, Somalia 2020. In *BioMed Research International* 2022. DOI: 10.1155/2022/9074294.

ISIDProMed (2019): PRO/AH/EDR> Undiagnosed pneumonia - China (HU): RFI. ProMed International Society for Infetious Diseases. Available online at https://promedmail.org/promed-post/?id=6864153.

Iwatsuki-Horimoto, Kiyoko; Nakajima, Noriko; Ichiko, Yurie; Sakai-Tagawa, Yuko; Noda, Takeshi; Hasegawa, Hideki; Kawaoka, Yoshihiro (2018): Syrian Hamster as an Animal Model for the Study of Human Influenza Virus Infection. In *Journal of Virology* 92 (4). DOI: 10.1128/JVI.01693-17.

Jackson, Cody B.; Farzan, Michael; Chen, Bing; Choe, Hyeryun (2022): Mechanisms of SARS-CoV-2 entry into cells. In *Nature reviews. Molecular cell biology* 23 (1), pp. 3–20. DOI: 10.1038/s41580-021-00418-x.

Jester, Barbara J.; Uyeki, Timothy M.; Jernigan, Daniel B. (2020): Fifty Years of Influenza A(H3N2) Following the Pandemic of 1968. In *American Journal of Public Health* 110 (5), pp. 669–676. DOI: 10.2105/AJPH.2019.305557.

Jiang, Wenming; Liu, Shuo; Hou, Guangyu; Li, Jinping; Zhuang, Qingye; Wang, Suchun et al. (2012): Chinese and Global Distribution of H9 Subtype Avian Influenza Viruses. In *PloS one* 7 (12). DOI: 10.1371/journal.pone.0052671.

Jinjarak, Yothin; Noy, Ilan; Ta, Quy (2021): Pandemics and Economic Growth: Evidence from the 1968 H3N2 Influenza. In *Economics of Disasters and Climate Change* 6 (1), pp. 73–93. DOI: 10.1007/s41885-021-00096-1.

Johnson, Bryan A.; Xie, Xuping; Bailey, Adam L.; Kalveram, Birte; Lokugamage, Kumari G.; Muruato, Antonio et al. (2021): Loss of furin cleavage site attenuates SARS-CoV-2 pathogenesis. In *Nature* 591 (7849), pp. 293–299. DOI: 10.1038/s41586-021-03237-4.

Jones, Jeremy C.; Baranovich, Tatiana; Marathe, Bindumadhav M.; Danner, Angela F.; Seiler, Jon P.; Franks, John et al. (2014): Risk Assessment of H2N2 Influenza Viruses from the Avian Reservoir. In *Journal of Virology* 88 (2), pp. 1175–1188. DOI: 10.1128/JVI.02526-13.

Joseph, Udayan; Linster, Martin; Suzuki, Yuka; Krauss, Scott; Halpin, Rebecca A.; Vijaykrishna, Dhanasekaran et al. (2014): Adaptation of Pandemic H2N2 Influenza A Viruses in Humans. In *Journal of Virology* 89 (4), pp. 2442–2447. DOI: 10.1128/JVI.02590-14.

Jung, Christoph; Kmiec, Dorota; Koepke, Lennart; Zech, Fabian; Jacob, Timo; Sparrer, Konstantin M. J.; Kirchhoff, Frank (2022): Omicron: What Makes the Latest SARS-CoV-2 Variant of Concern So Concerning? In *Journal of Virology* 96 (6), e0207721. DOI: 10.1128/jvi.02077-21.

Juozapaitis, Mindaugas; Aguiar Moreira, Étori; Mena, Ignacio; Giese, Sebastian; Riegger, David; Pohlmann, Anne et al. (2014): An infectious bat-derived chimeric influenza virus harbouring the entry machinery of an influenza A virus. In *Nature communications* 5. DOI: 10.1038/ncomms5448.

Kalthoff, Donata; Grund, Christian; Harder, Timm C.; Lange, Elke; Vahlenkamp, Thomas W.; Mettenleiter, Thomas C.; Beer, Martin (2010): Limited Susceptibility of Chickens, Turkeys, and Mice to Pandemic (H1N1) 2009 Virus. In *Emerging Infectious Diseases* 16 (4), pp. 703–705. DOI: 10.3201/eid1604.091491.

Kamins, A. O.; Restif, O.; Ntiamoa-Baidu, Y.; Suu-Ire, R.; Hayman, D. T. S.; Cunningham, A. A. et al. (2011): Uncovering the fruit bat bushmeat commodity chain and the true extent of fruit bat hunting in Ghana, West Africa. In *Biological conservation* 144 (12), pp. 3000–3008. DOI: 10.1016/j.biocon.2011.09.003.

Kan, Biao; Wang, Ming; Jing, Huaiqi; Xu, Huifang; Jiang, Xiugao; Yan, Meiying et al. (2005): Molecular Evolution Analysis and Geographic Investigation of Severe Acute Respiratory Syndrome Coronavirus-Like Virus in Palm Civets at an Animal Market and on Farms‡. In *Journal of Virology* 79 (18), pp. 11892–11900. DOI: 10.1128/JVI.79.18.11892-11900.2005.

Kandeil, Ahmed; Gomaa, Mokhtar R.; Shehata, Mahmoud M.; El Taweel, Ahmed N.; Mahmoud, Sara H.; Bagato, Ola et al. (2019): Isolation and Characterization of a Distinct Influenza A Virus from Egyptian Bats. In *Journal of Virology* 93 (2). DOI: 10.1128/JVI.01059-18.

Karakus, Umut; Thamamongood, Thiprampai; Ciminski, Kevin; Ran, Wei; Günther, Sira C.; Pohl, Marie O. et al. (2019): MHC class II proteins mediate cross-species entry of bat influenza viruses. In *Nature* 567 (7746), pp. 109–112. DOI: 10.1038/s41586-019-0955-3.

Kash, John C.; Basler, Christopher F.; García-Sastre, Adolfo; Carter, Victoria; Billharz, Rosalind; Swayne, David E. et al. (2004): Global Host Immune Response: Pathogenesis and Transcriptional Profiling of Type A Influenza Viruses Expressing the Hemagglutinin and Neuraminidase Genes from the 1918 Pandemic Virus. In *Journal of Virology* 78 (17), pp. 9499–9511. DOI: 10.1128/JVI.78.17.9499-9511.2004.

Kash, John C.; Tumpey, Terrence M.; Proll, Sean C.; Carter, Victoria; Perwitasari, Olivia; Thomas, Matthew J. et al. (2006): Genomic analysis of increased host immune and cell death responses induced by 1918 influenza virus. In *Nature* 443 (7111), pp. 578–581. DOI: 10.1038/nature05181.

Kawaoka, Y.; Krauss, S.; Webster, R. G. (1989): Avian-to-human transmission of the PB1 gene of influenza A viruses in the 1957 and 1968 pandemics. In *Journal of Virology* 63 (11), pp. 4603–4608.

Kim, Jeong-Ki; Negovetich, Nicholas J.; Forrest, Heather L.; Webster, Robert G. (2009): Ducks: The "Trojan Horses" of H5N1 influenza. In *Influenza and Other Respiratory Viruses* 3 (4), pp. 121–128. DOI: 10.1111/j.1750-2659.2009.00084.x.

Kim, Jihoon; Koo, Bon-Kyoung; Knoblich, Juergen A. (2020): Human organoids: model systems for human biology and medicine. In *Nature reviews. Molecular cell biology* 21 (10), pp. 571–584. DOI: 10.1038/s41580-020-0259-3.

King, Jacqueline; Staubach, Christoph; Lüder, Christiane; Koethe, Susanne; Günther, Anne; Stacker, Lina et al. (2022): Connect to Protect: Dynamics and Genetic Connections of Highly Pathogenic Avian Influenza Outbreaks in Poultry from 2016 to 2021 in Germany. In *Viruses* 14 (9). DOI: 10.3390/v14091849.

Kirsebom, Freja C. M.; Andrews, Nick; Stowe, Julia; Toffa, Samuel; Sachdeva, Ruchira; Gallagher, Eileen et al. (2022): COVID-19 vaccine effectiveness against the omicron (BA.2) variant in England. In *The Lancet. Infectious diseases* 22 (7), pp. 931–933. DOI: 10.1016/S1473-3099(22)00309-7.

Klenk, H. D.; Garten, W. (1994): Host cell proteases controlling virus pathogenicity. In *Trends in microbiology* 2 (2), pp. 39–43. DOI: 10.1016/0966-842X(94)90123-6.

Klenk, H.-D.; Matrosovich, M. N.; Stech, J. (2008): Avian Influenza: S. Karger AG (27).

Korber, Bette; Fischer, Will M.; Gnanakaran, Sandrasegaram; Yoon, Hyejin; Theiler, James; Abfalterer, Werner et al. (2020): Tracking Changes in SARS-CoV-2 Spike: Evidence that D614G Increases Infectivity of the COVID-19 Virus. In *Cell* 182 (4), 812-827.e19. DOI: 10.1016/j.cell.2020.06.043.

Kroidl, Inge; Mecklenburg, Ingo; Schneiderat, Peter; Müller, Katharina; Girl, Philipp; Wölfel, Roman et al. (2021): Vaccine breakthrough infection and onward transmission of SARS-CoV-2 Beta (B.1.351) variant, Bavaria, Germany, February to March 2021. In *Euro surveillance : bulletin Europeen sur les maladies transmissibles = European communicable disease bulletin* 26 (30). DOI: 10.2807/1560-7917.ES.2021.26.30.2100673.

Kuchipudi, Suresh V.; Nelli, Rahul K.; Gontu, Abhinay; Satyakumar, Rashmi; Surendran Nair, Meera; Subbiah, Murugan (2021): Sialic Acid Receptors: The Key to Solving the Enigma of Zoonotic Virus Spillover. In *Viruses* 13 (2). DOI: 10.3390/v13020262.

Kumar, Suresh; Karuppanan, Kalimuthu; Subramaniam, Gunasekaran (2022): Omicron (BA.1) and sub-variants (BA.1.1, BA.2, and BA.3) of SARS-CoV-2 spike infectivity and pathogenicity: A comparative sequence and structural-based computational assessment. In *Journal of medical virology* 94 (10), pp. 4780–4791. DOI: 10.1002/jmv.27927.

Kurhade, Chaitanya; Zou, Jing; Xia, Hongjie; Cai, Hui; Yang, Qi; Cutler, Mark et al. (2022): Neutralization of Omicron BA.1, BA.2, and BA.3 SARS-CoV-2 by 3 doses of BNT162b2 vaccine. In *Nature communications* 13 (1), p. 3602. DOI: 10.1038/s41467-022-30681-1.

Kutter, Jasmin S.; Meulder, Dennis de; Bestebroer, Theo M.; Lexmond, Pascal; Mulders, Ard; Richard, Mathilde et al. (2021a): SARS-CoV and SARS-CoV-2 are transmitted through the air between ferrets over more than one meter distance. In *Nature communications* 12 (1), p. 1653. DOI: 10.1038/s41467-021-21918-6.

Kutter, Jasmin S.; Meulder, Dennis de; Bestebroer, Theo M.; van Kampen, Jeroen J. A.; Molenkamp, Richard; Fouchier, Ron A. M. et al. (2021b): Small quantities of respiratory syncytial virus RNA only in large droplets around infants hospitalized with acute respiratory infections. In *Antimicrobial resistance and infection control* 10 (1), p. 100. DOI: 10.1186/s13756-021-00968-x.

Kutter, Jasmin S.; Spronken, Monique I.; Fraaij, Pieter L.; Fouchier, Ron am; Herfst, Sander (2018): Transmission routes of respiratory viruses among humans. In *Current Opinion in Virology* 28, pp. 142–151. DOI: 10.1016/j.coviro.2018.01.001.

Lal, Arush; Ashworth, Henry C.; Dada, Sara; Hoemeke, Laura; Tambo, Ernest (2020): Optimizing Pandemic Preparedness and Response Through Health Information Systems: Lessons Learned From Ebola to COVID-19. In *Disaster Medicine and Public Health Preparedness*, pp. 1–8. DOI: 10.1017/dmp.2020.361.

Laleye, Agnes Tinuke; Abolnik, Celia (2020): Emergence of highly pathogenic H5N2 and H7N1 influenza A viruses from low pathogenic precursors by serial passage in ovo. In *PloS one* 15 (10). DOI: 10.1371/journal.pone.0240290.

Lange, Elke; Kalthoff, Donata; Blohm, Ulrike; Teifke, Jens P.; Breithaupt, Angele; Maresch, Christina et al. (2009): Pathogenesis and transmission of the novel swine-origin influenza virus A/H1N1 after experimental infection of pigs. In *The Journal of General Virology* 90 (Pt 9), pp. 2119–2123. DOI: 10.1099/vir.0.014480-0.

Lau, Susanna K. P.; Woo, Patrick C. Y.; Li, Kenneth S. M.; Huang, Yi; Tsoi, Hoi-Wah; Wong, Beatrice H. L. et al. (2005): Severe acute respiratory syndrome coronavirus-like virus in Chinese horseshoe bats. In *Proceedings of the National Academy of Sciences of the United States of America* 102 (39), pp. 14040–14045. DOI: 10.1073/pnas.0506735102.

Le Sage, Valerie; Jones, Jennifer E.; Kormuth, Karen A.; Fitzsimmons, William J.; Nturibi, Eric; Padovani, Gabriella H. et al. (2021): Pre-existing heterosubtypic immunity provides a barrier to airborne transmission of influenza viruses. In *PLoS pathogens* 17 (2), e1009273. DOI: 10.1371/journal.ppat.1009273.

Lemieux, Jacob E.; Siddle, Katherine J.; Shaw, Bennett M.; Loreth, Christine; Schaffner, Stephen F.; Gladden-Young, Adrianne et al. (2020): Phylogenetic analysis of SARS-CoV-2 in Boston highlights the impact of superspreading events. In *Science (New York, N.Y.)*. DOI: 10.1126/science.abe3261.

Leroy, Eric M.; Kumulungui, Brice; Pourrut, Xavier; Rouquet, Pierre; Hassanin, Alexandre; Yaba, Philippe et al. (2005): Fruit bats as reservoirs of Ebola virus. In *Nature* 438 (7068), pp. 575–576. DOI: 10.1038/438575a.

Li, Aqian; Dai, Xinxian; Chen, Lei; Liu, Lin; Li, Chuan; Liu, Yang et al. (2022a): Immunogenicity and protective efficacy of an inactivated SFTS vaccine candidate in mice. In *Biosafety and Health* 4 (1), pp. 45–52. DOI: 10.1016/j.bsheal.2021.12.008.

Li, Chong; Wang, Shuoguo; Bing, Guoxia; Carter, Robert A.; Wang, Zejiang; Wang, Jinliang et al. (2017): Genetic evolution of influenza H9N2 viruses isolated from various hosts in China from 1994 to 2013. In *Emerging Microbes & Infections* 6 (11), e106. DOI: 10.1038/emi.2017.94.

Li, Lei; Honda-Okubo, Yoshikazu; Huang, Ying; Jang, Hyesun; Carlock, Michael A.; Baldwin, Jeremy et al. (2021): Immunisation of ferrets and mice with recombinant SARS-CoV-2 spike protein formulated with Advax-SM adjuvant protects against COVID-19 infection. In *Vaccine* 39 (40), pp. 5940–5953. DOI: 10.1016/j.vaccine.2021.07.087.

Li, Linjie; Liao, Hanyi; Meng, Yumin; Li, Weiwei; Han, Pengcheng; Liu, Kefang et al. (2022b): Structural basis of human ACE2 higher binding affinity to currently circulating Omicron SARS-CoV-2 sub-variants BA.2 and BA.1.1. In *Cell* 185 (16), 2952-2960.e10. DOI: 10.1016/j.cell.2022.06.023.

Li, Wendong; Shi, Zhengli; Yu, Meng; Ren, Wuze; Smith, Craig; Epstein, Jonathan H. et al. (2005): Bats are natural reservoirs of SARS-like coronaviruses. In *Science (New York, N.Y.)* 310 (5748), pp. 676–679. DOI: 10.1126/science.1118391.

Liao, Y.; Yuan, Q.; Torres, J.; Tam, J. P.; Liu, D. X. (2006): Biochemical and functional characterization of the membrane association and membrane permeabilizing activity of the severe acute respiratory syndrome coronavirus envelope protein. In *Virology* 349 (2), pp. 264–275. DOI: 10.1016/j.virol.2006.01.028.

Lin, Ruey-Wen; Chen, Guang-Wu; Sung, Hsiang-Hsuan; Lin, Ren-Jye; Yen, Li-Chen; Tseng, Yu-Ling et al. (2019): Naturally occurring mutations in PB1 affect influenza A virus replication fidelity, virulence, and adaptability. In *Journal of biomedical science* 26 (1), p. 55. DOI: 10.1186/s12929-019-0547-4.

Lindsley, William G.; Blachere, Francoise M.; Beezhold, Donald H.; Thewlis, Robert E.; Noorbakhsh, Bahar; Othumpangat, Sreekumar et al. (2016): Viable influenza A virus in airborne particles expelled during coughs versus exhalations. In *Influenza and Other Respiratory Viruses* 10 (5), pp. 404–413. DOI: 10.1111/irv.12390.

Lindstrom, Stephen E.; Cox, Nancy J.; Klimov, Alexander (2004): Genetic analysis of human H2N2 and early H3N2 influenza viruses, 1957-1972: evidence for genetic divergence and multiple reassortment events. In *Virology* 328 (1), pp. 101–119. DOI: 10.1016/j.virol.2004.06.009.

Liu, Haolin; Wei, Pengcheng; Kappler, John W.; Marrack, Philippa; Zhang, Gongyi (2022a): SARS-CoV-2 Variants of Concern and Variants of Interest Receptor Binding Domain Mutations and Virus Infectivity. In *Frontiers in immunology* 13, p. 825256. DOI: 10.3389/fimmu.2022.825256.

Liu, Wen-Chun; Nachbagauer, Raffael; Stadlbauer, Daniel; Strohmeier, Shirin; Solórzano, Alicia; Berlanda-Scorza, Francesco et al. (2021a): Chimeric Hemagglutinin-Based Live-Attenuated Vaccines Confer Durable Protective Immunity against Influenza A Viruses in a Preclinical Ferret Model. In *Vaccines* 9 (1). DOI: 10.3390/vaccines9010040.

Liu, William J.; Xiao, Haixia; Dai, Lianpan; Di Liu; Chen, Jianjun; Qi, Xiaopeng et al. (2021b): Avian influenza A (H7N9) virus: from low pathogenic to highly pathogenic. In *Frontiers of medicine* 15 (4), pp. 507–527. DOI: 10.1007/s11684-020-0814-5.

Liu, Yang; Liu, Jianying; Johnson, Bryan A.; Xia, Hongjie; Ku, Zhiqiang; Schindewolf, Craig et al. (2022b): Delta spike P681R mutation enhances SARS-CoV-2 fitness over Alpha variant. In *Cell reports* 39 (7), p. 110829. DOI: 10.1016/j.celrep.2022.110829.

Liu, Yang; Liu, Jianying; Plante, Kenneth S.; Plante, Jessica A.; Xie, Xuping; Zhang, Xianwen et al. (2022c): The N501Y spike substitution enhances SARS-CoV-2 infection and transmission. In *Nature* 602 (7896), pp. 294–299. DOI: 10.1038/s41586-021-04245-0.

Lopez Moreno, Gustavo; Nirmala, Jayaveeramuthu; Goodell, Christa; Culhane, Marie; Torremorell, Montserrat (2021): Shedding and transmission of a live attenuated influenza A virus vaccine in pre-weaned pigs under field conditions. In *PloS one* 16 (2). DOI: 10.1371/journal.pone.0246690.

Louten, Jennifer (2016): Virus Transmission and Epidemiology. In *Essential Human Virology*, pp. 71–92. DOI: 10.1016/B978-0-12-800947-5.00005-3.

Luis, Angela D.; O'Shea, Thomas J.; Hayman, David T. S.; Wood, James L. N.; Cunningham, Andrew A.; Gilbert, Amy T. et al. (2015): Network analysis of host-virus communities in bats and rodents reveals determinants of cross-species transmission. In *Ecology letters* 18 (11), pp. 1153–1162. DOI: 10.1111/ele.12491.

Ma, Wenjun; Kahn, Robert E.; Richt, Juergen A. (2008): The pig as a mixing vessel for influenza viruses: Human and veterinary implications. In *Journal of molecular and genetic medicine : an international journal of biomedical research* 3 (1), pp. 158–166.

MacLean, Oscar A.; Lytras, Spyros; Weaver, Steven; Singer, Joshua B.; Boni, Maciej F.; Lemey, Philippe et al. (2021): Natural selection in the evolution of SARS-CoV-2 in bats created a generalist virus and highly capable human pathogen. In *PLoS biology* 19 (3), e3001115. DOI: 10.1371/journal.pbio.3001115.

Magaña-Guerrero, Fátima Sofía; Quiroz-Mercado, Joaquín; Garfias-Zenteno, Nicolás; Garfias, Yonathan (2020): Comparative analysis of inflammatory response in the BALB/c and C57BL/6 mouse strains in an endotoxin-induced uveitis model. In *Journal of immunological methods* 476, p. 112677. DOI: 10.1016/j.jim.2019.112677.

Magouras, Ioannis; Brookes, Victoria J.; Jori, Ferran; Martin, Angela; Pfeiffer, Dirk Udo; Dürr, Salome (2020): Emerging Zoonotic Diseases: Should We Rethink the Animal-Human Interface? In *Frontiers in veterinary science* 7, p. 582743. DOI: 10.3389/fvets.2020.582743.

Maher, John A.; DeStefano, Joanne (2004): The ferret: an animal model to study influenza virus. In *Lab animal* 33 (9), pp. 50–53. DOI: 10.1038/laban1004-50.

Malone, Brandon; Urakova, Nadya; Snijder, Eric J.; Campbell, Elizabeth A. (2022): Structures and functions of coronavirus replication-transcription complexes and their relevance for SARS-CoV-2 drug design. In *Nature reviews. Molecular cell biology* 23 (1), pp. 21–39. DOI: 10.1038/s41580-021-00432-z.

Mandl, Judith N.; Ahmed, Rafi; Barreiro, Luis B.; Daszak, Peter; Epstein, Jonathan H.; Virgin, Herbert W.; Feinberg, Mark B. (2014): Reservoir Host Immune Responses to Emerging Zoonotic Viruses. In *Cell* 160 (1), pp. 20–35. DOI: 10.1016/j.cell.2014.12.003.

Mandl, Judith N.; Schneider, Caitlin; Schneider, David S.; Baker, Michelle L. (2018): Going to Bat(s) for Studies of Disease Tolerance. In *Frontiers in immunology* 9, p. 2112. DOI: 10.3389/fimmu.2018.02112.

Manzoor, Rashid; Igarashi, Manabu; Takada, Ayato (2017): Influenza A Virus M2 Protein: Roles from Ingress to Egress. In *International journal of molecular sciences* 18 (12). DOI: 10.3390/ijms18122649.

Mao, Binli; Le-Trilling, Vu Thuy Khanh; Wang, Kai; Mennerich, Denise; Hu, Jie; Zhao, Zhenyu et al. (2022): Obatoclax inhibits SARS-CoV-2 entry by altered endosomal acidification and impaired cathepsin and furin activity in vitro. In *Emerging Microbes & Infections* 11 (1), pp. 483–497. DOI: 10.1080/22221751.2022.2026739.

Margine, Irina; Krammer, Florian (2014): Animal Models for Influenza Viruses: Implications for Universal Vaccine Development. In *Pathogens* 3 (4), pp. 845–874. DOI: 10.3390/pathogens3040845.

Marí Saéz, Almudena; Weiss, Sabrina; Nowak, Kathrin; Lapeyre, Vincent; Zimmermann, Fee; Düx, Ariane et al. (2015): Investigating the zoonotic origin of the West African Ebola epidemic. In *EMBO molecular medicine* 7 (1), pp. 17–23. DOI: 10.15252/emmm.201404792.

Marshall, Nicolle; Priyamvada, Lalita; Ende, Zachary; Steel, John; Lowen, Anice C. (2013): Influenza Virus Reassortment Occurs with High Frequency in the Absence of Segment Mismatch. In *PLoS pathogens* 9 (6). DOI: 10.1371/journal.ppat.1003421.

Maruggi, Giulietta; Mallett, Corey P.; Westerbeck, Jason W.; Chen, Tiffany; Lofano, Giuseppe; Friedrich, Kristian et al. (2022): A self-amplifying mRNA SARS-CoV-2 vaccine candidate induces safe and robust protective immunity in preclinical models. In *Molecular Therapy* 30 (5), pp. 1897–1912. DOI: 10.1016/j.ymthe.2022.01.001.

Matrosovich, Mikhail N.; Matrosovich, Tatyana Y.; Gray, Thomas; Roberts, Noel A.; Klenk, Hans-Dieter (2004): Neuraminidase Is Important for the Initiation of Influenza Virus Infection in Human Airway Epithelium. In *Journal of Virology* 78 (22), pp. 12665–12667. DOI: 10.1128/JVI.78.22.12665-12667.2004.

McAuley, Julie L.; Gilbertson, Brad P.; Trifkovic, Sanja; Brown, Lorena E.; McKimm-Breschkin, Jennifer L. (2019): Influenza Virus Neuraminidase Structure and Functions. In *Frontiers in microbiology* 10, p. 39. DOI: 10.3389/fmicb.2019.00039.

McCallum, Matthew; Walls, Alexandra C.; Sprouse, Kaitlin R.; Bowen, John E.; Rosen, Laura E.; Dang, Ha V. et al. (2021): Molecular basis of immune evasion by the Delta and Kappa SARS-CoV-2 variants. In *Science (New York, N.Y.)* 374 (6575), pp. 1621–1626. DOI: 10.1126/science.abl8506.

McGuire, Liam P.; Fuller, Nathan W.; Dzal, Yvonne A.; Haase, Catherine G.; Silas, Kirk A.; Willis, Craig K. R. et al. (2022): Similar hibernation physiology in bats across broad geographic ranges. In *Journal of comparative physiology. B, Biochemical, systemic, and environmental physiology* 192 (1), pp. 171–181. DOI: 10.1007/s00360-021-01400-x.

Memish, Ziad A.; Mishra, Nischay; Olival, Kevin J.; Fagbo, Shamsudeen F.; Kapoor, Vishal; Epstein, Jonathan H. et al. (2013): Middle East respiratory syndrome coronavirus in bats, Saudi Arabia. In *Emerging Infectious Diseases* 19 (11), pp. 1819–1823. DOI: 10.3201/eid1911.131172.

Michelitsch, Anna; Wernike, Kerstin; Ulrich, Lorenz; Mettenleiter, Thomas C.; Beer, Martin (2021): SARS-CoV-2 in animals: From potential hosts to animal models. In *Advances in virus research* 110, pp. 59–102. DOI: 10.1016/bs.aivir.2021.03.004.

Møller Kirsebom, Freja Cordelia; Andrews, Nick; Stowe, Julia; Groves, Natalie; Chand, Meera; Ramsay, Mary; Bernal, Jamie Lopez (2022): Effectiveness of the COVID-19 vaccines against hospitalisation with Omicron sub-lineages BA.4 and BA.5 in England. In *The Lancet regional health. Europe* 23, p. 100537. DOI: 10.1016/j.lanepe.2022.100537.

Morales, Antonio C.; Hilt, Deborah A.; Williams, Susan M.; Pantin-Jackwood, Mary J.; Suarez, David L.; Spackman, Erica et al. (2009): Biologic characterization of H4, H6, and H9 type low pathogenicity avian influenza viruses from wild birds in chickens and turkeys. In *Avian diseases* 53 (4), pp. 552–562. DOI: 10.1637/8877-041509-Reg.1.

Morens, David M.; Fauci, Anthony S. (2020): Emerging Pandemic Diseases: How We Got to COVID-19. In *Cell* 182 (5), pp. 1077–1092. DOI: 10.1016/j.cell.2020.08.021.

Mostafa, Ahmed; Blaurock, Claudia; Scheibner, David; Müller, Christin; Blohm, Ulrike; Schäfer, Alexander et al. (2020): Genetic incompatibilities and reduced transmission in chickens may limit the evolution of reassortants between H9N2 and panzootic H5N8 clade 2.3.4.4 avian influenza virus showing high virulence for mammals. In *Virus Evolution* 6 (2). DOI: 10.1093/ve/veaa077.

Muik, Alexander; Lui, Bonny Gaby; Bacher, Maren; Wallisch, Ann-Kathrin; Toker, Aras; Couto, Carla Iris Cadima et al. (2022): Exposure to BA.4/5 S protein drives neutralization of Omicron BA.1, BA.2, BA.2.12.1, and BA.4/5 in vaccine-experienced humans and mice. In *Science immunology* 7 (78), eade9888. DOI: 10.1126/sciimmunol.ade9888.

Muñoz-Fontela, César; Dowling, William E.; Funnell, Simon G. P.; Gsell, Pierre-S; Riveros-Balta, A. Ximena; Albrecht, Randy A. et al. (2020): Animal models for COVID-19. In *Nature* 586 (7830), pp. 509–515. DOI: 10.1038/s41586-020-2787-6.

Munster, Vincent J.; Adney, Danielle R.; van Doremalen, Neeltje; Brown, Vienna R.; Miazgowicz, Kerri L.; Milne-Price, Shauna et al. (2016): Replication and shedding of MERS-CoV in Jamaican fruit bats (Artibeus jamaicensis). In *Scientific reports* 6, p. 21878. DOI: 10.1038/srep21878.

Nelson, Martha I.; Vincent, Amy L. (2015): Reverse zoonosis of influenza to swine: new perspectives on the human-animal interface. In *Trends in microbiology* 23 (3), pp. 142–153. DOI: 10.1016/j.tim.2014.12.002.

Nelson, Martha I.; Worobey, Michael (2018): Origins of the 1918 Pandemic: Revisiting the Swine "Mixing Vessel" Hypothesis. In *American journal of epidemiology* 187 (12), pp. 2498–2502. DOI: 10.1093/aje/kwy150.

Neuman, Benjamin W.; Kiss, Gabriella; Kunding, Andreas H.; Bhella, David; Baksh, M. Fazil; Connelly, Stephen et al. (2010): A structural analysis of M protein in coronavirus assembly and morphology. In *Journal of Structural Biology* 174 (1), pp. 11–22. DOI: 10.1016/j.jsb.2010.11.021.

Nguyen, Thi-Quyen; Rollon, Rare; Choi, Young-Ki (2021): Animal Models for Influenza Research: Strengths and Weaknesses. In *Viruses* 13 (6). DOI: 10.3390/v13061011.

Noton, Sarah L.; Medcalf, Elizabeth; Fisher, Dawn; Mullin, Anne E.; Elton, Debra; Digard, Paul (2007): Identification of the domains of the influenza A virus M1 matrix protein required for NP binding, oligomerization and incorporation into virions. In *The Journal of General Virology* 88 (Pt 8), pp. 2280–2290. DOI: 10.1099/vir.0.82809-0.

O'Donnell, Kyle L.; Pinski, Amanda N.; Clancy, Chad S.; Gourdine, Tylisha; Shifflett, Kyle; Fletcher, Paige et al. (2021): Pathogenic and transcriptomic differences of emerging SARS-CoV-2 variants in the Syrian golden hamster model. In *EBioMedicine* 73, p. 103675. DOI: 10.1016/j.ebiom.2021.103675.

Okda, Faten A.; Perry, S. Scott; Webby, Richard J.; Russell, Charles J. (2021): Interplay between H1N1 influenza a virus infection, extracellular and intracellular respiratory tract pH, and host responses in a mouse model. In *PloS one* 16 (5), e0251473. DOI: 10.1371/journal.pone.0251473.

Olivero, Jesús; Fa, Julia E.; Farfán, Miguel Á.; Márquez, Ana L.; Real, Raimundo; Juste, F. Javier et al. (2020): Human activities link fruit bat presence to Ebola virus disease outbreaks. In *Mam Rev* 50 (1), pp. 1–10. DOI: 10.1111/mam.12173.

Olsen, Björn; Munster, Vincent J.; Wallensten, Anders; Waldenström, Jonas; Osterhaus, Albert D. M. E.; Fouchier, Ron A. M. (2006): Global patterns of influenza a virus in wild birds. In *Science (New York, N.Y.)* 312 (5772), pp. 384–388. DOI: 10.1126/science.1122438.

Overbey, Katie N.; Zachos, Nicholas C.; Coulter, Caroline; Jacangelo, Joseph; Schwab, Kellogg J. (2021): Recovery of Infectious Human Norovirus GII.4 Sydney From Fomites via Replication in Human Intestinal Enteroids. In *Frontiers in cellular and infection microbiology* 11, p. 693090. DOI: 10.3389/fcimb.2021.693090.

Palese, P.; Tobita, K.; Ueda, M.; Compans, R. W. (1974): Characterization of temperature sensitive influenza virus mutants defective in neuraminidase. In *Virology* 61 (2), pp. 397–410. DOI: 10.1016/0042-6822(74)90276-1.

Pantin-Jackwood, Mary J.; Stephens, Christopher B.; Bertran, Kateri; Swayne, David E.; Spackman, Erica (2017): The pathogenesis of H7N8 low and highly pathogenic avian influenza viruses from the United States 2016 outbreak in chickens, turkeys and mallards. In *PloS one* 12 (5). DOI: 10.1371/journal.pone.0177265.

Parker, Matthew D.; Lindsey, Benjamin B.; Leary, Shay; Gaudieri, Silvana; Chopra, Abha; Wyles, Matthew et al. (2021): Subgenomic RNA identification in SARS-CoV-2 genomic sequencing data. In *Genome Research* 31 (4), pp. 645–658. DOI: 10.1101/gr.268110.120.

Pavlovic, J.; Zürcher, T.; Haller, O.; Staeheli, P. (1990): Resistance to influenza virus and vesicular stomatitis virus conferred by expression of human MxA protein. In *Journal of Virology* 64 (7), pp. 3370–3375. DOI: 10.1128/jvi.64.7.3370-3375.1990.

Peacock, Thomas P.; Goldhill, Daniel H.; Zhou, Jie; Baillon, Laury; Frise, Rebecca; Swann, Olivia C. et al. (2021): The furin cleavage site in the SARS-CoV-2 spike protein is required for transmission in ferrets. In *Nature microbiology* 6 (7), pp. 899–909. DOI: 10.1038/s41564-021-00908-w.

Peiris, J. S.M.; Lai, S. T.; Poon, L. L.M.; Guan, Y.; Yam, L. Y.C.; Lim, W. et al. (2003): Coronavirus as a possible cause of severe acute respiratory syndrome. In *The Lancet* 361 (9366), pp. 1319–1325. DOI: 10.1016/S0140-6736(03)13077-2.

Pekar, Jonathan E.; Magee, Andrew; Parker, Edyth; Moshiri, Niema; Izhikevich, Katherine; Havens, Jennifer L. et al. (2022): The molecular epidemiology of multiple zoonotic origins of SARS-CoV-2. In *Science (New York, N.Y.)* 377 (6609), pp. 960–966. DOI: 10.1126/science.abp8337.

Phan, Lan T.; Nguyen, Thuong V.; Luong, Quang C.; Nguyen, Thinh V.; Nguyen, Hieu T.; Le, Hung Q. et al. (2020): Importation and Human-to-Human Transmission of a Novel Coronavirus in Vietnam. In *The New England journal of medicine* 382 (9), pp. 872–874. DOI: 10.1056/nejmc2001272.

Pickering, Brad S.; Spengler, Jessica R.; Shadabi, Elnaz; Dalziel, Antonia E.; Lautner, Elizabeth A.; Silva, Primal (2019): The Biosafety Level 4 Zoonotic Laboratory Network (BSL4ZNet): Report of a workshop on live animal handling. In *Antiviral research* 172, p. 104640. DOI: 10.1016/j.antiviral.2019.104640.

Pickering, Bradley; Lung, Oliver; Maguire, Finlay; Kruczkiewicz, Peter; Kotwa, Jonathon D.; Buchanan, Tore et al. (2022): Divergent SARS-CoV-2 variant emerges in white-tailed deer with deer-to-human transmission. In *Nature microbiology* 7 (12), pp. 2011–2024. DOI: 10.1038/s41564-022-01268-9.

Pinto, Lawrence H.; Lamb, Robert A. (2006): The M2 proton channels of influenza A and B viruses. In *The Journal of biological chemistry* 281 (14), pp. 8997–9000. DOI: 10.1074/jbc.R500020200.

Piret, Jocelyne; Boivin, Guy (2020): Pandemics Throughout History. In *Frontiers in microbiology* 11, p. 631736. DOI: 10.3389/fmicb.2020.631736.

Pohlmann, Anne; King, Jacqueline; Fusaro, Alice; Zecchin, Bianca; Banyard, Ashley C.; Brown, Ian H. et al. (2022): Has Epizootic Become Enzootic? Evidence for a Fundamental Change in the Infection Dynamics of Highly Pathogenic Avian Influenza in Europe, 2021. In *mBio* 13 (4), e0060922. DOI: 10.1128/mbio.00609-22.

Powell, F. L.; Rothwell, L.; Clarkson, M. J.; Kaiser, P. (2009): The turkey, compared to the chicken, fails to mount an effective early immune response to Histomonas meleagridis in the gut. In *Parasite immunology* 31 (6), pp. 312–327. DOI: 10.1111/j.1365-3024.2009.01113.x.

Prather, Kimberly A.; Marr, Linsey C.; Schooley, Robert T.; McDiarmid, Melissa A.; Wilson, Mary E.; Milton, Donald K. (2020): Airborne transmission of SARS-CoV-2. In *Science (New York, N.Y.)* 370 (6514), pp. 303–304. DOI: 10.1126/science.abf0521#:~:text=They%20are%20highly%20concentrated%20near.

Puzelli, Simona; Rossini, Giada; Facchini, Marzia; Vaccari, Gabriele; Di Trani, Livia; Di Martino, Angela et al. (2014): Human Infection with Highly Pathogenic A(H7N7) Avian Influenza Virus, Italy, 2013. In *Emerging Infectious Diseases* 20 (10), pp. 1745–1749. DOI: 10.3201/eid2010.140512.

Rademan, Rochelle; Geldenhuys, Marike; Markotter, Wanda (2023): Detection and Characterization of an H9N2 Influenza A Virus in the Egyptian Rousette Bat in Limpopo, South Africa. In *Viruses* 15 (2), p. 498. DOI: 10.3390/v15020498.

Rajao, Daniela S.; Vincent, Amy L. (2015): Swine as a model for influenza A virus infection and immunity. In *ILAR journal* 56 (1), pp. 44–52. DOI: 10.1093/ilar/ilv002.

Ran, Wei; Schön, Jacob; Ciminski, Kevin; Kraft, Julian; Kessler, Susanne; Euchner, Sophie et al. (2022): Generation of an Attenuated Chimeric Bat Influenza A Virus Live-Vaccine Prototype. In *Microbiology spectrum* 10 (6), e0142422. DOI: 10.1128/spectrum.01424-22.

Randazzo, W.; Sánchez, G. (2020): Hepatitis A infections from food. In *Journal of applied microbiology* 129 (5), pp. 1120–1132. DOI: 10.1111/jam.14727.

Rascovan, Nicolás; Sjögren, Karl-Göran; Kristiansen, Kristian; Nielsen, Rasmus; Willerslev, Eske; Desnues, Christelle; Rasmussen, Simon (2019): Emergence and Spread of Basal Lineages of Yersinia pestis during the Neolithic Decline. In *Cell* 176 (1-2), 295-305.e10. DOI: 10.1016/j.cell.2018.11.005.

Redondo, Natalia; Zaldívar-López, Sara; Garrido, Juan J.; Montoya, Maria (2021): SARS-CoV-2 Accessory Proteins in Viral Pathogenesis: Knowns and Unknowns. In *Frontiers in immunology* 12, p. 708264. DOI: 10.3389/fimmu.2021.708264.

Reid, Ann H.; Taubenberger, Jeffery K.; Fanning, Thomas G. (2004): Evidence of an absence: the genetic origins of the 1918 pandemic influenza virus. In *Nature reviews. Microbiology* 2 (11), pp. 909–914. DOI: 10.1038/nrmicro1027.

Ren, Wenlin; Zhu, Yunkai; Wang, Yuyan; Shi, Hongyang; Yu, Yin; Hu, Gaowei et al. (2021): Comparative analysis reveals the species-specific genetic determinants of ACE2 required for SARS-CoV-2 entry. In *PLoS pathogens* 17 (3). DOI: 10.1371/journal.ppat.1009392.

Reperant, Leslie A.; M E Osterhaus, Albert D. (2013): The Human-Animal Interface. In *Microbiology spectrum* 1 (1). DOI: 10.1128/microbiolspec.OH-0013-2012.

Richard, Mathilde; van den Brand, Judith M. A.; Bestebroer, Theo M.; Lexmond, Pascal; Meulder, Dennis de; Fouchier, Ron A. M. et al. (2020): Influenza A viruses are transmitted via the air from the nasal respiratory epithelium of ferrets. In *Nature communications* 11 (1), p. 766. DOI: 10.1038/s41467-020-14626-0.

RKI (2021): Anzahl und Anteile von VOC und VOI in Deutschland. https://www.rki.de/DE/Content/InfAZ/N/Neuartiges_Coronavirus/Virusvariante.html. Available online at https://www.rki.de/DE/Content/InfAZ/N/Neuartiges_Coronavirus/Daten/VOC_VOI_T abelle.xlsx?__blob=publicationFile, updated on 5th January, 2023.

Rosenthal, Nadia; Brown, Steve (2007): The mouse ascending: perspectives for human-disease models. In *Nature cell biology* 9 (9), pp. 993–999. DOI: 10.1038/ncb437.

Rota, Paul A.; Oberste, M. Steven; Monroe, Stephan S.; Nix, W. Allan; Campagnoli, Ray; Icenogle, Joseph P. et al. (2003): Characterization of a novel coronavirus associated with severe acute respiratory syndrome. In *Science (New York, N.Y.)* 300 (5624), pp. 1394–1399. DOI: 10.1126/science.1085952.

Roth, Nicole; Gergen, Janina; Kovacikova, Kristina; Mueller, Stefan O.; Ulrich, Lorenz; Schön, Jacob et al. (2023): Assessment of Immunogenicity and Efficacy of CV0501 mRNA-Based Omicron COVID-19 Vaccination in Small Animal Models. In *Vaccines* 11 (2). DOI: 10.3390/vaccines11020318.

Rott, R. (1992): The pathogenic determinant of influenza virus. In *Veterinary microbiology* 33 (1-4), pp. 303–310. DOI: 10.1016/0378-1135(92)90058-2.

Rovida, Francesca; Cassaniti, Irene; Paolucci, Stefania; Percivalle, Elena; Sarasini, Antonella; Piralla, Antonio et al. (2021): SARS-CoV-2 vaccine breakthrough infections with the alpha variant are asymptomatic or mildly symptomatic among health care workers. In *Nature communications* 12 (1), p. 6032. DOI: 10.1038/s41467-021-26154-6.

Ruiz-Aravena, Manuel; McKee, Clifton; Gamble, Amandine; Lunn, Tamika; Morris, Aaron; Snedden, Celine E. et al. (2022): Ecology, evolution and spillover of coronaviruses from bats. In *Nature reviews. Microbiology* 20 (5), pp. 299–314. DOI: 10.1038/s41579-021-00652-2.

Ryt-Hansen, Pia; Larsen, Inge; Kristensen, Charlotte Sonne; Krog, Jesper Schak; Larsen, Lars Erik (2019): Limited impact of influenza A virus vaccination of piglets in an enzootic infected sow herd. In *Research in veterinary science* 127, pp. 47–56. DOI: 10.1016/j.rvsc.2019.10.015.

Saito, Takehiko; Watanabe, Chiaki; Takemae, Nobuhiro; Chaisingh, Arunee; Uchida, Yuko; Buranathai, Chantanee et al. (2009): Pathogenicity of highly pathogenic avian influenza viruses of H5N1 subtype isolated in Thailand for different poultry species. In *Veterinary microbiology* 133 (1-2), pp. 65–74. DOI: 10.1016/j.vetmic.2008.06.020.

Sallam, Malik (2021): COVID-19 Vaccine Hesitancy Worldwide: A Concise Systematic Review of Vaccine Acceptance Rates. In *Vaccines* 9 (2). DOI: 10.3390/vaccines9020160.

Samji, Tasleem (2009): Influenza A: Understanding the Viral Life Cycle. In *The Yale Journal of Biology and Medicine* 82 (4), pp. 153–159.

Scarpa, Fabio; Sanna, Daria; Benvenuto, Domenico; Borsetti, Alessandra; Azzena, Ilenia; Casu, Marco et al. (2022): Genetic and Structural Data on the SARS-CoV-2 Omicron

BQ.1 Variant Reveal Its Low Potential for Epidemiological Expansion. In *International journal of molecular sciences* 23 (23). DOI: 10.3390/ijms232315264.

Scheibner, David; Salaheldin, Ahmed H.; Bagato, Ola; Zaeck, Luca M.; Mostafa, Ahmed; Blohm, Ulrike et al. (2023): Phenotypic effects of mutations observed in the neuraminidase of human origin H5N1 influenza A viruses. In *PLoS pathogens* 19 (2), e1011135. DOI: 10.1371/journal.ppat.1011135.

Schlottau, Kore; Rissmann, Melanie; Graaf, Annika; Schön, Jacob; Sehl, Julia; Wylezich, Claudia et al. (2020): SARS-CoV-2 in fruit bats, ferrets, pigs, and chickens: an experimental transmission study. In *The Lancet. Microbe* 1 (5), e218-e225. DOI: 10.1016/S2666-5247(20)30089-6.

Schoeman, Dewald; Gordon, Bianca; Fielding, Burtram C. (2022): Coronaviruses. In *Encyclopedia of Infection and Immunity*, pp. 241–258. DOI: 10.1016/B978-0-12-818731-9.00052-5.

Scholtissek, C.; Rohde, W.; Hoyningen, V. von; Rott, R. (1978): On the origin of the human influenza virus subtypes H2N2 and H3N2. In *Virology* 87 (1), pp. 13–20. DOI: 10.1016/0042-6822(78)90153-8.

Schön, Jacob; Ran, Wei; Gorka, Marco; Schwemmle, Martin; Beer, Martin; Hoffmann, Donata (2020): A modified live bat influenza A virus-based vaccine prototype provides full protection against HPAIV H5N1. In *NPJ Vaccines* 5. DOI: 10.1038/s41541-020-0185-6.

Schroeder, Simon; Mache, Christin; Kleine-Weber, Hannah; Corman, Victor M.; Muth, Doreen; Richter, Anja et al. (2021): Functional comparison of MERS-coronavirus lineages reveals increased replicative fitness of the recombinant lineage 5. In *Nature communications* 12 (1), p. 5324. DOI: 10.1038/s41467-021-25519-1.

Schubert, Katharina; Karousis, Evangelos D.; Jomaa, Ahmad; Scaiola, Alain; Echeverria, Blanca; Gurzeler, Lukas-Adrian et al. (2020): SARS-CoV-2 Nsp1 binds the ribosomal mRNA channel to inhibit translation. In *Nature structural & molecular biology* 27 (10), pp. 959–966. DOI: 10.1038/s41594-020-0511-8.

Seekings, Amanda H.; Howard, Wendy A.; Nuñéz, Alejandro; Slomka, Marek J.; Banyard, Ashley C.; Hicks, Daniel et al. (2020): The Emergence of H7N7 Highly Pathogenic Avian Influenza Virus from Low Pathogenicity Avian Influenza Virus Using an in ovo Embryo Culture Model. In *Viruses* 12 (9). DOI: 10.3390/v12090920.

Sha, Tim Wai; Weber, Michaela; Kasumba, Dacquin M.; Noda, Takeshi; Nakano, Masahiro; Kato, Hiroki; Fujita, Takashi (2020): Influenza A virus NS1 optimises virus infectivity by enhancing genome packaging in a dsRNA-binding dependent manner. In *Virology Journal* 17 (1), p. 107. DOI: 10.1186/s12985-020-01357-3.

Shalhoub, Sarah; Omrani, Ali S. (2016): Middle East respiratory syndrome. In *BMJ (Clinical research ed.)* 355, i5281. DOI: 10.1136/bmj.i5281.

Shaw, George M.; Hunter, Eric (2012): HIV Transmission. In *Cold Spring Harbor Perspectives in Medicine* 2 (11). DOI: 10.1101/cshperspect.a006965.

Shaw, Megan L.; Stone, Kathryn L.; Colangelo, Christopher M.; Gulcicek, Erol E.; Palese, Peter (2008): Cellular proteins in influenza virus particles. In *PLoS pathogens* 4 (6), e1000085. DOI: 10.1371/journal.ppat.1000085.

Shi, Jianzhong; Zeng, Xianying; Cui, Pengfei; Yan, Cheng; Chen, Hualan (2023): Alarming situation of emerging H5 and H7 avian influenza and effective control strategies. In *Emerging Microbes & Infections* 12 (1). DOI: 10.1080/22221751.2022.2155072.

Shuai, Huiping; Chan, Jasper Fuk-Woo; Yuen, Terrence Tsz-Tai; Yoon, Chaemin; Hu, Jing-Chu; Wen, Lei et al. (2021): Emerging SARS-CoV-2 variants expand species tropism to murines. In *EBioMedicine* 73, p. 103643. DOI: 10.1016/j.ebiom.2021.103643.

Sieczkarski, Sara B.; Whittaker, Gary R. (2002): Influenza virus can enter and infect cells in the absence of clathrin-mediated endocytosis. In *Journal of Virology* 76 (20), pp. 10455–10464. DOI: 10.1128/JVI.76.20.10455-10464.2002.

Simmonds, Peter; Aiewsakun, Pakorn; Katzourakis, Aris (2019): Prisoners of war - host adaptation and its constraints on virus evolution. In *Nature reviews. Microbiology* 17 (5), pp. 321–328. DOI: 10.1038/s41579-018-0120-2.

Singer, Shepherd R.; Angulo, Frederick J.; Swerdlow, David L.; McLaughlin, John M.; Hazan, Itay; Ginish, Netanel et al. (2021): Effectiveness of BNT162b2 mRNA COVID-19 vaccine against SARS-CoV-2 variant Beta (B.1.351) among persons identified through contact tracing in Israel: A prospective cohort study. In *EClinicalMedicine* 42, p. 101190. DOI: 10.1016/j.eclinm.2021.101190.

Slomka, Marek J.; Seekings, Amanda H.; Mahmood, Sahar; Thomas, Saumya; Puranik, Anita; Watson, Samantha et al. (2018): Unexpected infection outcomes of China-origin H7N9 low pathogenicity avian influenza virus in turkeys. In *Scientific reports* 8 (1), p. 7322. DOI: 10.1038/s41598-018-25062-y.

Smith, Gavin J. D.; Vijaykrishna, Dhanasekaran; Bahl, Justin; Lycett, Samantha J.; Worobey, Michael; Pybus, Oliver G. et al. (2009): Origins and evolutionary genomics of the 2009 swine-origin H1N1 influenza A epidemic. In *Nature* 459 (7250), pp. 1122–1125. DOI: 10.1038/nature08182.

Smith, Jacqueline; Smith, Nikki; Le Yu; Paton, Ian R.; Gutowska, Maria Weronika; Forrest, Heather L. et al. (2015): A comparative analysis of host responses to avian influenza infection in ducks and chickens highlights a role for the interferon-induced transmembrane proteins in viral resistance. In *BMC genomics* 16 (1), p. 574. DOI: 10.1186/s12864-015-1778-8.

Snijder, Eric J.; Limpens, Ronald W. A. L.; Wilde, Adriaan H. de; Jong, Anja W. M. de; Zevenhoven-Dobbe, Jessika C.; Maier, Helena J. et al. (2020): A unifying structural and functional model of the coronavirus replication organelle: Tracking down RNA synthesis. In *PLoS biology* 18 (6), e3000715. DOI: 10.1371/journal.pbio.3000715.

Soares, Miguel P.; Teixeira, Luis; Moita, Luis F. (2017): Disease tolerance and immunity in host protection against infection. In *Nature reviews. Immunology* 17 (2), pp. 83–96. DOI: 10.1038/nri.2016.136.

Sola, Isabel; Almazán, Fernando; Zúñiga, Sonia; Enjuanes, Luis (2015): Continuous and Discontinuous RNA Synthesis in Coronaviruses. In *Annual review of virology* 2 (1), pp. 265–288. DOI: 10.1146/annurev-virology-100114-055218.

Somerville, Mari; Curran, Janet A.; Dol, Justine; Boulos, Leah; Saxinger, Lynora; Doroshenko, Alexander et al. (2021): Public health implications of SARS-CoV-2 variants of concern: a rapid scoping review. In *BMJ Open* 11 (12). DOI: 10.1136/bmjopen-2021-055781.

Song, Huai-Dong; Tu, Chang-Chun; Zhang, Guo-Wei; Wang, Sheng-Yue; Zheng, Kui; Lei, Lian-Cheng et al. (2005): Cross-host evolution of severe acute respiratory syndrome coronavirus in palm civet and human. In *Proceedings of the National Academy of Sciences of the United States of America* 102 (7), pp. 2430–2435. DOI: 10.1073/pnas.0409608102.

Souza-Neto, Jayme A.; Powell, Jeffrey R.; Bonizzoni, Mariangela (2018): Aedes aegypti vector competence studies: A review. In *Infection, genetics and evolution : journal of molecular epidemiology and evolutionary genetics in infectious diseases* 67, pp. 191–209. DOI: 10.1016/j.meegid.2018.11.009.

Stadlbauer, Daniel; Waal, Leon de; Beaulieu, Edith; Strohmeier, Shirin; Kroeze, Edwin J. B. Veldhuis; Boutet, Philippe et al. (2021): AS03-adjuvanted H7N9 inactivated split virion vaccines induce cross-reactive and protective responses in ferrets. In *NPJ Vaccines* 6. DOI: 10.1038/s41541-021-00299-3.

Steinhauer, D. A. (1999): Role of hemagglutinin cleavage for the pathogenicity of influenza virus. In *Virology* 258 (1), pp. 1–20. DOI: 10.1006/viro.1999.9716.

Storm, Nadia; van Jansen Vuren, Petrus; Markotter, Wanda; Paweska, Janusz T. (2018): Antibody Responses to Marburg Virus in Egyptian Rousette Bats and Their Role in Protection against Infection. In *Viruses* 10 (2). DOI: 10.3390/v10020073.

Streicker, Daniel G.; Turmelle, Amy S.; Vonhof, Maarten J.; Kuzmin, Ivan V.; McCracken, Gary F.; Rupprecht, Charles E. (2010): Host phylogeny constrains cross-species emergence and establishment of rabies virus in bats. In *Science (New York, N.Y.)* 329 (5992), pp. 676–679. DOI: 10.1126/science.1188836.

Stubbs, Thomas M.; te Velthuis, Aartjan J. W. (2014): The RNA-dependent RNA polymerase of the influenza A virus. In *Future virology* 9 (9), pp. 863–876. DOI: 10.2217/fvl.14.66.

Su, Shuo; Wong, Gary; Shi, Weifeng; Liu, Jun; Lai, Alexander C.K.; Zhou, Jiyong et al. (2016): Epidemiology, Genetic Recombination, and Pathogenesis of Coronaviruses. In *Trends in microbiology* 24 (6), pp. 490–502. DOI: 10.1016/j.tim.2016.03.003.

Subudhi, Sonu; Rapin, Noreen; Bollinger, Trent K.; Hill, Janet E.; Donaldson, Michael E.; Davy, Christina M. et al. (2017): A persistently infecting coronavirus in hibernating Myotis lucifugus, the North American little brown bat. In *The Journal of General Virology* 98 (9), pp. 2297–2309. DOI: 10.1099/jgv.0.000898.

Suguitan, Amorsolo L.; Matsuoka, Yumiko; Lau, Yuk-Fai; Santos, Celia P.; Vogel, Leatrice; Cheng, Lily I. et al. (2012): The Multibasic Cleavage Site of the Hemagglutinin of Highly Pathogenic A/Vietnam/1203/2004 (H5N1) Avian Influenza Virus Acts as a Virulence Factor in a Host-Specific Manner in Mammals. In *Journal of Virology* 86 (5), pp. 2706–2714. DOI: 10.1128/JVI.05546-11.

Sun, Honglei; Xiao, Yihong; Liu, Jiyu; Wang, Dayan; Li, Fangtao; Wang, Chenxi et al. (2020): Prevalent Eurasian avian-like H1N1 swine influenza virus with 2009 pandemic viral genes facilitating human infection. In *Proceedings of the National Academy of Sciences of the United States of America* 117 (29), pp. 17204–17210. DOI: 10.1073/pnas.1921186117.

Sun, Shihui; Gu, Hongjing; Cao, Lei; Chen, Qi; Ye, Qing; Yang, Guan et al. (2021): Characterization and structural basis of a lethal mouse-adapted SARS-CoV-2. In *Nature communications* 12. DOI: 10.1038/s41467-021-25903-x.

Sun, Wanying; Cheng, Samuel S.M.; Lam, Kristy N.T.; Kwan, Tsz C.; Wong, Ricky W.K.; Lau, Leo H.K. et al. (2022): Natural Reassortment of Eurasian Avian-Like Swine H1N1 and Avian H9N2 Influenza Viruses in Pigs, China. In *Emerging Infectious Diseases* 28 (7), pp. 1509–1512. DOI: 10.3201/eid2807.220642.

Suratekar, Rohit; Ghosh, Pritha; Niesen, Michiel J. M.; Donadio, Gregory; Anand, Praveen; Soundararajan, Venky; Venkatakrishnan, A. J. (2022): High diversity in Delta variant

across countries revealed by genome-wide analysis of SARS-CoV-2 beyond the Spike protein. In *Molecular systems biology* 18 (2), e10673. DOI: 10.15252/msb.202110673.

Suzuki, Rigel; Yamasoba, Daichi; Kimura, Izumi; Wang, Lei; Kishimoto, Mai; Ito, Jumpei et al. (2022): Attenuated fusogenicity and pathogenicity of SARS-CoV-2 Omicron variant. In *Nature* 603 (7902), pp. 700–705. DOI: 10.1038/s41586-022-04462-1.

Tan, Sophia T.; Kwan, Ada T.; Rodríguez-Barraquer, Isabel; Singer, Benjamin J.; Park, Hailey J.; Lewnard, Joseph A. et al. (2023): Infectiousness of SARS-CoV-2 breakthrough infections and reinfections during the Omicron wave. In *Nature medicine*. DOI: 10.1038/s41591-022-02138-x.

Taubenberger, Jeffery K. (2006): The Origin and Virulence of the 1918 "Spanish" Influenza Virus1. In *Proceedings of the American Philosophical Society* 150 (1), pp. 86–112.

Taubenberger, Jeffery K.; Morens, David M. (2006): 1918 Influenza: the Mother of All Pandemics. In *Emerging Infectious Diseases* 12 (1), pp. 15–22. DOI: 10.3201/eid1201.050979.

Taubenberger, Jeffery K.; Morens, David M. (2010): Influenza: The Once and Future Pandemic. In *Public Health Reports* 125 (Suppl 3), pp. 16–26.

Taubenberger, Jeffery K.; Morens, David M. (2020): The 1918 Influenza Pandemic and Its Legacy. In *Cold Spring Harbor Perspectives in Medicine* 10 (10). DOI: 10.1101/cshperspect.a038695.

Tegally, Houriiyah; Moir, Monika; Everatt, Josie; Giovanetti, Marta; Scheepers, Cathrine; Wilkinson, Eduan et al. (2022): Emergence of SARS-CoV-2 Omicron lineages BA.4 and BA.5 in South Africa. In *Nature medicine* 28 (9), pp. 1785–1790. DOI: 10.1038/s41591-022-01911-2.

Tegally, Houriiyah; Wilkinson, Eduan; Giovanetti, Marta; Iranzadeh, Arash; Fonseca, Vagner; Giandhari, Jennifer et al. (2021): Detection of a SARS-CoV-2 variant of concern in South Africa. In *Nature* 592 (7854), pp. 438–443. DOI: 10.1038/s41586-021-03402-9.

Tong, Suxiang; Li, Yan; Rivailler, Pierre; Conrardy, Christina; Castillo, Danilo A. Alvarez; Chen, Li-Mei et al. (2012): A distinct lineage of influenza A virus from bats. In *Proceedings of the National Academy of Sciences of the United States of America* 109 (11), pp. 4269–4274. DOI: 10.1073/pnas.1116200109.

Tong, Suxiang; Zhu, Xueyong; Li, Yan; Shi, Mang; Zhang, Jing; Bourgeois, Melissa et al. (2013): New world bats harbor diverse influenza A viruses. In *PLoS pathogens* 9 (10), e1003657. DOI: 10.1371/journal.ppat.1003657.

Tostanoski, Lisa H.; Wegmann, Frank; Martinot, Amanda J.; Loos, Carolin; McMahan, Katherine; Mercado, Noe B. et al. (2020): Ad26 vaccine protects against SARS-CoV-2 severe clinical disease in hamsters. In *Nature medicine* 26 (11), pp. 1694–1700. DOI: 10.1038/s41591-020-1070-6.

Towner, Jonathan S.; Amman, Brian R.; Sealy, Tara K.; Carroll, Serena A. Reeder; Comer, James A.; Kemp, Alan et al. (2009): Isolation of genetically diverse Marburg viruses from Egyptian fruit bats. In *PLoS pathogens* 5 (7), e1000536. DOI: 10.1371/journal.ppat.1000536.

Trimpert, Jakob; Adler, Julia M.; Eschke, Kathrin; Abdelgawad, Azza; Firsching, Theresa C.; Ebert, Nadine et al. (2021): Live attenuated virus vaccine protects against SARS-CoV-2 variants of concern B.1.1.7 (Alpha) and B.1.351 (Beta). In *Science advances* 7 (49), eabk0172. DOI: 10.1126/sciadv.abk0172.

Tu, Changchun; Crameri, Gary; Kong, Xiangang; Chen, Jinding; Sun, Yanwei; Yu, Meng et al. (2004): Antibodies to SARS coronavirus in civets. In *Emerging Infectious Diseases* 10 (12), pp. 2244–2248. DOI: 10.3201/eid1012.040520.

Ulrich, Lorenz; Michelitsch, Anna; Halwe, Nico; Wernike, Kerstin; Hoffmann, Donata; Beer, Martin (2021): Experimental SARS-CoV-2 Infection of Bank Voles. In *Emerging Infectious Diseases* 27 (4), pp. 1193–1195. DOI: 10.3201/eid2704.204945.

United Nations (2022): Day of 8 billion. Available online at https://www.un.org/development/desa/pd/sites/www.un.org.development.desa.pd/files/wpp2022_summary_of_results.pdf.

Uraki, Ryuta; Halfmann, Peter J.; Iida, Shun; Yamayoshi, Seiya; Furusawa, Yuri; Kiso, Maki et al. (2022): Characterization of SARS-CoV-2 Omicron BA.4 and BA.5 isolates in rodents. In *Nature* 612 (7940), pp. 540–545. DOI: 10.1038/s41586-022-05482-7.

Uraki, Ryuta; Ito, Mutsumi; Furusawa, Yuri; Yamayoshi, Seiya; Iwatsuki-Horimoto, Kiyoko; Adachi, Eisuke et al. (2023): Humoral immune evasion of the omicron subvariants BQ.1.1 and XBB. In *The Lancet. Infectious diseases* 23 (1), pp. 30–32. DOI: 10.1016/S1473-3099(22)00816-7.

Uriu, Keiya; Kimura, Izumi; Shirakawa, Kotaro; Takaori-Kondo, Akifumi; Nakada, Taka-aki; Kaneda, Atsushi et al. (2021): Neutralization of the SARS-CoV-2 Mu Variant by Convalescent and Vaccine Serum. In *The New England journal of medicine* 385 (25), pp. 2397–2399. DOI: 10.1056/NEJMc2114706.

van Riel, Debby; Munster, Vincent J.; Wit, Emmie de; Rimmelzwaan, Guus F.; Fouchier, Ron A. M.; Osterhaus, Albert D. M. E.; Kuiken, Thijs (2007): Human and avian influenza viruses target different cells in the lower respiratory tract of humans and other mammals. In *The American journal of pathology* 171 (4), pp. 1215–1223. DOI: 10.2353/ajpath.2007.070248.

Vandegrift, Kurt J.; Yon, Michele; Surendran Nair, Meera; Gontu, Abhinay; Ramasamy, Santhamani; Amirthalingam, Saranya et al. (2022): SARS-CoV-2 Omicron (B.1.1.529) Infection of Wild White-Tailed Deer in New York City. In *Viruses* 14 (12). DOI: 10.3390/v14122770.

Veneti, Lamprini; Seppälä, Elina; Larsdatter Storm, Margrethe; Valcarcel Salamanca, Beatriz; Alnes Buanes, Eirik; Aasand, Nina et al. (2021): Increased risk of hospitalisation and intensive care admission associated with reported cases of SARS-CoV-2 variants B.1.1.7 and B.1.351 in Norway, December 2020 -May 2021. In *PloS one* 16 (10), e0258513. DOI: 10.1371/journal.pone.0258513.

Viboud, Cécile; Simonsen, Lone; Fuentes, Rodrigo; Flores, Jose; Miller, Mark A.; Chowell, Gerardo (2016): Global Mortality Impact of the 1957–1959 Influenza Pandemic. In *The Journal of Infectious Diseases* 213 (5), pp. 738–745. DOI: 10.1093/infdis/jiv534.

Vidaña, Beatriz; Brookes, Sharon M.; Everett, Helen E.; Garcon, Fanny; Nuñez, Alejandro; Engelhardt, Othmar et al. (2021): Inactivated pandemic 2009 H1N1 influenza A virus human vaccines have different efficacy after homologous challenge in the ferret model. In *Influenza and Other Respiratory Viruses* 15 (1), pp. 142–153. DOI: 10.1111/irv.12784.

Viglietta, Marine; Bellone, Rachel; Blisnick, Adrien Albert; Failloux, Anna-Bella (2021): Vector Specificity of Arbovirus Transmission. In *Frontiers in microbiology* 12. DOI: 10.3389/fmicb.2021.773211.

Virtanen, Jenni; Aaltonen, Kirsi; Kegler, Kristel; Venkat, Vinaya; Niamsap, Thanakorn; Kareinen, Lauri et al. (2022): Experimental Infection of Mink with SARS-COV-2 Omicron Variant and Subsequent Clinical Disease. In *Emerging Infectious Diseases* 28 (6), pp. 1286–1288. DOI: 10.3201/eid2806.220328.

Vries, Erik de; Du, Wenjuan; Guo, Hongbo; Haan, Cornelis A.M. de (2019): Influenza A Virus Hemagglutinin–Neuraminidase–Receptor Balance: Preserving Virus Motility. In *Trends in microbiology* 28 (1), pp. 57–67. DOI: 10.1016/j.tim.2019.08.010.

Walia, Rasna R.; Anderson, Tavis K.; Vincent, Amy L. (2019): Regional patterns of genetic diversity in swine influenza A viruses in the United States from 2010 to 2016. In *Influenza and Other Respiratory Viruses* 13 (3), pp. 262–273. DOI: 10.1111/irv.12559.

Walther, Trevenan; Karamanska, Rositsa; Chan, Renee W. Y.; Chan, Michael C. W.; Jia, Nan; Air, Gillian et al. (2013): Glycomic analysis of human respiratory tract tissues and correlation with influenza virus infection. In *PLoS pathogens* 9 (3), e1003223. DOI: 10.1371/journal.ppat.1003223.

Wang, Chia C.; Prather, Kimberly A.; Sznitman, Josué; Jimenez, Jose L.; Lakdawala, Seema S.; Tufekci, Zeynep; Marr, Linsey C. (2021): Airborne transmission of respiratory viruses. In *Science (New York, N.Y.)* 373 (6558). DOI: 10.1126/science.abd9149.

Wang, Liang; Didelot, Xavier; Bi, Yuhai; Gao, George F. (2022a): SARS-CoV-2 transmissibility compared between variants of concern and vaccination status. In *Briefings in bioinformatics* 23 (2). DOI: 10.1093/bib/bbab594.

Wang, Mei-Yue; Zhao, Rong; Gao, Li-Juan; Gao, Xue-Fei; Wang, De-Ping; Cao, Ji-Min (2020a): SARS-CoV-2: Structure, Biology, and Structure-Based Therapeutics Development. In *Frontiers in cellular and infection microbiology* 10, p. 587269. DOI: 10.3389/fcimb.2020.587269.

Wang, Ning; Shang, Jian; Jiang, Shibo; Du, Lanying (2020b): Subunit Vaccines Against Emerging Pathogenic Human Coronaviruses. In *Frontiers in microbiology* 11, p. 298. DOI: 10.3389/fmicb.2020.00298/full#B162.

Wang, Qian; Guo, Yicheng; Iketani, Sho; Nair, Manoj S.; Li, Zhiteng; Mohri, Hiroshi et al. (2022b): Antibody evasion by SARS-CoV-2 Omicron subvariants BA.2.12.1, BA.4 and BA.5. In *Nature* 608 (7923), pp. 603–608. DOI: 10.1038/s41586-022-05053-w.

Wang, Qian; Iketani, Sho; Li, Zhiteng; Liu, Liyuan; Guo, Yicheng; Huang, Yiming et al. (2022c): Alarming antibody evasion properties of rising SARS-CoV-2 BQ and XBB subvariants. In *Cell*. DOI: 10.1016/j.cell.2022.12.018.

Washington, Nicole L.; Gangavarapu, Karthik; Zeller, Mark; Bolze, Alexandre; Cirulli, Elizabeth T.; Schiabor Barrett, Kelly M. et al. (2021): Emergence and rapid transmission of SARS-CoV-2 B.1.1.7 in the United States. In *Cell* 184 (10), 2587-2594.e7. DOI: 10.1016/j.cell.2021.03.052.

Wei, Chaojie; Yuan, Yufeng; Cheng, Zhenshun (2020): A super-spreader of SARS-CoV-2 in incubation period among health-care workers. In *Respiratory research* 21 (1), p. 327. DOI: 10.1186/s12931-020-01592-w.

Wei, Sung-Hsi; Yang, Ji-Rong; Wu, Ho-Sheng; Chang, Ming-Chuan; Lin, Jen-Shiou; Lin, Chi-Yung et al. (2013): Human infection with avian influenza A H6N1 virus: an epidemiological analysis. In *The Lancet. Respiratory medicine* 1 (10), pp. 771–778. DOI: 10.1016/S2213-2600(13)70221-2.

WHO (2009): Pandemic Influenza Preparedness and Response: A WHO Guidance Document. THE WHO PANDEMIC PHASES. Available online at https://www.ncbi.nlm.nih.gov/books/NBK143061/.

WHO (2015): Summary of probable SARS cases with onset of illness from 1 November 2002 to 31 July 2003. Available online at https://www.who.int/publications/m/item/summary-of-probable-sars-cases-with-onset-of-illness-from-1-november-2002-to-31-july-2003.

WHO (2016): Tool for influenza pandemic risk assessment (TIPRA) (No. WHO/OHE/PED/GIP/2016.2). Available online at https://apps.who.int/iris/bitstream/handle/10665/250130/WHO-OHE-PED-GIP-?sequence=1.

WHO (2022): Middle East respiratory syndrome coronavirus (MERS-CoV) - Saudi Arabia. Available online at https://www.who.int/emergencies/disease-outbreak-news/item/2022-DON422.

WHO (2023): Statement on the update of WHO's working definitions and tracking system for SARS-CoV-2 variants of concern and variants of interest. Available online at https://www.who.int/news/item/16-03-2023-statement-on-the-update-of-who-s-working-definitions-and-tracking-system-for-sars-cov-2-variants-of-concern-and-variants-of-interest.

WHO as of 1st december (2022): Tracking SARS-CoV-2 Variants. Available online at https://www.who.int/activities/tracking-SARS-CoV-2-variants.

WHO as of 24th March (2023): WHO Coronavirus (COVID-19) Dashboard. Available online at https://covid19.who.int/.

Wilkinson, Gerald S.; Adams, Danielle M. (2019): Recurrent evolution of extreme longevity in bats. In *Biology letters* 15 (4), p. 20180860. DOI: 10.1098/rsbl.2018.0860.

Winkler, Emma S.; Chen, Rita E.; Alam, Fahmida; Yildiz, Soner; Case, James Brett; Uccellini, Melissa B. et al. (2022): SARS-CoV-2 Causes Lung Infection without Severe Disease in Human ACE2 Knock-In Mice. In *Journal of Virology* 96 (1), e0151121. DOI: 10.1128/JVI.01511-21.

WOAH (2021): Avian Influenza. (Including Infection with High Pathogenicity Avian Influenza Viruses). Chapter 3.3.4. OIE: Paris, France. Available online at https://www.woah.org/fileadmin/Home/fr/Health_standards/tahm/3.03.04_AI.pdf.

WOAH (2022): Manual of Diagnostic Tests and Vaccines for Terrestrial Animals 2022. Available online at https://www.woah.org/fileadmin/Home/eng/Health_standards/tahm/A_summry.htm.

Wong, Julius; Layton, Daniel; Wheatley, Adam K.; Kent, Stephen J. (2019): Improving immunological insights into the ferret model of human viral infectious disease. In *Influenza and Other Respiratory Viruses* 13 (6), pp. 535–546. DOI: 10.1111/irv.12687.

Worobey, Michael; Han, Guan-Zhu; Rambaut, Andrew (2014): A synchronized global sweep of the internal genes of modern avian influenza virus. In *Nature* 508 (7495), pp. 254–257. DOI: 10.1038/nature13016.

Worobey, Michael; Levy, Joshua I.; Malpica Serrano, Lorena; Crits-Christoph, Alexander; Pekar, Jonathan E.; Goldstein, Stephen A. et al. (2022): The Huanan Seafood Wholesale Market in Wuhan was the early epicenter of the COVID-19 pandemic. In *Science (New York, N.Y.)* 377 (6609), pp. 951–959. DOI: 10.1126/science.abp8715.

Wu, Aiping; Peng, Yousong; Huang, Baoying; Ding, Xiao; Wang, Xianyue; Niu, Peihua et al. (2020): Genome Composition and Divergence of the Novel Coronavirus (2019-nCoV) Originating in China. In *Cell host & microbe* 27 (3), pp. 325–328. DOI: 10.1016/j.chom.2020.02.001.

Xiao, Han; Killip, Marian J.; Staeheli, Peter; Randall, Richard E.; Jackson, David (2013): The human interferon-induced MxA protein inhibits early stages of influenza A virus infection by retaining the incoming viral genome in the cytoplasm. In *Journal of Virology* 87 (23), pp. 13053–13058. DOI: 10.1128/JVI.02220-13.

Xiao, Kangpeng; Zhai, Junqiong; Feng, Yaoyu; Zhou, Niu; Zhang, Xu; Zou, Jie-Jian et al. (2020): Isolation of SARS-CoV-2-related coronavirus from Malayan pangolins. In *Nature* 583 (7815), pp. 286–289. DOI: 10.1038/s41586-020-2313-x.

Xiao, Yinghong; Rouzine, Igor M.; Bianco, Simone; Acevedo, Ashley; Goldstein, Elizabeth Faul; Farkov, Mikhail et al. (2016): RNA Recombination Enhances Adaptability and Is Required for Virus Spread and Virulence. In *Cell host & microbe* 19 (4), pp. 493–503. DOI: 10.1016/j.chom.2016.03.009.

Xie, Xuping; Zou, Jing; Kurhade, Chaitanya; Liu, Mingru; Ren, Ping; Pei-Yong, Shi (2022): Neutralization of SARS-CoV-2 Omicron sublineages by 4 doses of the original mRNA vaccine. In *Cell reports* 41 (9), p. 111729. DOI: 10.1016/j.celrep.2022.111729.

Xu, Huafeng; Palpant, Timothy; Weinberger, Cody; Shaw, David E. (2022): Characterizing Receptor Flexibility to Predict Mutations That Lead to Human Adaptation of Influenza Hemagglutinin. In *Journal of Chemical Theory and Computation* 18 (8), pp. 4995–5005. DOI: 10.1021/acs.jctc.1c01044.

Yadav, Rohitash; Chaudhary, Jitendra Kumar; Jain, Neeraj; Chaudhary, Pankaj Kumar; Khanra, Supriya; Dhamija, Puneet et al. (2021): Role of Structural and Non-Structural Proteins and Therapeutic Targets of SARS-CoV-2 for COVID-19. In *Cells* 10 (4). DOI: 10.3390/cells10040821.

Yan, Renhong; Zhang, Yuanyuan; Li, Yaning; Xia, Lu; Guo, Yingying; Zhou, Qiang (2020): Structural basis for the recognition of SARS-CoV-2 by full-length human ACE2. In *Science (New York, N.Y.)* 367 (6485), pp. 1444–1448. DOI: 10.1126/science.abb2762.

Yang, Jiaan; Zhang, Peng; Cheng, Wen Xiang; Lu, Youyong; Gang, Wu; Ren, Gang (2021a): Exposing structural variations in SARS-CoV-2 evolution. In *Scientific reports* 11 (1), p. 22042. DOI: 10.1038/s41598-021-01650-3.

Yang, Jianmei; Lee, Jinhwa; Ma, Jingjiao; Lang, Yuekun; Nietfeld, Jerome; Li, Yuhao et al. (2017): Pathogenicity of modified bat influenza virus with different M genes and its reassortment potential with swine influenza A virus. In *The Journal of General Virology* 98 (4), pp. 577–584. DOI: 10.1099/jgv.0.000715.

Yang, Tzu-Jing; Yu, Pei-Yu; Chang, Yuan-Chih; Liang, Kang-Hao; Tso, Hsian-Cheng; Ho, Meng-Ru et al. (2021b): Effect of SARS-CoV-2 B.1.1.7 mutations on spike protein structure and function. In *Nature structural & molecular biology* 28 (9), pp. 731–739. DOI: 10.1038/s41594-021-00652-z.

Ye, Zi-Wei; Yuan, Shuofeng; Yuen, Kit-San; Fung, Sin-Yee; Chan, Chi-Ping; Jin, Dong-Yan (2020): Zoonotic origins of human coronaviruses. In *International Journal of Biological Sciences* 16 (10), pp. 1686–1697. DOI: 10.7150/ijbs.45472.

York, Ashley; Hengrung, Narin; Vreede, Frank T.; Huiskonen, Juha T.; Fodor, Ervin (2013): Isolation and characterization of the positive-sense replicative intermediate of a

negative-strand RNA virus. In *Proceedings of the National Academy of Sciences of the United States of America* 110 (45), E4238-45. DOI: 10.1073/pnas.1315068110.

Yuan, Shuofeng; Ye, Zi-Wei; Liang, Ronghui; Tang, Kaiming; Zhang, Anna Jinxia; Lu, Gang et al. (2022): Pathogenicity, transmissibility, and fitness of SARS-CoV-2 Omicron in Syrian hamsters. In *Science (New York, N.Y.)* 377 (6604), pp. 428–433. DOI: 10.1126/science.abn8939.

Zaki, Ali M.; van Boheemen, Sander; Bestebroer, Theo M.; Osterhaus, Albert D. M. E.; Fouchier, Ron A. M. (2012): Isolation of a novel coronavirus from a man with pneumonia in Saudi Arabia. In *The New England journal of medicine* 367 (19), pp. 1814–1820. DOI: 10.1056/NEJMoa1211721.

Zanobini, Patrizio; Bonaccorsi, Guglielmo; Lorini, Chiara; Haag, Mendel; McGovern, Ian; Paget, John; Caini, Saverio (2022): Global patterns of seasonal influenza activity, duration of activity and virus (sub)type circulation from 2010 to 2020. In *Influenza and Other Respiratory Viruses* 16 (4), pp. 696–706. DOI: 10.1111/irv.12969.

Zettler, Silja; Renner, Simone; Kemter, Elisabeth; Hinrichs, Arne; Klymiuk, Nikolai; Backman, Mattias et al. (2020): A decade of experience with genetically tailored pig models for diabetes and metabolic research. In *Animal Reproduction* 17 (3). DOI: 10.1590/1984-3143-AR2020-0064.

Zhang, Xinghai; Li, Yuanguo; Jin, Song; Wang, Tiecheng; Sun, Weiyang; Zhang, Yiming et al. (2022): H9N2 influenza virus spillover into wild birds from poultry in China bind to human-type receptors and transmit in mammals via respiratory droplets. In *Transboundary and emerging diseases* 69 (2), pp. 669–684. DOI: 10.1111/tbed.14033.

Zhou, Bin; Ma, Jingjiao; Liu, Qinfang; Bawa, Bhupinder; Wang, Wei; Shabman, Reed S. et al. (2014): Characterization of uncultivable bat influenza virus using a replicative synthetic virus. In *PLoS pathogens* 10 (10), e1004420. DOI: 10.1371/journal.ppat.1004420.

Zhou, Bin; Thao, Tran Thi Nhu; Hoffmann, Donata; Taddeo, Adriano; Ebert, Nadine; Labroussaa, Fabien et al. (2021): SARS-CoV-2 spike D614G change enhances replication and transmission. In *Nature* 592 (7852), pp. 122–127. DOI: 10.1038/s41586-021-03361-1.

Zhou, Peng; Yang, Xing-Lou; Wang, Xian-Guang; Hu, Ben; Zhang, Lei; Zhang, Wei et al. (2020): A pneumonia outbreak associated with a new coronavirus of probable bat origin. In *Nature* 579 (7798), pp. 270–273. DOI: 10.1038/s41586-020-2012-7.

Zhu, Na; Zhang, Dingyu; Wang, Wenling; Li, Xingwang; Yang, Bo; Song, Jingdong et al. (2020): A Novel Coronavirus from Patients with Pneumonia in China, 2019. In *The New England journal of medicine* 382 (8), pp. 727–733. DOI: 10.1056/nejmoa2001017.

Zhu, Zhaoqin; Yang, Yuqin; Feng, Yanling; Shi, Bisheng; Chen, Lixiang; Zheng, Ye et al. (2013): Infection of inbred BALB/c and C57BL/6 and outbred Institute of Cancer Research mice with the emerging H7N9 avian influenza virus. In *Emerging Microbes & Infections* 2 (8), e50-. DOI: 10.1038/emi.2013.50.

ZOONOSES (1951). In *The Lancet* 257 (6653), pp. 518–519.

9　Appendix

9.1　Eigenständigkeitserklärung

Hiermit erkläre ich, dass diese Arbeit bisher von mir weder an der Mathematisch-Naturwissenschaftlichen Fakultät der Universität Greifswald noch einer anderen wissenschaftlichen Einrichtung zum Zwecke der Promotion eingereicht wurde.

Ferner erkläre ich, dass ich diese Arbeit selbstständig verfasst und keine anderen als die darin angegebenen Hilfsmittel und Hilfen benutzt und keine Textabschnitte eines Dritten ohne Kennzeichnung übernommen habe.

_____

Nico Joël Halwe

9.3   Publications

9.3.1 Publications included in this dissertation

I)   **Halwe NJ**, Gorka M, Hoffmann B, Rissmann M, Breithaupt A, Schwemmle M, Beer M, Kandeil A, Ali MA, Kayali G, Hoffmann D, Balkema-Buschmann A. **Egyptian Fruit Bats (Rousettus aegyptiacus) Were Resistant to Experimental Inoculation with Avian-Origin Influenza A Virus of Subtype H9N2, But Are Susceptible to Experimental Infection with Bat-Borne H9N2 Virus.** *Viruses.* **2021** Apr 14;13(4):672. doi: 10.3390/v13040672

II)   **Halwe NJ**, Hamberger L, Sehl-Ewert J, Mache C, Schön J, Ulrich L, Calvelage S, Tönnies M, Fuchs J, Bandawane P, Loganathan M, Abbad A, Carreño JM, Bermúdez-González MC, Simon V, Kandeil A, El-Shesheny R,. Ali MA, Kayali G, Budt M, Hippenstiel S, Hocke AC, Krammer F, Wolff T, Schwemmle M, Ciminski K, Hoffmann D, Beer M **The bat-borne influenza A virus H9N2 exhibits a set of unexpected pre-pandemic features.** Submitted to *Nature Medicine*, **2023** (Contacted potential reviewers on the 19th of May, 2023)

III)   Ulrich L*, **Halwe NJ***, Taddeo A*, Ebert N*, Schön J, Devisme C, Trüeb BS, Hoffmann B, Wider M, Fan X, Bekliz M, Essaidi-Laziosi M, Schmidt ML, Niemeyer D, Corman VM, Kraft A, Godel A, Laloli L, Kelly JN, Calderon BM, Breithaupt A, Wylezich C, Berenguer Veiga I, Gultom M, Osman S, Zhou B, Adea K, Meyer B, Eberhardt CS, Thomann L, Gsell M, Labroussaa F, Jores J, Summerfield A, Drosten C, Eckerle IA, Wentworth DE, Dijkman R, Hoffmann D, Thiel V, Beer M, Benarafa C. **Enhanced fitness of SARS-CoV-2 variant of concern Alpha but not Beta.** *Nature.* **2022** Feb;602(7896):307-313. doi: 10.1038/s41586-021-04342-0.

IV)   Barut GT*, **Halwe NJ***, Taddeo A*, Kelly JN*, Schön J, Ebert N, Ulrich L, Devisme C, Steiner S, Trüeb BS, Hoffmann B, Veiga IB, Leborgne NGF, Moreira EA, Breithaupt A, Wylezich C, Höper D, Wernike K, Godel A, Thomann L, Flück V, Stalder H, Brügger M, Esteves BIO, Zumkehr B, Beilleau G, Kratzel A, Schmied K, Ochsenbein S, Lang RM, Wider M, Machahua C, Dorn P, Marti TM, Funke-Chambour M, Rauch A, Widera M, Ciesek S, Dijkman R, Hoffmann D, Alves MP, Benarafa C, Beer M, Thiel

V. **The spike gene is a major determinant for the SARS-CoV-2 Omicron-BA.1 phenotype.** *Nat Commun.* **2022** Oct 7;13(1):5929. doi: 10.1038/s41467-022-33632-y

9.3.2 Publications not included in this dissertation

V)‡   Zhou B*, Thao TTN*, Hoffmann D*, Taddeo A*, Ebert N, Labroussaa F, Pohlmann A, King J, Steiner S, Kelly JN, Portmann J, **Halwe NJ**, Ulrich L, Trüeb BS, Fan X, Hoffmann B, Wang L, Thomann L, Lin X, Stalder H, Pozzi B, de Brot S, Jiang N, Cui D, Hossain J, Wilson MM, Keller MW, Stark TJ, Barnes JR, Dijkman R, Jores J, Benarafa C*, Wentworth DE*, Thiel V*, Beer M*. **SARS-CoV-2 spike D614G change enhances replication and transmission.** *Nature.* **2021** Apr;592(7852):122-127. doi: 10.1038/s41586-021-03361-1

‡*Awarded with the Charles C. Shepard Science Award 2022*
(https://www.cdc.gov/os/shepardaward/winners/Awards22.html)

VI)   Ulrich L*, Michelitsch A*, **Halwe N***, Wernike K, Hoffmann D, Beer M. **Experimental SARS-CoV-2 Infection of Bank Voles.** *Emerg Infect Dis.* **2021** Apr;27(4):1193-1195. doi: 10.3201/eid2704.204945

VII)   Hoffmann D*, Corleis B*, Rauch S, Roth N, Mühe J, **Halwe NJ**, Ulrich L, Fricke C, Schön J, Kraft A, Breithaupt A, Wernike K, Michelitsch A, Sick F, Wylezich C, Hoffmann B, Thran M, Thess A, Mueller SO, Mettenleiter TC, Petsch B, Dorhoi A[†], Beer M[†]. **CVnCoV and CV2CoV protect human ACE2 transgenic mice from ancestral B BavPat1 and emerging B.1.351 SARS-CoV-2.** *Nat Commun.* **2021** Jun 30;12(1):4048. doi: 10.1038/s41467-021-24339-7

VIII)   Roth N, Gergen J, Kovacikova K, Mueller SO, Ulrich L, Schön J, **Halwe NJ**, Fricke C, Corleis B, Dorhoi A, Hoffmann D, Beer M, Maione D, Petsch B, Rauch S. **Assessment of Immunogenicity and Efficacy of CV0501 mRNA-Based Omicron COVID-19 Vaccination in Small Animal Models.** *Vaccines.* **2023**; 11(2):318. https://doi.org/10.3390/vaccines11020318

IX)   Corleis B, Hoffmann D, Rauch S, Fricke C, Roth N, Gergen J, Kovacikova K, Schlottau K, **Halwe NJ**, Ulrich L, Schön J, Wernike K, Widera M, Ciesek S, Mueller SO,

Mettenleiter TC, Maione D, Petsch B, Beer M & Dorhoi A et al. **Efficacy of an unmodified bivalent mRNA vaccine against SARS-CoV-2 variants in female small animal models.** *Nat Commun.* **2023**; 14, 816. https://doi.org/10.1038/s41467-023-36110-1

9.4   Oral and poster presentations

04.06. – 05.06.2020   Junior Scientist Zoonoses Meeting 2020, Leipzig, Germany. Poster presentation: **Molecular biology and spill over potential of bat-influenza-viruses**

<u>Nico Joël Halwe</u>, Anne Balkema-Buschmann, Melanie Rissmann, Donata Hoffmann, Martin Beer (poster presentations for young scientists were cancelled due to the COVID-19 pandemic)

24.03. – 26.03.2021   30th Annual meeting of the Society for Virology, Online, Poster talk: **Egyptian fruit bats are resistant to infection with avian-origin Influenza A virus of subtype H9N2 but reveal susceptibility to bat-borne H9N2**

<u>Nico Joël Halwe</u>, Marco Gorka, Bernd Hoffmann, Melanie Rissmann, Angele Breithaupt, Martin Beer, Ahmed Kandeil, Mohamed A. Ali, Ghazi Kayali, Donata Hoffmann, Anne Balkema-Buschmann

30.03. – 02.04.2022   31st Annual meeting of the Society for Virology, Munich, Germany. Oral presentation: **Viral fitness determination of SARS-CoV-2 VOCs Alpha and Beta by competitive infection and transmission experiments in ferrets, hamsters and two mouse models**

<u>Nico Joël Halwe</u>, Lorenz Ulrich, Adriano Taddeo, Nadine Ebert, Jacob Schön, Christelle Devisme, Bernd Hoffmann, Anna Kraft, Angele Breithaupt, Claudia Wylezich, Volker Thiel, Charaf Benarafa, Donata Hoffmann, Martin Beer

23.06 – 24.06.2022   Junior Scientist Zoonoses Meeting, Hanover, Germany. Poster presentation:

In vivo **competitive infection and transmission of SARS-CoV-2 VoCs Alpha, Delta and Omicron**

Nico Joël Halwe, Lorenz Ulrich, Jacob Schön, Bernd Hoffmann, Angele Breithaupt, Volker Thiel, Charaf Benarafa, Donata Hoffmann, Martin Beer

05.10. – 07.10.2022   Zoonoses 2022 – International Symposium on Zoonoses Research, Berlin, Germany. Oral presentation:

SARS-CoV-2 VOC Omicron subvariants: viral host range, immune escape and virulence levels

Nico Joël Halwe, Lorenz Ulrich, Jacob Schön, Bernd Hoffmann, Angele Breithaupt, Claudia Wylezich, Kerstin Wernike, Dirk Höper, Volker Thiel, Charaf Benarafa, Donata Hoffmann, Martin Beer

28.03. – 31.03.2023   32nd Annual meeting of the Society for Virology, Ulm, Germany. Oral presentation:

The bat-derived H9N2 Influenza A virus possesses concerning zoonotic features

Nico Joël Halwe, Lea Hamberger, Julia Sehl-Ewert, Jacob Schön, Lorenz Ulrich, Jonas Fuchs, Ahmed Kandeil, Rabeh El-Shesheny, Ghazi Kayali, Martin Schwemmle, Kevin Ciminski, Donata Hoffmann, Martin Beer

04.05. – 07.05.2023   8th European Congress of Virology, Gdansk, Poland. Oral presentation:

The bat-derived H9N2 Influenza A virus possesses concerning zoonotic features

Nico Joël Halwe, Lea Hamberger, Julia Sehl-Ewert, Jacob Schön, Lorenz Ulrich, Jonas Fuchs, Ahmed Kandeil, Rabeh El-Shesheny, Pooja Bandawane, Madhumathi Loganathan, Anass Abbad, Juan Manuel Carreño, Viviana Simon, Ghazi Kayali, Florian Krammer, Martin Schwemmle, Kevin Ciminski, Donata Hoffmann, Martin Beer

14.05. – 18.05.2023   XVIth   International   Nidovirus   Symposium,   Montreux,
                             Switzerland. Flash oral and poster presentation:
                             **A multi-species approach to *in vivo* characterize SARS-CoV-
                             2 VOC Alpha, Delta and Omicron subvariant fitness
                             advantages**
                             Nico Joël Halwe, Lorenz Ulrich, Jacob Schön, Bernd Hoffmann,
                             Angele Breithaupt, Claudia Wylezich, Kerstin Wernike, Dirk
                             Höper, Volker Thiel, Charaf Benarafa, Donata Hoffmann, Martin
                             Beer

14.05. – 18.05.2023   XVIth   International   Nidovirus   Symposium,   Montreux,

10 Danksagung

Ich möchte mich an dieser Stelle mit einem riesigen Dankeschön bei allen Personen bedanken, die mich von Anfang bis Abgabe dieser Doktorarbeit unterstützt und motiviert haben.

Zunächst bedanke ich mich herzlich bei **Prof. Dr. Stefan Finke** für die freundliche Übernahme des Erstgutachtens und der universitären Betreuung, sowie allen weiteren Gutachtern für die Beurteilung dieser Arbeit.

Ein sehr großes Dankeschön an meinen Institutsleiter und Mentor **Prof. Dr. Martin Beer**, der mir die Gelegenheit gegeben hat an diesen hochaktuellen und spannenden Projekten zu forschen, sowie mich stets durch die gesamte Doktorarbeit hindurch mit viele Ratschlägen versorgt hat, die maßgeblich zum Erfolg dieser Arbeit beigetragen haben!

Meiner Arbeitsgruppenleiterin **PD Dr. Donata Hoffmann** möchte ich außerordentlich für ihre tägliche Betreuung, ihre kontinuierliche Ansprechbarkeit, ihr Vertrauen und damit einhergehend ihre außerordentliche Unterstützung während meiner gesamten Doktorarbeit danken!

Darüber hinaus bedanke ich mich natürlich auch bei der gesamten AG D. Hoffmann mit **Lorenz, Jacob, Mareen, Kore, Doris und Anna** für die vielen lustigen Gespräche, die allseits fröhliche Stimmung im Labor, sowie für etliche Kaffeerunden, diverse coole Aktivitäten außerhalb des Labors und die daraus entstandenen, neuen Freundschaften!

Ebenfalls möchte ich mich bei den Tierpflegern und den Pathologen für ihre tatkräftige Unterstützung während meiner Tierversuche bedanken! Mein weiterer Dank gebührt allen weiteren FLI-internen oder externen Kooperationspartnern für herausragende, gemeinsame Publikationen! An dieser Stelle möchte ich besonders **Prof. Dr. Martin Schwemmle, Prof. Dr. Volker Thiel, Prof. Dr. Charaf Benarafa und PD Dr. Anne Balkema-Buschmann** erwähnen, die als hervorragende Supervisor an den Veröffentlichungen in dieser Dissertation mitgewirkt haben!

Ich möchte mich zudem bei allen neu dazu gewonnenen Freundschaften am FLI bedanken, sei es innerhalb oder außerhalb des Instituts für Virusdiagnostik! Ihr habt maßgeblich dazu beigetragen, dass ich mich hier oben weit entfernt meiner Heimat wohlgefühlt habe!

An dieser Stelle möchte ich vor allem **Paul, Benedikt** und meine Freundin **Felicitas** namentlich nennen! Ich bin extrem froh, euch kennengelernt zu haben!

Zusätzlich dazu möchte ich all meinen langjährigen Freunden aus meiner Heimat danken, bei denen ich auch in stressigen Phasen immer meinen Kopf frei bekommen konnte: Vor allem **Yannik, Lucas, Matthias H., Matthias B., Fabian und Kevin.**

Abschließend gebührt der größte und herzlichste Dank natürlich meiner Familie. <u>**Meinem Bruder**</u>, da ich durch ihn das Interesse an der Virologie erst für mich entdeckt habe und natürlich <u>**Meinen Eltern**</u>, ihr habt mich von klein auf bis zu diesem Punkt unterstützt und gefördert. Ich bin wer ich bin nur durch euch, hierfür bin ich euch unendlich dankbar!!!